Universitat Politècnica de València
Departamento de Máquinas y Motores Térmicos

UNIVERSITAT
POLITÈCNICA
DE VALÈNCIA

Doctoral Thesis

ANALYSIS AND CFD-GUIDED OPTIMIZATION OF ADVANCED COMBUSTION SYSTEMS IN COMPRESSION-IGNITED ENGINES

Presented by:
Cássio Spohr Fernandes

Supervised by:
Dra. Gabriela Bracho León

in fulfillment of the requirements for the degree of
Doctor of Philosophy

Valencia, April 2023

Ph.D. Thesis

ANALYSIS AND CFD-GUIDED OPTIMIZATION OF ADVANCED COMBUSTION SYSTEMS IN COMPRESSION-IGNITED ENGINES

Written by: Mr. Cássio Spohr Fernandes
Supervised by: Dra. Gabriela Bracho León

Examination committee:

Chairman: Dr. Jesús Benajes
Secretary: Dra. María Arántzazu Gómez Esteban
Member: Dr. Angelo Onorati

Reviewing board:

Dr. Adrián Pandal
Dr. Walter Vera Tudela
Dra. Luisa Monico

Valencia, April 2023

Abstract

Reducing emissions of pollutant gases from internal combustion engines (ICE) is one of the biggest challenges to combat global warming. As the engines will continue to be used by industry for decades, it is necessary to develop new technologies. In this context, the present doctoral thesis was motivated by the need to further improve engines, both from a technical engineering and social point of view, due to the effects of greenhouse gases.

The main objective of this thesis is to develop an optimization methodology for compression ignition (CI) engine combustion systems by coupling optimization algorithms with computer simulation. With the optimization of the combustion systems, it is possible to increase the efficiency of the engines, thus reducing fuel consumption, concomitantly with the reduction of gas emissions, in particular nitrogen oxides (NO_x) and soot.

In the first step, different optimization algorithms are addressed in order to elect the best candidate for this methodology. From this point on, the first optimization is focused on a CI engine operating with conventional fuel in order to validate the methodology and also to evaluate the current state of evolution of these engines. With the goal of reducing fuel consumption while keeping NO_x and soot levels below the values of a real engine, the optimization process begins. The results obtained confirm that a new combustion system specifically for this engine could generate a reduction in fuel consumption while keeping gas emissions below the stipulated value. Furthermore, it is concluded that CI engines using conventional fuel are already at a very high-efficiency level, and it is difficult to improve them without the use of an after-treatment system.

Thus, the second optimization block is based on the use of CI engines operating on an alternative fuel, which in this case is OME. This study aimed to design a specific combustion system for an engine using this fuel that delivers efficiency on the same order of magnitude as a diesel engine. While searching for better efficiency, the NO_x emissions are a restriction of the optimization system so that the combustion system does not emit more gases than a real engine. In this case, soot is not considered due to the characteristics of the fuel not producing this kind of pollutant. The results showed that a combustion system designed specifically for this operation could deliver high efficiencies, including the efficiency obtained was around 2.2 % higher compared to the real diesel engine. In addition, it was possible to halve the NO_x emissions when the engine operates with OME.

The last optimization block concerns a new engine architecture that makes it possible to eliminate NO_x emissions. The oxy-fuel combustion model is

exciting since nitrogen is eliminated from the intake mixture, and thus no emissions containing N_2 are generated. Furthermore, with the use of this combustion mode, it is possible to capture CO_2 from the exhaust gas, which can then be sold to the market. Since this is a new and little-researched topic, the results are promising. They show that it was possible to obtain a specific combustion system capable of delivering efficiency levels close to conventional engines. Furthermore, NO_x emissions were eliminated, as well as soot emissions. Additionally, this system was able to reduce CO and HC emissions to levels similar to conventional engines.

Moreover, the results presented in this doctoral thesis provide an extended database to explore the CI engine operation. Additionally, this work showed the potential of computational simulation allied with mathematical methods in order to design combustion systems for different applications.

Resumen

Reducir las emisiones de gases contaminantes de los motores de combustión interna alternativos (MCIA) es uno de los mayores retos para combatir el calentamiento global. Dado que los motores seguirán siendo utilizados por la industria durante décadas, es necesario desarrollar nuevas tecnologías. En este contexto, la presente tesis doctoral viene motivada por la necesidad de seguir mejorando los motores, tanto desde el punto de vista de la ingeniería técnica como desde el punto de vista social, debido a los efectos de los gases de efecto invernadero.

El objetivo principal de esta tesis es desarrollar una metodología de optimización para sistemas de combustión de motores de encendido por compresión (MEC) mediante el acoplamiento de algoritmos de optimización con simulación por ordenador. Con la optimización de los sistemas de combustión es posible aumentar la eficiencia de los motores, reduciendo así el consumo de combustible junto con la reducción de emisiones contaminantes, en particular óxidos de nitrógeno (NO_x) y hollín.

En el primer paso, se abordan diferentes algoritmos de optimización con el fin de elegir el mejor candidato para esta metodología. A partir de aquí, la primera optimización se centra en un motor de encendido por compresión que funciona con combustible convencional para validar la metodología y también para evaluar el estado actual de evolución de estos motores. Con el objetivo de reducir el consumo de combustible manteniendo los niveles de NO_x y hollín por debajo de los valores de un motor real, se inicia el proceso de optimización. Los resultados obtenidos confirman que un nuevo sistema de combustión específico para este motor podría generar una reducción del consumo de combustible manteniendo las emisiones de gases por debajo del valor estipulado. Además, se concluye que los motores MEC que utilizan combustible convencional se encuentran ya en un nivel de eficiencia muy elevado, y es difícil mejorarlos sin utilizar un sistema de postratamiento.

Así pues, el segundo bloque de optimización se basa en el uso de motores MEC que funcionan con un combustible alternativo, que en este caso es el OME. El objetivo de este estudio es diseñar un sistema de combustión específico para un motor que utilice este combustible y que ofrezca un rendimiento del mismo orden de magnitud que un motor diésel. En la búsqueda de una mayor eficiencia, las emisiones de NO_x son una restricción del sistema de optimización para que el sistema de combustión no emita más gases que un motor real. En este caso, el hollín no se tiene en cuenta debido a que las características del combustible no producen este tipo de contaminante. Los resultados mostraron que un sistema de combustión diseñado específicamente para

esta operación podía ofrecer altas eficiencias, incluso la eficiencia obtenida fue alrededor de 2,2 % mayor en comparación con el motor diesel real. Además, fue posible reducir a la mitad las emisiones de NO_x cuando el motor funciona con OME.

El último bloque de optimización se refiere a una nueva arquitectura de motor que permite eliminar las emisiones de NO_x. El modelo de oxicombustión resulta apasionante, ya que se elimina el nitrógeno de la mezcla de admisión y, por tanto, no se generan emisiones que contengan N_2. Además, con el uso de este modo de combustión, es posible capturar CO_2 de los gases de escape, que luego puede venderse en el mercado. Dado que se trata de un tema nuevo y poco investigado, los resultados son prometedores. Demuestran que fue posible obtener un sistema de combustión específico capaz de ofrecer niveles de eficiencia cercanos a los de los motores convencionales. Además, se eliminaron las emisiones de NO_x, así como las de hollín. Adicionalmente, este sistema fue capaz de reducir las emisiones de CO y HC a niveles similares a los motores convencionales.

Por otra parte, los resultados presentados en esta tesis doctoral proporcionan una base de datos ampliada para explorar el funcionamiento del motor CI. Adicionalmente, este trabajo mostró el potencial de la simulación computacional aliada con métodos matemáticos para diseñar sistemas de combustión para diferentes aplicaciones.

Resum

Reduir les emissions de gasos contaminants dels motors de combustió interna alternatius (MCIA) és un dels majors reptes per a combatre el camvi climàtic. Atés que els motors continuaran sent utilitzats per la indústria durant dècades, és necessari desenvolupar noves tecnologies. En aquest context, la present tesi doctoral ve motivada per la necessitat de continuar millorant els motors, tant des del punt de vista de l'enginyeria tècnica com des del punt de vista social, degut a l'efecte dels gasos d'efecte d'hivernacle.

L'objectiu principal d'aquesta tesi és desenvolupar una metodologia d'optimització per a sistemes de combustió de motors d'encesa provocada mitjançant l'acoblament d'algorismes d'optimització amb simulació per ordinador. Amb l'optimització dels sistemes de combustió és possible augmentar l'eficiència dels motors, reduint així el consum de combustible, concomitantment amb la reducció d'emissions de gasos, en particular òxids de nitrogen (NO_x) i sutge.

En el primer pas, s'aborden diferents algorismes d'optimització amb la finalitat d'elegir el millor candidat per a aquesta metodologia. A partir d'ací, la primera optimització se centra en un motor d'encesa per compressió que funciona amb combustible convencional per a validar la metodologia i també per a avaluar l'estat actual d'evolució d'aquests motors. Amb l'objectiu de reduir el consum de combustible mantenint els nivells de NO_x i sutge per davall dels valors d'un motor real, s'inicia el procés d'optimització. Els resultats obtinguts confirmen que un nou sistema de combustió específic per a aquest motor podria generar una reducció del consum de combustible mantenint les emissions de gasos per davall del valor estipulat. A més, es conclou que els motors d'encesa per compressió que utilitzen combustible convencional es troben ja en un nivell d'eficiència molt elevat, i és difícil millorar-los sense utilitzar un sistema de posttractament.

Així doncs, el segon bloc d'optimització es basa en l'ús de motors d'encesa per compressió que funcionen amb un combustible alternatiu, que en aquest cas és el OME. L'objectiu d'aquest estudi és dissenyar un sistema de combustió específic per a un motor que utilitze aquest combustible i que oferisca un rendiment del mateix ordre de magnitud que un motor dièsel. En la cerca d'una major eficiència, les emissions de NO_x són una restricció del sistema d'optimització perquè el sistema de combustió no emeta més gasos que un motor real. En aquest cas, el sutge no es té en compte pel fet que les característiques del combustible no produeixen aquest tipus de contaminant. Els resultats van mostrar que un sistema de combustió dissenyat específicament per a aquesta operació podia oferir altes eficiències, fins i tot l'eficiència obtin-

guda va ser al voltant de 2,2 % major en comparació amb el motor dièsel real. A més, va ser possible reduir a la meitat les emissions de NO_x quan el motor funciona amb OME.

L'últim bloc d'optimització es refereix a una nova arquitectura del motor que permet eliminar les emissions de NO_x. El model de oxicombustió resulta apassionant, ja que s'elimina el nitrogen de la mescla d'admissió i, per tant, no es generen emissions que continguen N_2. A més, amb l'ús d'aquesta manera de combustió, és possible capturar CO_2 dels gasos de fuita, que després pot vendre's en el mercat. Atés que es tracta d'un tema nou i poc investigat, els resultats són prometedors. Demostren que va ser possible obtindre un sistema de combustió específic capaç d'oferir nivells d'eficiència pròxims als dels motors convencionals. A més, es van eliminar les emissions de NO_x, així com les de sutge. Addicionalment, aquest sistema va ser capaç de reduir les emissions de CO i HC a nivells similars als motors convencionals.

D'altra banda, els resultats presentats en aquesta tesi doctoral proporcionen una base de dades ampliada per a explorar el funcionament del motor CI. Addicionalment, aquest treball va mostrar el potencial de la simulació computacional aliada amb mètodes matemàtics per a dissenyar sistemes de combustió per a diferents aplicacions.

"Success does not happen by accident. It is hard work, perseverance, learning, study, sacrifice and, above all, love for what you are doing or learning to do."
Edson Arantes do Nascimento, Pelé

"A minha família."

Acknowledgements

After more than four years, it is time to finish my Ph.D. studies, and I would like to thank everyone that has been part of this journey in some way. First of all, I would like to sincerely thank my supervisor Prof. Gabriela Bracho for all her teachings and help during the development of this research. Thank you very much for your patience in all these years, the continuous knowledge you have passed on, and your attention to the smallest details in all the activities. This gratitude also extends to the management of CMT-Motores Térmicos, Prof. Francisco Payri, Prof. José María Desantes, Prof. Jesús Benajes, and Prof. Vicente Macian, for receiving me and for the opportunity to be part of the research center. I would also like to extend my gratitude to all the members of the administrative department, Amparo, Haby, Elena, Elvira, and Carmina, for all their help over the past years.

Secondly, I would like to thank Prof. Ricardo Novella, Dr. Josep Gómez-Soriano, and Dr. Jose Manuel Pastor for their advice, indispensable knowledge, and time spent helping me improve my work.

I would also like to thank Prof. Tommaso Lucchini and all the other members of the Politecnico di Milano's internal combustion engine group for receiving me as a visiting researcher and for so much knowledge shared with me.

Not least, I would like to thank from the bottom of my heart all the companions and friends during these years as we have shared many stories, joys, worries, and so many different emotions along this path. In alphabetical order to avoid any problems, Alba, Álvaro, André, Antonio, Augusto, Brayan, Daiana, Dani, Diego, Douglas, Felipe, Ibrahim, Jácson, Paula, Rafael, Rodrigo, Santiago, and Vitor, my many thanks to you all.

Finally, I would like to thank those who made all of this possible, my family. It has been a long time separated by 10000 km, but you have always been there and are the most important people in my life. Seu Eron, Dona Elenita, Ane, Thobias, and Alice, thank you very much for the incentive, support in all decisions, and for believing in me.

I want to thanks the Universitat Politecnica de Valencia for his predoctoral contract (FPI-2019-S2-20-555), which is included within the framework of Programa de Apoyo para la Investigacion y Desarrollo (PAID).

Contents

List of Figures

List of Tables

Nomenclature

Acronyms

aTDC	After top dead center
BC	Boundary conditions
BDC	Bottom dead center
BMEP	Brake mean effective pressure
BPF	By-pass valve
BSFC	$Ba_{0.5}Sr_{0.5}Co_{0.8}Fe_{0.2}O_{3-\delta}$
bTDC	Before top dead center
C15	Conquerors 15
C22	Conquerors 22
CA10	Crank angle at 10% mass fraction burned
CA25	Crank angle at 25% mass fraction burned
CA50	Crank angle at 50% mass fraction burned
CA75	Crank angle at 75% mass fraction burned
CA90	Crank angle at 90% mass fraction burned
CAD	Crank angle degree
CAPSO	Centripetal accelerated particle swarm optimization
CAS	Cryogenic air separation
CFD	Computational Fluid Dynamics
CI	Compression ignition
CR-RC	Compression ratio
DE	Differential evolution

DMDF	Dual-mode dual-fuel
DOC	Diesel oxydation catalysts
$dP/d\theta$	Pressure gradient
DPF	Diesel particulate filter
ECN	Engine combustion network
EGR	Exhaust Gas Cecirculation
EU	European union
EVO	Exhaust vale opening
GA	Genetic algorithms
GHG	Greenhouse gases
HCCI	Homogeneous charge compression ignition
HE	Heat exchanger
HRR	Heat release rate
HR	Heat release
ICE	Internal combustion engine
ID	Ignition delay
IMEP	Indicated mean effective pressure
IP	Injection pressure
ISFC	Indicated specific fuel consumption
IVC	Intake valve closing
LHV	Low heating value
LOL	Lift-off length
LTC	Low temperature combustion
M-PSO	Mutation particle swarm optimization
MD	Medium duty
MIEC	Mixed ionic-electronic conducting membrane
NIE	Net indicated efficiency
NN	Neural network
NS	Novelty search
OF	Objective function
Opt	Optimized
PCCI	Premixed charge compression ignition
PM	Particulate matter
PPCI	Partially premixed compression ignition

PSO	Particle swarm optimization
RCCI	Reactivity controlled compression ignition
RIF	Representative interactive flamelet
RoHR	Rate of heat release
ROI	Rate of injection
rpm	Engine speed
SA	Spray angle
SHADE	Successful history-based adaptive differential evolution
SI	Spark ignition
SOC	Start of combustion
SOI	Start of injection
TDC	Top dead center
VGT	Variable geometry turbine
VIM	Virtual injection model

Greek symbols

α	Pressure ratio
β	Volume ratio
ϵ	Dissipation rate
η_{th}	Thermal efficiency
γ	Specific heat
λ	Air-fuel ratio
μ	Micro
ρ	Density

Latin symbols

$\dot{M}$	Momentum flux
$\dot{m}$	Mass flow rate
A	Nozzle area
C_3H_3	Propynyl
CO	Carbon monoxide
CO_2	Carbon dioxide
d_o	Nozzle outlet diameter
exp	Experimental
H_2O	Water

HC	Hydrocarbon
HVO	Hydrotreated Vegetable Oil
k	Turbulent kinetic energy
m	Mass
m_{air}	Air mass
N_2	Nitrogen
NO	Nitrogen monoxide
NO_x	Nitrogen oxides
O_2	Oxygen
OME	Oxymethylene dimethyl ether
p	Pressure (general)
P_{IVC}	IVC pressure.
$POMDME$	Polyoxymethylene ether
sim	Simulated
T	Temperature (general)
t	Time (general)
T_f	Fuel temperature.
T_{air}	Air temperature.
$T_{cyl.head}$	Cylinder head temperature.
T_{IVC}	IVC temperature.
T_{liner}	Liner temperature.
T_{piston}	Piston temperature.
U	Velocity (general)
u_t	Turbulence viscosity
Z	Mixture fraction
P_{max}	Maximum pressure
T_{max}	Maximum temperature

Chapter 1

Introduction

This initial chapter presents the motivation for studying the combustion phenomena in compression-ignited engines, as well as the interest in developing robust methodologies for the design of efficient and non-polluting power systems. The first section introduces an overview of the current energy demand scenario and the trends in global emissions regulations. Next, the objectives of this thesis and the partial goals are defined. Finally, the outline of the document is listed, providing a summary of the contents of each part of the manuscript.

1.1 General context

Since the development of the first engines, the concepts of spark-ignition (SI) and compression-ignited (CI) engines were developed by Nikolaus Otto and Rudolf Diesel during the last decades of the XIX century. The importance and usage of Internal combustion engines (ICE) grew in an unimaginable way in the last three decades, and currently they still play a dominant role in the fields of power, propulsion, and energy [1]. Thanks to the research and development performed by the industries, engines have become much more efficient and cleaner.

Despite the efforts and improvements done in recent years for producing clean propulsion systems, during the last decade the transportation sector contributed in about 16% of CO_2 emissions, as illustrates Figure 1.1. In

order to improve this scenario, new technologies are being considered, such as electric mobility or fuel cell vehicles.

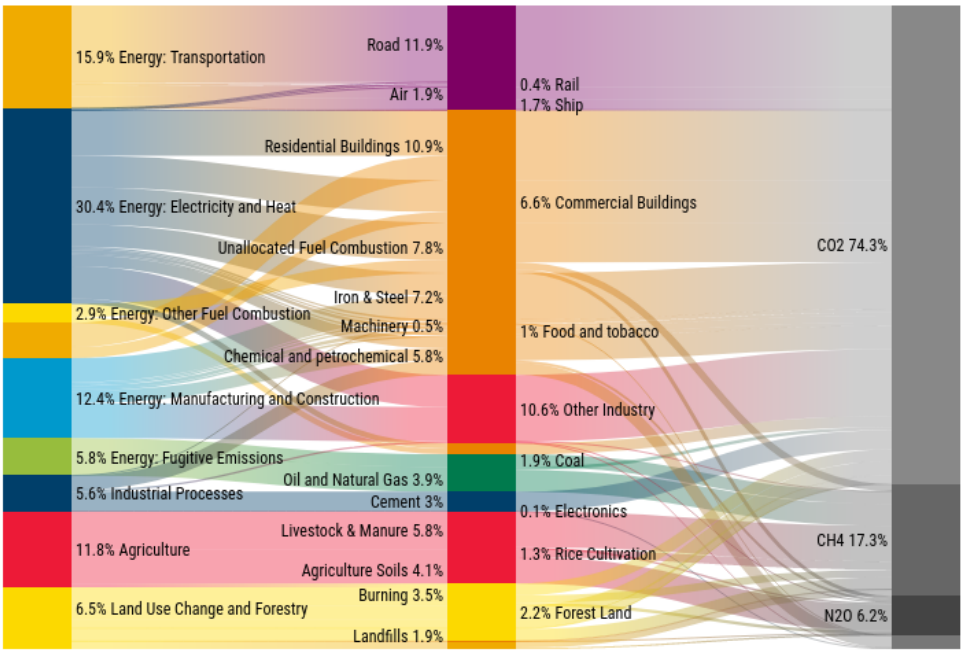

Figure 1.1: World Greenhouse Gas Emissions in 2016. Source: www.wri.org [2].

Strict regulations have been established trying to control and reduce Greenhouse Gases (GHG) emissions [3]. Since 1992, the European Union (EU) has introduced increasingly stricter limits on vehicle emissions through a series of 'Euro' standards. The EURO I, II, and III promoted improvements in pollutant exhaust gases. Moreover, EURO IV and V led to the introduction of catalytic control. Since the application of the Euro Normative, the limits of nitrogen oxides (NO_x) and particulates (PM) have been reduced by 95% and 97% respectively. Figure 1.2 shows the evolution of the emissions standards for the last 30 years, and it can be seen how the actual engines have fewer emissions than the former engines.

To attend the limits of the aforementioned Normative researchers have been studying new technologies and systems, mainly focused on some paths like:

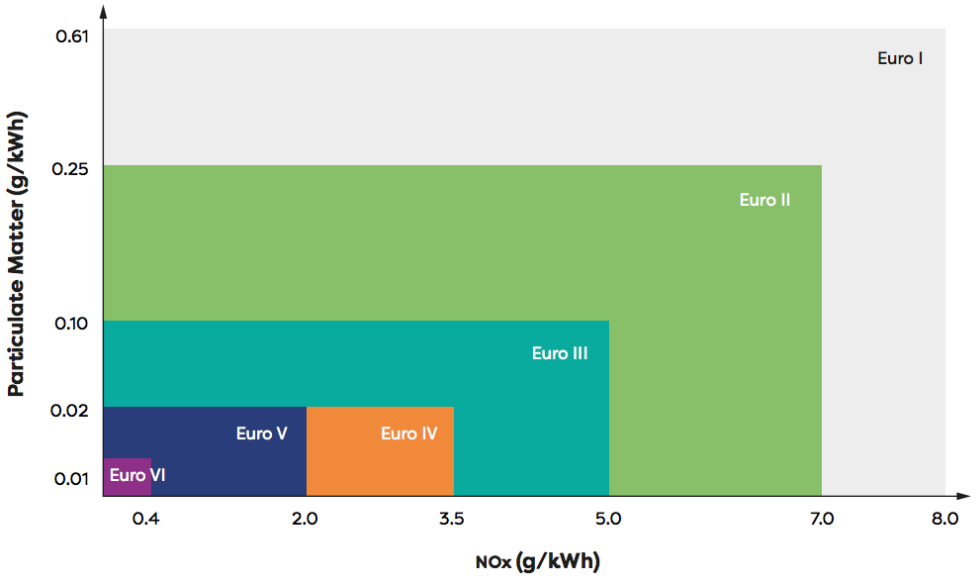

Figure 1.2: European emissions standards for the last 30 years. Source: www.aecc.eu.

- Improve the efficiency and reduce the emissions in ICE through injection, air-management, and combustion systems optimization.
- Replacement of internal combustion engines with electric batteries.
- Utilization of new alternative and sustainable fuels.

The idea of replacing current engines with electric motors have been suggested years ago and, in recent years, this idea has been gaining even more strength. Electric vehicles can be a good alternative in the cities where the distances are short and could be easily covered by the autonomy of the batteries. When it comes to the transportation sector dominated by heavy-duty (HD) and medium-duty (MD) engines, electrification is not an option yet due to the high energy requirements [4, 5]. However, their development is not yet mature and far from being implemented in all countries. For this reason, many research activities have been dedicated to optimizing the current technical definitions of ICEs, as a potential mid-term solution for reducing the CO_2 emissions of the transportation sector. Strategies like increase fuel

injection pressure or implementation of Exhaust gas recirculation (EGR) have become conventional for the control of NO_x emissions. Furthermore, the after-treatment system has been installed in almost all vehicles nowadays.

Moreover, the utilization of new sustainable fuels as hydrogen or alternative low carbon content fuels [6] is a path for reducing emissions. Among the various renewable fuels, Oxymethylene Ethers (OMEs) have gained attention since they produce lower levels of PM and carbon oxide (CO) emissions as is reported in previous studies [7, 8]. Therefore, there is an advance in combustion process that can provide CO_2 saving.

To analyze this huge range of possibilities a common approach is to combine the experimental studies with Computational Fluid Dynamics (CFD) simulations during the design process of the combustion systems. With the CFD simulation is possible to test different configurations computationally, thus saving affordable time and cost. Even with this powerful tool, it is difficult to carry out a parametric study involving all the possibilities and in this aspect, optimization techniques combined with simulation are gaining ground. This coupling between CFD and optimization allows a robust analysis with great precision combined and reasonable costs.

In this context, the research work of this Thesis is focused on the development of a robust optimization methodology for the design and analysis of CI combustion systems. The target is to maximize the efficiency of the engine, meanwhile the pollutant emissions are reduced. The implemented tools and methods are useful for future engine designs and for testing alternative fuels or different oxidant compositions.

1.2 Background

In previous works carried out at CMT-Motores Térmicos, engines with different combustion strategies, fuels, and combustion systems have been studied in order to provide alternative solutions to reduce pollutant emissions and improve engine performance. These works present both experiments and computational simulation results, which constitute a valuable database of CI engines.

In 2014 Winklinger [9] developed a combustion model that can be coupled with CFD platforms for numerical simulation of the turbulent combustion process of fuel sprays. The combustion model developed was coupled with the software OpenFOAM®, and it was validated. To allow the utilization of precise chemical processes at an acceptable computing cost, a tabulation

approach was used to store pre-calculated turbulent flamelet solutions. The combustion model simulates turbulent processes in a mostly non-premixed combustion environment. Furthermore, it can simulate phenomena such as autoignition and flame lift-off.

De Lima in [10] focused on the development and analysis of a new combustion concept for a two-stroke CI engine with scavenge loop through poppet-valves in the cylinder head. Her investigation intended to improve the understanding about this new system and evaluated the pollutant emissions and engine efficiency of this concept. The results for premixed LTC concept showed a drastic reduction in NO_x emissions, while the soot emissions were kept below the engine reference. However, CO and HC were increased due to extremely low combustion temperatures combined with the existence of over-mixed lean mixtures, resulting in a dramatic decrease in combustion efficiency. However, after the optimization procedure it was possible to recover efficiency while reducing emissions simultaneously.

Monsalve in [11] contributed to the understanding of dual-fuel combustion mode in compression ignition employing diesel, gasoline, and ethanol inside the chamber of a metal engine. The results revealed that decreasing the reactivity gradient between low and high reactivity fuel enhances RCCI performance at low loads. At the same time, he achieved NO levels under the EURO VI limit with minimal soot emissions. However, Monsalve demonstrated that limiting fuel reactivity was not an effective strategy for extending engine operation to higher loads.

In 2018, Hernández-López in [12] and Gómez-Soriano in [13] used computer simulation coupled with genetic algorithms (GA) for internal combustion engine optimization. Hernández-López focused primarily on developing the methodology, coupling CFD simulations and GA, for combustion analysis. The target in his optimization was to increase engine efficiency and reduce the pollutant emissions. In addition, a CI engine using an alternative fuel was optimized. In both cases, results show that it is possible to use the developed methodology successfully, being possible to reduce NO_x and soot emission levels and to increase engine efficiency. Gómez-Soriano further explored the optimization methodology focused on the analysis of combustion noise. The obtained results show that it was possible to reduce combustion noise, improve engine efficiency while contaminant emissions were kept below the baseline engine values. In these studies, the optimum (or best case) design was obtained after a huge amount of calculations, beyond five thousand simulations.

Sari in [14] proposed a dual mode dual-fuel concept (DMDF) achieving clean combustion across the entire engine operating map and enabling a reduc-

tion in HC and CO. Moreover, the use of low carbon fuels has been proposed for the reduction of CO_2 emissions in which the fuel life cycle or well-to-wheel concept was considered while its combustion performance was evaluated.

Due to the new emissions regulations the development of cleaner fuels is also necessary. In order to study the physical-chemical properties of surrogate diesel fuels García-Carrero in [15] performed a study to understand the properties of those fuels. Some quantitative diesel-like spray parameters were tested in an optical vessel. The study was carried out comparing the following fuels: diesel, dodecane, HVO, and OME_x in Spray A ECN condition. The main contribution of her study was the extensive database for multiple fuels. In this data, it is possible to find fundamental combustion parameters that enable the validation of new models and computational codes. Furthermore, the data of the alternative fuels and diesel blends allow to validate CFD results using these new alternatives.

Lewiski in [16] experimentally studied the influence of piston geometry and the use of alternative fuels with new geometries on an optical engine. To analyze the combustion behavior and soot formation for several geometries a CI engine was used. The combustion process was affected by different flame behavior caused by each geometry. Furthermore, due to the optical techniques used in the work it was possible to know the temporal and spatial distribution of the soot. Regarding alternative fuels, results showed a nonappearance of soot for the use of pure OME_x. Using until 50% of diesel with OME_x mixture reduced the soot formation to a lower level than the pure diesel fuel, but it was necessary to improve the injection duration due to the necessity of injecting more fuel to maintain the same energy in the cycle.

Based on this background summary, it can be seen that combustion comprehension is still a hot topic for engine development, both from experimental and numerical points of view. Computer simulations are indispensable in the design of combustion systems, since they can accelerate the design process with reasonable costs. Moreover, numerical analysis can provide additional insights of complex phenomena in sophisticated combustion processes that sometimes are difficult to obtain experimentally.

1.3 Objectives

The fundamental objective of this thesis is to develop a numerical platform for the optimization of combustion systems in CI engines that enables to perform exhaustive analysis of the combustion phenomena with a reasonable computational cost. The platform should be flexible, allowing to study the

effect of the geometry of the piston, setting conditions, the type of fuel or the composition of the oxidant on the thermodynamic parameters and pollutant formation. The methodology implemented combines state-of-the art CFD simulations with advanced evolutionary algorithms in order to obtain the best cases that would provide the highest engine efficiency and lowest pollutant emissions levels.

The fulfillment of this general objective is achieved through the completion of the following partial objectives:

- Development and validation of the computational engine model that reproduces a full load engine operating condition of a conventional compression ignition system. For this purpose, the OpenFOAM® software coupled with LibICE libraries was used, where the CFD model was calibrated with available experimental data in order to guarantee the reliability of the results.
- Implementation of the optimization algorithm. The evolutionary algorithm should handle the high dimension of parameters (typical of this kind of problem), which are non-linear, with a big search space, and where the function evaluation corresponds to the CFD simulation. This integration also implies the development of additional tools for fast and accurate pre-processing and post-processing of the data automatically.
- Assessment of the influence of the comburent on the combustion performance, replacing the traditional diesel fuel by sustainable OME_x to quantify the effect on the thermodynamic variables and pollutant formation.
- Analysis of the effect of the oxidant composition on combustion and pollutant production. This involves the depletion of the nitrogen in the gas trapped in the cylinder, which is replaced by water and CO_2. The engine architecture is optimized to provide suitable thermodynamic conditions in the exhaust line.

1.4 Thesis outline

The thesis is organized into eight chapters starting with this introduction (**chapter 1**), which presents the general context. The main contents of each chapter are given below:

Chapter 2 details the literature review of the combustion process in compression-ignited engines, the strategies most common for optimizing combustion systems, and current alternatives that are being implemented nowadays to improve the performance of these power plants.

Chapter 3 presents a literature review of the available optimization algorithms, their characteristics, potential, and the suitability for engine design process. This review has been fundamental for the selection of the approach used in this research work.

Chapter 4 describes the tools and methods implemented in this thesis. It starts presenting the characteristics of the engine used as baseline for the calibration and validation of the models. Afterward, details of all the physical models (spray, turbulence, combustion, pollutant emissions, etc) and numerical schemes chosen for the simulations are given. It shows the mesh independence study and the heat transfer model evaluation. Lastly, the benchmark of the optimization algorithm is presented, followed by an explanation of the complementary tools and scripts coupled to automatize the whole procedure for the calculations.

Chapter 5 presents the results of the combustion chamber optimization of a conventional diesel CI engine. The results are divided into two blocks, the first one shows the results of the optimization algorithm, like the convergence of the parameters. The second block is composed of engine results, where the optimized combustion chamber design and the thermodynamic variables are analyzed.

In **chapter 6**, the developed optimization methodology is applied to analyze the effect of the comburent on the combustion system design. Conventional diesel fuel is replaced by oxymethylether (OME), therefore the physical properties and chemical mechanisms should be adapted. Like in chapter 5 the results will be divided into different groups, one for the optimization and algorithm results, the second one for the analysis and evaluation of the optimum combustion system. The last part presents a sensitivity study performed with a neural network methodology to understand the influence of the operating setting on the optimized case.

Chapter 7 is dedicated to the analysis of the combustion performance when the oxidant composition is different from the conventional air. The target was to design a system able to operate in conditions similar to oxy-fuel, with absence of nitrogen in the mass trapped in the cylinder, and then avoiding the formation of NO_x emissions. The combustion chamber was redesigned to maximize efficiency and to reduce soot production. Results are used to analyze if this concept has potential for future power plants.

Lastly, **chapter 8** summarizes the most relevant findings of this research work and the main conclusions. In addition, some ideas for future directions are proposed from the knowledge and experience acquired during the development of this thesis.

References

[1] Heywood, John B. *Internal Combustion Engine Fundamentals. N. York: McGraw-Hill*. 1988.

[2] Ge, Mengpin and Friedrich, Johannes. *4 Charts Explain Greenhouse Gas Emissions by Countries and Sectors*. 2020.

[3] Intergovernmental Panel on Climate Change. *Climate Change 2014 Mitigation of Climate Change*. 2014. DOI: 10.1017/cbo9781107415416.

[4] García, Antonio, Monsalve-Serrano, Javier, Martinez-Boggio, Santiago, and Gaillard, Patrick. "Impact of the hybrid electric architecture on the performance and emissions of a delivery truck with a dual-fuel RCCI engine". In: *Applied Energy* 301.February (2021), p. 117494. DOI: 10.1016/j.apenergy.2021.117494.

[5] García, Antonio, Monsalve-Serrano, Javier, Lago Sari, Rafael, and Martinez-Boggio, Santiago. "Energy sustainability in the transport sector using synthetic fuels in series hybrid trucks with RCCI dual-fuel engine". In: *Fuel* 308.August 2021 (2022), p. 122024. DOI: 10.1016/j.fuel.2021.122024.

[6] Valentino, Gerardo, Allocca, Luigi, and Marchitto, Luca. "PIV investigation of high swirl flow on spray structure and its effect on emissions in a diesel-like environment". In: *SAE 2011 World Congress and Exhibition* (2011). DOI: 10.4271/2011-01-1286.

[7] Iannuzzi, Stefano Emanuele, Barro, Christophe, Boulouchos, Konstantinos, and Burger, Jakob. "Combustion behavior and soot formation/oxidation of oxygenated fuels in a cylindrical constant volume chamber". In: *Fuel* 167 (2016), pp. 49–59. DOI: 10.1016/j.fuel.2015.11.060.

[8] Lautenschütz, Ludger et al. "Physico-chemical properties and fuel characteristics of oxymethylene dialkyl ethers". In: *Fuel* 173 (2016), pp. 129–137. DOI: 10.1016/j.fuel.2016.01.060.

[9] Winklinger, JF. "Implementation of a combustion model based on the flamelet concept and its application to turbulent reactive sprays [Tesis doctoral no publicada]". In: *Universitat Politècnica de València* (2014). DOI: https://doi.org/10.4995/Thesis/10251/48488.

[10] De Lima Moradell, DA. "Analysis of combustion concepts in a poppet valve two-stroke downsized compression ignition engine designed for passenger car applications [Tesis doctoral no publicada]". In: *Universitat Politècnica de València* (2016). DOI: https://doi.org/10.4995/Thesis/10251/68502.

[11] Monsalve Serrano, J. "Dual-fuel compression ignition: towards clean, highly efficient combustion [Tesis doctoral no publicada]". In: *Universitat Politècnica de València* (2016). DOI: https://doi.org/10.4995/Thesis/10251/75109.

[12] Hernández López, Alberto. "Optimization and analysis by CFD of mixing-controlled combustion concepts in compression ignition engines [Tesis doctoral no publicada]". PhD thesis. 2018. DOI: https://doi.org/10.4995/Thesis/10251/103826.

[13] Gómez Soriano, J. "Computational assessment of combustion noise of automotive compression-ignited engines [Tesis doctoral]". In: *Universitat Politècnica de València* (2018). DOI: https://doi.org/10.4995/Thesis/10251/112726.

[14] Lago Sari, R. "Dual Mode Dual Fuel Combustion: Implementation on a Real Medium Duty Engine Platform [Tesis doctoral]". In: *Universitat Politècnica de València* (2021). DOI: https://doi.org/10.4995/Thesis/10251/165366.

[15] García Carrero, AA. "Experimental Study of the Fuel Effect on Diffusion Combustion and Soot Formation under Diesel Engine-Like Conditions [Tesis doctoral]". In: *Universitat Politècnica de València* (2021). DOI: https://doi.org/10.4995/Thesis/10251/179997.

[16] Vargas Lewiski, FD. "Analysis of the combustion process and soot formation in a single cylinder optical engine fueled with e-fuels and using different piston geometries [Tesis doctoral]". In: *Universitat Politècnica de València* (2021). DOI: 10.4995/Thesis/10251/180351.

Chapter 2

Literature review: New technologies and fuels for pollutant emissions reduction in compression ignition engines

2.1 Introduction

This chapter presents some fundamentals of the combustion process in compression ignition engines. In order to do this, a thorough literature study is offered, addressing the problems that conventional diesel combustion has experienced recently. First, a general description of the diesel combustion phases is given. Then, the relevant parameters used to optimize the engine are described. Moreover, alternative technologies for minimizing pollutant emission formation have been widely explored. Therefore, a literature review of sustainable fuels and promising engine architectures has been performed.

2.2 The combustion process in CI engines

2.2.1 Formation of air-fuel mixture

In compression engines, only the air is compressed instead of a mixture. The fuel is compressed until very high pressure levels and is introduced in the combustion chamber near the end of the compression stroke, just before the top dead center (TDC). The mixture formation occurs very quickly inside the combustion chamber, where ignition starts without any external energy source, only by heat transfer from the compressed air to the fuel, thus causing the auto-ignition. In this combustion process, highly ignitable fuels must be used, and high temperatures must be ensured. A proper mixing of the combustible with the air is of great importance in this type of engine for achieving good combustion performance with high efficiency and avoiding contaminants formation.

In diesel engines, energy conversion is influenced by the injection rate and the rate of mixture production. Due to the heterogeneity of the mixture, different air-fuel ratios (λ) are formed: the areas around the spray are typically very rich, with a $\lambda \approx 0$. In contrast, the areas outside of the spray have pure air, $\lambda \approx \infty$.

The injection process primarily dominates internal mixture generation. For this reason, the injection system must ensure an adequate injection pressure, introduce the fuel, promote the spray propagation, and distribute it accordingly in the chamber in a very short period. Then, the liquid fuel should break up quickly, creating droplets, evaporating and mixing with the air, and initiating the combustion (autoignition). The burning then continues as the fuel and air combine to provide the ideal combustion environment. Therefore, the fuel-air mixture regulates the way that diesel burns [1, 2].

2.2.2 Air motion

The airflow in the combustion chamber can be shaped by the design of the combustion chamber and the intake port. In CI engines, it is characterized by the swirl motion. The swirl is essentially the rotational speed around the axis of the cylinder and can be defined by the design of the intake port. It increases with higher engine speed. The responsibility of the swirl is to promote the break up of the liquid fuel and help in the mixing of it with the available air.

The air between the piston crown and the cylinder head is pushed into the piston bowl more and more during the compression stroke, which also increases the swirl and thus causes the squish flow. The increase in squish flow interferes

with air swirl and, as a result, promotes the momentum transfer between the injected spray and combustion chamber air, which is crucial for the production of mixtures. The piston gap can be created with a very turbulent flow by properly designing the bowl geometry, which enhances the mixture formation and speeds up combustion.

2.2.3 Fuel atomization and evaporation

The fuel jet has a cone-shaped configuration at the nozzle exit during the injection process. The fuel is injected in liquid phase with high-velocity. It enters the combustion chamber in order to interact with the high-density, high-temperature air available, and it atomizes within the chamber producing significantly smaller droplets than the nozzle diameter [1, 3]. In the first phase of the atomization, the initial droplets appear, named primary breakup. Fuel temperature and composition determine the volatility property, which is an essential parameter in spray breakup.

The second phase is known as a secondary breakup, which is responsible for fragmenting the first droplets into smaller particles. The formation of latter droplets is essential for fast heating and evaporation of the fuel affecting the ignition delay directly. The primary driving mechanism behind secondary atomization is aerodynamic forces. The air density, spray cone angle, injection pressure, and injection pressure curve are significantly affecting factors.

The fuel should be vaporized to start the chemical reactions. Then, a heterogeneous combination of air and liquid fuel droplets of various sizes and distributions is present in the mixture. The heat transfer from the heated air to the liquid fuel is of paramount importance. This process is fundamentally influenced by the kinetic energy of the spray and the injection pressure. High velocities facilitate droplet creation as well as mass transport and heat transfer. Therefore, the smaller the droplets, the earlier the temperatures lead to evaporation, and the more fuel is vaporized.

The liquid phase of the spray stops penetrating when the fuel injection and evaporation rates are equal. The liquid length is the distance between the nozzle exit and the tip of the liquid region. It is an important parameter in the engine's combustion process. Longer liquid lengths may cause impingement inside the piston bowl, resulting in increased emission formation.

2.2.4 Combustion process

The combustion process refers to the release of the fuel's energy within the engine cylinder for conversion to useful work. The combustion process can be

described by the rate of heat release (RoHR). Moreover, it can be classified as a combination of premixed and non-premixed combustion where the non-premixed phase is dominant [1, 4, 5]. Figure 2.1 presents the RoHR trace and allows to identify the different phases of combustion.

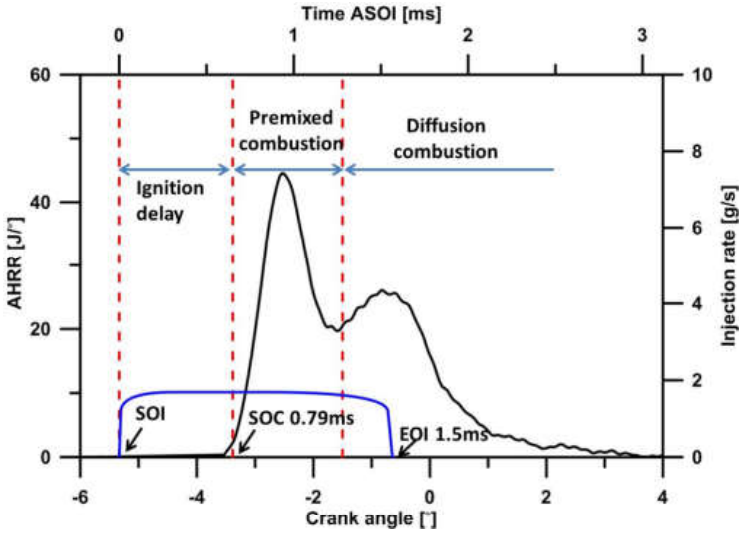

Figure 2.1: Combustion process definition by comparison of the fuel injection rate against the RoHR. Source [6].

In their respective order, the main phases are:

- **Ignition delay:** Ignition delay (ID) is generally defined as the time between the start of injection (SOI) and the start of combustion (SOC). The fuel is injected into the combustion chamber where it mixes with the air available inside the chamber. As the mass inside the combustion chamber contains oxygen, once the air mixes with the fuel, chemical pre-reactions occur, creating a proper condition for the autoignition of the mixture. As shown in Figure 2.1, in this phase there is no apparent increment of RoHR. This parameter influences the efficiency, emissions, and combustion noise [7].
- **Autoignition:** The spontaneous ignition of unburned gas in advance of the flame front is known as autoignition and it is assessed in terms of a cetane number. It has a significant role in the emissions formation and in the performance of diesel engines [2, 5]. The autoignition process consists of sequences of physical and chemical processes. Higgins et al. in [5] summarize the autoignition process for the case of Diesel spray:

  - Physical induction: During this time, the injected fuel atomizes, englobes, and mixes with air before beginning to vaporize as it enters the chamber. The vaporization absorbs heat, causing the temperature of the liquid fuel inside the combustion chamber to drop, delaying the ignition chemistry. It lasts until the simultaneous rise in pressure and chemiluminescence is detectable. When the appropriate temperatures are reached just downstream of the liquid length, the first ignition stage can begin, defining the end of the physical induction period.
  - First-stage ignition: The first stage ignition period lasts from the first detectable rise in pressure and chemiluminescence until rapid heat release begins. During this time, fuel is consumed in a broad averaged fuel-rich region of the spray between the liquid length and the penetration tip of the spray. At this stage, chain-branching reactions consume fuel, producing radicals and releasing small amounts of energy that increase pressure and temperature. Some authors have described this stage as a low-temperature ignition process or cold flame [8, 9].
  - Second-stage ignition: Begins with a significant heat release, followed by a sudden increase in premixed-burn pressure. Due to the high temperatures provided by the heat released in the first stage, a hydrogen peroxide dissociation reaction dominates the chemistry and produces a significant heat release [1, 10].

- **Premixed phase:** In this phase, all fuel mixed during the ID is rapidly burned. The mixing of fuel and air from the ignition delay phase produces an increment in temperature and pressure in the region between the liquid length and the tip of the spray. This rise in combustion chamber conditions promotes appropriate inflammability conditions that react with the air-fuel mixture prepared during the ID. At this point, the combustion process begins, and both temperature and pressure increase rapidly, as shown in Figure 2.1. Moreover, this phase of combustion is controlled by the injection rate and is faster than the non-premixed phase, as studied in different works [11–13]. The duration of this phase can be defined as the period between the SOC and the first local minimum in RoHR.

  This phase also affects the formation of pollutant emissions, which depends on the equivalence ratio and temperature field inside the combustion chamber. In [14] Dec, it was observed that the premixed combustion

phase occurs under fuel-rich conditions, which means at high equivalence ratios with values between 2-4, and leads to the initial soot formation. These conditions are not favorable to the NO_x formation because there is little oxygen amount present, and adiabatic flame temperatures are lower than those required for significant thermal NO production [14]. However, the remaining fuel burns as a diffusion flame with higher temperatures and more oxygen once this flame occurs, nearly stoichiometric equivalence ratios in conditions nearly the proper conditions for thermal NO production [14, 15].

- **Non-premixed or diffusion phase:** This phase begins after all the fuel mixed during the ID phase is completely burned. This phase is also known as the non-premixed, diffusion, or mixing-controlled phase. In this stage, the flame front generated on the premixed phase is consolidated, controlled by the in-cylinder air-fuel mixing process, and produced in oxygen/fuel stoichiometric conditions [1]. During this phase, it can be assumed that the fuel jet is at stationary condition, thus maintaining a nearly constant flame structure until the end of injection. As the mixing rate controls the burning rate, the fuel consumption is determined by the rate at which fuel and air are mixed in proper conditions for burning [14, 16]. Convection becomes the dominant process during the injection event due to the momentum created by the spray. As a result, after the end of injection, the structure of the flame undergoes one final significant alteration, and the process is thereafter dominated by the diffusion of oxygen and fuel. Furthermore, some authors [1, 17] consider this phase as an independent phase, which begins after the end of the injection and is called as late combustion phase. Figure 2.2 presents the most extended model about diffusion flame model proposed by Dec [14] that was continued by Flynn et al. in [18]. The lift-off length is the distance between the injector tip and the lifted flame's point (LOL). Similar to a non-reactive and evaporative jet, this zone experiences physical processes such as atomization, air entrainment, and evaporation. The presence of a diffusive flame downstream influences these processes. The rich fuel-air mixture has an equivalence ratio between 2-4. Then comes a premixed reaction zone, which consumes all of the oxygen mixed with the jet, raising the temperature. Since the normal diffusion flame structure develops after the LOL, it is safe to presume that there is no oxygen concentration inside the diffusive flame. The internal volume of the diffusive flame is formed of unburned fuel, rich premixed combustion products, and soot precursors. Moreover, the reaction surface surrounds

this region, and the fuel is oxidized to CO_2 and H_2O. The diffusion flame is formed by a thin layer of stoichiometric surface with a high amount of oxygen available. When the flame front reaches the premixed combustion products, they have been oxidized, and most part of the fuel energy is released. The thermal NO production zone has oxygen which leads to lean mixtures, and high temperature contributes to the NO_x formation [19]. The emissions behavior is presented in Figure 2.3.

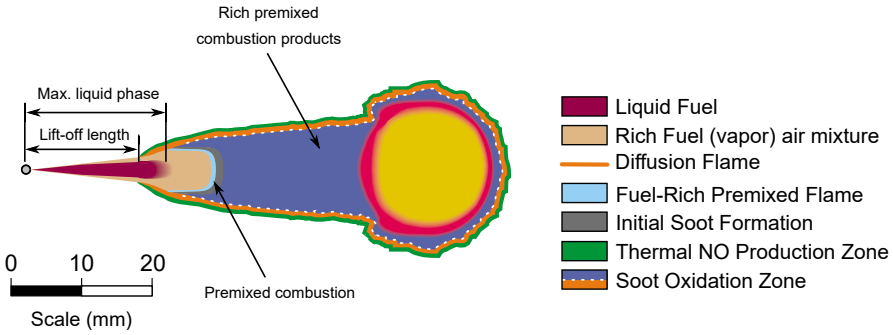

Figure 2.2: Diffusive flame structure according to the conceptual model proposed by Dec. Adapted from [14].

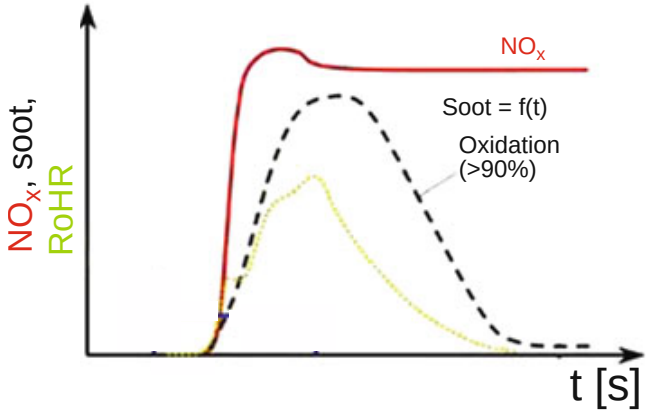

Figure 2.3: NO_x and soot concentrations in a combustion chamber as a function of time. Source [7].

2.2.5 Soot formation

In general terms, soot can be considered a solid substance composed of carbon and hydrogen [20]. Unburned fuel turns into soot when it transitions from the vapor phase to a solid phase at high temperatures above 1600 K in fuel-rich areas. Other molecules available as hydrocarbons can be transformed into soot or may condense depending on the surrounding conditions. Overall, the rich regions are located in the spray core or in the piston bowl once the spray is blocked by the walls of the cylinder. The high soot formation in a CI engine is related to poor combustion, which leads to low-efficiency values. Moreover, soot emissions are extremely hazardous to the health of humans and the environment.

Figure 2.4 shows in sequence the first steps of the soot formation process in a scheme. The process starts with fuel pyrolysis, which is the process of organic compounds altering their structure in the presence of high temperatures without significant oxidation, generating the precursors. The next step is nucleation, where the soot particles are formed from gas-phase reactants. The nucleation is restricted to the region near the reaction zone due to the higher temperatures, radical, and ion concentration in both combustion phases [21]. In this step, the initial aromatic rings formed determine the amount of soot produced. Moreover, two propynyl radicals, C_3H_3, are formed. The next step is the surface growth, which happens simultaneously with nucleation. This process is characterized by the mass addition to the surface of a nucleated soot particle. The soot particles easily accept the hydrocarbons in the gas phase leading to an increment of soot mass. At the same time, the number of particles remains constant. The last step is composed of coalescence and agglomeration together. In the coalescence, the particles collide, decreasing the number of particles but maintaining constant the mass of two soot particles combined. Agglomeration is the process when primary particles stick together to form a large group of primary particles.

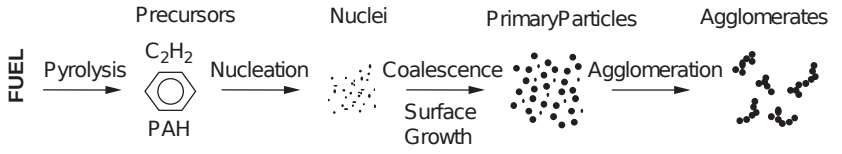

Figure 2.4: Soot formation scheme proposed by Tree and Svensson. Source [20].

2.3 Strategies for combustion system design

The combustion system is an essential part of the CI engines where the mixture preparation takes place for proper energy conversion from thermal energy into mechanical work. An extensive literature review has been done to list the strategies that enhance combustion behavior, reduce emission levels, and increase efficiency. The design process of a combustion system is done by considering a variety of parameters that affect its operation and performance. For instance, the most relevant characteristics that play an important role in the design strategy are: the physical configuration of the engine (such as piston geometry), the injection system hardware, the admission pipe shape, and the operating settings, among others. Moreover, the performance and layout of the combustion chamber depend on the type of comburent. As stated in the previous chapter, the trend nowadays is to move towards sustainable fuels, introducing a new variable in the design process puzzle. Of course, all the aforementioned factors must be adapted to different technologies and novel combustion concepts that are being developed at the moment. The different parameters that are dominant on the definition of a combustion system as well as the trending technologies are explained below.

2.3.1 Strategies based on the physical characteristics or geometric parameters

The physical features that have a high impact on the engine are the compression ratio (CR) and the piston bowl geometry. Optimizing the physical characteristics of an engine can be done experimentally, and through a computational simulation [22–26]. The numerical methods become an advantageous alternative since they can provide accurate estimations and allow to test of several geometries with no need to manufacture the parts of the system (that might not be used later), saving resources and time.

Compression ratio

The compression ratio is the ratio between the maximum volume and the minimum volume of the cylinder. It compares the ratio between the volume on the bottom dead center (BDC) and the top dead center (TDC). Analyzing the Equation 2.1 it is possible to see that increasing the CR (r_c) also increases the thermal efficiency $\eta_t h$ of the engine:

$$\eta_{th} = 1 - \frac{1}{r_c^{\gamma-1}} \left[\frac{\alpha\beta^{\gamma} - 1}{\alpha\gamma(\beta - 1) + \alpha - 1} \right] \tag{2.1}$$

where γ represents the charge-specific heat ratio, α is the pressure ratio associated with the constant volume portion of the heat release, and β means the volume ratio associated with the constant pressure portion of the heat release. Some advantages and drawbacks of a high CR are listed here [27–29]:

Advantages

- Shorten ID due to the higher temperature in the compression phase that helps to reduce HC and CO emissions. Moreover, it helps to reduce combustion noise and combustion stability.
- With low r_c, the soot emissions can grow at low-speed and mid-load due to the longer ID, which increases the premixing phase.
- Lower exhaust temperature and more tolerance of higher BMEP at high speeds. Maximum torque is limited by exhaust gas temperature.
- Improved usability for cold starts.

Drawbacks

- Late combustion event to control the peak of in-cylinder pressure and higher NO_x emissions.
- Higher in-cylinder pressure increases friction.
- Heat release losses are higher through the piston and cylinder head due to the lower distance between the cylinder surface at TDC.
- Air utilization becomes difficult, which decreases maximum torque/power at high loads, consequently reducing the efficiency at high loads.

Combustion chamber design

The combustion chamber design is one of the most critical parameters discussed in the CI engine optimization once it can directly affect the combustion rate and heat transfer. The combustion chamber is defined as the volume that exists in the squish region together with the volume of the piston bowl shape. Usually, CI engines have an axisymmetric bowl with an injector located on the axis of the combustion chamber. The development of the combustion chamber is focused on promoting the best fuel-air mixing process. The geometry

of the combustion system is special to guide the fuel and vapor diffusion to achieve a sufficient degree of air-fuel mixture and fast combustion. During the design stage of a new combustion chamber, four essential characteristics must be taken into account: improvement of mixing, reduction of pollutant emissions, adjustment of the ratio between the surface and volume of the bowl, and improve the volumetric efficiency [29].

Figure 2.5 shows most of the conventional bowl profiles used in CI engines nowadays. The bathtub bowl geometry is used to reduce the heat transfer losses through the surface area reduction and improves the engine efficiency, and fuel consumption [23, 26]. Another type of bowl is the re-entrant or ω-shaped bowl, which is focused on reducing soot emissions. This type of geometry promotes the amplification of the swirl velocity, increasing turbulence levels and the mixing rate [29, 30]. Moreover, this geometry preserves the fuel sprays kinetic energy, preventing the mixture from stagnating near the piston bottom. The stock bowl can promote low NO_x and soot emissions while delivering poor combustion efficiency [31]. The stepped lib bowl is used to redirect the spray to the cylinder head, avoiding the spray penetration into the squish region, which helps to reduce the soot formed during the combustion and reduces the soot-in-oil and CO emissions. Furthermore, some authors indicate that this geometry can provide better air-fuel mixing and complete combustion [32–35]. The wave-stepped lib bowl has the potential to reduce even more soot emissions when compared with the stepped-lib [6].

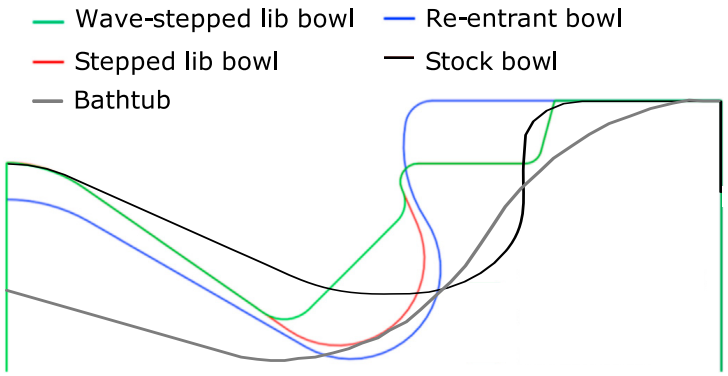

Figure 2.5: CI engine piston bowl geometries examples. Adapted from [23, 36].

Many engines with an extensive speed operation range use a narrow and deep piston shape, generating a high turbulent flow in the piston gap, accelerating the diffusion combustion, and decreasing the combustion duration.

Moreover, commercial vehicles have engines with broad and flat piston bowl shapes. A critical factor that should be considered together with the bowl shape definition is the included angle of the sprays, which should match the piston bowl design to prevent that liquid fuel reaches the bowl bottom. According to different works, an absolute optimum nozzle angle exists for each combustion chamber design, which is usually capable of simultaneously improving efficiency and emissions [37, 38].

2.3.2 Strategies based on the injection system

Other parameters that play an important role in engine optimization are related to the fuel injection components. This system is fundamental because it directly affects the mixing process. The essential task of the injection system is to meter and deliver an appropriate quantity of fuel, for a given engine operating condition of speed and load, to each cylinder at the appropriate time. The strategies to optimize the injection system are based on improving the fuel injection parameters by modifying the profile and timing of the rate of injection (ROI) through the best match between injection pressure (IP) [38], the start of injection (SOI), the number of injector nozzles, nozzle hole diameter, and the spray included angle.

In diesel engines, when the fuel injection is done at low pressure, the diameters of fuel droplets will enlarge. ID will be increased, thus leading to higher emissions of NO_x and CO. When high injection pressure is used, the droplet diameter becomes smaller, assisting the atomization and evaporation process, improving the ID time, which reduces the smoke and CO emissions [39, 40].

The second parameter is the number of injector nozzle holes. In general, the increment in the number of injector nozzles enhances the fuel-air mixing, especially in the bowl region, because the fuel is better to spread in the chamber domain, englobing more efficiently the air. However, the number of holes cannot increase too much because, at some point, there could start happening spray-to-spray interaction disturbing the mixture process. Another essential parameter is the nozzle hole diameter which correlates with the number of injector nozzles and defines the shape and profile of the injection rate. With a small nozzle diameter, a larger number of holes is necessary to maintain the energy target. The diameter influences the interaction between the fuel spray and the piston geometry and could improve fuel consumption and reduce NO_x emissions [29, 41]. Small diameters produce smaller droplet sizes that favor atomization and evaporation. Moreover, the liquid spray penetration decreases

when the nozzle diameter is small, avoiding wall impingement with the piston surface or the liner.

The final parameter, called the SOI, determines the crank angle at which the fuel injection will begin. Moving the SOI, it is possible to control the RoHR peak, the peak of in-cylinder pressure, and the in-cylinder temperature. Moving the SOI for values before the TDC, advancing the SOI, longer the ignition delay increasing the amount of fuel burned during the premixed combustion phase resulting in a peak of RoHR and the peak of pressure. This rise in pressure also increases the in-cylinder temperature affecting the emissions, especially the NO_x and soot emissions [42, 43].

2.3.3 Strategies based on air management system

The main objective of the air management components is to deliver an intake charge at the necessary conditions for optimum combustion of a steady or transient engine operating point. The essential parameters to optimize the air management system are the EGR rate, intake pressure, and swirl number. These parameters are used to control the air properties admitted to the combustion chamber.

The main objective of introducing EGR into the intake manifold is to control and reduce the NO_x emissions and consists of recirculating some exhaust gas to the engine admission. On the opposite, this strategy increases soot emissions, and specific fuel consumption [44, 45]. It can be defined by the ratio between the recirculation mass of gas that comes from the exhaust and the total in-cylinder mass as expressed in Equation 2.2.

$$EGR = \frac{m_{EGR}}{m_{EGR} + m_{air}} \tag{2.2}$$

The composition of the EGR is mainly N_2, CO_2, H_2O and O_2 and the main effects on combustion are: reduction of O_2 concentration which leads a lower flame temperature. With less concentration of O_2, there is a lower gas temperature during the combustion due to the higher specific heat of the CO_2 and H_2O. Moreover, the possibility of the dissociation of products that also participate in the combustion process since CO_2 and H_2O show a potential to dissociate at higher temperatures [46]. These effects reduce the combustion rate and temperature, promoting the NO_x reduction while compromising the efficiency, increasing the CO, HC, and soot emissions [47, 48].

The intake pressure is the pressure of the fresh air that enters the cylinder. Due to the presence of turbochargers in actual engines, it is necessary to

calibrate this parameter because it also influences the trapped mass amount and the air-fuel mixing process. The increment of the intake pressure also increases the in-cylinder density and the amount of O_2 improving the air-fuel mixing process. In general, higher values of intake pressure lead to a better efficiency value, reducing the soot emissions, however at the same time, there is an augmentation of in-cylinder pressure and temperature, which promotes NO_x emissions formation [49].

Finally, the swirl number is the ratio of the axial flux of angular momentum to the axial flux of linear momentum. To simplify, the swirl number is the rotational air motion around the cylinder axis, and its intensity comes from the intake and piston geometry. A higher swirl level improves the air-fuel mixing, which leads to better efficiency and reduces the soot emissions because the fuel finds easier the available oxygen inside the combustion chamber [38]. Moreover, the swirl affects the heat transfer and heat losses and could reduce the spray penetration [50, 51].

2.4 Alternative fuels for CI engines

A consensus has not yet been achieved in the current debates over the energy source that will power the next generation of engines concerning the global energy demand increment and how it affects GHG emissions, particularly in the transportation sector. Diverse alternatives for reducing GHG emissions are being studied, and one of them evidences the necessity of exploring the potential of alternative fuels. This new fuel range includes alcohols, natural gas, biodiesel, hydrogen, and ammonia, among others [52]. Additionally, the generation of fuels from renewable sources, primarily renewable energy and biomass, is crucial for a sustainable fuel supply for the total transformation of the transportation sector [53].

Among the various renewable fuels, Polyoxymethylene ethers (OME, also abbreviated as DMM, PODE, POMDME) could be valuable alternatives due to the lower levels of PM and CO emissions [54–59]. Figure 2.6 shows the production of the OME from potential sources. Comparing OME production to conventional diesel made from fossil fuels and synthetic diesel made using Fischer-Tropsch synthesis, OME production is economically competitive from the standpoint of atomic economy, and OME kept the majority of C-O bonds from reactants. OME is also environmentally beneficial from the perspective of life cycle analysis since it may be created utilizing eco-friendly energy from biomass [60, 61] or from CO_2 [62]. Additionally, if the OME were used to reduce widespread PM air pollution, large-scale manufacture of OME via a

green path would be essential. The OME can be obtained from renewables or CO_2 sources employing gasification or chemical reduction. Synthesis gases can be converted to methanol serving for the OME production by the reaction of H_2 and CO_2 [63, 64].

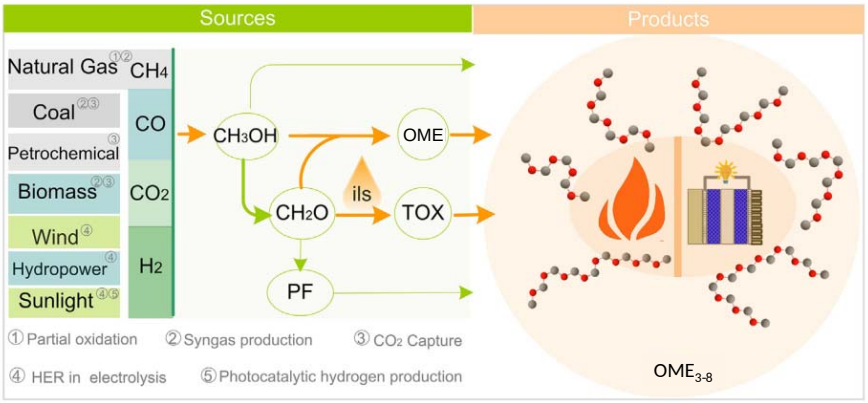

Figure 2.6: OME production from potential resources. Adapted from [65].

According to Bae and Kim in [52], there are critical points for using alternative fuels. Among the important points are the following:

- Energy sustainability and relief energy concerns.
- Improve engine efficiency and reduce pollutant emissions.
- Compensate for the unbalanced use of fossil fuels.

At the same time, the following aspects should be considered:

- Chemical and physical properties since these properties determine whether or not the fuel is suitable for engine applications.
- Comparable LHV is important since this quantity directly affects the released energy and fuel consumption.
- When it comes to the commercial acceptance of alternative fuels, material compatibility with existing engine hardware or fuel supply infrastructure is crucial. In the alternative, high additional costs would be incurred for hardware alterations.

- One of the challenges that producers and consumers face daily is the cost of manufacturing. While production costs have fallen over the past few decades due to technological advancements, alternative fuels still cost more than traditional gasoline and diesel.

In recent years, many studies have been developed focusing on utilizing the OME in addition to or substituting diesel in CI engines. When compared to conventional diesel, the OME shows a greater content of O_2 in its composition (CH_3-O-(CH_2-O)$_x$-CH_3) avoiding soot emissions formed in the combustion process [57, 66]. The x in the chemical structure of the OME is the chain length, where OME_1 is the simplest structure. Moreover, due to the O_2 present in the OME, it is also feasible to lower NO_x emissions through the use of a higher EGR rate [62]. To use OME_1 as fuel, it is necessary to adjust the injection system to avoid problems with vapor lock and compensate for the LHV differences with longer injections or higher injection pressures to maintain the same cycle energy [54, 67, 68]. Better results in terms of soot, HC, and CO emissions have been found in several studies with OME_x in CI engines [36, 57, 69, 70]. Some significant results were found in the works of Ma et al. [69], and García et al. in [71]. In the first one, the authors obtained a soot reduction of around 68% in an experiment using OME_x blend with diesel without any modification of the injection system. In the second one, the OME_x allowed a reduction of soot to values around zero when the engine was operating at full load. Moreover, it is possible to control the NO_x emissions through a higher EGR rate due to the amount of oxygen in the fuel [62, 71].

2.5 Alternative combustion systems

CI engines are used as stationary and moving power sources all over the world. There are significant concerns about the future of CI engines given the increasingly strict environmental regulations, greenhouse gas regulations, and demand for fossil fuels. The demand for transportation and electrical power is increasing to meet economic demand. Based on this, we could ask ourselves the following question: does it exist any method that will enable the CI engine to satisfy these current and upcoming industry demands? Interesting improvements to efficiency and pollution reduction using conventional diesel fuel, almost eliminating sulfur, have been developed. The new methods studied have been able to lower the oxygen content of the intake air by using EGR, which results in lower peak combustion temperatures and considerable

NO_x reductions. Modern CI engines now make use of after-treatment innovations, including diesel particulate filters (DPF), deNO_x catalysts, and diesel oxidation catalysts (DOC). The ongoing studies on improved combustion have opened up fascinating possibilities for increasing the efficiency of CI engines as well as significantly reducing the emissions profile. The ability to manage power output by fuel supply and maintain a high compression ratio may be improved while maintaining some fuel and air premixing. To achieve these objectives, a number of different tactics have been used.

In the scenario of pollutant emissions reduction, a large variety of alternative combustion system strategies are already developed and studied. These alternative combustion concepts intend to eliminate both NO_x and soot emissions by means of avoiding the trade-off between them. Among these alternatives, some of the most conventional combustion modes are homogeneous charge compression ignition (HCCI), premixed charge compression ignition (PCCI), and reactivity-controlled compression ignition (RCCI). Moreover, the concepts of the argon cycle and oxy-fuel combustion are also gaining weight recently.

The HCCI combustion concept is characterized by early fuel injection, which allows completely full air-fuel mixing during the compression stroke, and it was proposed considering the combustion of diesel [72]. This homogeneous charge is squeezed in the direction of the TDC, increasing its temperature and pressure. At some point, the environment within the combustion chamber will provide enough energy to activate the initiation reactions at various locations depending on the thermal stratification of the combustion chamber. After the start of the reactions, the burning occurs rapidly inside the combustion chamber. The fast combustion reduces the heat transfer losses and in-cylinder temperature, and the volumetric combustion is close to an ideal cycle [73]. More applications, operation details, and several information about this concept can be found in [74–80].

When compared to HCCI combustion, the PPCI approach was considered to be more practical and cost-effective. In comparison to mixing controlled combustion, premixed combustion dominates substantially more. By pre-igniting the diesel fuel, the PPCI combustion mode increases the reactivity of the mixture. Because of the two-stage igniting behavior of diesel-like fuels, the PPCI combustion process mainly shows a two-stage heat release. The first stage of heat release is due to the reactions at low temperatures releasing approximately 7% of the energy. The second stage occurs due to reactions at high temperatures and releases the remaining energy. To further explore the PPCI mode, the reader is referred to some works [81–85].

The RCCI concept can be defined as a partially premixed combustion strategy based on the dual-fuel operation. This technology uses two fuels: one highly reactive and one less reactive [86]. The fuels are delivered to the engine using separate injection systems. Low reactivity has a port fuel injection, and high reactivity fuel is direct injection. The combustion control is possible by altering the relative quantities or timings of injection of the two fuels. The RCCI method combines different fuels as gasoline and diesel. In this combination, the combustion timing can be advanced through the control of the diesel fuel injection, with a higher amount of fuel is possible to obtain the advantage of its higher reactivity. On the other hand, a small quantity of diesel fuel can be directly injected into the cylinder shortly before the optimum combustion time to provide a pilot ignition that ignites the balance of the mixture. This method provides a higher flexibility to control the combustion timing and a wider operation range compared to HCCI engines working with a single fuel. More information about this combustion method can be found in [87–94].

Additionally, the current trend is to design combustion systems that not only provide good performance but also facilitate the capture of emissions, such as CO_2, that can be used later as raw material for the chemical industry. Two of the most recent methods applied to engines are argon gas induction and oxy-fuel combustion. The argon gas induction on compression ignition engines is a technology that can be applied in combination with hydrogen and biofuels. One of the most difficult issues is that argon heats extremely fast when it is compressed. The mixture, therefore, combusts before reaching the appropriate pressure level, reducing the engine efficiency. As a result, new strategies are necessary to manage the combustion process in an argon engine. This technology has been little studied so far. Prashanth et al. in [95] studied the influence of argon gas induction with air in a CI engine fueled with diesel at varying percentages. Between the most relevant results obtained are a significantly higher NO_x, CO_2 and CO reduction whereas the thermal efficiency also was reduced. However, the HC emissions increased. The peak of in-cylinder pressure and corresponding in-cylinder temperature decreased along the exhaust gas temperatures. Increased argon induction percentages have no effect on the particular fuel consumption. More information about this combustion mode can be found in [96].

In this thesis, the oxy-fuel concept will be the focus once the other technologies such as HCCI, PCCI, and RCCI have already been extensively studied and the argon gas induction has recently started to be explored. Oxy-fuel combustion is a promising concept focused on removing and purifying exhaust gases, CO_2 gases [97]. This technology is most commonly applied in power

plants [98–102]. This concept can be defined as a combustion process that occurs in highly oxygen-enriched environments and uses a high EGR rate to manage the combustion temperatures and prevent overheating problems [103, 104]. The advantage of this concept is the removal of N_2 from the intake gas, which leads to theoretical zero emissions of NO_x; however, with the disadvantage of the expensive cost to produce pure O_2.

Considering this, the oxy-fuel combustion technology could be one of the most promising concepts to reduce emissions in ICE. An essential drawback of this concept is the expensive value of obtaining high-purity oxygen. The solutions used to apply this technology in stationary applications may not be an economical choice for transport applications once, which can increase the weight of the vehicles, leading to higher values of fuel consumption. In light of this, different alternatives are being evaluated in order to obtain the most beneficial system.

Some options to obtain oxygen with the necessary purity have been searched. Between the most relevant alternatives are the cryogenic air separation (CAS) and the oxygen transport membranes that are also known as mixed ionic-electronic conducting membranes (MIECs) [105, 106]. However, the CAS technology presents a higher cost, thus making MIECs better alternatives for obtaining oxygen.

Bauman et al. [107] developed an MIEC with high O_2 permeation and a production capacity around 62 ml/min/cm^2 of O_2 at 1000 °C made of $Ba_{0.5}Sr_{0.5}Co_{0.8}Fe_{0.2}O_{3-\delta}$ (BSFC).In another study, Catalán-Martinez et al. [108] studied experimentally and numerically the effect of temperature, gas composition, feeding flow, and sweep inlet flow on the MIEC BSFC performance. Through the application of experimental analysis with one-dimensional and CFD simulations, their results show that with the temperature increment, from 700 °C to 1000 °C, it is possible to improve the O_2 transport. In terms of feed and sweep inlet flows, the O_2 flux exhibits asymptotic behavior. Thus, considering these previous studies, the MIEC BSFC can use the exhaust gas and provide the needed oxygen amount for the proper engine performance in oxy-fuel combustion mode. Furthermore, Desantes et al. [109] presented a patent combining an MIEC with an ICE in a synergistic approach to utilize waste heat from the engine to supply the requisite thermal power for the membrane.

As this technology is still recent, its applications in engines are still limited, although some studies have been found. One of the first works to mention the application of oxy-fuel combustion in engines was Osman in [110]. In this work, pure oxygen and water were injected into the combustion chamber of

a CI engine. Water injection helps to control the in-cylinder temperature because it has a higher specific heat, so it is possible to obtain results where HC, CO, NO_x and soot emissions are reduced. Van Blarigan et al. in [111] performed experiments on an SI engine operating in oxy-fuel combustion mode using methane as a fuel for both dry and wet EGR. Aiming to determine the combustion performance of the engine and compare it with an engine operating under methane-air conditions. From the experimental analysis, results indicate that the engine efficiency is reduced in oxy-fuel combustion due to the lower ratio of specific heat of the EGR when compared to a regular engine. Tan and Hu in [112] studied the emissions of a CI engine focusing on the concentration of the intake gas components aiming for the best ratio between the amounts and thus reducing NO_x emissions. According to the results, NO_x emissions increased as the concentration of N_2 was changed from 79% to 40% with the engine operating with only O_2 and N_2 forming the intake gas mixture. On the other hand, adding CO_2 to the intake gas leads to a considerable reduction of NO_x, and it was even possible to reduce NO_x emissions to 0 when the composition was 50% O_2 and CO_2. The application of oxy-fuel combustion has been further explored in engines operating in Homogenous Charge Compression Ignition (HCCI) mode [113–116]. In these studies, in general, they aimed to experiment and understand how this new mode of oxy-fuel combustion affects combustion characteristics, feasibility, and application for pollutant emission control. The most important results include that it is possible to operate an engine in HCCI mode using only CO_2 and O_2 in the intake gas. Due to the lower specific heat of CO_2, higher compression ratios are required to maintain the same combustion phasing. However, increasing CO_2 in the mixture shows a potential to eliminate NO_x emissions and still reduce soot and CO emission levels.

To the correct application of the oxy-fuel combustion concept in combination with the MIEC in ICE, the engine must deliver to the membrane an exhaust gas with a determining condition for the correct operation of the membrane [117]. This means that the exhaust gases of the engine should reach the pressure and temperature requirements for optimal operation of the MIEC. Serrano et al. [118] evaluated the potential of this concept in engines to reduce pollutant emissions. Furthermore, their concept is co-active with CO_2-capture technologies approaches. They proposed a 1D ICE model using two strategies to recover the exhaust gas energy for oxygen production. The O_2 generation was achieved by using Catalán-Martinez et al. [108] BSCF MIEC model. At high engine speeds, they observed that the oxy-fuel combustion system produces comparable brake power and efficiency to a normal CI engine. The particular break fuel consumption increases at low engine speeds. Serrano et

al. [119] evaluated the oxy-fuel technology coupled with an MIEC in a SI engine through experimental and theoretical techniques considering thermal-mechanical constraints. The results show a fall in indicated efficiency that could be compensated by knocking reduction, allowing for spark optimization with an EGR rate range of 60% to 70% to maintain combustion stability.

The engine model was defined to adapt the original oxy-fuel combustion engine proposed in [109] and already studied by Serrano et al. in [118]. Figure 2.7 presents the computational model for 1D study. The orange line represents the fuel flow; the black line represents the N_2 flow. The red and blue lines represent, respectively, the exhaust gas flow and the blend of O_2, CO_2, and H_2O, which enters the cylinder. Moreover, the acronyms VGT, HE, and BPV mean variable geometry turbine, heat exchange, and by-pass valve, respectively. Furthermore, the terms accompanying the VGT (N/A-1 and G/O) mean nitrogen and air intake, and 1 is the air intake order for the N/A nomenclature. The G/O regards the gas mixture of O_2, CO_2, and H_2O that enters the compressor and, subsequently, the engine. The G/N term accompanying the heat exchanger means exhaust gas and nitrogen. More details can be found in [109].

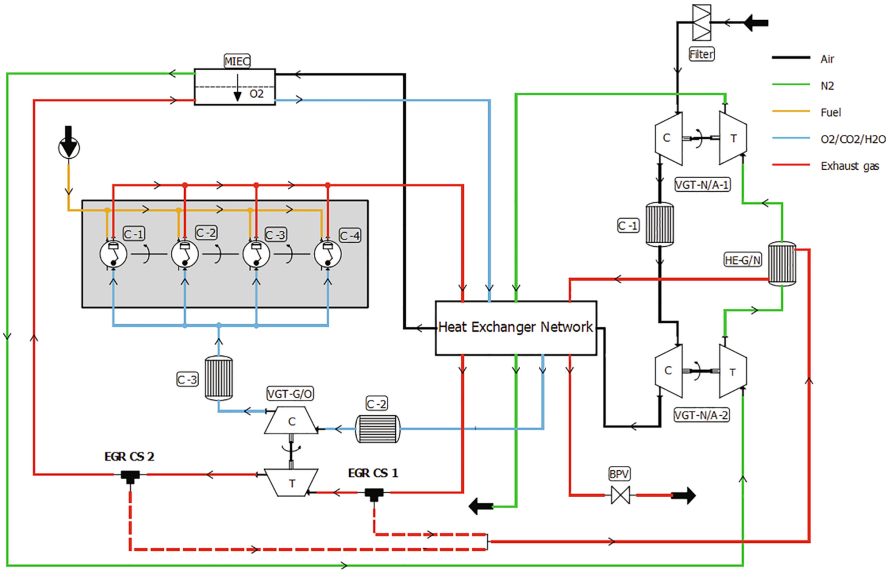

Figure 2.7: Implementation model of oxy-fuel combustion concept applied in a CI engine coupled with a MIEC technology. Adapted from [118].

2.6 Summary and conclusions

As demonstrated throughout this chapter, many approaches for engine optimization strategies for pollutant emissions reduction and efficiency increment were discussed. Moreover, advanced combustion concepts and alternatives for fossil fuel replacement in CI engines that have been used in recent years were presented. However, even though CI engines are highly efficient, it is still necessary to explore alternatives for more environmentally friendly use. In this regard, this thesis emphasizes three main alternatives: novel combustion system configuration involving piston geometry, injection, and air management systems to improve the mixing process. The second alternative is the use of alternative fuels due to their properties of low emissions production. The combustion process is similar to conventional diesel fuel, which contributes to their use. The last alternative evaluated is the oxy-fuel combustion concept. This method is a new technology that makes it possible, in addition to the elimination of NO_x emissions, to capture the CO_2 that can be stored and used in different sectors later on. Although several research has previously been conducted using these technologies, there are still other subjects that might be investigated, which are outlined below:

- In the case of combustion system configuration, they demonstrated significant pollutant emissions using a different configuration of parameters in CI engines. However, what could be a better way to develop a new combustion system?
- Because OME is a relatively new e-fuel, there are various aspects of the combustion process that are yet unknown. In this approach, using simultaneous numerical simulations to examine pure OME combustion in an engine will increase understanding of this fuel and yield valuable discoveries.
- In the same way as OME utilization, oxy-fuel combustion is a new combustion mode that has been little discussed in CI engines to reduce pollutant emissions. The simulation models can be applied to understand the phenomena, its feasibility, and how it affects the combustion in CI.

References

[1] Heywood, John B. *Internal Combustion Engine Fundamentals. N. York: McGraw-Hill.* 1988.

[2] Stone, R. and Ball, J.K. *Automotive Engineering Fundamentals*. Premiere Series Bks. SAE International, 2004.

[3] Xuan, T. "Optical investigations on Diesel spray dynamics and in-flame soot formation [Tesis doctoral]". In: *Universitat Politècnica de València* (2017). DOI: 10.4995/Thesis/10251/94626.

[4] Dumouchel, Christophe. "On the experimental investigation on primary atomization of liquid streams". In: *Experiments in Fluids* 45.3 (2008), pp. 371–422. DOI: 10.1007/s00348-008-0526-0.

[5] Aradi, Allen, Higgins, Brian, and Siebers, Dennis L. "Diesel-Spray Ignition and Premixed-Burn Behavior". In: (2000). DOI: https://doi.org/10.4271/2000-01-0940.

[6] Vargas Lewiski, FD. "Analysis of the combustion process and soot formation in a single cylinder optical engine fueled with e-fuels and using different piston geometries [Tesis doctoral]". In: *Universitat Politècnica de València* (2021). DOI: 10.4995/Thesis/10251/180351.

[7] Klaus Mollenhauer, Helmut Tschöke. *Handbook of Diesel Engines*. Springer Berlin, Heidelberg, 2010. DOI: https://doi.org/10.1007/978-3-540-89083-6.

[8] Skeen, Scott, Manin, Julien, and Pickett, Lyle M. "Visualization of Ignition Processes in High-Pressure Sprays with Multiple Injections of n-Dodecane". In: *SAE International Journal of Engines* 8.2 (2015), pp. 696–715. DOI: https://doi.org/10.4271/2015-01-0799.

[9] Pickett, Lyle M., Kook, Sanghoon, and Williams, Timothy C. "Visualization of Diesel Spray Penetration, Cool-Flame, Ignition, High-Temperature Combustion, and Soot Formation Using High-Speed Imaging". In: *SAE International Journal of Engines* 2.1 (2009), pp. 439–459. DOI: https://doi.org/10.4271/2009-01-0658.

[10] Westbrook, C. K. et al. "The effects of pressure, temperature, and concentration on the reactivity of alkanes: Experiments and modeling in a rapid compression machine". In: *Symposium (International) on Combustion* 27.1 (1998), pp. 371–378. DOI: 10.1016/S0082-0784(98)80425-6.

[11] Plee, Steven L. and Ahmad, Tanvir. "Relative Roles of Premixed and Diffusion Burning in Diesel Combustion". In: *1983 SAE International Fall Fuels and Lubricants Meeting and Exhibition*. SAE International, 1983. DOI: https://doi.org/10.4271/831733.

[12] Dec, John E. and Espey, Christoph. "Ignition and Early Soot Formation in a DI Diesel Engine Using Multiple 2-D Imaging Diagnostics". In: *International Congress & Exposition*. SAE International, 1995. DOI: https://doi.org/10.4271/950456.

[13] Espey, Christoph and Dec, John E. "Chemiluminescence Imaging of Autoignition in a DI Diesel Engine". In: *International Fall Fuels and Lubricants Meeting and Exposition*. SAE International, 1998. DOI: https://doi.org/10.4271/982685.

[14] Dec, John E. "A Conceptual Model of DI Diesel Combustion Based on Laser-Sheet Imaging*". In: *International Congress & Exposition*. SAE International, 1997. DOI: https://doi.org/10.4271/970873.

[15] Musculus, Mark P. B. "On the Correlation between NOx Emissions and the Diesel Premixed Burn". In: *SAE 2004 World Congress & Exhibition*. SAE International, 2004. DOI: https://doi.org/10.4271/2004-01-1401.

[16] Glassman, Irvin and Yetter, Richard A. "Chapter 9 - Combustion of Nonvolatile Fuels". In: *Combustion (Fourth Edition)*. Ed. by Irvin Glassman and Richard A. Yetter. Fourth Edition. Burlington: Academic Press, 2008, pp. 495–550. DOI: https://doi.org/10.1016/B978-0-12-088573-2.00009-9.

[17] Hsu, Bertrand D. *Diesel-Engine Combustion Analysis Practical Combustion Analysis*. 2022.

[18] Westbrook, Charles K. et al. "Diesel Combustion: An Integrated View Combining Laser Diagnostics, Chemical Kinetics, And Empirical Validation". In: *Future Transportation Technology Conference & Exposition*. SAE International, 1999. DOI: https://doi.org/10.4271/1999-01-0509.

[19] Dec, John E. and Canaan, Robert E. "PLIF Imaging of NO Formation in a DI Diesel Engine". In: *International Congress & Exposition*. SAE International, 1998. DOI: https://doi.org/10.4271/980147.

[20] Tree, Dale R. and Svensson, Kenth I. "Soot processes in compression ignition engines". In: *Progress in Energy and Combustion Science* 33.3 (2007), pp. 272–309. DOI: 10.1016/j.pecs.2006.03.002.

[21] Bartok, W. and Sarofim, A.F. *Fossil Fuel Combustion: A Source Book*. Wiley, 1991.

[22] Wickman, D. D., Senecal, P. K., and Reitz, R. D. "Diesel engine combustion chamber geometry optimization using genetic algorithms and multi-dimensional spray and combustion modeling". In: *SAE Technical Papers* 110 (2001), pp. 487–507. DOI: 10.4271/2001-01-0547.

[23] Benajes, Jesús, Pastor, José V., García, Antonio, and Monsalve-Serrano, Javier. "An experimental investigation on the influence of piston bowl geometry on RCCI performance and emissions in a heavy-duty engine". In: *Energy Conversion and Management* 103 (2015), pp. 1019–1030. DOI: 10.1016/j.enconman.2015.07.047.

[24] Benajes, Jesús, García, Antonio, Pastor, José Manuel, and Monsalve-Serrano, Javier. "Effects of piston bowl geometry on reactivity controlled compression ignition heat transfer and combustion losses at different engine loads". In: *Energy* 98 (2016), pp. 64–77. DOI: 10.1016/j.energy.2016.01.014.

[25] Benajes, Jesus et al. "Optimization of the combustion system of a medium duty direct injection diesel engine by combining CFD modeling with experimental validation". In: *Energy Conversion and Management* 110 (2016), pp. 212–229. DOI: 10.1016/j.enconman.2015.12.010.

[26] Kakaee, Amir Hasan, Nasiri-Toosi, Ali, Partovi, Babak, and Paykani, Amin. "Effects of piston bowl geometry on combustion and emissions characteristics of a natural gas/diesel RCCI engine". In: *Applied Thermal Engineering* 102 (2016), pp. 1462–1472. DOI: 10.1016/j.applthermaleng.2016.03.162.

[27] Reddy, Abhishek G, Pratap Singh, Nirmal, V Sai Krishna, Kolluri R, Priyedarshi, Anurag, and Singh, SN. "Effect Of Compression Ratio On The Performance Of Diesel Engine At Different Loads". In: *Journal of Engineering Research and Applications www.ijera.com ISSN* 5.102 (2015), pp. 2248–962262.

[28] Funayama, Yoshihiro, Nakajima, Hiroshi, and Shimokawa, Kiyohiro. "A Study on the Effects of a Higher Compression Ratio in the Combustion Chamber on Diesel Engine Performance". In: *SAE 2016 World Congress and Exhibition*. SAE International, 2016. DOI: https://doi.org/10.4271/2016-01-0722.

[29] Miles, Paul C. and Andersson, Öivind. "A review of design considerations for light-duty diesel combustion systems". In: *International Journal of Engine Research* 17.1 (2016), pp. 6–15. DOI: 10.1177/1468087415604754.

[30] Kidoguchi, Yoshiyuki, Yang, Changlin, and Miwa, Kei. "Effect of high squish combustion chamber on simultaneous reduction of NOx and particulate from a direct-injection diesel engine". In: *SAE Technical Papers* 724 (1999). DOI: 10.4271/1999-01-1502.

[31] Dempsey, Adam B., Walker, N. Ryan, and Reitz, Rolf D. "Effect of Piston Bowl Geometry on Dual Fuel Reactivity Controlled Compression Ignition (RCCI) in a Light-Duty Engine Operated with Gasoline/Diesel and Methanol/Diesel". In: *SAE International Journal of Engines* 6.1 (2013), pp. 78–100. DOI: https://doi.org/10.4271/2013-01-0264.

[32] Dolak, Jonathan George, Shi, Yu, and Reitz, Rolf. "A computational investigation of stepped-bowl piston geometry for a light duty engine operating at low load". In: *SAE Technical Papers* (2010). DOI: 10.4271/2010-01-1263.

[33] Dahlstrom, Jessica, Andersson, Oivind, Tuner, Martin, and Persson, Håkan. "Experimental Comparison of Heat Losses in Stepped-Bowl and Re-Entrant Combustion Chambers in a Light Duty Diesel Engine". In: *SAE Technical Papers* (2016). DOI: 10.4271/2016-01-0732.

[34] Busch, Stephen, Zha, Kan, Perini, Federico, and Reitz, Rolf D. "Piston Bowl Geometry Impacts on Late-Cycle Flow and Mixing in a Small-Bore Diesel Engine." In: (2017).

[35] Leach, Felix, Ismail, Riyaz, Davy, Martin, Weall, Adam, and Cooper, Brian. "The effect of a stepped lip piston design on performance and emissions from a high-speed diesel engine". In: *Applied Energy* 215.November 2017 (2018), pp. 679–689. DOI: 10.1016/j.apenergy.2018.02.076.

[36] Pastor, José V. et al. "Effect of a novel piston geometry on the combustion process of a light-duty compression ignition engine: An optical analysis". In: *Energy* 221 (2021). DOI: 10.1016/j.energy.2021.119764.

[37] Shi, Yu and Reitz, Rolf D. "Assessment of optimization methodologies to study the effects of bowl geometry, spray targeting and swirl ratio for a heavy-duty diesel engine operated at High-Load". In: *SAE International Journal of Engines* 1.1 (2009), pp. 537–557. DOI: 10.4271/2008-01-0949.

[38] Genzale, Caroline L., Reitz, Rolf D., and Wickman, David D. "A computational investigation into the effects of spray targeting, bowl geometry and swirl ratio for low-temperature combustion in a heavy-duty diesel engine". In: *SAE Technical Papers* 2007.724 (2007), pp. 776–790. DOI: 10.4271/2007-01-0119.

[39] Çelikten, Ismet. "An experimental investigation of the effect of the injection pressure on engine performance and exhaust emission in indirect injection diesel engines". In: *Applied Thermal Engineering* 23.16 (2003), pp. 2051–2060. DOI: 10.1016/S1359-4311(03)00171-6.

[40] Divekar, Prasad S., Chen, Xiang, Tjong, Jimi, and Zheng, Ming. "Energy efficiency impact of EGR on organizing clean combustion in diesel engines". In: *Energy Conversion and Management* 112 (2016), pp. 369–381. DOI: 10.1016/j.enconman.2016.01.042.

[41] Kim, Byong Seok, Yoon, Wook Hyeon, Ryu, Sung Hyup, and Ha, Ji Soo. "Effect of the injector nozzle hole diameter and number on the spray characteristics and the combustion performance in medium-speed diesel marine engines". In: *SAE Technical Papers* 724 (2005). DOI: 10.4271/2005-01-3853.

[42] Agarwal, Avinash Kumar et al. "Effect of fuel injection timing and pressure on combustion, emissions and performance characteristics of a single cylinder diesel engine". In: *Fuel* 111 (2013), pp. 374–383. DOI: 10.1016/j.fuel.2013.03.016.

[43] Kweon, Chol Bum et al. "Effect of injection timing on detailed chemical composition and particulate size distributions of diesel exhaust". In: *SAE Technical Papers* (2003). DOI: 10.4271/2003-01-1794.

[44] Ladommatos, N., Abdelhalim, S., and Zhao, H. "The effects of exhaust gas recirculation on diesel combustion and emissions". In: *International Journal of Engine Research* 1.1 (2000), pp. 107–126. DOI: 10.1243/1468087001545290.

[45] Mito, Yuko, Tanaka, Daisuke, Lee, Seang Wock, Daisho, Yasuhiro, and Kusaka, Jin. "The effect of intake, injection parameters and fuel properties on diesel combustion and emissions". In: *SAE Technical Papers* (2003). DOI: 10.4271/2003-01-1793.

[46] Tufail, K. *Turbocharging and air-path management for light-duty diesel engines*. x. Woodhead Publishing Limited, 2009, pp. 175–214. DOI: 10.1533/9781845697457.1.175.

[47] Sher, Eran. "Handbook of Air Pollution From Internal Combustion Engines". In: San Diego: Academic Press, 1998, pp. 653–663. DOI: https://doi.org/10.1016/B978-012639855-7/50056-9.

[48] Squaiella, Lucas Lázaro Ferreira, Martins, Cristiane Aparecida, and Lacava, Pedro T. "Strategies for emission control in diesel engine to meet Euro VI". In: *Fuel* 104 (2013), pp. 183–193. DOI: 10.1016/j.fuel.2012.07.027.

[49] Han, Sangwook and Bae, Choongsik. "The influence of fuel injection pressure and intake pressure on conventional and low temperature diesel combustion". In: *SAE Technical Papers* (2012). DOI: 10.4271/2012-01-1721.

[50] Miles, Paul C. and Andersson, Öivind. "A review of design considerations for light-duty diesel combustion systems". In: *International Journal of Engine Research* 17.1 (2016), pp. 6–15. DOI: 10.1177/1468087415604754.

[51] Broatch, Alberto, Olmeda, Pablo, García, Antonio, Salvador-Iborra, Josep, and Warey, Alok. "Impact of swirl on in-cylinder heat transfer in a light-duty diesel engine". In: *Energy* 119 (2017), pp. 1010–1023. DOI: 10.1016/j.energy.2016.11.040.

[52] Bae, Choongsik and Kim, Jaeheun. "Alternative fuels for internal combustion engines". In: *Proceedings of the Combustion Institute* 36.3 (2017), pp. 3389–3413. DOI: 10.1016/j.proci.2016.09.009.

[53] König, Andrea, Marquardt, Wolfgang, Mitsos, Alexander, Viell, Jörn, and Dahmen, Manuel. "Integrated design of renewable fuels and their production processes: recent advances and challenges". In: *Current Opinion in Chemical Engineering* 27 (2020), pp. 45–50. DOI: 10.1016/j.coche.2019.11.001.

[54] Iannuzzi, Stefano Emanuele, Barro, Christophe, Boulouchos, Konstantinos, and Burger, Jakob. "Combustion behavior and soot formation/oxidation of oxygenated fuels in a cylindrical constant volume chamber". In: *Fuel* 167 (2016), pp. 49–59. DOI: 10.1016/j.fuel.2015.11.060.

[55] Lautenschütz, Ludger et al. "Physico-chemical properties and fuel characteristics of oxymethylene dialkyl ethers". In: *Fuel* 173 (2016), pp. 129–137. DOI: 10.1016/j.fuel.2016.01.060.

[56] Liu, Haoye, Wang, Zhi, Zhang, Jun, Wang, Jianxin, and Shuai, Shijin. "Study on combustion and emission characteristics of Polyoxymethylene Dimethyl Ethers/diesel blends in light-duty and heavy-duty diesel engines". In: *Applied Energy* 185 (2017), pp. 1393–1402. DOI: 10.1016/j.apenergy.2015.10.183.

[57] Omari, Ahmad, Heuser, Benedikt, and Pischinger, Stefan. "Potential of oxymethylenether-diesel blends for ultra-low emission engines". In: *Fuel* 209.May (2017), pp. 232–237. DOI: 10.1016/j.fuel.2017.07.107.

[58] Tan, Yong Ren et al. "Sooting characteristics of polyoxymethylene dimethyl ether blends with diesel in a diffusion flame". In: *Fuel* 224.November 2017 (2018), pp. 499–506. DOI: 10.1016/j.fuel.2018.03.051.

[59] Ferraro, Federica, Russo, Carmela, Schmitz, Robert, Hasse, Christian, and Sirignano, Mariano. "Experimental and numerical study on the effect of oxymethylene ether-3 (OME3) on soot particle formation". In: *Fuel* 286.P1 (2021), p. 119353. DOI: 10.1016/j.fuel.2020.119353.

[60] Zhang, Xiaolei, Kumar, Amit, Arnold, Ulrich, and Sauer, Jörg. "Biomass-derived oxymethylene ethers as diesel additives: A thermodynamic analysis". In: *Energy Procedia* 61 (2014), pp. 1921–1924. DOI: 10.1016/j.egypro.2014.12.242.

[61] Zhang, Xiaolei et al. "An optimized process design for oxymethylene ether production from woody-biomass-derived syngas". In: *Biomass and Bioenergy* 90.x (2016), pp. 7–14. DOI: 10.1016/j.biombioe.2016.03.032.

[62] Deutz, Sarah et al. "Cleaner production of cleaner fuels: Wind-to-wheel-environmental assessment of CO2-based oxymethylene ether as a drop-in fuel". In: *Energy and Environmental Science* 11.2 (2018), pp. 331–343. DOI: 10.1039/c7ee01657c.

[63] Burger, Jakob, Siegert, Markus, Ströfer, Eckhard, and Hasse, Hans. "Poly(oxymethylene) dimethyl ethers as components of tailored diesel fuel: Properties, synthesis and purification concepts". In: *Fuel* 89.11 (2010), pp. 3315–3319. DOI: 10.1016/j.fuel.2010.05.014.

[64] Burger, Jakob, Ströfer, Eckhard, and Hasse, Hans. "Production process for diesel fuel components poly(oxymethylene) dimethyl ethers from methane-based products by hierarchical optimization with varying model depth". In: *Chemical Engineering Research and Design* 91.12 (2013), pp. 2648–2662. DOI: 10.1016/j.cherd.2013.05.023.

[65] Wang, Dan, Zhu, Gangli, Li, Zhen, Xue, Machen, and Xia, Chungu. "Conceptual design of production of eco-friendly polyoxymethylene dimethyl ethers catalyzed by acid functionalized ionic liquids". In: *Chemical Engineering Science* 206 (2019), pp. 10–21. DOI: 10.1016/j.ces.2019.05.017.

[66] Härtl, Martin, Seidenspinner, Philipp, Jacob, Eberhard, and Wachtmeister, Georg. "Oxygenate screening on a heavy-duty diesel engine and emission characteristics of highly oxygenated oxymethylene ether fuel OME1". In: *Fuel* 153 (2015), pp. 328–335. DOI: 10.1016/j.fuel.2015.03.012.

[67] Pellegrini, Leonardo et al. "Combustion behaviour and emission performance of neat and blended polyoxymethylene dimethyl ethers in a light-duty diesel engine". In: *SAE Technical Papers* (2012). DOI: 10.4271/2012-01-1053.

[68] Pélerin, Dominik, Gaukel, Kai, Härtl, Martin, Jacob, Eberhard, and Wachtmeister, Georg. "Potentials to simplify the engine system using the alternative diesel fuels oxymethylene ether OME1 and OME3-6 on a heavy-duty engine". In: *Fuel* 259.January 2019 (2020). DOI: 10.1016/j.fuel.2019.116231.

[69] Ma, Xiao et al. "PLII-LEM and OH∗ Chemiluminescence Study on Soot Formation in Spray Combustion of PODEn-Diesel Blend Fuels in a Constant Volume Vessel". In: *SAE Technical Papers* 2017-October (2017). DOI: 10.4271/2017-01-2329.

[70] Liu, Haoye et al. "Recent progress in the application in compression ignition engines and the synthesis technologies of polyoxymethylene dimethyl ethers". In: *Applied Energy* 233-234.June 2018 (2019), pp. 599–611. DOI: 10.1016/j.apenergy.2018.10.064.

[71] García, Antonio et al. "Potential of e-Fischer Tropsch diesel and oxymethyl-ether (OMEx) as fuels for the dual-mode dual-fuel concept". In: *Applied Energy* 253.July (2019), p. 113622. DOI: 10.1016/j.apenergy.2019.113622.

[72] Gray, Allen W. and Ryan, Thomas W. "Homogeneous charge compression ignition (HCCI) of diesel fuel". In: *SAE Technical Papers* 412 (1997). DOI: 10.4271/971676.

[73] Jin, Chao and Zheng, Zunqing. "A review on homogeneous charge compression ignition and low temperature combustion by optical diagnostics". In: *Journal of Chemistry* 2015 (2015). DOI: 10.1155/2015/910348.

[74] Christensen, Magnus, Hultqvist, Anders, and Johansson, Bengt. "Demonstrating the multi fuel capability of a homogeneous charge compression ignition engine with variable compression ratio". In: *SAE Technical Papers* 724 (1999). DOI: 10.4271/1999-01-3679.

[75] Hyvönen, Jari, Haraldsson, Göran, and Johansson, Bengt. "Supercharging HCCI to extend the operating range in a multi-cylinder VCR-HCCI engine". In: *SAE Technical Papers* 2003.724 (2003). DOI: 10.4271/2003-01-3214.

[76] Tanaka, Shigeyuki, Ayala, Ferran, Keck, James C., and Heywood, John B. "Two-stage ignition in HCCI combustion and HCCI control by fuels and additives". In: *Combustion and Flame* 132.1-2 (2003), pp. 219–239. DOI: 10.1016/S0010-2180(02)00457-1.

[77] Song, H. H. and Edwards, C. F. "Understanding chemical effects in low-load-limit extension of homogeneous charge compression ignition engines via recompression reaction". In: *International Journal of Engine Research* 10.4 (2009), pp. 231–250. DOI: 10.1243/14680874JER03409.

[78] Yao, Mingfa, Zheng, Zhaolei, and Liu, Haifeng. "Progress and recent trends in homogeneous charge compression ignition (HCCI) engines". In: *Progress in Energy and Combustion Science* 35.5 (2009), pp. 398–437. DOI: 10.1016/j.pecs.2009.05.001.

[79] Stanglmaier, Rudolf H and Roberts, Charles E. "(HCCI): Benefits , Compromises , and Future Engine Applications". In: *Engineering* 724 (2012).

[80] Martins, Mario et al. "HCCI of wet ethanol on dedicated cylinder of a diesel engine using exhaust heat recovery". In: *SAE Technical Papers* September (2018). DOI: 10.4271/2018-36-0191.

[81] Jain, Ayush, Singh, Akhilendra Pratap, and Agarwal, Avinash Kumar. "Effect of fuel injection parameters on combustion stability and emissions of a mineral diesel fueled partially premixed charge compression ignition (PCCI) engine". In: *Applied Energy* 190 (2017), pp. 658–669. DOI: 10.1016/j.apenergy.2016.12.164.

[82] Chaichan, Miqdam T. "Combustion and emission characteristics of E85 and diesel blend in conventional diesel engine operating in PPCI mode". In: *Thermal Science and Engineering Progress* 7.April (2018), pp. 45–53. DOI: 10.1016/j.tsep.2018.04.013.

[83] Ma, Cheng et al. "Analysis of PPCI mode and multi-objective comprehensive optimization for a dual-fuel engine". In: *Fuel* 303.April (2021), p. 121296. DOI: 10.1016/j.fuel.2021.121296.

[84] Hu, Jiancun, Chen, Ziqiang, Yao, Ye, Shi, Lei, and Deng, Kangyao. "Study on control-oriented emission predictions of PPCI diesel engine with two-stage fuel injection". In: *Fuel* 320.January (2022), p. 123984. DOI: 10.1016/j.fuel.2022.123984.

[85] Ma, Cheng et al. "Multi-objective optimization of dual-fuel engine performance in PPCI mode based on preference decision". In: *Fuel* 312.October 2021 (2022), p. 122901. DOI: 10.1016/j.fuel.2021.122901.

[86] Reitz, Rolf D. and Duraisamy, Ganesh. "Review of high efficiency and clean reactivity controlled compression ignition (RCCI) combustion in internal combustion engines". In: *Progress in Energy and Combustion Science* 46 (2015), pp. 12–71. DOI: 10.1016/j.pecs.2014.05.003.

[87] Mancaruso, Ezio and Vaglieco, Bianca Maria. "UV-Visible Spectroscopic Measurements of Dual-Fuel PCCI Engine". In: *SAE International Journal of Fuels and Lubricants* 4.2 (2011), pp. 271–281. DOI: 10.4271/2011-24-0061.

[88] Splitter, Derek, Hanson, Reed, Kokjohn, Sage, Wissink, Martin, and Reitz, Rolf. "Injection effects in low load RCCI dual-fuel combustion". In: *SAE Technical Papers* (2011). DOI: 10.4271/2011-24-0047.

[89] Kokjohn, S. L., Hanson, R. M., Splitter, D. A., and Reitz, R. D. "Fuel reactivity controlled compression ignition (RCCI): A pathway to controlled high-efficiency clean combustion". In: *International Journal of Engine Research* 12.3 (2011), pp. 209–226. DOI: 10.1177/1468087411401548.

[90] Mancaruso, Ezio and Vaglieco, Bianca Maria. "UV-visible imaging of PCCI engine running with ethanol/diesel fuel". In: *SAE Technical Papers* (2012). DOI: 10.4271/2012-01-1238.

[91] Mancaruso, Ezio and Vaglieco, Bianca Maria. "Characterization of PCCI combustion in a single cylinder CI engine fuelled with RME and bio-ethanol". In: *SAE Technical Papers* 2 (2013). DOI: 10.4271/2013-01-1672.

[92] Splitter, Derek, Wissink, Martin, Delvescovo, Dan, and Reitz, Rolf. "RCCI engine operation towards 60% thermal efficiency". In: *SAE Technical Papers* 2.X (2013). DOI: 10.4271/2013-01-0279.

[93] Splitter, Derek A. and Reitz, Rolf D. "Fuel reactivity effects on the efficiency and operational window of dual-fuel compression ignition engines". In: *Fuel* 118 (2014), pp. 163–175. DOI: 10.1016/j.fuel.2013.10.045.

[94] Mancaruso, Ezio, Todino, Michele, and Vaglieco, Bianca Maria. "Analysis of dual fuel combustion in single cylinder research engine fueled with methane and diesel by ir diagnostics". In: *SAE Technical Papers* 2019-April.April (2019). DOI: 10.4271/2019-01-1165.

[95] Prashanth, K, Shaik, Amjad, T, Srinivasa Rao, and B, Pavan Bharadwaja. "Experimental investigation of argon gas induction on diesel engine performance and emission characteristics : A comprehensive study on de-NO x techniques". In: *Process Safety and Environmental Protection* 152 (2021), pp. 471–481. DOI: 10.1016/j.psep.2021.06.036.

[96] Moneib, Hany A., Abdelaal, Mohsen, Selim, Mohamed Y.E., and Abdallah, Osama A. "NOx emission control in SI engine by adding argon inert gas to intake mixture". In: *Energy Conversion and Management* 50.11 (2009), pp. 2699–2708. DOI: 10.1016/j.enconman.2009.05.032.

[97] Abraham, B M, Asbury, J G, Lynch, E P, and Teotia, A P.S. "Coal-oxygen process provides CO/sub 2/ for enhanced recovery". In: *Oil Gas J.; (United States)* (1982).

[98] Hanak, Dawid P., Powell, Dante, and Manovic, Vasilije. "Techno-economic analysis of oxy-combustion coal-fired power plant with cryogenic oxygen storage". In: *Applied Energy* 191 (2017), pp. 193–203. DOI: 10.1016/j.apenergy.2017.01.049.

[99] Kimura, N., Omata, K., Kiga, T., Takano, S., and Shikisima, S. "The characteristics of pulverized coal combustion in O2/CO2 mixtures for CO2 recovery". In: *Energy Conversion and Management* 36.6-9 (1995), pp. 805–808. DOI: 10.1016/0196-8904(95)00126-X.

[100] Sanz, Wolfgang, Jericha, Herbert, Bauer, Bernhard, and Göttlich, Emil. "Qualitative and Quantitative Comparison of Two Promising Oxy-Fuel Power Cycles for CO2 Capture". In: *Journal of Engineering for Gas Turbines and Power* 130.3 (2008). 031702. DOI: 10.1115/1.2800350.

[101] Wei, Xiaoyu, Manovic, Vasilije, and Hanak, Dawid P. "Techno-economic assessment of coal- or biomass-fired oxy-combustion power plants with supercritical carbon dioxide cycle". In: *Energy Conversion and Management* 221.July (2020), p. 113143. DOI: 10.1016/j.enconman.2020.113143.

[102] Biyiklioğlu, Onur and Tat, Mustafa Ertunc. "Tribological assessment of NiCr, Al2O3/TiO2, and Cr3C2/NiCr coatings applied on a cylinder liner of a heavy-duty diesel engine". In: *International Journal of Engine Research* 22.7 (2021), pp. 2267–2280. DOI: 10.1177/1468087420930164.

[103] Pamminger, Michael, Wang, Buyu, Hall, Carrie M., Vojtech, Ryan, and Wallner, Thomas. "The impact of water injection and exhaust gas recirculation on combustion and emissions in a heavy-duty compression ignition engine operated on diesel and gasoline". In: *International Journal of Engine Research* 21.8 (2020), pp. 1555–1573. DOI: 10.1177/1468087418815290.

[104] Mobasheri, Raouf and Khabbaz, Seyed Alireza. "Modeling the effects of high EGR rates in conjunction with optimum multiple injection techniques in a heavy duty di diesel engine". In: *SAE Technical Papers* 1 (2014). DOI: 10.4271/2014-01-1124.

[105] Mancini, N. D. and Mitsos, A. "Conceptual design and analysis of ITM oxy-combustion power cycles". In: *Physical Chemistry Chemical Physics* 13.48 (2011), pp. 21351–21361. DOI: 10.1039/c1cp23027a.

[106] Portillo, Esmeralda, Alonso-Fariñas, Bernabé, Vega, Fernando, Cano, Mercedes, and Navarrete, Benito. "Alternatives for oxygen-selective membrane systems and their integration into the oxy-fuel combustion process: A review". In: *Separation and Purification Technology* 229.January (2019), p. 115708. DOI: 10.1016/j.seppur.2019.115708.

[107] Baumann, S. et al. "Ultrahigh oxygen permeation flux through supported Ba0.5Sr0.5Co0.8Fe0.2O3-δ membranes". In: *Journal of Membrane Science* 377.1-2 (2011), pp. 198–205. DOI: 10.1016/j.memsci.2011.04.050.

[108] Catalán-Martínez, D., Santafé-Moros, A., Gozálvez-Zafrilla, J. M., García-Fayos, J., and Serra, J. M. "Characterization of oxygen transport phenomena on BSCF membranes assisted by fluid dynamic simulations including surface exchange". In: *Chemical Engineering Journal* 387.October 2019 (2020), p. 124069. DOI: 10.1016/j.cej.2020.124069.

[109] Desantes, J. et al. "Motor de combustion interna de hidrocarburos auto transportable que no emite gases nocivos ni CO2; secuestra CO2 atmosférico y fabrica CO2 líquido subcrítico". In: (Patent WO 2020/193833 A1).

[110] Osman, Azmi. "Feasibility study of a novel combustion cycle involving oxygen and water". In: *SAE Technical Papers* 3 (2009). DOI: 10.4271/2009-01-2808.

[111] Van Blarigan, Andrew et al. "Experimental Study of Methane Fuel Oxycombustion in a Spark-Ignited Engine". In: *Journal of Energy Resources Technology* 136.1 (2014). DOI: 10.1115/1.4024974.

[112] Tan, Qinming and Hu, Yihuai. "A study on the combustion and emission performance of diesel engines under different proportions of O2 & N2 & CO2". In: *Applied Thermal Engineering* 108 (2016), pp. 508–515. DOI: 10.1016/j.applthermaleng.2016.07.151.

[113] Kang, Zhe et al. "Study of the Combustion Characteristics of a HCCI Engine Coupled with Oxy-Fuel Combustion Mode". In: *SAE International Journal of Engines* 10.3 (2017), pp. 908–916. DOI: 10.4271/2017-01-0649.

[114] Mobasheri, Raouf, Izza, Nadia, Aitouche, Abdel, Peng, Jun, and Bakir, Boualem. "Investigation of oxyfuel combustion on engine performance and emissions in a di Diesel HCCI Engine". In: *2019 8th International Conference on Systems and Control, ICSC 2019* (2019), pp. 411–416. DOI: 10.1109/ICSC47195.2019.8950525.

[115] Mohammed, Abdulrahman, Masurier, Jean Baptiste, Elkhazraji, Ali, and Johansson, Bengt. "Oxy-Fuel HCCI Combustion in a CFR Engine with Carbon Dioxide as a Thermal Buffer". In: *SAE Technical Papers* 2019-September.September (2019). DOI: 10.4271/2019-24-0119.

[116] Mobasheri, Raouf, Aitouche, Abdel, Peng, Zhijun, and Li, Xiang. "A numerical study of the effects of oxy-fuel combustion under homogeneous charge compression ignition regime". In: *International Journal of Engine Research* 23.4 (2022), pp. 649–660. DOI: 10.1177/1468087421993359.

[117] Arnau, F.J., García-Cuevas, L.M., Novella, R., and Gutiérrez, F. "Adapting an internal combustion engine to oxy-fuel combustion with in-situ oxygen production". In: *ASME - ICEF. The Internal Combustion Engine Fall Conference. Virtual Conference, Online:* (October 13-15, 2021).

[118] Serrano, J.R., Arnau, F.J., García-Cuevas, L.M., and Farias, V.H. "Oxy-fuel combustion feasibility of compression ignition engines using oxygen separation membranes for enabling carbon dioxide capture". In: *Energy Conversion and Management* 247 (2021), p. 114732. DOI: 10.1016/j.enconman.2021.114732.

[119] Serrano, J.R., Martin, J., Gomez-Soriano, J., and Raggi, R. "Theoretical and experimental evaluation of the spark-ignition premixed oxy-fuel combustion concept for future CO 2 captive powerplants". In: *Energy Conversion and Management* 244 (2021), p. 114498. DOI: 10.1016/j.enconman.2021.114498.

Chapter 3

Literature review: optimization methods

3.1 Introduction

This chapter presents some of the different optimization algorithms available for internal combustion engine (ICE) applications. As ICE's have become increasingly complex, making the task of increasing efficiency and reducing pollutant emissions more difficult, it has become necessary to develop more and more optimization methods that can consider every parameter of these powerplants.

For a long time, parametric studies were the primary option for optimization methods. This approach evaluates the effect of each variable in isolation. Nevertheless, it is well known that in engine development it is essential to evaluate the system globally, considering the cross-effects between each component of the engine. Moreover, the optimizations were performed experimentally, which implies a significant amount of iterations and work hours, raising the costs.

With the development of new technologies, different alternatives for engine optimization have been developed. Among these new alternatives, optimization algorithms arise as an interesting option. These algorithms are capable of evaluating several input parameters and their cross-effects simultaneously. Furthermore, with the evolution of computer codes, it is possible to use simulation software coupled with the algorithms to reproduce the behavior of

the engine, thus reducing the costs of an optimization study. These automated systems are responsible for significantly advancing the optimization approaches discussed in this chapter.

3.2 Optimization algorithms

Due to the significant number of parameters to be inspected in a combustion system definition, an additional technique must be applied to explore all the possibilities. Optimization procedures can be used to identify and propose guidelines for potential alternatives to optimize the combustion system performance. In the past, the optimization process was done experimentally, making the procedure more expensive. Nowadays, an option to reduce cost is to perform the same optimization approach using CFD models to reproduce the engine behavior. Moreover, it is possible to couple the CFD model with mathematical algorithms in an automated arrangement to develop the best combustion system possible. However, for this to be attainable, it is necessary to analyze the selected optimization algorithm, its strengths and weaknesses, and how to apply it to the specific problem.

Optimization algorithms can be grouped into two different categories: evolutionary algorithms and non-evolutionary algorithms. Non-evolutionary algorithms are statistical approaches that find the best combination from a previously set original population. In general, they are efficient methods for processes with a moderate number of variables. They are fast convergent methods, but the cost increases exponentially as the number of analyzed parameters grows. Examples of these algorithms are the methods of response surface and 2^k factorial.

On the other hand, evolutionary algorithms are thought of differently. From a population, the individuals evolve due to constraints of the environment, in a way that leads to an evolution of the individuals in the population. Those individuals defined at the beginning of the process are called parents, while the individuals in the new generations are known as children. For each problem, the appropriate requirements will influence how the new generations are affected. The stopping criterion is when one of the children reaches a particular quality value or a certain number of pre-established generations.

The major part of these systems are based on organic principles found in cells or animals, however, the main distinction is how the beginning population evolves and achieves the ultimate optimum. Some approaches are described in this subsection, including particle swarm optimization and tech-

niques developed from it, differential evolution, genetic algorithm, and neural network.

3.2.1 Particle Swarm Optimization

Kennedy and Eberhart in [1] developed a particle swarm optimization (PSO) algorithm. It was inspired by the social behavior of birds flocking to search for food. The basic concept is to use the previous experiences and expertise acquired by older birds to influence the behavior of other birds. Thus, the algorithm is simple; the potential solutions are tested, compared, and adjusted. Moreover, the PSO uses a force motion-based technique to move the candidate solution using concepts of velocity and position and information exchange.

The candidate solutions are called particles, and each particle is improved by moving them around the search space of each parameter. All the particles store their best position, and the method stores the global best position reached among all the particles during the process. The particles go to another position based on the velocity function calculated considering the local and global best positions. Figure 3.1 shows a working scheme of the PSO.

Some of the advantages of the PSO include rapid convergence, minimal objective evaluation compared to evolutionary algorithms, easy implementation, and few tuning parameters [2]. However, when applied to engine optimization, the basic PSO is considered effective with good performance, although the algorithm still has some drawbacks as it is highly sensitive to meta-parameters, which could lead to the function getting stuck in local minimums, and therefore it is not guaranteed that an optimum solution will be found. Some improvements can be applied to the PSO [2, 3] to avoid these inconveniences.

3.2.2 Mutation applied to PSO

This method is presented by Chen et al. in [4]. It is defined by introducing a mutation operator with an adaptive mutation probability into the basic PSO algorithm named M-PSO. Moreover, this method replaces the particles that fly out of the solution space with random particles generated during the search process. However, performing this algorithm without control is comparable to flipping a coin. There is no procedure to follow, and it is up at random that the particle will find a better optimum.

In the recent literature, different applications for the M-PSO can be found. Wang et al. in [5] applied the algorithm to demonstrate the improvement of the method in multi-objective optimization. This approach can speed up the convergence process, and by using the mutation system, it can increase

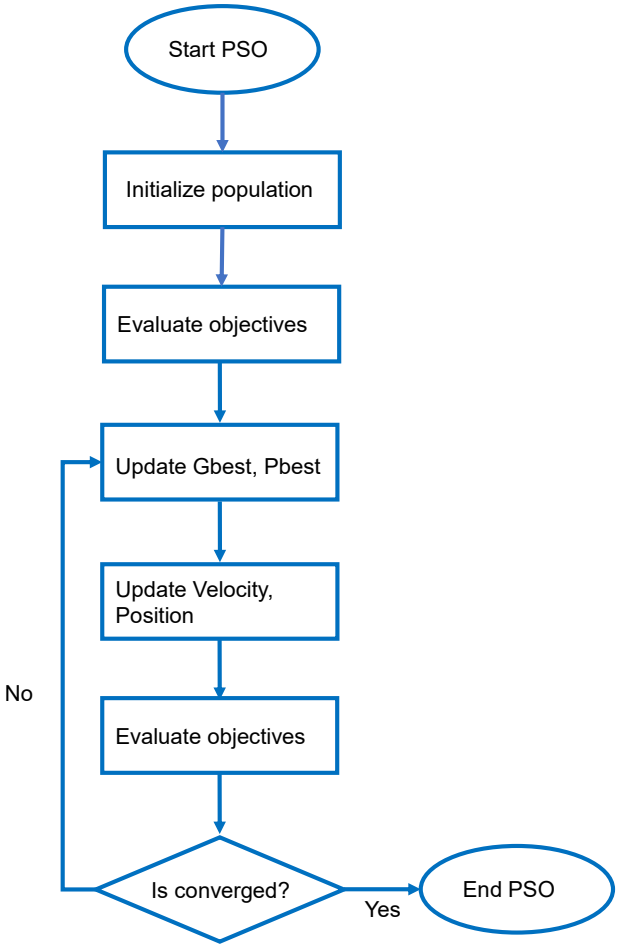

Figure 3.1: Basic PSO optimization scheme.

the randomness of the algorithm, improving the applicability of PSO. Furthermore, increasing the mutation factor can enhance the accuracy of the optimized solution while decreasing the convergence rate. Likewise, when the particle population is low, increasing the population speeds up the optimization process and allows it to reach an optimum outcome in less time. The acceleration constants have a crucial effect on the convergence speed at a greater population level. The weighted optimization technique is a trade-off helpful analysis for converting a multi-objective optimization into a single one.

3.2.3 Centripetal accelerated particle swarm optimization

Centripetal accelerated particle swarm optimization (CAPSO) is one of the most successful proposals to improve the PSO [6]. This new algorithm is based on Newton's laws of motion. CAPSO improves the shortcomings of PSO by quickening the convergence and avoiding local optima. In PSO, if a particle falls into a local optimum, it will sometimes be unable to escape. CAPSO applies mechanical rules of motion and specific terms to the PSO equations to solve the difficulties mentioned earlier. In this method, each particle has four specifications: location, velocity, acceleration, and centripetal acceleration. However, CAPSO does not appear to be a viable alternative when the number of assessments increases. Another technique, with the same acronym, is proposed in [7], which introduces chaos into accelerated PSO.

3.2.4 LSHADE and jSO

Differential Evolution (DE) algorithms are frequently considered one of the most effective population-based evolutionary algorithms for single objectives problems [8, 9]. This paradigm has been used previously and reported a successful improvement of the algorithm capabilities.

Success-History based Adaptive DE (SHADE) was developed from the DE algorithms, which uses mechanisms to adjust different parameters based on success-history adaptation [10]. The LSHADE method incorporates linear population size reduction, which enables a continuous cutback of the population size according to the employed linear function. Setting a large initial population to reduce gradually during the optimization process is necessary. As the algorithm stores in memory the information about the crossover and scale factor performed in all generations, this can lead to a high processing and storage requirement due to a large number of initial particles in comparison to the basic PSO.

Another application of the DE algorithms is the jSO, which is an improved variant of the LSHADE algorithm [11]. This is a single-objective optimization algorithm with a weighted variant of the mutation strategy. The jSO algorithm also uses the linear reduction of population size mechanism technique. However, several characteristics differ, including the initial population at the start of the process and the parameter p, which is connected to current-to-best mutation. In addition, this algorithm has already been used successfully in engineering-related problems and modified to achieve better results [12, 13].

3.2.5 Novelty search

Lehman and Stanley in [14] proposed the Novelty Search paradigm in evolutionary and bio-inspired optimization algorithms. It has recently been used to enhance several optimization algorithms. This concept is based on the idea of an algorithm focusing on an objective function to avoid being trapped in a local optimum, due to the gradient of the employed objective function. Individuals are representations of domain solutions in population-based bio-inspired algorithms. According to the Novelty Search paradigm, nature has no goal other than to evolve, and any consequence of this evolution is due to natural selection. It is merely the accumulation of several occurrences throughout time. Because they do not explore new solutions, evolutionary and bio-inspired algorithms may miss the fundamental solution to the problem, even if they are not necessarily the best match [15]. The main idea of the Novelty Search concept is to avoid and correct that the objective function can direct the optimization solution to a dead end [16].

As said before, bio-inspired or evolutionary algorithms may not find the optimal solution. Analyzing this fact mathematically, this happens because sometimes the best solution to the problem may be located in a region not so attractive to the algorithm, causing the algorithm to no longer search for solutions in this zone [16]. Two main alternatives are trying to solve this problem. The first one is based on the study and adaptation of the objective function to avoid a local optimum of the problem. This approach changes the problem to obtain a solution in a determined search region, which cannot be applied to real problems. The second alternative is to make changes in the algorithm to explore all the search space, including the unattractive regions, while trying to find the best solution. This second strategy has already been applied in the M-PSO algorithm.

This thesis defined the second approach as modifying the PSO algorithm with the Novelty Search concept to improve the optimization process, thus obtaining a new algorithm named Novelty Swarm (NS). The new algorithm is presented in Section 4.5.1, where all the equations are shown. Moreover, the CEC2005 benchmark solutions comparing the NS against other algorithms are presented.

3.2.6 Genetic algorithm

Genetic algorithms (GA) were inspired by human DNA and evolution. Each member of the population can be considered as a chromosome composed of a specific number of genes. The genes represent the parameters that will be

optimized. Traditionally, each member is an array of numbers. This population produces new generations of chromosomes by genetic operators, which combine the genes, or the specific parameters, of each chromosome to obtain a unique individual with a better combination of genes. Figure 3.2 summarizes the GA process.

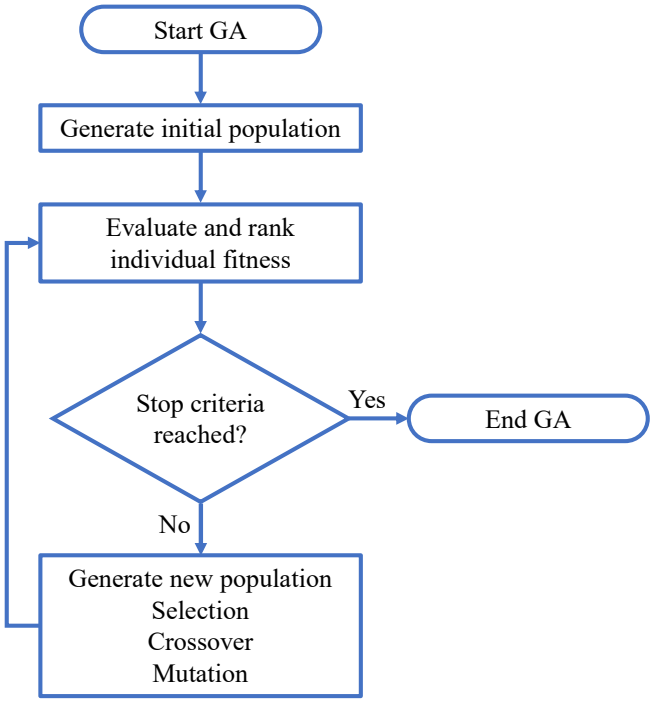

Figure 3.2: Example of GA flowchart application. Adapted from [17].

The first stage is to generate a random beginning population. Each member of the initial population is one chromosome composed of genes. In the following step, the GA evaluates and ranks all the individuals in terms of fitness value. If the convergence criteria are obtained, the algorithm stops. However, if convergence criteria are unobtained, a new generation population is established from the initial population through the arrangement of the better chromosomes. In general, the combination is controlled by three different operators. The first is the selection operator, which is responsible for select-

ing which chromosomes will be responsible for passing on their genes based on the evaluation and ranking of each member of the population. The second is the crossover operator, which is responsible for combining the genes from the parent chromosomes to create a new individual. As the algorithm evolves and the population increases, this algorithm tends to generate similar individuals since only the best characteristics are propagated. The last is the mutation operator, which is responsible for adding mutations to the new chromosomes to create more diversity in the population [17–19].

3.2.7 Neural network

The neural networks (NN) are machine learning models that consist of input neurons that receive the data, one or more hidden layers of neurons with the degrees of freedom of the neural network, and a final layer of output neurons that provide the model result. Figure 3.3 shows a typical architecture of the NN. The lines connecting the neurons are associated with weights and a numeric value.

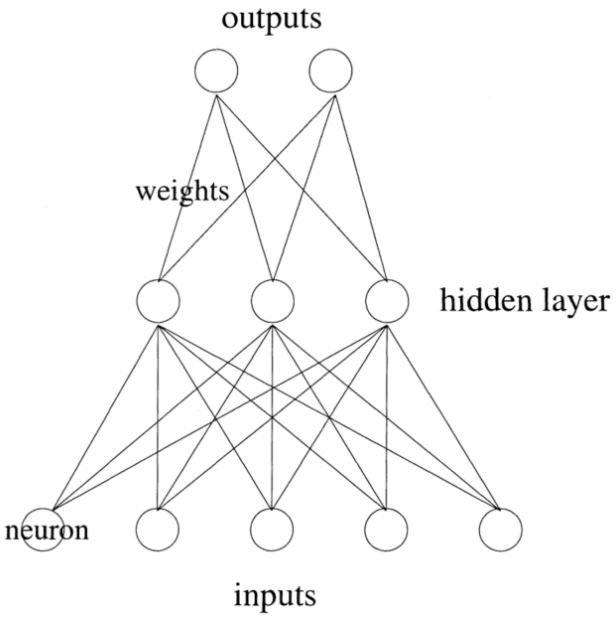

Figure 3.3: NN architecture example. Adapted from [20].

The output, h_i, of neuron i in the hidden layer is calculated by Equation 3.1 as follow,

$$h_i = \sigma(\sum_{j=1}^{N} V_{ij} x_j + T_i^{hid}) \tag{3.1}$$

where $\sigma()$ is called activation function, N the number of inputs, V_{ij} the weights, x_j inputs to the input neurons, and T_i^{hid} the threshold terms of the hidden neurons. The primary goal of the activation function is to introduce non-linearity into the NN, to bound the value of the neuron.

The model training is controlled by methods based on an algorithm called gradient descent, which allows varying the weights of the connections and the biases of the neurons to minimize the model error from the gradient of a cost function. For the operation of this algorithm, it is necessary to know the gradient, and for this purpose, the error back-propagation algorithm is used. This is used to calculate the partial derivatives of a cost function concerning any bias, weight, or skew of the network. From the calculation of the partial derivatives, it is possible to find out how the cost function varies with these parameters within the complex structure of the neural network. An example of a cost function is:

$$C(w,b) = \frac{1}{n} \cdot \sum_{x} \left\| y(x) - a^L(x) \right\|^2 \tag{3.2}$$

where the set of network weights is given by w, the set of biases by b, n is the number of entries 'x' of the environment, a^L represents the output vector, L is the number of layers and $y(x)$ the desired output value. The sum is applied to all entries in the training database.

The analysis of how much responsibility each neuron has in error is performed from the output or error signal to the first layers since, in this type of unidirectional structure, the error of the last layers depends on the error of the previous ones. It is recursively operated layer after layer moving the error backward. In this way, the analysis will serve to know how much to modify each parameter of each neuron in an efficient way, effectively using neurons by means of a single backward propagation.

Returning to the operation of the gradient descent algorithm [21], to locate the minimum an iterative process is triggered, in which each parameter (weights and biases) is subtracted from the partial derivative of the cost function concerning each of them at the evaluation point, multiplied by a learning speed or ratio. The learning speed varies on how fast the algorithm can converge. If the ratio is too low, the computational cost will increase, and the

solution could be a more inefficient local point. At the same time, if the ratio is too high, it could result in the minimum not being found, and the algorithm would not be able to converge if the minimum is not found, entering in an infinite loop.

Equation 3.3 presents the variation of each parameter defined as θ from the gradient of the cost function ($C(z_t\ , \theta)$) and the learning ratio (α), where z_t is an example of the iteration 't' that includes an input part 'x' and a target part 'y'.

$$\theta_{i+1} = \theta_i - \alpha \cdot \frac{\partial C(z_t, \theta)}{\partial \theta} \tag{3.3}$$

The iterative process must always start with small and random values of the weights and biases, both positive and negative. When the change in the parameter update is less than a particular value, denoted as the stop criterion, the execution of the algorithm is terminated.

The number of data used to calculate the gradient of the cost function before the parameters are updated consists of a hyperparameter denoted as 'batch size'. The training data can be divided into as many batches as there are data, and their grouping is random. When divided, Equation 3.3 varies according to Equation 3.4, where 'B' is the batch size.

$$\theta_{i+1} = \theta_i - \alpha \cdot \frac{1}{B} \sum_{t'=Bt+1}^{B(t+1)} \frac{\partial C(z_{t'}, \theta)}{\partial \theta} \tag{3.4}$$

On the other hand, the hyperparameter defined as a number of 'epochs' represents the number of times the learning algorithm uses the total training data. Combining it with the previous hyperparameter, if the data-set has a total of 500 samples, it is divided into blocks of 1 and 25 epochs are defined. Consequently, the parameters will be updated a total of 12500 times, the number of blocks times the number of epochs. From this idea, it is easy to deduce that the larger the number of batches, the more updates there will be per epoch, and the more updates per epoch, the faster the algorithm will learn.

3.3 Summary and conclusions

In this chapter, a review of several essential optimization methods used in recent years has been made. It can be seen that over time optimization algorithms have gained robustness and the ability to solve highly complex problems

in engineering applications. However, at the same time that the algorithms have become more powerful, the case studies, such as the optimization of combustion systems, have also evolved in complexity.

Considering that the non-evolutionary models have limitations due to the complexity of the problem and the need to use several input parameters, these methods have only been briefly described. On the other hand, evolutionary models show great potential for optimizing combustion systems, since they always seek to obtain better individuals. With the passing of iterations of the evolutionary algorithms, the suitability of the population for each problem is checked and evaluated. Generally, these algorithms are applied to issues that have not been extensively explored or are dependent on many input parameters. For these reasons, the novel algorithm, Novelty Swarm, was chosen as the optimization method in this thesis.

References

[1] Kennedy, J. and Eberhart, R. "Particle swarm optimization". In: *Proceedings of ICNN 95 - International Conference on Neural Networks*. IEEE, 1995. DOI: 10.1109/icnn.1995.488968.

[2] Karra, Prashanth and Kong, Song Charng. "Application of particle swarm optimization for diesel engine performance optimization". In: *SAE Technical Papers* (2010). DOI: 10.4271/2010-01-1258.

[3] Bergh, FVD. "An analysis of particle swarm optimizers. PhD Thesis". In: *University of Pretoria, South Africa* (2001). DOI: http://repository.up.ac.za/bitstream/handle/2263/24297/00thesis.pdf.

[4] Chen, Junfeng, Ren, Ziwu, and Fan, Xinnan. "Particle swarm optimization with adaptive mutation and its application research in tuning of PID parameters". In: *2006 1st International Symposium on Systems and Control in Aerospace and Astronautics*. 2006, 5 pp.–994. DOI: 10.1109/ISSCAA.2006.1627490.

[5] Wang, Xi, Ting, David S.K., and Henshaw, Paul. "Mutation particle swarm optimization (M-PSO) of a thermoelectric generator in a multivariable space". In: *Energy Conversion and Management* 224.June (2020), p. 113387. DOI: 10.1016/j.enconman.2020.113387.

[6] Beheshti, Zahra and Siti, Siti Mariyam. "CAPSO: Centripetal accelerated particle swarm optimization". In: *Information Sciences* 258 (2014), pp. 54–79. DOI: 10.1016/j.ins.2013.08.015.

[7] Gandomi, Amir Hossein, Yun, Gun Jin, Yang, Xin She, and Talatahari, Siamak. "Chaos-enhanced accelerated particle swarm optimization". In: *Communications in Nonlinear Science and Numerical Simulation* 18.2 (2013), pp. 327–340. DOI: 10.1016/j.cnsns.2012.07.017.

[8] Neri, Ferrante and Tirronen, Ville. "Recent advances in differential evolution: A survey and experimental analysis". In: 33.1-2 (2010), pp. 61–106. DOI: 10.1007/s10462-009-9137-2.

[9] Das, Swagatam, Mullick, Sankha Subhra, and Suganthan, P. N. "Recent advances in differential evolution-An updated survey". In: *Swarm and Evolutionary Computation* 27 (2016), pp. 1–30. DOI: 10.1016/j.swevo.2016.01.004.

[10] Tanabe, Ryoji and Fukunaga, Alex. "Evaluating the performance of SHADE on CEC 2013 benchmark problems". In: *2013 IEEE Congress on Evolutionary Computation, CEC 2013* 1 (2013), pp. 1952–1959. DOI: 10.1109/CEC.2013.6557798.

[11] Brest, Janez, Maučec, Mirjam Sepesy, and Bošković, Borko. "Single objective real-parameter optimization: Algorithm jSO". In: *2017 IEEE Congress on Evolutionary Computation, CEC 2017 - Proceedings* (2017), pp. 1311–1318. DOI: 10.1109/CEC.2017.7969456.

[12] Shen, Yong, Liang, Ziyuan, Kang, Hongwei, Sun, Xingping, and Chen, Qingyi. "A Modified jSO Algorithm for Solving Constrained Engineering Problems". In: *Symmetry* 13.1 (2021). DOI: 10.3390/sym13010063.

[13] Poláková, Radka and Valenta, Daniel. "jSO and GWO Algorithms Optimize Together". In: *CEUR Workshop Proceedings* 3226 (2022), pp. 159–166.

[14] Lehman, Joel and Stanley, Kenneth O. "Exploiting open-endedness to solve problems through the search for novelty". In: *Artificial Life - ALIFE* (2008).

[15] Lehman, Joel and Stanley, Kenneth O. "Efficiently evolving programs through the search for novelty". In: *Proceedings of the 12th Annual Genetic and Evolutionary Computation Conference, GECCO '10* (2010), pp. 837–844. DOI: 10.1145/1830483.1830638.

[16] Lehman, Joel and Stanley, Kenneth O. "Novelty Search and the Problem with Objectives". In: *Genetic Programming Theory and Practice IX*. Ed. by Rick Riolo, Ekaterina Vladislavleva, and Jason H. Moore. New York, NY: Springer New York, 2011, pp. 37–56. DOI: 10.1007/978-1-4614-1770-5_3.

[17] Voratas Kachitvichyanukul. “Comparison of Three Evolutionary Algorithms :” in: *Industrial Engineering & Management Systems* 11.3 (2012), pp. 215–223.

[18] Clow, Brian and White, Tony. “An evolutionary race: A comparison of genetic algorithms and particle swarm optimization used for training neural networks”. In: *Proceedings of the International Conference on Artificial Intelligence, IC-AI'04* 2 (2004), pp. 582–588.

[19] Hassan, Rania, Cohanim, Babak, De Weck, Olivier, and Venter, Gerhaid. “A comparison of particle swarm optimization and the genetic algorithm”. In: *Collection of Technical Papers - AIAA/ASME/ASCE/AHS/ASC Structures, Structural Dynamics and Materials Conference* 2.April (2005), pp. 1138–1150. DOI: 10.2514/6.2005-1897.

[20] Wang, Sun-Chong. “Artificial Neural Network”. In: *Interdisciplinary Computing in Java Programming*. Boston, MA: Springer US, 2003, pp. 81–100. DOI: 10.1007/978-1-4615-0377-4_5.

[21] Bengio, Yoshua. “Practical Recommendations for Gradient-Based Training of Deep Architectures”. In: *Neural Networks: Tricks of the Trade: Second Edition*. Ed. by Grégoire Montavon, Geneviève B. Orr, and Klaus-Robert Müller. Berlin, Heidelberg: Springer Berlin Heidelberg, 2012, pp. 437–478. DOI: 10.1007/978-3-642-35289-8_26.

Chapter 4

Methodology: Computational tools and numerical model implementation

4.1 Introduction

This doctoral thesis aims to propose a methodology for optimizing the combustion system to reduce pollutant emissions and increase the efficiency of a CI engine. The methodology is based on CFD simulations of the combustion process combined with optimization algorithms. The optimization process implies many simulations that should be prepared, launched, and post-processed in an automated way.

Figure 4.1 presents an overview of the workflow presented in this thesis. The first step is to prepare the model of the combustion process. For this purpose, a reference condition is used relevant to the max power of the engine. The results of the reference model have been validated using experimental data from the same engine, which was tested in CMT-Motores Térmicos laboratories. The second step consists of the calibration of each model used to replicate the physical and chemical phenomena inside the combustion chamber. The following step is the development of the optimization methodology, which comprises the algorithm description and its evaluation compared to benchmark functions. Afterward, the integration between the algorithm and

CFD is presented. Finally, all the tools that have been used to automate the optimization system are presented.

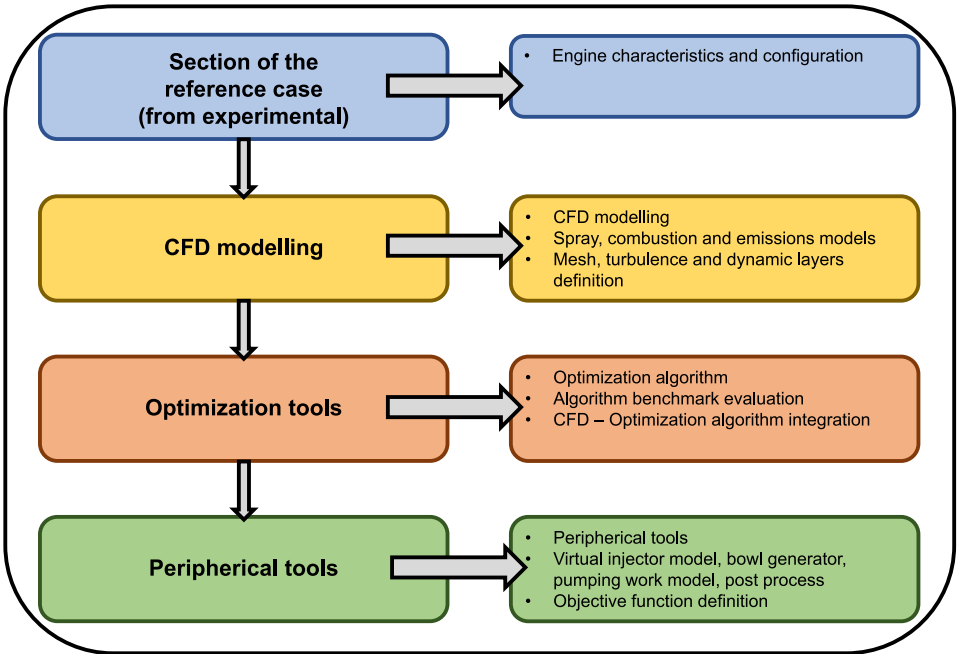

Figure 4.1: Methodology overview.

4.2 Engine characteristics description

An MD CI engine was employed in this thesis. A four-cylinder, 2.2 L diesel engine with turbocharger and common-rail injection. The main specifications of the engine and the injection characteristics are summarized in Table 4.1. The engine was tested at the experimental facilities available at CMT-Motores Térmicos at Universitat Politècnica de València. The experimental data obtained were used to calibrate the CFD engine model. During the experiments, the soot yield was measured with an AVL 439 opacimeter to obtain the particulate mass, and later it was converted to soot density. A Horiba MEXA-7100 gas analyzer measured volumetric concentrations of O_2,CO_2, CO, NO_x, and HC at the exhaust tailpipe.

Moreover, of the engine specification, the boundary conditions of the engine fueled with diesel operating at 3750 rpm and full power were used to

Table 4.1: Engine and injection system configuration.

Engine type	Direct-injection diesel engine
Volume [l]	2.2
Number of cylinders [-]	4
Bore [mm]	85
Stroke [mm]	96
Connecting rod length [mm]	152
Compression ratio [-]	16:1
Nozzle hole number	10
Nozzle hole diameter [μm]	112
Injector total area [m^2]	9.85e-06
Included spray angle [deg]	154
Engine speed [rpm]	3750
IMEP [bar]	18

reproduce the combustion process correctly. These settings were obtained from the experimental data using the CALMEC software and configurated to the CFD model to reproduce the gas characteristics on the IVC instant. The values are summarized in Table 4.2.

Table 4.2: Engine conditions used as boundary conditions of the CFD model.

IVC [cad aTDC]	-112
EVO [cad aTDC]	116
Temperature at IVC [K]	470
Pressure at IVC [bar]	3.89
Fuel mass [mg/cc]	62.4
Number of injections [-]	1
SOI [deg]	-11.5
Injection pressure [bar]	1800
EGR rate [%]	0
Swirl number [-]	2

The indicated mean effective pressure (IMEP), maximum cylinder pressure (P_{max}), pressure gradient (dP/d$theta$), combustion phasing angles, and rate of heat release (RoHR) are the most relevant combustion characteristics studied in this thesis. The experimental data were used to generate the initial thermodynamic conditions and the boundary conditions of wall temperatures and IVC configuration for the first CFD model. The in-cylinder pressure trace

was used as input for an in-house combustion analysis software (CALMEC) to characterize the necessary conditions [1, 2]. This software simplifies the combustion phenomena that occur inside the engine cylinder. From the solution of the equation of the first law of thermodynamics, it is possible to calculate precisely the instantaneous evolution of the energy released by the combustion process. For this, it is necessary to consider the combustion chamber as the control volume independent of the local conditions where this energy is being released.

4.3 Computational approach

To ensure the quality of the results obtained through computer simulation, it is necessary to consider several aspects during the definition and execution of the calculation model. The objective of the computational approach section is to obtain a robust CFD model capable of reproducing the combustion process that takes place inside the combustion chamber of an engine. The CFD simulations were carried out by using the OpenFOAM® technology CFD software [3] with the Lib-ICE code [4–8] coupled to perform the combustion system simulation including a complete pack of solvers for internal combustion engine simulations. The model was developed to accurately represent the cylinder original geometry, taking into account an axis-symmetric sector of the combustion chamber specified in relation to the number of injector holes to shorten the computing time needed to run all the simulations. For the simulations of the experimental case, the sector represents 1/10 of the combustion chamber. A dynamic mesh layering technique was used to reproduce the movement of the piston, which is available in Lib-ICE tools [4, 6].

4.3.1 CFD software and models

The simulations were performed in a closed cycle, which means they start at the instant of intake valve closing (IVC) and end at the exhaust valve opening (EVO) instant. This cycle involves the piston motion and the volume variation during the simulation.

Because of the large number of simulations required during the optimization process, the computational model must be robust enough to reproduce the physics of the problem in a reasonable amount of time. The domain was simplified considering an axisymmetric division of the combustion chamber defined as a function of the number of nozzles. Therefore, the domain of the combustion chamber was 1/10 of the entire geometry.

It is known that the combustion process depends on physical and chemical properties. Several sub-models were used to reproduce each phenomenon in the CFD simulations.

Spray definition

To reproduce the spray properties in OpenFOAM®, the liquid characteristics were simulated using a "Blob" injection method with Lagrangian particles [9–11]. The algorithms of Kelvin Helmholtz (KH)-Rayleigh Taylor (RT) were used to reproduce the spray atomization. The evaporation model is based on the Spalding number.

In all simulations, the in-cylinder gas turbulence was modeled using the Reynolds-Averaged Navier Stokes (RANS) procedure with a re-normalized group (RNG $k-\epsilon$) [12].

An N-Heptane surrogate fuel was used to reproduce the physical fuel properties of the Diesel [13, 14], It is well-known for providing a reasonable assessment of spray parameters such as liquid length. The chemistry model of the fuel was reproduced by a chemical kinetic mechanism that contains 162 species and 1543 reactions.

Combustion model definition

The Representative Interactive Flamelet (RIF) model approach was used for the combustion simulation. The model is based on the laminar flamelet concept and assumes that the smallest turbulence time and length scale are much larger than the chemical scales and that it exists a locally undisturbed sheet where reactions occur [15]. This sheet can be treated as an ensemble of stretched counter-flow diffusion flames, called flamelets, that configures the flames structures as a set of unsteady diffusion flames representing diesel combustion. Thus, the temporal evolution of all reacting scalars depends on the mixture fraction (Z) variable. Moreover, the mixture fraction is related to the local fuel-to-air ratio for non-premixed combustion. The local chemical composition is estimated from the Z present in the CFD domain, assuming that a β-pdf can represent its sub-grid. Then, the transport equations for mixture fraction and its variance should be solved by:

$$\frac{\partial \bar{\rho}\widetilde{Z}}{\partial t} + \nabla\left(\bar{\rho}\tilde{U}\widetilde{Z}\right) - \nabla\left(\widetilde{\mu_t}\nabla\widetilde{Z}\right) = \dot{S}_Z \tag{4.1}$$

$$\frac{\partial \bar{\rho}\widetilde{Z''^2}}{\partial t} + \nabla\left(\bar{\rho}\tilde{U}\widetilde{Z''^2}\right) - \nabla\left(\widetilde{\mu_t}\nabla\widetilde{Z''^2}\right) = 2\frac{\widetilde{\mu_t}}{Sc}\left|\nabla\widetilde{Z}\right|^2 - \bar{\rho}\tilde{\chi} \tag{4.2}$$

where ρ is the density, U represent the velocity, and μ_t means the turbulence viscosity. The liquid mass evaporation rate per unit volume is represented by the $\dot{S}_Z$ and the sink term in 4.1 represents the average scalar dissipation rate being a function of the turbulent time scale and mixture fraction variance as the following equation:

$$\tilde{\chi} = C_\chi \frac{\tilde{\varepsilon}}{\tilde{k}} \widetilde{Z''^2} \tag{4.3}$$

where C_χ was set to 2 in this work, ϵ and k represents the dissipation rate and the turbulent kinetic energy, respectively.

Multiple flamelets can be used to properly account for local flow and turbulence effects on flame structure and predict flame stabilization. Each one represents a specific portion of the injected fuel mass, and the chemical composition in each cell is then computed from the mixture fraction and flamelet marker distribution as follows:

$$\tilde{Y}_i(\vec{x}) = \sum_{i=1}^{N_f} M_j \int_0^1 Y_{j,i}(\tilde{Z}) P(\tilde{Z}, \widetilde{Z''^2}) dZ \tag{4.4}$$

The transport equation that must be solved for each flamelet marker is represented by:

$$\frac{\partial \bar{\rho} \widetilde{M_j}}{\partial t} + \nabla \left(\bar{\rho} \tilde{U} \widetilde{M_j} \right) - \nabla \left(\frac{\widetilde{\mu_t}}{Sc_t} \nabla \widetilde{M_j} \right) = \dot{S_{M_J}} \tag{4.5}$$

where the term corresponding to the source term $\dot{S}_Z$ is now $\dot{S}_{M_J}$ only for a specified range of the injection duration while being kept at zero for points outside this range. Moreover, the flamelet markers must satisfy the following relation:

$$Z = \sum_{i=1}^{N_f} M_j \tag{4.6}$$

The local flame structure is defined by the following flamelet equation that is solved assuming unity Lewis number [16] in the mixture fraction space:

$$\rho \frac{\partial Y_i}{\partial t} = \rho \frac{\chi_Z}{2} \frac{\partial^2 Y_i}{\partial Z^2} + \dot{\omega}_i \tag{4.7}$$

$$\rho\frac{\partial h_s}{\partial t} = \rho\frac{\chi_Z}{2}\frac{\partial^2 h_s}{\partial Z^2} + \dot{q}_s + \frac{dp}{dt} \tag{4.8}$$

wherein the Equation 4.7 Y_i is the mass fraction of the species i, and the $\dot{\omega}_i$ is the chemical source term of species i. In Equation 4.8, the h_s represents the sensible enthalpy and $\dot{q}_s$ the heat released by the chemical reactions. Both equations are solved on a 1-D mesh with the finite volume method by employing an ODE stiff solver to solve the chemical problem to compute $\dot{\omega}_i$. The effects of mixing related to turbulence and flow-field are grouped into the scalar dissipation rate term χ_Z as:

$$\chi_Z = \widehat{\chi_{st,J}}\frac{f(Z)}{f(Z_{st})} \tag{4.9}$$

In Equation 4.9 the $f(Z)$ has an *er fc*-profile [17], while the scalar dissipation rate at stoichiometric mixture fraction conditions $\widehat{\chi_{st,J}}$ for each flamelet is computed as an average of the local values in each computational cell through the next equation:

$$\widehat{\chi_{st,J}} = \frac{\int_V M_j \chi_{st,l}^{3/2}\rho P(Z_{st})dV'}{\int_V M_j \chi_{st,l}^{1/2}\rho P(Z_{st})dV'} \tag{4.10}$$

where P is the β-pdf function, whose parameters depend on the mixture fraction and variance, and for each cell of the domain, the local stoichiometric scalar dissipation rate is computed based on the Hellstrom formulation [16]:

$$\chi_{st,l} = \frac{\chi}{\int_0^1 \frac{f(Z)}{f(Z_{st})}\tilde{P}(Z)dZ} \tag{4.11}$$

In the mixture fraction space, the flamelet equations (Equation 4.7 and 4.8) are initialized by the pure mixing solution as:

$$Y_i(Z) = (1-Z)\cdot Y_{i,air} + Z\cdot Y_{i,fuel} \tag{4.12}$$

$$h_s(Z) = (1-Z)\cdot h_s(T_{air}) + Z\cdot h_s(T_{fuel}) \tag{4.13}$$

where $Y_{i,air}$ and $Y_{i,fuel}$ represent the species mass fraction on the air and fuel sides, respectively. T_{air} and T_{fuel} are the temperature on the air and fuel. The $Y_{i,air}$ is initialized according to the initial conditions in the CFD domain considering only the species of CO_2, O_2, H_2O, and N_2, and they are kept fixed during the simulation. Moreover, the T_{air} is initialized according to the initial

conditions in the domain and then varies with the pressure derivative (dp/dt) term. For the fuel, T_{fuel} is kept constant during the simulation.

The operation of the RIF combustion model is represented in Figure 4.2. This figure illustrates the mutual interactions between the CFD and flamelets domains. At each time-step, an average stoichiometric scalar dissipation rate values are passed to each flamelet, which solves the Equations 4.7 and 4.8 accordingly. The chemical composition in the CFD domain is computed from the mixture fraction, its variance, and the flamelet marker distribution. Temperature is updated from new chemical composition and total enthalpy, whose variation is only due to flow and spray evaporation. More information about its implementation with Lib-ICE is available in [8, 18–21].

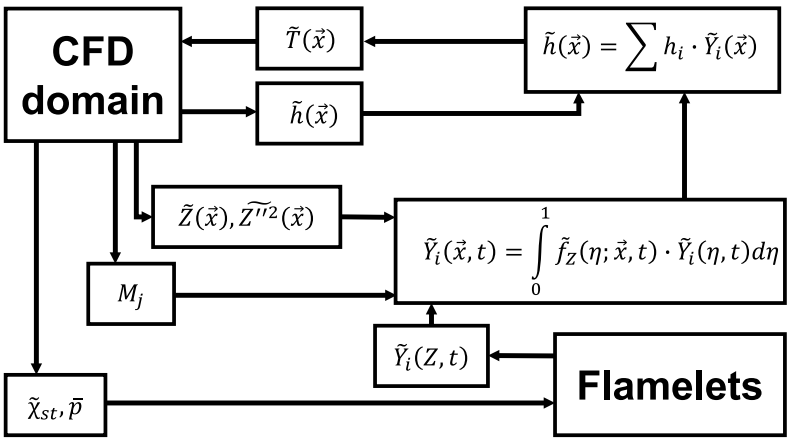

Figure 4.2: Operation of the representative interactive flamelet model (RIF) and interaction between flamelets and CFD domain. Adapted from [22].

Emissions modeling

Concerning the emissions, the Zeldovich mechanism [23] was used to evaluate NO_x emissions. In this model, the NO_x emissions are considered only NO, and its principal source is the oxidation of atmospheric nitrogen. The mechanism of NO formation is assumed to be formed as:

$$N + NO \leftrightarrow N_2 + O \tag{4.14}$$

$$N + O_2 \leftrightarrow NO + O \tag{4.15}$$

$$N + OH \leftrightarrow NO + H \tag{4.16}$$

The semi-empirical model presented by Leung et al. [24] was used to determine soot production and oxidation.

4.4 Model validation

The present section shows the validation and calibration of the models used in this work. First, different meshes configurations will be evaluated to establish the one that will be used to perform the optimizations based on the better compromise between result quality and time of the simulation. Furthermore, the turbulence models $k-\epsilon$, $k-\epsilon$ RNG, and $k-\omega$ SST are evaluated. Moreover, the Angelberger, Han and Reitz, Hu et al., and Rakopoulos heat transfer models were tested to analyze how each one affects the simulation and the better option for this study.

The usual validation method in CI engines is performed by comparing the in-cylinder pressure and the rate of heat release (RoHR) traces obtained from the simulations against experimental results. Furthermore, the simulations are defined by the closed engine cycle, from IVC to EVO instants.

4.4.1 Mesh independence study

One of the most critical conditions in a CFD simulation is the mesh definition which provides an accurate solution in a reasonable time. Thus, a mesh independence study was performed to estimate the best discretization of the domain, aiming for the best trade-off between results quality and simulation time. The meshes were generated with a dedicated tool to produce hexahedral meshes oriented with the spray angle. This tool is based on python code developed in Politecnico di Milano and described in [6]. The code was customized in this thesis to obtain a better cell morphology according to the piston bowl shape. The 2D area is divided into three regions: the spray, layer, and piston. The mesh is generated from a set of parameters imposed by the user. Figure 4.3 shows all the meshes tested in this study at TDC. The number of processors, cells at IVC, and TDC of each mesh are described in Table 4.3.

Figure 4.4 compares the experimental and simulated results in terms of in-cylinder pressure and RoHR of all meshes. In general, all simulations performed for the different meshes show pressure results in agreement with the

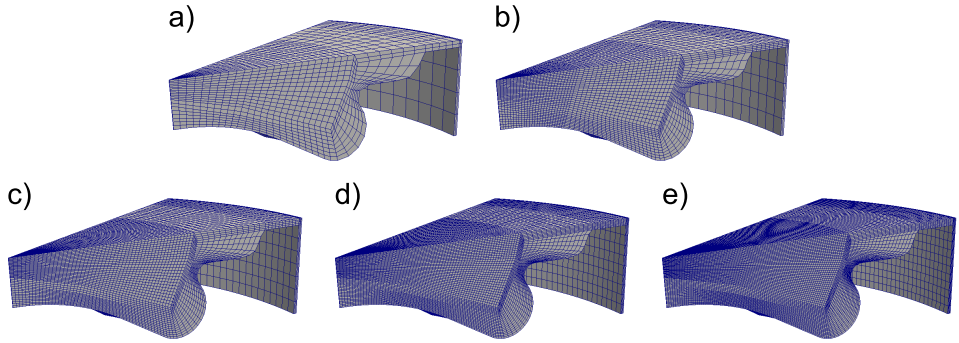

Figure 4.3: Mesh independence consideration: representation of the tested meshes in the first strategy: a) Mesh 1, b) Mesh 2, c) Mesh 3, d) Mesh 4, and e) Mesh 5.

Table 4.3: Mesh independence study: Tested mesh cells.

Case	Cells in IVC	Cells in TDC	Number of processors
Mesh 1	161310	9120	9
Mesh 2	264105	25560	9
Mesh 3	398160	53880	9
Mesh 4	655275	108075	9
Mesh 5	958080	178320	9

experimental values. When it comes to RoHR, it can be seen that the more refined the mesh, the higher the peak in the premixed phase of combustion. At the same time this occurs, more refined meshes show a reduction in heat transfer values during the diffusive phase of combustion. This effect increases the combustion duration in this stage.

Figure 4.5 shows the comparison between the NO_x emissions results and the simulation time needed to complete a simulation for each mesh. Notably, the CFD model has more deviation in the emission predictions for coarse meshes, overestimating the experimental value due to higher in-cylinder temperatures. After a certain mesh configuration, the calculations stabilize and converge to emission values closer to the experimental ones. On the other hand, it is also possible to see that the more refined the mesh is, the more computational time is required to perform the calculation as depicted in the right side plot in Figure 4.5.

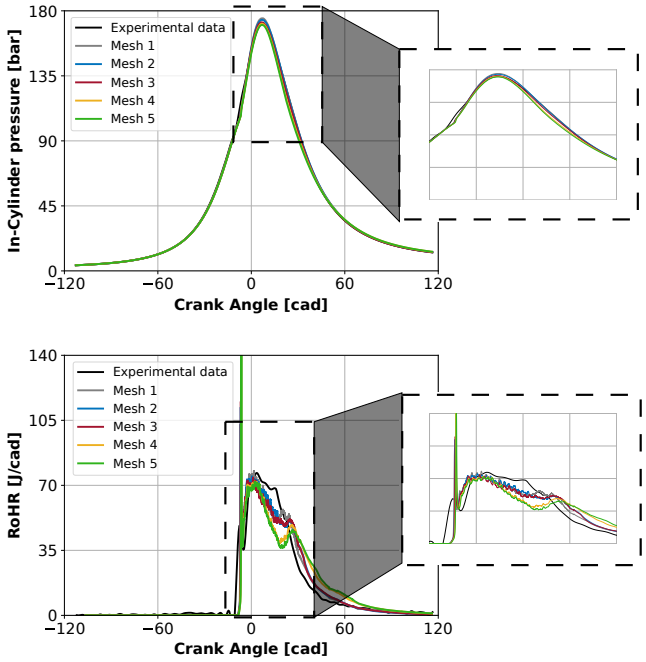

Figure 4.4: Mesh independence study: In-cylinder pressure and RoHR comparison between experimental data and simulations results.

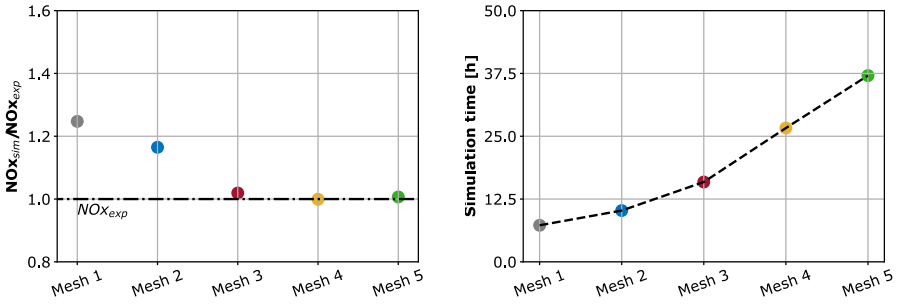

Figure 4.5: Mesh independence study: effect of the mesh in NO_x emissions (left) and simulation time (right).

After this analysis, Mesh 3 was chosen because it has a good relationship between results and computational time. This mesh will be called "fine mesh" in the thesis. However, considering the high number of simulations performed

during the optimization process, employing a different strategy to the use of nine processors for each case is very costly. The next step was to obtain a new mesh configuration to reduce the computational time or processor number. It was decided to discretize the domain using fewer number of cells (with bigger sizes) in the regions where the gradients are not so high, but applying a refinement to the piston wall, by using a boundary layer. Again, 5 different meshes were tested. Besides, in this second strategy, the number of processors used for the simulation was reduced to 4. This number was selected based on the capabilities of the cluster used in this research to ensure that 40 different simulations can be launched simultaneously during the optimization process, as explained later on. Figure 4.6 shows all the meshes tested in TDC instant, and Table 4.4 describes the number of cells in IVC, TDC, and also the number of processors used for each simulation.

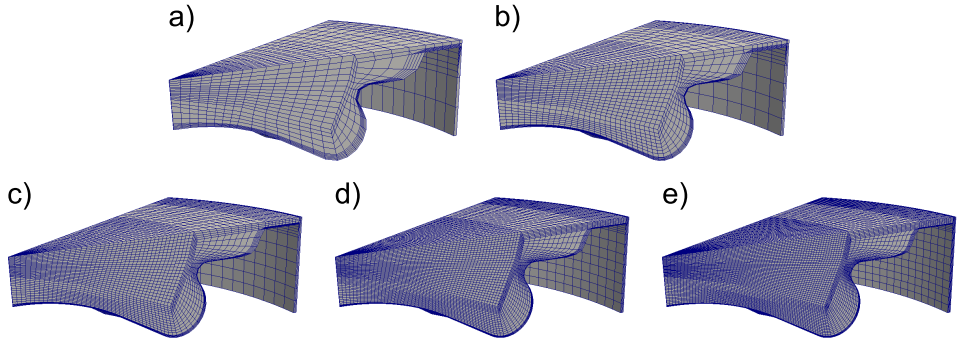

Figure 4.6: Mesh independence study: representation of the tested meshes in the second strategy: a) Mesh 1, b) Mesh 2, c) Mesh 3, d) Mesh 4, and e) Mesh 5.

Table 4.4: Mesh independence study: Tested mesh cells in the second strategy (with additional boundary layers).

Case	Cells in IVC	Cells in TDC	Number of processors
Mesh 1	84040	6564	4
Mesh 2	112527	12492	4
Mesh 3	203100	26628	4
Mesh 4	332790	53205	4
Mesh 5	490914	134856	4

With the results of these new CFD simulations for the simplified mesh, a comparison against the experimental results of in-cylinder pressure and RoHR is presented in Figure 4.7. All tested meshes agree with the experimental data for in-cylinder pressure. The simulations well reproduce the compression phase. Some differences appear in the maximum pressure value, where using a coarse mesh leads to higher pressure values due to the less amount of cells which causes more instabilities during the calculations. On the other hand, in terms of RoHR, it is possible to see that there are differences between the meshes. The bottom of Figure 4.7 shows the RoHR trace over the cycle simulation, showing that as the mesh refinement increases, the diffusive phase of combustion increases since with more cells in the mesh, it is possible to obtain a better representation of all physical and chemical phenomena that occur during the combustion process. Moreover, using a finer mesh, the peak of RoHR during the premixed phase increases considerably because the finer mesh is capable of better reproducing the start of the combustion inside the chamber.

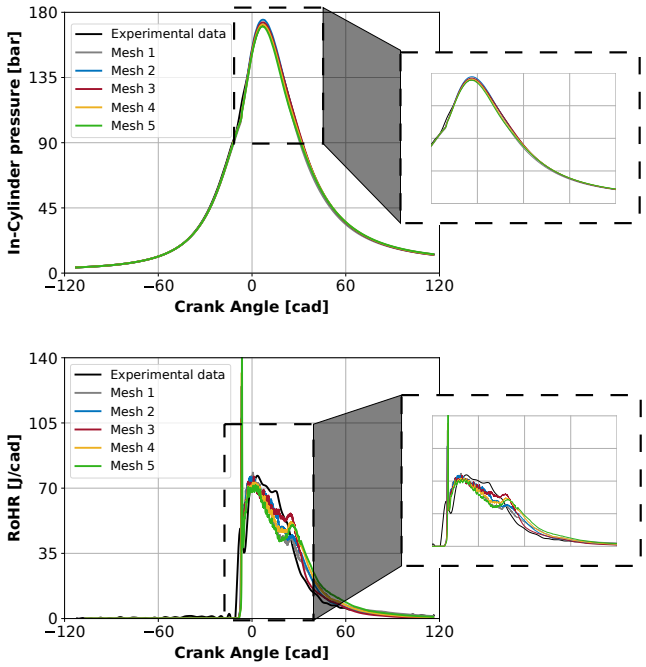

Figure 4.7: Mesh independence study, second strategy: In-cylinder pressure and, RoHR comparison between experimental data and simulations results.

Moreover, the NO_x emissions of each mesh configuration were compared against the experimental value, which can be seen in the left part of Figure 4.8. The more refined the mesh, the better the predictions of NO_x emissions from the computational code, and closer to the experimental values are the results, but increasing the simulation time and amount of resources needed. On the other hand, Mesh 1, which is very simplified, can perform the simulation in a shorter time and is not able to predict emissions correctly.

From the analysis of the two strategies used to define the best configuration, Mesh 3 was selected for the simulations during the different optimizations in this thesis. This mesh configuration presents results in agreement with the experimental data, within a feasible error range of NO_x emissions (lower than 20%) while the time of the simulation is around 15h using 4 processors. At the first moment this error value, around 20% in NO_x emissions, may seem excessive. However, in the case of an optimization process where thousands of simulations will be performed, an increase of 4 hours in the time for each of the simulations is reflected in an increase of several days and resources for the study. An important point to note is, even with this difference between the experimental and simulated value, this mesh configuration manages to capture the combustion behavior in CI engines well. From now on, this mesh will be called "coarse mesh," and it will be used to perform all the subsequent simulations.

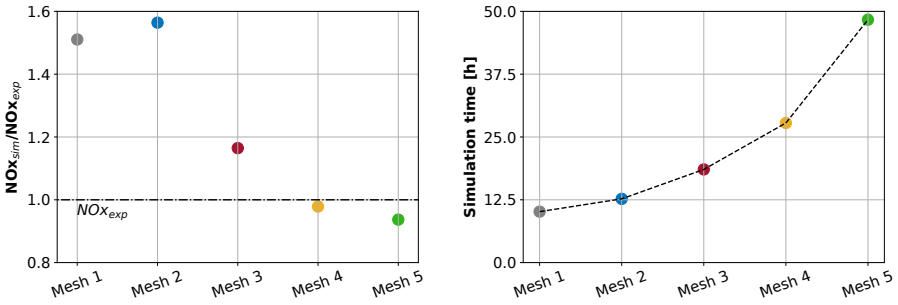

Figure 4.8: Mesh independence study, second part: effect of the mesh in NO_x emissions (left) and simulation time (right).

4.4.2 Turbulence modelling evaluation

The turbulence modeling is one of the most critical and limiting factors for accurate CFD simulations. The in-cylinder turbulence used in this thesis

was modeled by Reynolds-Averaged Navier Stokes (RANS) due to its faster calculation time when compared to simulations using other methodologies, such as Large Eddy Simulation (LES). Considering the variety of models used to simulate CI engines, the standard $k-\epsilon$, $k-\epsilon$ RNG (Re-Normalized Group), and $k-\omega$ SST (Shear Stress Transport) models were evaluated. The standard $k-\epsilon$ model uses two transport different partial equations (PDE) with two variables, the turbulent kinetic energy (TKE) and the rate of the dissipation of TKE. This model shows a good prediction far from the regions of the wall, which has a significant effect in ICE due to the complex geometry combined with high Reynolds numbers [25–29]. The model $k-\epsilon$ RNG accounts for critical physical aspects of flame propagation at engine conditions, such as compressibility effects [30, 31]. This model uses RNG methods to account for the effects of smaller scales of motion. Moreover, it can be used to derive a turbulence model similar to the $k-\epsilon$, resulting in a modified form of the ϵ equation, which attempts to account for the different scales of motion through changes to the production term. Another alternative tested was the $k-\omega$ SST model. This model uses the original $k-\omega$ model behavior in the regions near the walls, providing a better description of flow curvature and boundary layer development on the flat wall after jet impingement. In the regions far from the walls, this model approximates the behavior of the $k-\epsilon$ model that is appropriate for free jet flows [22, 32].

Each model was tested using the coarse mesh shown in 4.4.1, which were performed with a real operation condition of injection, geometry, and the original boundary conditions at IVC. Figure 4.9 shows the results of in-cylinder pressure and RoHR for all tested turbulence models. Both $k-\epsilon$ and $k-\epsilon$ RNG agree with the experimental data since one model is derived from the other for both in-cylinder pressure and RoHR. When using the $k-\epsilon$ model as a basis for the $k-\epsilon$ RNG approach, we observed similar results for both cases in terms of in-cylinder pressure and RoHR. Additionally, the models were able to accurately replicate the variation in tangential velocity and turbulence intensity. Moreover, they are widely used to predict the penetration and diffusion of jets. Little differences are observed in the diffusive phase of the combustion, where the model $k-\epsilon$ RNG presents a slight duration and reproduces better the experimental setup due to its better capability to predict more realistic large-scale flame structures.

On the other hand, the model $k-\omega$ SST agrees with the experimental values during the compression and premixed phase of the cycle. However, the combustion in the diffusive phase has lower values when compared to the other models, and presents a shorter diffusive phase. Once the $k-\omega$ SST model is coupled with the methodology of $k-\omega$ and $k-\epsilon$ in the same model, this

difference comes from the mesh used to perform the simulation. As reported by Zhou et al. in [22], it was necessary to adopt a mesh twice as refined as the mesh adopted for the simulation using the $k - \epsilon$ model, especially in the near nozzle region thus compromising the trade-off between simulation result and time. The lower energy release can be seen in the value of the maximum in-cylinder pressure, which is lower than the experimental and reflected in lower combustion efficiency as shown in the bottom graph of Figure 4.9.

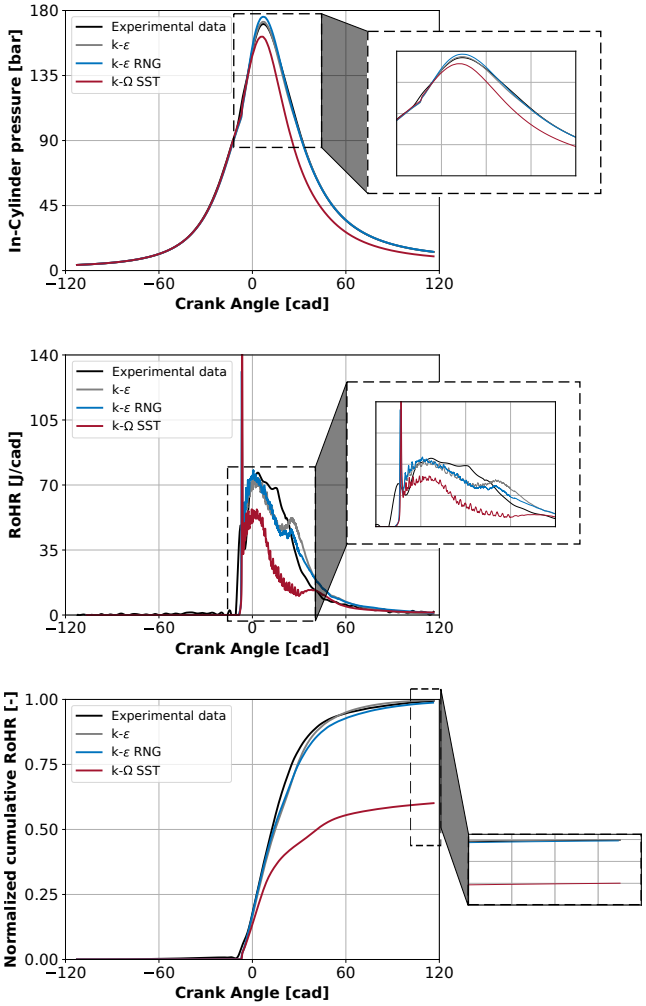

Figure 4.9: Turbulence modeling study: In-cylinder pressure, RoHR, and normalized cumulative RoHR.

Figure 4.10 compares the temperature distribution fields of the standard $k-\epsilon$, $k-\epsilon$ RNG, and $k-\omega$ SST cases between crank angles -5 and 15. It is possible to see that for the simulation using the $k-\epsilon$ RNG model, there is a higher temperature after the crank angle 5 inside the combustion chamber compared to the simulation of the $k-\omega$ SST case. This higher temperature from compression causes the fuel to ignite earlier. Also, the spray for the $k-\epsilon$ RNG case appears thinner than the $k-\omega$ SST case, causing more fuel to impingement on the cylinder head. At the same time, the highest temperatures appear around the stoichiometric zone, represented by the white line, and it can be seen that for the $k-\epsilon$ RNG case, this zone extends to the piston step and also almost until the squish zone, which is not happening for the $k-\omega$ SST case.

Based on the results obtained, it was decided that the $k-\epsilon$ RNG model will be used as a basis for all the following simulations since it presents results closer to the experimental one when compared to the other two models. Moreover, the simulations using $k-\epsilon$ RNG and $k-\epsilon$ models took around 14 hours, while the simulation using the $k-\omega$ SST model needed 3 times as long to complete. An important remark for the results obtained for the $k-\omega$ SST model is that the simulation presents a different trend from those found in the literature [22, 32]. Still, it is essential to note that the variables adopted for this model are the software standards without any adjustment. The model is also more susceptible to errors since the mesh is not so refined.

4.4.3 Mesh layering study

The correct definition of the dynamic mesh layers parameter is important because it directly affects the simulation quality. This parameter is responsible for adding new layers of cells to the domain as the piston moves up and down. Thus, an inappropriate value can result in the addition of insufficient cells or tiny cells that distort the mesh, decreasing the quality of the results.

With the defined mesh and the turbulence model already selected, five different mesh layering configurations were tested, and the specifications are shown in Table 4.5. Moreover, this parameter influences the case generation, requiring more or less time for the correct creation of the moving mesh used in all the simulations and increasing the cells number that are added to the domain.

Figure 4.11 shows the comparison of the results between these five tested cases against experimental data. The differences in in-cylinder pressure are not sensitive to variations of the layering size, being the maximum variation of

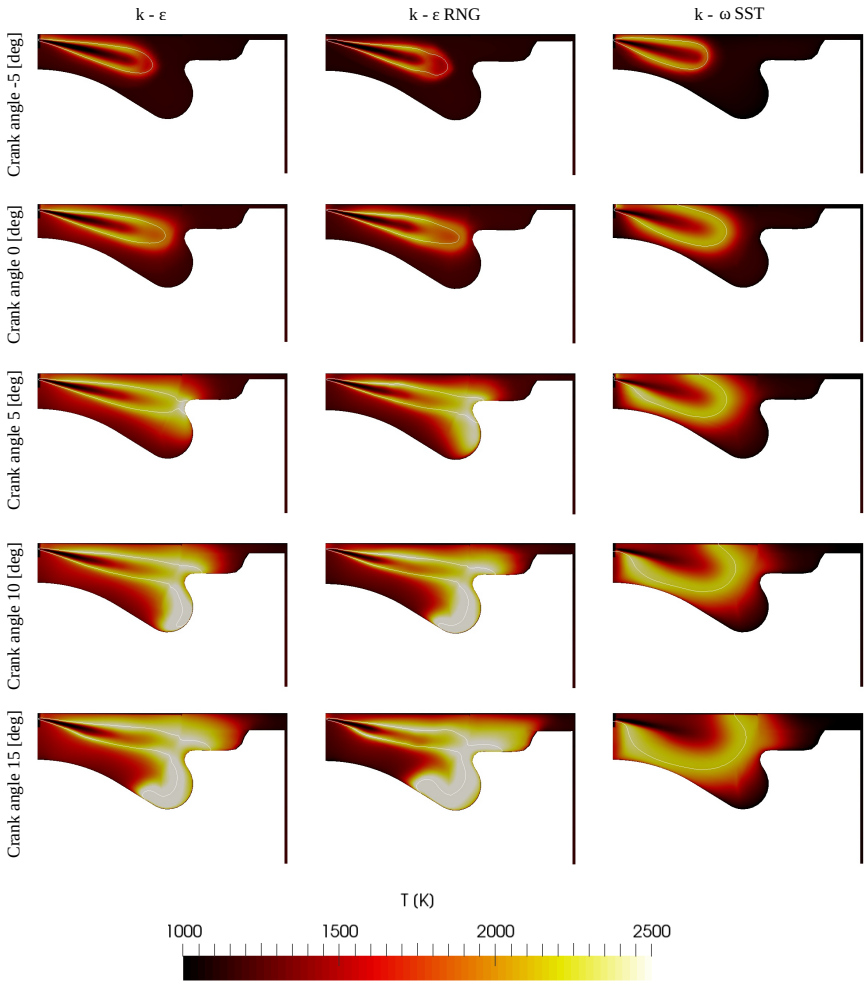

Figure 4.10: Temperature contours: comparison between $k-\epsilon$, $k-\epsilon$ RNG, and $k-\omega$ SST models.

1.5% for Case 5. There is a more significant difference between the results for the in-cylinder mean temperature, where Cases 4 and 5 show a temperature peak a little closer to the experimental trace but with more difference at the end of the cycle. Besides this, the Cases 1 and 2, more refined cases, the differences between the peak of the in-cylinder temperature are higher, showing results equal to the experimental during the expansion. With the RoHR, it is possible to observe consistent behavior. As smaller cells are added with the mesh movement, less constant with is the RoHR, there is a higher

Table 4.5: Dynamic mesh layering definition.

Case	Minimum value	Maximum value
Case 1	2.5E-5	1.0E-4
Case 2	5.0E-5	2.0E-4
Case 3	1.0E-4	4.0E-4
Case 4	2.0E-4	8.0E-4
Case 5	4.0E-4	1.6E-3

difference between the maximum and minimum value of heat transfer, during the diffusive phase of combustion, thus causing a slower phase. Analyzing the normalized cumulative RoHR is possible to see that the differences are small, the size of the layer added in the domain does not affect, in absolute values, the amount of energy transferred during the simulation.

Based on the results, the configuration of Case 3 was chosen for the next simulations due to the good agreement between the results. Once this setup presents intermediate results in terms of in-cylinder pressure and temperature, a lower peak in RoHR during the premixed phase of the combustion obtained values similar to the experimental values for the total energy released during the cycle. Moreover, as already mentioned, the dynamic mesh layering definition impacts the time to generate each case since the processing time was 9180s, 4260s, 1980s, 1260s, and 720s for each case (1, 2, 3, 4, and 5), respectively. Case 3 shows the better trade-off between time-results quality thus being defined as the basis for the next simulations.

4.4.4 Heat transfer evaluation

A critical aspect of a CFD simulation and combustion system optimization proceeding is the study of heat transfer over the combustion chamber walls [33–37]. The correct analysis of this parameter influences the power and efficiency of the engine since the more heat is lost by the walls, the less power is transferred to the crankshaft. Furthermore, this also affects the thermal energy going out with the exhaust gases, which is a critical aspect of the after-treatment system. Another effect of the importance of the heat transfer evaluation is the NO_x formation since it mostly depends on the temperature inside the combustion chamber.

To provide a reliable prediction of the heat transfer with the boundaries, all the heat transfer models available in the OpenFOAM-based code combined with LibICE were tested to define the best option for the optimization process.

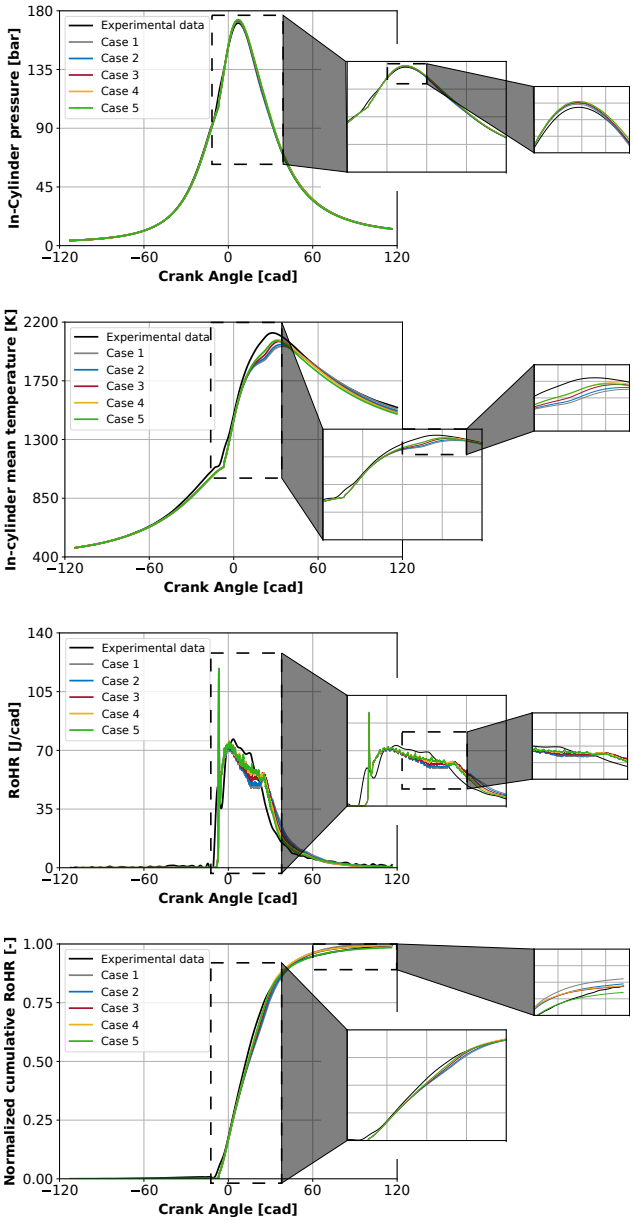

Figure 4.11: Dynamic mesh layering study: In-cylinder pressure, in-cylinder mean temperature, RoHR, and normalized cumulative RoHR comparison.

The simulations were performed using the Angelberger, Han and Reitz, Hu et al., and Rakopoulos models [38–41].

Figure 4.12 compares in-cylinder pressure, temperature, RoHR, and cumulative HR of all tested cases against the experimental data. It is possible to see that the Han and Reitz model [39] underestimates the in-cylinder pressure and temperature values compared to the experimental data. The temperature difference can cause an improper prediction of NO_x emissions once this compound depends on the temperature, and its production grows exponentially with temperatures higher than 1800 K. On the other hand, the different models present a behavior similar to the experimental data, with little overestimating the in-cylinder pressure. Moreover, the Huh et al. [40] model has a higher maximum pressure value, almost reaching 180 bar of pressure, which is the operation security limit established for the engine. Angelberger and Rakopoulos models show similar behavior for all outputs computed in Figure 4.12. It is possible to see some differences in the maximum value of in-cylinder temperature, where the Rakopoulos model underestimate the value. Thus, the normalized cumulative RoHR of all cases shows a good agreement with the experimental data regarding combustion characteristics with a combustion performance of around 99%.

Figure 4.13 compares the results of the heat transfer rate through each wall of the combustion chamber. The total heat transfer rate value corresponds to the sum of the liner, cylinder head, and piston heat transfer. The Han and Reitz model [39] shows the most discrepant results seeming to overestimate the heat transfer for all boundaries. Besides, Huh et al. [40] seems to underestimate the heat transfer through the piston. Angerlberger and Rakopoulos models [38, 41] show similar results. The Angelberger model was chosen for future simulations due to the quality of the results, the smaller peak in the premixed phase of the combustion than the Rakopoulos model, and also because it is already used in simulations of internal combustion engines [42, 43].

The differences between the results for each of the models can occur due to several factors. The turbulent Prandt number was used to simplify and calculate the turbulent thermal diffusivity as the ratio of turbulent viscosity to Prandt number, which allows the results to be fine-tuned using the Prandt value in each of the models. Also, with the simplifications of each of the models, it is possible to comprehend that not all the effects within the combustion chamber can be captured in the simulations. However, it is possible to understand the behavior and how the heat transfer is split into each of the wall regions. In addition, it is important to know that each of the models can best reproduce specific results in their inherent characteristics. Thus, the Huh et

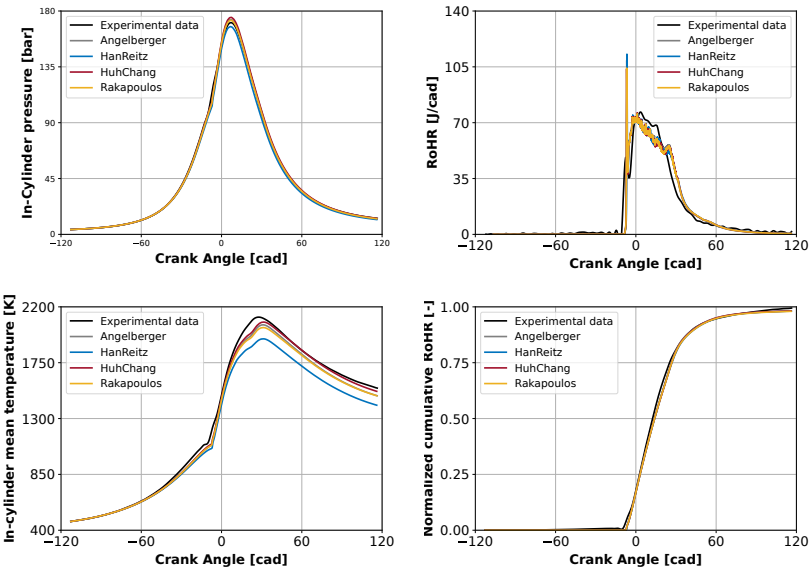

Figure 4.12: Wall heat transfer model evaluation: In-cylinder pressure (top-left), RoHR (top-right), In-cylinder mean temperature (bottom-left), and normalized cumulative RoHR (bottom-right).

al. model is expected to provide better results when applied to cases with a high compression ratio. The Angelberger model reproduces wall heat transfer well in diesel engines, especially at high compression ratios, on the other hand, in spark ignition engines, it underestimates heat transfer. The Han and Reitz model has a fairly simple formulation but manages to capture the trends during compression and expansion correctly. However, some difficulties are encountered just after TDC, where it fails to capture negative trends. It can be used for both SI and CI engines at high and low speeds. The Rakopoulos model is accepted for heat transfer calculation for both SI and CI engines and shows good prediction during the compression stroke, but with some less predictive results right after TDC since cylinder pressure is a key parameter in its equation [37, 41, 44].

4.4.5 Numerical results: validation and discussion

After defining the mesh, models, and sub-models that will be used in all simulations during the optimizations, it can be pointed out that:

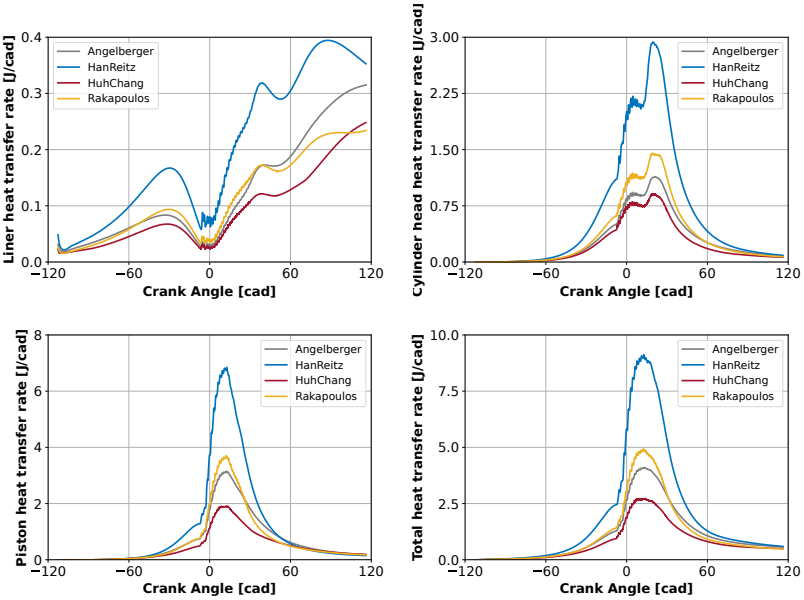

Figure 4.13: Comparison of the heat transfer rate for all cylinder components and total heat transfer.

- The mesh and the layering configuration were established based on the trade-off between the quality of the results and simulation time.
- The turbulence model selected is the RANS method, specifically the $k-\epsilon$ RNG model, due to its capability to provide good results with a less fine mesh in a faster computational time.
- Angelberger heat transfer model was coupled with the turbulence approach in order to estimate the wall heat transfer quantities.

Table 4.6 resumes all the models and sub-models selected to perform the simulations.

To resume the suitability of the model configuration, both cases, fine and coarse mesh, were simulated and compared again with all the actualized configurations and the operating conditions described in Table 4.1 and Table 4.2. Figure 4.14 shows a comparison between the fine and coarse mesh.

Figure 4.15 shows the in-cylinder temperature, RoHR, and normalized cumulative HR. Those figures present good agreement between experiments and simulations for both meshes. In terms of in-cylinder pressure, there are

Table 4.6: Models specifications.

	Model
Turbulence	RNG $k-\epsilon$ [RANS]
Combustion	RIF
Wall heat transfer	Angelberger
Injector	Blob injector
Break-up	KH-RT
Evaporation	standard
Collision	off
NO_x	Zeldovich
Soot	Leung Lindstedt Jones

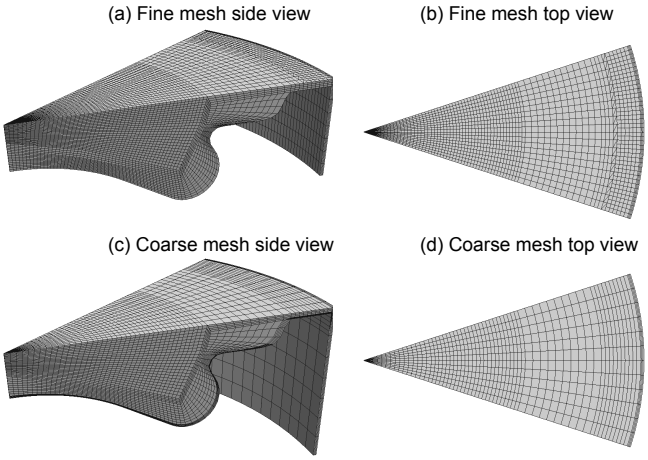

Figure 4.14: Comparison between the tested meshes: side (a) and top view (b) for fine mesh, and side (c) and top view (d) for coarse mesh.

almost no differences. For RoHR there is a peak of heat release in the premixed phase of combustion as a result of the RIF combustion model used. On the other hand, during the diffusion phase of combustion, the two meshes present a behavior very similar to the experiment, which also happens for the normalized cumulative HR.

Moreover, the results related to performance and pollutant emissions, especially those related to NO_x and soot models, are shown in Table 4.7. In terms of emissions, the fine mesh best reproduces the experimental values meanwhile presents a higher fuel consumption. However, the difference in val-

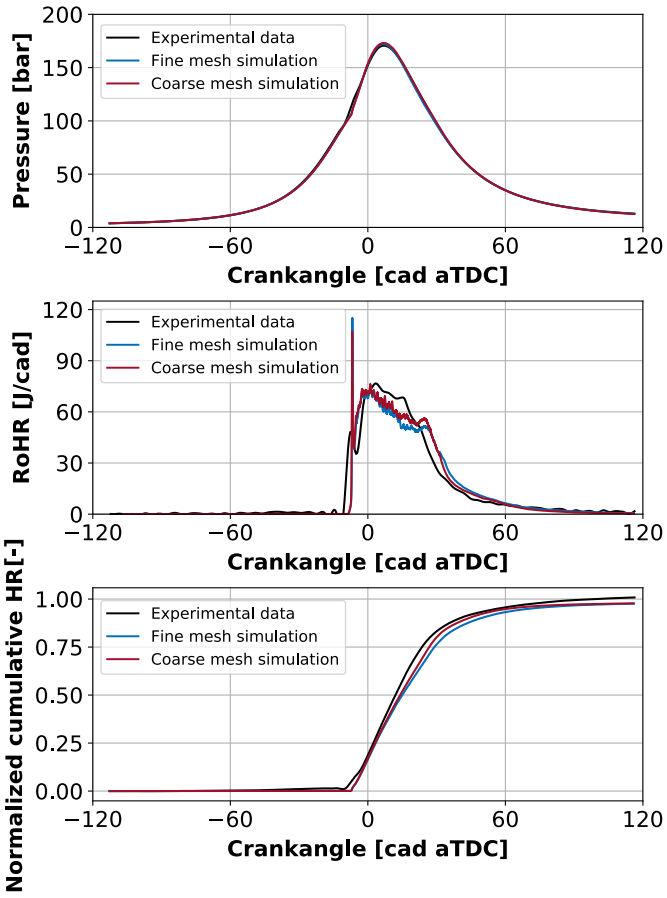

Figure 4.15: Comparison of experimental data with simulations of fine and coarse meshes. The results for OpenFOAM simulation show the in-cylinder pressure (top), RoHR (middle), and normalized cumulative HR (bottom).

ues found for the coarse mesh is within an admissible confidence interval due to its simplification to improve computational times.

In general, the simulations show a good agreement with the experimental data in terms of IMEP, ISFC, and combustion characteristics (RoHR and normalized cumulative RoHR), showing that one can use both without any loss of information during simulations. As already mentioned, to perform all the optimization processes, a thousand simulations are necessary. With this in mind, fine mesh provides more accurate results in pressure and pollutant emissions values when compared to coarse mesh. Still, the more computational time for each simulation or higher processing capacity is necessary to

Table 4.7: Comparison between the experimental and CFD simulation values.

	IMEP [bar]	NO_x [ppm]	YSoot [-]	ISFC [g/kWh]
Experimental data	22.36	1253	4.18E-06	191.8
Fine mesh simulation	22.26	1277	3.03E-06	192.9
Coarse mesh simulation	22.50	1459	2.09E-06	191.1

maintain the same computational time, which increases the costs. Based on these results, the coarse mesh will be used to perform the simulations.

4.5 Optimization algorithm

The present section shows the optimization algorithm used in this thesis, its integration with the Novelty Search (NS) concept, and all the necessary equations. In addition, benchmark results are presented comparing the algorithms already shown in Section 3.2.

4.5.1 Novelty swarm optimization algorithm

To perform the optimization process in this work, the Novelty Swarm (NS) algorithm was applied [45]. This new algorithm is based on the particle swarm optimization algorithm (PSO) [46] with some modifications to couple the Novelty Search concept in its execution. The PSO algorithm is inspired by the social behavior of bird flocks offering a fast rate of convergence and a low cost to evaluate the objective function, and can be applied in problems with large scale domain of candidate solutions and can have a simple mathematical implementation. Nonetheless, some drawbacks of the PSO are that the algorithm can be trapped in a local minimum point and not find the global optimum of the function. Moreover, the PSO has a strong connection with the meta-parameters values, thus making the algorithm an excellent choice for applying this new concept. During the PSO execution, the algorithm requires little information as the position x_i and velocity v_i of each particle, according to the following expressions:

$$x_i(t+1) = x_i(t) + v_i(t+1), \tag{4.17}$$

$$\begin{aligned} v_i(t+1) =& w \cdot \beta \cdot v_i(t) + c_1 \cdot \tau \cdot (p_i - x_i(t)) \\ &+ c_2\ \gamma \cdot (g - x_i(t)), \end{aligned} \tag{4.18}$$

where w means the inertia weight, c_1 and c_2 represent the individual and social weight respectively, and t means the iteration. Typical values for the inertia weight w are in the range of [0.5,1.5] and the values of c_1 and c_2 vary in the range of [1,3]. Also, in the previous Equation (4.18), p_i means the instant best position of x_i (local best position), and g denotes the global best position obtained from the algorithm until the current iteration. The variables β, τ and γ are random vectors being that each element is a different element of distribution between 0 and 1.

The integration between PSO and the Novelty Search concept has already been used in previous works with successful results improving the algorithm exploration inside the search space as presented in [47]. The particles are divided into two groups named families: the first family is composed of particles called "conquerors" that aim to "conquer" the best solution to the problem. These particles are mathematically controlled by the PSO equations (Eq. 4.17 and Eq. 4.18). The other family is named "explorers" particles. These particles should "explore" all the search space independent of the results, always searching for and the best solution to the problem avoiding the PSO from getting stuck in a local minimum. Moreover, the Novelty Search concept is applied in this family of particles. All the particles generated by the algorithm (conquerors + explorers) are stored in a repository. Maintaining all the information of the optimization process, the new explorers particles can avoid the regions close to the particles already observed. The repository is defined by the following Equation (4.19):

$$\mathrm{MC}\ (t) = \frac{\sum\limits_{x \in \mathcal{R}(t)} x}{\mathrm{card}(\mathcal{R}(t))}, \tag{4.19}$$

where $\mathcal{R}(t)$ is the repository in the iteration t, $\mathrm{card}(\mathcal{R}(t))$ is the number of elements of $\mathcal{R}(t)$ and MC (t) is the point that summarizes the behavior of the system in the iteration t. In this expression, the MC (t) is defined to be analogous to a centre of mass.

To adapt the PSO algorithm with the Novelty Search concept, a new velocity equation is necessary to guide the explorers particles behavior considering this modification. Therefore the Equation (4.20) was defined to avoid the particle dependency from the old global best position and now considering the new center of mass as follows,

$$v_i(t+1) = w \cdot \delta \cdot v_i(t) + c_1 \cdot \phi \cdot (p_i - x_i(t)) + \\ + c_3 \cdot \rho \cdot \exp\left(-\alpha \cdot \left|\frac{x_i(t) - \text{MC}\ (t)}{x_{max} - x_{min}}\right|\right) \cdot (x_i(t) - \text{MC}\ (t)), \tag{4.20}$$

where x_{max}, x_{min} are vectors that represent the boundaries of the search space. The variables δ, ϕ, and ρ represent random vectors like in Equation (4.18). The quotient is given in Equation (4.21) which is part of the Equation (4.20) and should be carried out componentwise.

$$\frac{x_i(t) - \text{MC}\ (t)}{x_{max} - x_{min}} \tag{4.21}$$

4.5.2 NS Benchmark results

This section reports the results obtained from the CEC2005 benchmark. This is a well-known and referenced series of problems for evaluating and comparing computational intelligence problems. The algorithms PSO [48], M-PSO [48, 49], CAPSO [50], LSHADE [51], and jSO [51, 52] already presented in Section 3.2 were compared against the NS algorithm. The CEC2005 benchmark [53] is a collection of functions that compare the effectiveness of optimization methods. This set of functions is made up of 25 separate functions that may be classified as follows:

- 5 unimodal functions, represented by the functions Func 1 to Func 5.
- 20 multimodal functions, defined by Func 6 to Func 25.

In all functions, the optimum is moved further from the origin to prevent finding it in the domain's center. The general properties of each function are shown in Table 4.8. In this table, the "Domain" column denotes the search space limit, the "Init." or initial column indicates the search space area where the particles are initiated, the "F(x*)" column represents the minimum value of each function, and the "Accuracy" column specifies the maximum inaccuracy permitted before the problem is deemed settled. It was used the Python3 [54] programming language to run the test, with Numpy [55] as a dependent package. The evaluation was run on a PC with a 2.20 GHz Intel Xenon E5-4620 processor and 512 GB of RAM. For each algorithm, each benchmark function was run 25 times for 2, 10, and 30 dimensions. Table 4.9 lists the parameter parameters for each algorithm. A sensitivity analysis was

performed to identify a suitable parameter, altering the value from 1 to 10. It was decided on a value of 5 and ran a sensitivity analysis to determine the best number of NS particles to use, resulting in 60 and 30 for the conqueror particles and explorer particles, respectively.

Table 4.8: CEC2005 functions execution data [53].

Func.	**Domain**	**Init.**	**F(x*)**	**Accuracy**
Func1	$[-100, 100]^D$	$[-100, 100]^D$	-4.50E+02	-4.50E+02 + 1.00E-06
Func2	$[-100, 100]^D$	$[-100, 100]^D$	-4.50E+02	-4.50E+02 + 1.00E-06
Func3	$[-100, 100]^D$	$[-100, 100]^D$	-4.50E+02	-4.50E+02 + 1.00E-06
Func4	$[-100, 100]^D$	$[-100, 100]^D$	-4.50E+02	-4.50E+02 + 1.00E-06
Func5	$[-100, 100]^D$	$[-100, 100]^D$	-3.10E+02	-3.10E+02 + 1.00E-06
Func6	$[-100, 100]^D$	$[-100, 100]^D$	3.90E+02	3.90E+02 + 1.00E-02
Func7	$[-600, 600]^D$	$[0, 600]^D$	-1.80E+02	-1.80E+02 + 1.00E-02
Func8	$[-32, 32]^D$	$[-32, 32]^D$	-1.40E+02	-1.40E+02 + 1.00E-02
Func9	$[-5, 5]^D$	$[-5, 5]^D$	-3.30E+02	-3.30E+02 + 1.00E-02
Func10	$[-5, 5]^D$	$[-5, 5]^D$	-3.30E+02	-3.30E+02 + 1.00E-02
Func11	$[-0.5, 0.5]^D$	$[-0.5, 0.5]^D$	9.00E+01	9.00E+01 + 1.00E-02
Func12	$[-\pi, \pi]^D$	$[-\pi, \pi]^D$	-4.60E+02	-4.60E+02 + 1.00E-02
Func13	$[-3, 1]^D$	$[-3, 1]^D$	-1.30E+02	-1.30E+02 + 1.00E-02
Func14	$[-100, 100]^D$	$[-100, 100]^D$	-3.00E+02	-3.00E+02 + 1.00E-02
Func15	$[-5, 5]^D$	$[-5, 5]^D$	1.20E+02	1.20E+02 + 1.00E-02
Func16	$[-5, 5]^D$	$[-5, 5]^D$	1.20E+02	1.20E+02 + 1.00E-02
Func17	$[-5, 5]^D$	$[-5, 5]^D$	1.20E+02	1.20E+02 + 1.00E-01
Func18	$[-5, 5]^D$	$[-5, 5]^D$	1.00E+01	1.00E+01 + 1.00E-01
Func19	$[-5, 5]^D$	$[-5, 5]^D$	1.00E+01	1.00E+01 + 1.00E-01
Func20	$[-5, 5]^D$	$[-5, 5]^D$	1.00E+01	1.00E+01 + 1.00E-01
Func21	$[-5, 5]^D$	$[-5, 5]^D$	3.60E+02	3.60E+02 + 1.00E-01
Func22	$[-5, 5]^D$	$[-5, 5]^D$	3.60E+02	3.60E+02 + 1.00E-01
Func23	$[-5, 5]^D$	$[-5, 5]^D$	3.60E+02	3.60E+02 + 1.00E-01
Func24	$[-5, 5]^D$	$[-5, 5]^D$	2.60E+02	2.60E+02 + 1.00E-01
Func25	$[-5, 5]^D$	$[-2, 5]^D$	2.60E+02	2.60E+02 + 1.00E-01

The cost of computing the mass center from 3000 to 15000 particles was calculated to determine the number of particles q that should have been taken randomly from the repository. As a balance between costing time and including as many particles as feasible, the maximum repository size of $p = 12000$ and a minimum relevant number of particles to compute the mass center is

Table 4.9: Setting of algorithms parameters.

	NS	**PSO**	**M-PSO**	**CAPSO**	**LSHADE**	**jSO**
w	0.9	0.9	0.9	-	-	-
$c1$	2.0	2.0	2.0	-	-	-
$c2$	2.0	2.0	2.0	-	-	-
$c3$	2.0	-	-	-	-	-
Mutation	0.05	-	0.05	-	-	-
Particles	60	60	60	60	-	-
Explorer Particles	30	-	-	-	-	-
α	5.0	-	-	-	-	-
NP_0	-	-	-	-	$18{\cdot}D$	$18{\cdot}D$
NP_{min}	-	-	-	-	4	4
H	-	-	-	-	6	6
NA_g	-	-	-	-	$2.6{\cdot}NP_g$	$2.6{\cdot}NP_g$
p	-	-	-	-	0.11	0.11
Reference	-	[48]	[48, 49]	[50]	[51]	[51, 52]

$q = 10000$. The execution ends when the optimum is obtained (with a specified error set for each function) or when the maximum number of function evaluations have been finished (even if the optimum has not been reached). For 2-dimensional space, the maximum iterations are 10000, and for 10 and 30-dimensional space, they are 100000. The CEC2005 benchmark establishes the final standards (see the 5th column of Table 4.8).

Figures 4.16 and 4.17 show the evolution of the error of the results of CEC2005 functions 15 until 25 for all tested algorithms for 10 dimensions case. Moreover, when the number of function evaluations is 1000 in relation to the fitness function, NS is the best algorithm for a 10-dimensional space. In 6 of the benchmark functions, the new method shows better results, followed by PSO, which presents accurate results in 3 of the functions, thus making the NS a good option for the optimization process. The completed results of all tested functions for all dimensions are presented in the Annex 4.8.

Tables 4.10 and 4.11 show the bidirectional Friedman analysis results of variation from ranks was performed according to [56]. From Table 4.10, the NS shows a better performance than the other algorithms for the cases of 2 and 30 dimensions. Focusing on the comparison between the composition of the functions. Using Table 4.11 as a guide, it is possible to see that, the NS algorithm performance is even better than the other test algorithms.

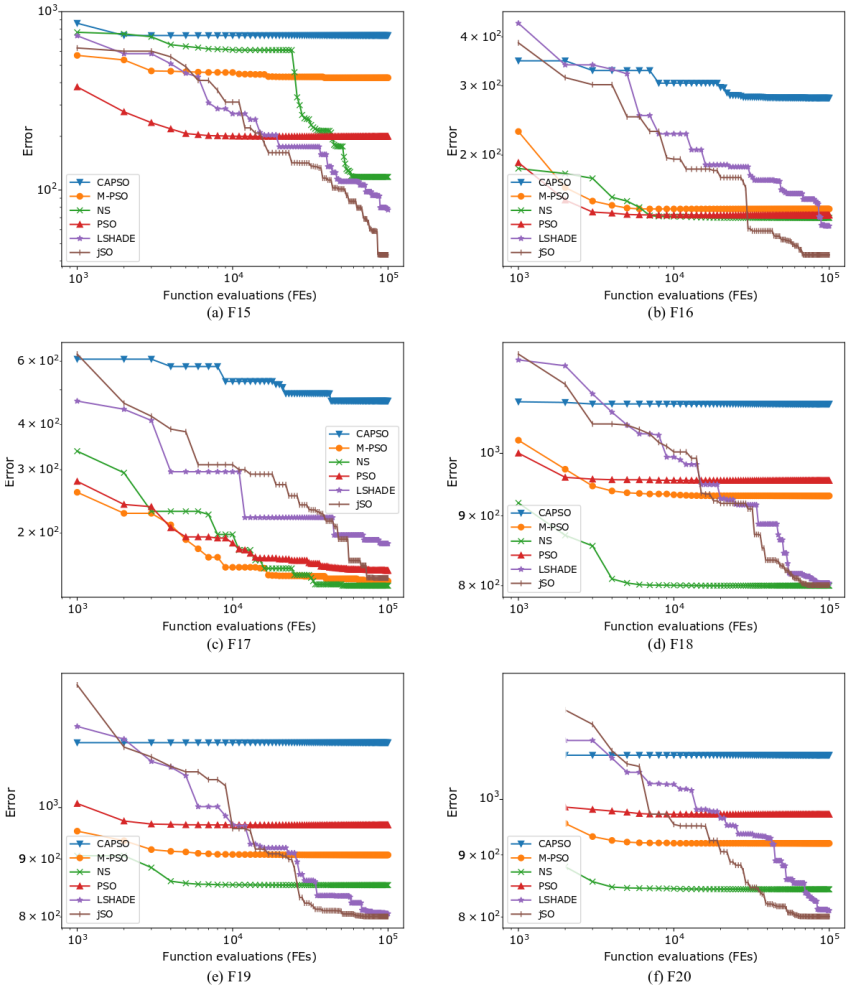

Figure 4.16: Functions 15 to 20 convergence for the composition 10 dimensional benchmark for the different algorithms.

Table 4.10: F1 - F25: Friedman mean rank for CEC2005 comparison.

	NS	PSO	M-PSO	CAPSO	LSHADE	jSO
2 dimensions	2.1	3.4	2.8	5.8	3.5	3.5
10 dimensions	3.2	4.0	3.2	6.0	3.1	1.7
30 dimensions	2.0	3.2	2.2	6.0	4.3	3.3

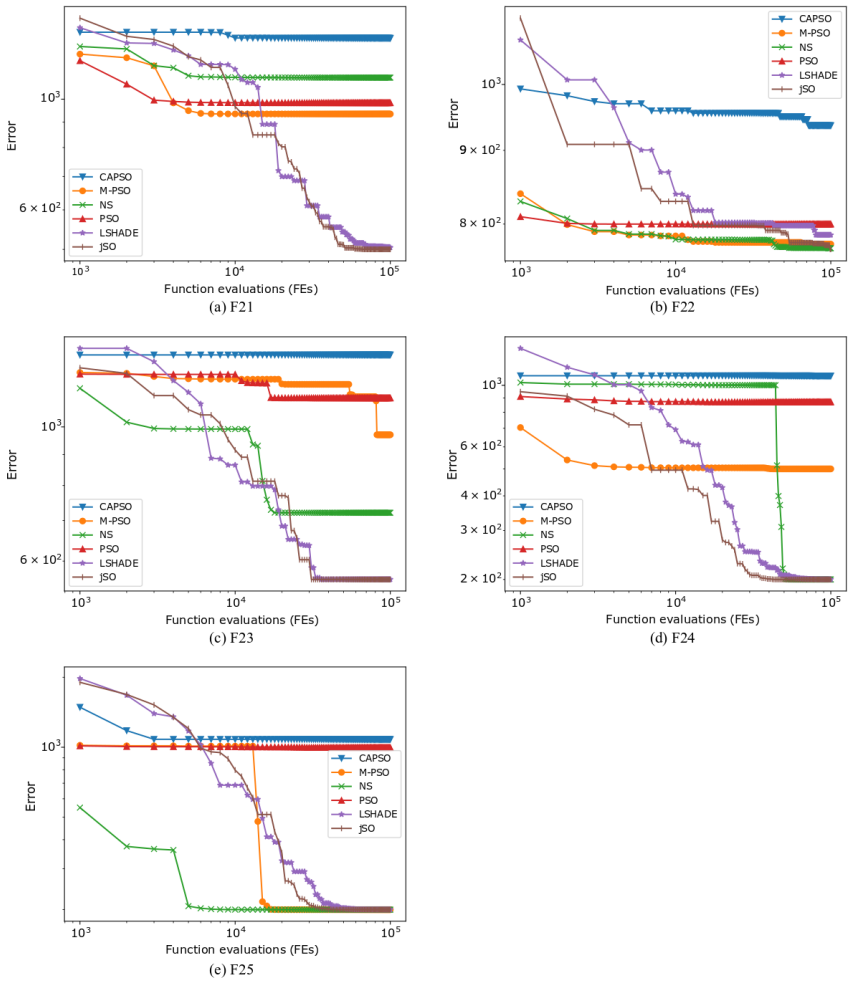

Figure 4.17: Functions 21 to 25 convergence for the composition 10 dimensional benchmark for the different algorithms.

However, because the optimum is more easily found in elementary functions, the search space does not need to be exhaustively investigated. In these situations, the NS algorithm performs less well than the other methods.

The algorithm complexity is calculated following the methodology of Suganthan et al. in [53] where $T0$ is the average execution time of a function using simple calculations (*log*, *exp*, and similar). $T1$ denotes the execution time of CEC2005 Function 3 for the stated dimension and 200000 function

Table 4.11: Composition functions F15 - F25: Friedman mean rank for CEC2005 comparison.

	NS	PSO	M-PSO	CAPSO	LSHADE	jSO
2 dimensions	1.3	3.9	3.0	6.0	3.5	3.5
10 dimensions	3.0	4.6	4.0	6.0	2.3	1.1
30 dimensions	1.8	4.1	2.7	6.0	3.8	2.5

evaluations, and $T2$ is the average execution time of 5 optimization methods employing the selected algorithm of the same function.

Table 4.12 presents the complexity calculations of the tested algorithms. When the results are analyzed, it is possible to see that NS has more complexity, which is reflected in computational time, than the other PSO-based algorithms (PSO, M-PSO, and CAPSO). This complexity increases with the number of dimensions due to the computational cost of sampling particles in the repository. This increased cost disadvantages the NS when compared to other PSO-based algorithms for simple functions; nevertheless, when it comes to more challenging issues, the NS looks to be an excellent choice. Furthermore, for simple and complicated functions, the NS outperforms the LSHADE and jSO algorithms.

The algorithm assessments have revealed that NS produces excellent results in the optimal search while raising the computational charge of the calculations, even when just a few evaluations are needed. Furthermore, NS stands out in composition functions, particularly those with several variables.

4.6 Optimization methodology

This section describes the methodology that couples the NS algorithm with CFD calculation. This step is an essential aspect of simulation work due to the high number of different combustion systems tested, and it is impossible to test these systems experimentally. Figure 4.18 shows a global scheme of the optimization methodology. Three blocks are present, coupling each respective part of the work. In the first one, the initial CFD case used as a model for the optimization is calibrated and validated against experimental data, as already shown in previous sections. In the second block, the NS algorithm is implemented and configured, which means that all variables used as inputs and their ranges are set in the algorithm routine. Moreover, the objective function is defined based on the outputs of interest, like emissions and engine

Table 4.12: Calculation of algorithm complexity according to CEC2005 [53].

T0		T1		$\hat{T}2$	$\frac{\hat{T}2-T1}{T0}$
8.56	two-dimensions	2.67	NS	61.29	6.85
			PSO	16.59	1.62
			M-PSO	36.56	3.96
			CAPSO	39.40	4.29
			LSHADE	46.66	5.14
			jSO	42.60	5.01
	ten-dimensions	5.12	NS	81.12	8.88
			PSO	37.66	3.80
			M-PSO	40.58	4.14
			CAPSO	42.11	4.32
			LSHADE	115.61	12.91
			jSO	118.69	13.27
	thirty-dimensions	11.15	NS	141.90	15.27
			PSO	43.92	3.83
			M-PSO	51.05	4.66
			CAPSO	48.54	4.37
			LSHADE	245.60	27.39
			jSO	251.58	28.09

efficiency, and after all the definitions, the optimization process starts. The last block comprises all the cases produced throughout the NS execution and an extensive examination of the results.

Considering that the optimization process requires a high number of simulations, it is necessary to automate each step as much as possible. Block 3, shown in Figure 4.18, represents the NS algorithm initialization and steps to create, and evaluate each case until the end of the optimization process. The first action to be taken is the NS initializing, which will generate the first hundred particles between "Conquerors" and "Explorers" using the Latin hypercube methodology to generate an initial database for the optimization process. With this database, the algorithm will generate the first 40 particles (30 conquerors and 10 explorers), starting the optimization. Each of these 40 particles is a CFD case to be simulated. For this to be possible, tools are attached to generate the bowl profile, create the mesh and generate the injection rate of each case in different combustion systems. These tools will be presented in Sections 4.7.1, 4.7.2, and 4.7.3 of this thesis. Once generated, the cases are simulated, and their results are used to evaluate each new combustion system. From this point on wards, NS updates the global best value

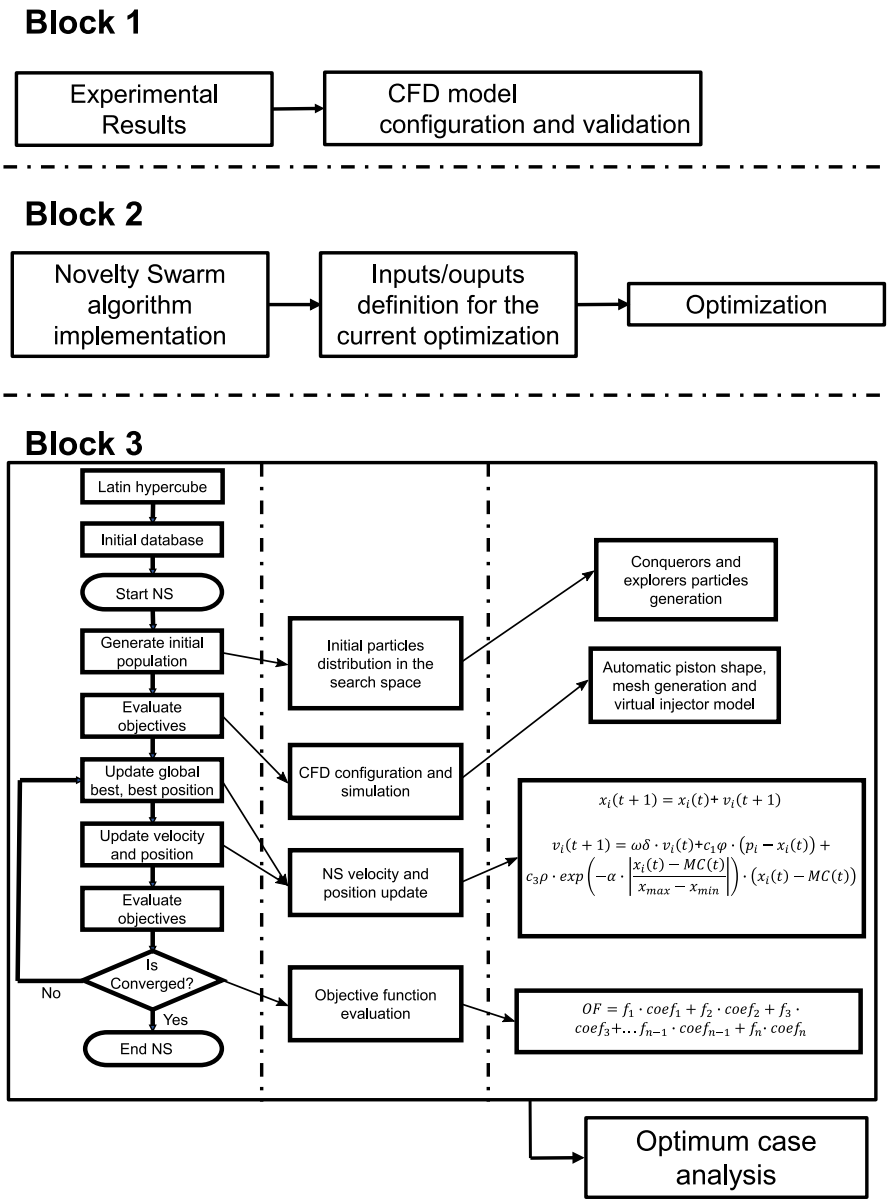

Figure 4.18: Scheme of the optimization methodology.

and best position values and then updates the velocity and positions to create new particles. These particles are also simulated and evaluated, repeating the process until reaching the stopping criterion or a maximum number of 1000

evaluated particles. This whole process is controlled by Python and Matlab routines.

The objective function that evaluates all cases of optimization is defined in advance based on the proposed objective. For example, if the objective is to improve the efficiency of the engine, maintaining the emissions below the determined value, such as NO_x emissions, efficiency will be the main parameter or the parameter to optimize, and the emissions will be the constraint of the process. Each parameter, the optimization parameter, and the constraints are particular to each studied case. In this thesis, the objective function decreases as more favorable results are obtained, and the smallest value obtained is considered the optimized case.

4.7 Computational tools

This section presents the tools coupled with the NS algorithm to automatize the optimization process. These tools are fundamental to generate the CFD cases once the NS defines the parameters to set up each combustion system.

4.7.1 Injector model - Virtual injection model

One of the main factors that have a critical influence on the combustion process in CI engines is fuel injection. A virtual injection model (VIM) was used to provide a robust and reliable rate of injection (ROI) for each simulation. This model is an in-house 0D model [57, 58] that uses the the total mass fuel of the cycle, the number of holes, injection pressure, and the engine speed to calculate a mass flow rate curve for each case.

The model is calibrated against experimental data from a real injector to predict the results correctly. The injection profile has a trapezoidal form, and the code assumes an incompressible flow between the inlet and outlet orifices, solving the equations of Bernoulli and continuity between these two points.

The left side of Figure 4.19 shows the experimental injection profiles against the simulated one, and the right side shows a set of ROI curves generated by the code for different injection pressure levels.

4.7.2 Bowl geometry model

Due to its importance in the combustion process, one of the most important steps in the generation of a combustion chamber geometry is the capacity to create a reliable piston shape bowl. So, to generate the shape of the piston,

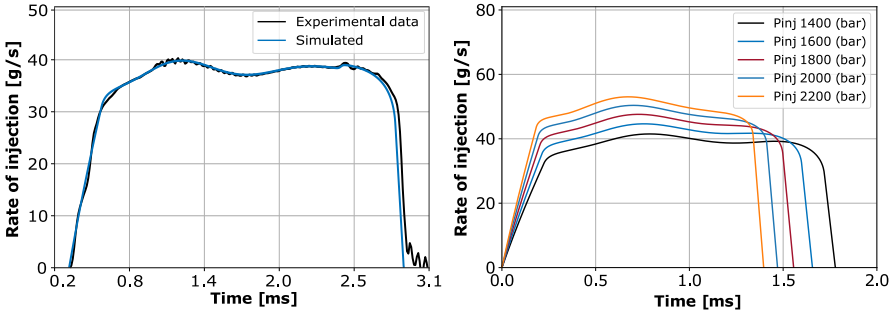

Figure 4.19: Rate of injection comparison: experimental data versus simulated values (Left-hand side) and a comparison between several ROI generated for several injection pressure values.

an automatic tool was implemented using Bezier polynomial curves [42, 59] defined by several control points. These points are dimensionless, independent from each other, and have their own variation range in order to set a specific part of the piston bowl geometry. Considering that the piston bowl directly impacts the compression ratio (CR) of the engine, the squish height is adjusted in order to maintain a constant CR value. In Figure 4.20, the original piston bowl geometry is represented by the dashed line and compared with different geometries generated using Bezier curves and all the points used to guide the geometry. As well, the geometrical points (GP) are indicated. In that figure, the 'p' points are fixed and maintain the piston diameter constant. This method offers a wide range of possible combustion chamber designs, ranging from wide, open bowls to small, extremely re-entrant ones. However, in some cases there, the proposed inputs could not generate a bowl that meets the CR, the NS discards these inputs and generate a new one.

4.7.3 Pumping work model

A procedure linked to the optimization process calculates the pumping effort required to obtain the appropriate intake boost in order to determine the net indicated efficiency (NIE). This model is based on basic thermodynamic modeling with the following assumptions:

- Because the work of the compressor and turbine are assumed equal, no mechanical losses are considered.
- The efficiency of the turbine and compressor efficiencies are assumed to be constant.

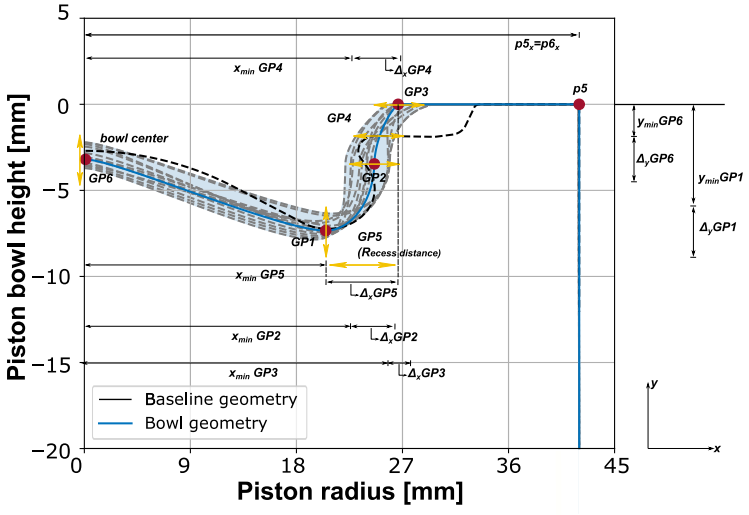

Figure 4.20: Parameters definition: points of Bezier curve and examples of piston bowl shape.

- To reproduce the aftercooler effect, a continuous pressure decrease is considered between the engine intake valve and the compressor.

For each of the cases simulated during the optimization process it is assumed that the IVC pressure as input of the model. The turbocharger has been chosen to have a compressor, turbine efficiency, and mechanical efficiency of 70%, 72% and, 90%, respectively. The pressure differences are calculated by scaling the experimental pressure values to reproduce the same behavior, but now using the values obtained in each simulation as a basis. These assumptions have already been employed successfully in other investigations [60, 61].

4.7.4 Post-processing

A notable amount of this thesis has been carried out in the post-processing definition. In order to systematically analyze the outputs and calculate the OF of each case during the optimization, an automatic routine to evaluate the simulations was created. This routine is Python-based, and it is launched after the end of the calculation. Figure 4.21 shows a diagram divided into different parts that represent each step of the post-processing routine. At the first moment, all the output files are read, and the interesting information

is stored. The second step is the calculation of the engine outputs to evaluate and compare the cases. The maximum pressure (P_{max}) and temperature (T_{max}) came directly from the OpenFOAM files. Moreover, all the final emissions as NO_x, soot, CO, and CO_2 obtained from the simulations are stored. The IMEP, pressure gradient (dp/da), ISFC and efficiency are calculated and saved. The next step is calculating the objective function established before the initialization of the optimization process. The function is calculated with the objective parameter and the constraints together with the respective coefficients. The last step of the post-processing routine is the feedback on the NS with the evaluation of the set of inputs of each simulation, so it is possible to automate the entire optimization process.

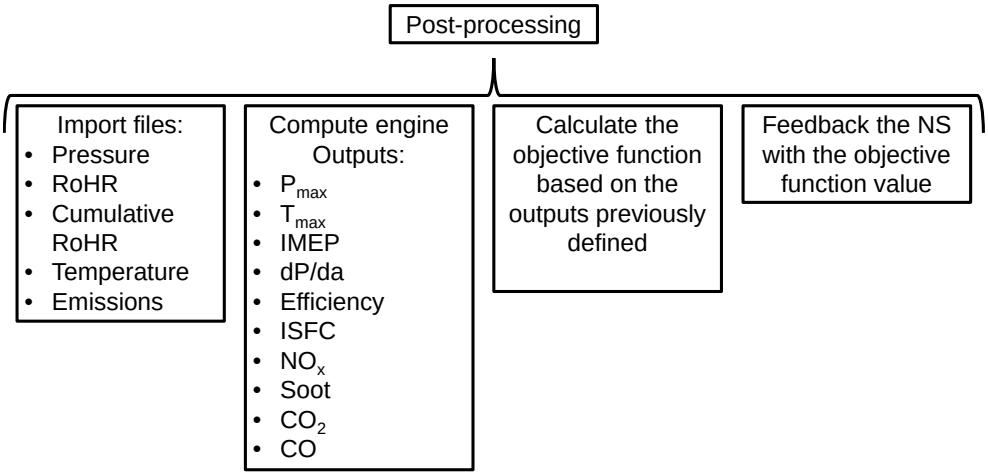

Figure 4.21: Diagram of the post-process sequence of each case during the optimization.

4.8 Summary and conclusions

In this section, it was presented the engine characteristics and the numerical tools used in this thesis. In the engine characteristics section were presented the real engine with its data. After this, all the computational approach was detailed. All the models used to calculate combustion and evaluate emissions were described. Additionally, the model validation presents all the tests to define the best mesh, turbulence, and heat transfer models in order to reproduce the real engine better. Moreover, the optimization algorithm has been

explained in detail. The algorithm was compared against others in this subsection by evaluating the benchmark functions. Finally, the approach used throughout the optimizations for this thesis, as well as the most significant improvements, were explained. Furthermore, the tools coupled with the optimization algorithm were shown.

The tools and approaches given in this chapter, along with the information obtained from the literature review chapter, guarantee that the aims proposed for this doctoral thesis may be fulfilled.

3.A Annex:

This Appendix shows the average differences between the optimal value calculated by the algorithm compared to the actual optimal value for the 25 iterations performed for each of the functions. In addition, the standard deviation for each 25 runs of each of the functions are also shown. These differences can be seen in Tables 4.13 - 4.18 below. For average results equal to zero, the correction is applied according to Table 4.8.

Table 4.13: Synthesis of the optimization results for functions 1 to 14 of the two-dimensional CEC2005 benchmark. The optimum result is highlighted in bold.

		NS	PSO	M-PSO	CAPSO	LSHADE	jSO
$f1$	Mean	**0.00E+4**	**0.00E+4**	**0.00E+4**	2.56E+00	**0.00E+4**	**0.00E+4**
	Std.	0.00E+00	0.00E+00	0.00E+00	6.95E+00	0.00E+00	0.00E+00
	Rank	**3.00E+00**	**3.00E+00**	**3.00E+00**	6.00E+00	**3.00E+00**	**3.00E+00**
$f2$	Mean	**0.00E+4**	**0.00E+4**	**0.00E+4**	1.84E+01	**0.00E+4**	**0.00E+4**
	Std.	0.00E+00	0.00E+00	0.00E+00	3.56E+01	0.00E+00	0.00E+00
	Rank	**3.00E+00**	**3.00E+00**	**3.00E+00**	6.00E+00	**3.00E+00**	**3.00E+00**
$f3$	Mean	**0.00E+4**	1.99E+02	**0.00E+4**	6.08E+03	6.55E+00	2.97E-07
	Std.	0.00E+00	3.36E+02	0.00E+00	6.85E+03	3.09E+01	1.46E-06
	Rank	**1.50E+00**	5.00E+00	**1.50E+00**	6.00E+00	4.00E+00	3.00E+00
$f4$	Mean	**0.00E+4**	**0.00E+4**	**0.00E+4**	1.57E+01	**0.00E+4**	**0.00E+4**
	Std.	0.00E+00	0.00E+00	0.00E+00	2.10E+01	0.00E+00	0.00E+00
	Rank	**3.00E+00**	**3.00E+00**	**3.00E+00**	6.00E+00	**3.00E+00**	**3.00E+00**
$f5$	Mean	**0.00E+4**	**0.00E+4**	**0.00E+4**	**0.00E+4**	3.98E-01	4.09E-01
	Std.	0.00E+00	0.00E+00	0.00E+00	0.00E+00	1.44E+00	9.08E-01
	Rank	**2.50E+00**	**2.50E+00**	**2.50E+00**	**2.50E+00**	5.00E+00	6.00E+00
$f6$	Mean	1.54E-01	1.97E+00	**1.59E-3**	2.56E+02	6.08E-01	6.39E-02
	Std.	3.79E-01	6.56E+00	7.79E-03	1.04E+03	1.77E+00	1.16E-01
	Rank	3.00E+00	5.00E+00	**1.00E+00**	6.00E+00	4.00E+00	2.00E+00
$f7$	Mean	1.12E-02	**0.00E+4**	5.88E-03	7.22E-01	1.03E-02	2.17E-03
	Std.	1.25E-02	0.00E+00	1.10E-02	1.07E+00	3.70E-02	6.95E-03
	Rank	5.00E+00	**1.00E+00**	3.00E+00	6.00E+00	4.00E+00	2.00E+00
$f8$	Mean	**0.00E+4**	1.68E+01	1.52E+01	1.36E+01	9.51E+00	8.56E+00
	Std.	0.00E+00	7.33E+00	8.54E+00	9.03E+00	8.39E+00	8.42E+00
	Rank	**1.00E+00**	6.00E+00	5.00E+00	4.00E+00	3.00E+00	2.00E+00
$f9$	Mean	**0.00E+4**	**0.00E+4**	**0.00E+4**	1.03E+00	**0.00E+4**	1.17E-03
	Std.	0.00E+00	0.00E+00	0.00E+00	1.71E+00	0.00E+00	5.72E-03
	Rank	**2.50E+00**	**2.50E+00**	**2.50E+00**	6.00E+00	**2.50E+00**	5.00E+00
$f10$	Mean	**0.00E+4**	**0.00E+4**	**0.00E+4**	8.45E-01	1.30E-02	8.90E-03
	Std.	0.00E+00	0.00E+00	0.00E+00	1.11E+00	3.93E-02	2.34E-02
	Rank	**2.00E+00**	**2.00E+00**	**2.00E+00**	6.00E+00	5.00E+00	4.00E+00
$f11$	Mean	1.02E-02	**0.00E+4**	1.73E-03	3.42E-01	4.29E-02	4.92E-02
	Std.	9.19E-03	0.00E+00	4.80E-03	3.47E-01	6.49E-02	6.59E-02
	Rank	3.00E+00	**1.00E+00**	2.00E+00	6.00E+00	4.00E+00	5.00E+00
$f12$	Mean	**0.00E+4**	**0.00E+4**	**0.00E+4**	3.36E+01	4.10E-03	5.48E-02
	Std.	0.00E+00	0.00E+00	0.00E+00	1.21E+02	2.00E-02	1.38E-01
	Rank	**2.00E+00**	**2.00E+00**	**2.00E+00**	6.00E+00	4.00E+00	5.00E+00
$f13$	Mean	**0.00E+4**	4.74E-03	2.37E-03	1.58E-02	9.64E-04	**0.00E+4**
	Std.	0.00E+00	8.43E-03	6.41E-03	2.37E-02	4.72E-03	0.00E+00
	Rank	**1.5.00E+00**	5.00E+00	4.00E+00	6.00E+00	3.00E+00	**1.5.00E+00**
$f14$	Mean	1.69E-02	**1.24E-2**	1.69E-02	1.34E-01	1.51E-02	1.73E-02
	Std.	6.31E-03	9.33E-03	6.29E-03	2.32E-01	6.69E-03	1.90E-02
	Rank	4.00E+00	**1.00E+00**	3.00E+00	6.00E+00	2.00E+00	5.00E+00

Table 4.14: Synthesis of the optimization results for functions 15 to 25 of the two-dimensional CEC2005 benchmark. The optimum result is highlighted in bold.

		NS	PSO	M-PSO	CAPSO	LSHADE	jSO
	Mean	**0.00E+4**	**0.00E+4**	4.00E+00	8.64E+01	1.12E-04	7.04E-01
$f15$	Std.	0.00E+00	0.00E+00	1.96E+01	9.08E+01	5.48E-04	2.66E+00
	Rank	**1.50E+00**	**1.50E+00**	5.00E+00	6.00E+00	3.00E+00	4.00E+00
	Mean	**0.00E+4**	1.20E+01	1.60E+01	1.49E+02	1.61E+01	5.86E+00
$f16$	Std.	0.00E+00	3.25E+01	3.67E+01	1.19E+02	3.66E+01	2.10E+01
	Rank	**1.00E+00**	3.00E+00	4.00E+00	6.00E+00	5.00E+00	2.00E+00
	Mean	1.63E+00	5.61E+00	3.62E+01	1.97E+02	**7.6461E-1**	6.53E+00
$f17$	Std.	8.00E+00	2.08E+01	4.83E+01	1.56E+02	2.10E+00	2.13E+01
	Rank	2.00E+00	3.00E+00	5.00E+00	6.00E+00	**1.00E+00**	4.00E+00
	Mean	**2.81E+1**	2.60E+02	6.46E+01	3.59E+02	1.73E+02	2.57E+02
$f18$	Std.	7.22E+01	1.62E+02	9.36E+01	1.69E+02	1.20E+02	1.08E+02
	Rank	**1.00E+00**	5.00E+00	2.00E+00	6.00E+00	3.00E+00	4.00E+00
	Mean	**2.11E+2**	2.80E+02	2.34E+02	3.69E+02	2.37E+02	2.64E+02
$f19$	Std.	4.14E+01	1.20E+02	7.26E+01	1.12E+02	7.83E+01	7.41E+01
	Rank	**1.00E+00**	5.00E+00	2.00E+00	6.00E+00	3.00E+00	4.00E+00
	Mean	**0.00E+4**	2.48E+02	2.24E+02	4.18E+02	2.42E+02	2.22E+02
$f20$	Std.	0.00E+00	1.14E+02	7.08E+01	1.70E+02	8.95E+01	1.04E+02
	Rank	**1.00E+00**	5.00E+00	3.00E+00	6.00E+00	4.00E+00	2.00E+00
	Mean	**5.72E+1**	2.74E+02	2.24E+02	3.99E+02	2.40E+02	2.15E+02
$f21$	Std.	8.92E+01	1.65E+02	1.41E+02	1.59E+02	1.68E+02	1.50E+02
	Rank	**1.00E+00**	5.00E+00	3.00E+00	6.00E+00	4.00E+00	2.00E+00
	Mean	**1.73E+2**	3.13E+02	2.24E+02	3.50E+02	2.38E+02	2.10E+02
$f22$	Std.	7.14E+01	1.27E+02	8.10E+01	1.18E+02	8.60E+01	3.80E+01
	Rank	**1.00E+00**	5.00E+00	3.00E+00	6.00E+00	4.00E+00	2.00E+00
	Mean	1.73E+02	2.61E+02	**1.4534E+2**	3.99E+02	2.69E+02	3.55E+02
$f23$	Std.	1.18E+02	2.20E+02	2.27E+02	2.14E+02	2.05E+02	1.79E+02
	Rank	2.00E+00	3.00E+00	**1.00E+00**	6.00E+00	5.00E+00	4.00E+00
	Mean	**1.96E+2**	2.00E+02	2.00E+02	2.78E+02	1.98E+02	2.00E+02
$f24$	Std.	1.06E+01	0.00E+00	1.14E-06	1.47E+02	8.72E+00	9.53E-04
	Rank	**1.00E+00**	4.00E+00	4.00E+00	6.00E+00	2.00E+00	4.00E+00
	Mean	1.94E+02	1.98E+02	**1.6610E+2**	3.25E+02	3.41E+02	3.93E+02
$f25$	Std.	1.85E+01	1.70E+02	3.53E+01	2.31E+02	1.62E+02	1.57E+02
	Rank	2.00E+00	3.00E+00	**1.00E+00**	4.00E+00	5.00E+00	6.00E+00

Table 4.15: Synthesis of the optimization results for functions 1 to 14 of the ten-dimensional CEC2005 benchmark. The optimum result is highlighted in bold.

		NS	PSO	M-PSO	CAPSO	LSHADE	jSO
$f1$	Mean	**0.00E+4**	4.13E+00	**0.00E+4**	3.11E+03	9.65E-05	**0.00E+4**
	Std.	0.00E+00	2.02E+01	0.00E+00	2.12E+03	5.76E-05	0.00E+00
	Rank	**2.00E+00**	5.00E+00	**2.00E+00**	6.00E+00	4.00E+00	**2.00E+00**
$f2$	Mean	**0.00E+4**	4.46E+00	**0.00E+4**	6.36E+03	3.01E+01	1.19E-01
	Std.	0.00E+00	1.51E+01	0.00E+00	6.17E+03	1.61E+01	3.48E-01
	Rank	**1.50E+00**	4.00E+00	**1.50E+00**	6.00E+00	5.00E+00	3.00E+00
$f3$	Mean	**0.00E+4**	1.56E+05	**0.00E+4**	3.27E+07	6.07E+05	3.22E+05
	Std.	0.00E+00	1.46E+05	0.00E+00	4.96E+07	3.08E+05	1.95E+05
	Rank	**1.50E+00**	3.00E+00	**1.50E+00**	6.00E+00	5.00E+00	4.00E+00
$f4$	Mean	**0.00E+4**	1.26E+01	**0.00E+4**	7.92E+03	5.96E+01	1.80E+00
	Std.	0.00E+00	4.17E+01	0.00E+00	7.87E+03	2.92E+01	2.44E+00
	Rank	**1.50E+00**	4.00E+00	**1.50E+00**	6.00E+00	5.00E+00	3.00E+00
$f5$	Mean	2.78E-05	1.76E+02	**8.87E-6**	2.67E+03	1.11E+01	1.12E-04
	Std.	2.96E-05	8.62E+02	1.38E-05	3.15E+03	4.34E+00	1.82E-04
	Rank	2.00E+00	5.00E+00	**1.00E+00**	6.00E+00	4.00E+00	3.00E+00
$f6$	Mean	6.99E+01	3.17E+04	3.64E+01	7.91E+08	4.06E+01	2.05E+01
	Std.	1.98E+02	1.55E+05	6.56E+01	1.34E+09	2.44E+01	**2.40E+1**
	Rank	4.00E+00	5.00E+00	2.00E+00	6.00E+00	3.00E+00	**1.00E+00**
$f7$	Mean	6.94E-01	1.20E+00	**6.30E-1**	2.91E+02	7.90E-01	1.83E-01
	Std.	3.76E-01	2.38E+00	4.14E-01	2.27E+02	1.08E-01	**1.36E-1**
	Rank	3.00E+00	5.00E+00	2.00E+00	6.00E+00	4.00E+00	**1.00E+00**
$f8$	Mean	2.03E+01	**2.03E+1**	2.04E+01	2.04E+01	2.04E+01	2.03E+01
	Std.	6.94E-02	7.28E-02	7.50E-02	6.28E-02	6.47E-02	**8.83E-2**
	Rank	3.00E+00	2.00E+00	4.50E+00	4.50E+00	6.00E+00	**1.00E+00**
$f9$	Mean	1.25E+00	3.06E+00	4.81E-01	7.84E+01	**3.21E-2**	4.62E-01
	Std.	1.10E+00	1.35E+00	5.80E-01	2.09E+01	1.25E-02	8.33E-01
	Rank	4.00E+00	5.00E+00	3.00E+00	6.00E+00	**1.00E+00**	2.00E+00
$f10$	Mean	2.07E+01	1.87E+01	2.06E+01	8.90E+01	1.22E+01	**1.08E+1**
	Std.	1.07E+01	6.94E+00	1.16E+01	2.91E+01	2.81E+00	4.77E+00
	Rank	5.00E+00	3.00E+00	4.00E+00	6.00E+00	2.00E+00	**1.00E+00**
$f11$	Mean	4.91E+00	**4.11E+0**	4.26E+00	8.91E+00	5.24E+00	4.69E+00
	Std.	1.73E+00	1.41E+00	1.60E+00	1.81E+00	7.81E-01	7.53E-01
	Rank	4.00E+00	**1.00E+00**	2.00E+00	6.00E+00	5.00E+00	3.00E+00
$f12$	Mean	1.72E+03	1.71E+03	1.48E+03	4.30E+04	**2.30E+2**	2.45E+02
	Std.	3.02E+03	3.66E+03	4.10E+03	2.69E+04	1.10E+02	3.24E+02
	Rank	5.00E+00	4.00E+00	3.00E+00	6.00E+00	**1.00E+00**	2.00E+00
$f13$	Mean	7.43E-01	6.10E-01	7.15E-01	1.24E+01	4.45E-01	**3.88E-1**
	Std.	2.20E-01	2.44E-01	2.72E-01	6.26E+00	1.06E-01	1.76E-01
	Rank	5.00E+00	3.00E+00	4.00E+00	6.00E+00	2.00E+00	**1.00E+00**
$f14$	Mean	3.25E+00	**2.96E+0**	3.05E+00	4.00E+00	3.21E+00	3.08E+00
	Std.	3.58E-01	4.93E-01	5.08E-01	3.77E-01	2.13E-01	3.40E-01
	Rank	5.00E+00	**1.00E+00**	3.00E+00	6.00E+00	4.00E+00	2.00E+00

Table 4.16: Synthesis of the optimization results for functions 15 to 25 of the ten-dimensional CEC2005 benchmark. The optimum result is highlighted in bold.

		NS	PSO	M-PSO	CAPSO	LSHADE	jSO
	Mean	2.27E+02	2.41E+02	3.32E+02	7.30E+02	7.23E+01	**4.49E+1**
$f15$	Std.	2.03E+02	1.64E+02	2.14E+02	9.66E+01	2.27E+01	3.18E+01
	Rank	3.00E+00	4.00E+00	5.00E+00	6.00E+00	2.00E+00	**1.00E+00**
	Mean	1.42E+02	1.52E+02	1.49E+02	3.06E+02	1.35E+02	**1.12E+2**
$f16$	Std.	2.08E+01	5.67E+01	2.20E+01	9.78E+01	1.66E+01	8.56E+00
	Rank	3.00E+00	5.00E+00	4.00E+00	6.00E+00	2.00E+00	**1.00E+00**
	Mean	**1.49E+2**	1.57E+02	1.57E+02	4.94E+02	1.87E+02	1.53E+02
$f17$	Std.	2.61E+01	2.96E+01	3.35E+01	2.23E+02	1.26E+01	2.14E+01
	Rank	**1.00E+00**	3.00E+00	4.00E+00	6.00E+00	5.00E+00	2.00E+00
	Mean	8.23E+02	9.34E+02	8.38E+02	1.08E+03	7.87E+02	**7.52E+2**
$f18$	Std.	1.67E+02	9.88E+01	1.98E+02	8.83E+01	7.07E+01	1.23E+02
	Rank	3.00E+00	5.00E+00	4.00E+00	6.00E+00	2.00E+00	**1.00E+00**
	Mean	8.62E+02	9.35E+02	8.37E+02	1.13E+03	7.96E+02	**7.70E+2**
$f19$	Std.	1.59E+02	9.83E+01	1.80E+02	7.64E+01	4.59E+01	7.75E+01
	Rank	4.00E+00	5.00E+00	3.00E+00	6.00E+00	2.00E+00	**1.00E+00**
	Mean	8.39E+02	9.19E+02	8.63E+02	1.10E+03	8.02E+02	**7.78E+2**
$f20$	Std.	1.51E+02	1.24E+02	1.78E+02	9.72E+01	4.91E+01	7.25E+01
	Rank	3.00E+00	5.00E+00	4.00E+00	6.00E+00	2.00E+00	**1.00E+00**
	Mean	9.18E+02	8.45E+02	8.22E+02	1.30E+03	4.97E+02	**4.84E+2**
$f21$	Std.	3.32E+02	3.71E+02	3.64E+02	1.81E+02	5.39E+01	1.14E+02
	Rank	5.00E+00	4.00E+00	3.00E+00	6.00E+00	2.00E+00	**1.00E+00**
	Mean	7.85E+02	8.07E+02	7.94E+02	9.56E+02	7.86E+02	**7.70E+2**
$f22$	Std.	4.03E+01	4.99E+01	4.56E+01	6.45E+01	5.98E+00	9.72E+00
	Rank	2.00E+00	5.00E+00	4.00E+00	6.00E+00	3.00E+00	**1.00E+00**
	Mean	8.94E+02	1.07E+03	9.27E+02	1.31E+03	5.73E+02	**5.43E+2**
$f23$	Std.	2.09E+02	1.81E+02	2.42E+02	5.64E+01	5.38E+01	4.36E+01
	Rank	3.00E+00	5.00E+00	4.00E+00	6.00E+00	2.00E+00	**1.00E+00**
	Mean	3.28E+02	6.94E+02	4.08E+02	1.14E+03	2.00E+02	**2.00E+2**
$f24$	Std.	2.11E+02	2.99E+02	2.12E+02	1.36E+02	3.53E-02	0.00E+00
	Rank	3.00E+00	5.00E+00	4.00E+00	6.00E+00	2.00E+00	**1.00E+00**
	Mean	2.92E+02	8.76E+02	3.48E+02	1.15E+03	**2.00E+2**	**2.00E+2**
$f25$	Std.	2.04E+02	2.34E+02	1.88E+02	1.58E+02	2.22E-03	0.00E+00
	Rank	3.00E+00	4.00E+00	5.00E+00	6.00E+00	**1.50E+00**	**1.50E+00**

Table 4.17: Synthesis of the optimization results for functions 1 to 14 of the thirty-dimensional CEC2005 benchmark. The optimum result is highlighted in bold.

		NS	PSO	M-PSO	CAPSO	LSHADE	jSO
	Mean	**0.00E+4**	5.45E+02	**0.00E+4**	5.92E+04	9.28E+02	5.46E+02
$f1$	Std.	0.00E+00	5.12E+02	0.00E+00	2.97E+04	1.52E+02	8.45E+01
	Rank	**1.50E+00**	3.00E+00	**1.50E+00**	6.00E+00	5.00E+00	4.00E+00
	Mean	**0.00E+4**	7.59E+02	**0.00E+4**	1.10E+05	2.68E+04	2.02E+04
$f2$	Std.	0.00E+00	1.80E+03	0.00E+00	4.91E+04	3.90E+03	3.08E+03
	Rank	**1.50E+00**	3.00E+00	**1.50E+00**	6.00E+00	5.00E+00	4.00E+00
	Mean	**0.00E+4**	6.88E+06	**0.00E+4**	4.70E+08	6.11E+07	4.62E+07
$f3$	Std.	0.00E+00	3.71E+06	0.00E+00	4.19E+08	1.45E+07	9.84E+06
	Rank	**1.50E+00**	3.00E+00	**1.50E+00**	6.00E+00	5.00E+00	4.00E+00
	Mean	**0.00E+4**	1.83E+03	**0.00E+4**	1.07E+05	3.53E+04	3.11E+04
$f4$	Std.	0.00E+00	1.58E+03	0.00E+00	4.46E+04	4.07E+03	3.66E+03
	Rank	**1.50E+00**	3.00E+00	**1.50E+00**	6.00E+00	5.00E+00	4.00E+00
	Mean	**4.73E+3**	5.74E+03	5.01E+03	2.76E+04	8.51E+03	7.09E+03
$f5$	Std.	1.45E+03	1.63E+03	1.96E+03	5.37E+03	5.10E+02	6.09E+02
	Rank	**1.00E+00**	3.00E+00	2.00E+00	6.00E+00	5.00E+00	4.00E+00
	Mean	7.87E+04	2.82E+07	**6.88E+4**	3.37E+10	1.04E+07	4.19E+06
$f6$	Std.	2.56E+05	4.11E+07	2.55E+05	3.21E+10	3.20E+06	8.96E+05
	Rank	2.00E+00	5.00E+00	**1.00E+00**	6.00E+00	4.00E+00	3.00E+00
	Mean	1.23E+01	6.39E+02	**9.77E+0**	1.76E+03	1.03E+02	6.27E+01
$f7$	Std.	3.84E+00	5.19E+02	4.51E+00	7.15E+02	1.79E+01	8.47E+00
	Rank	2.00E+00	5.00E+00	**1.00E+00**	6.00E+00	4.00E+00	3.00E+00
	Mean	2.10E+01	**2.09E+1**	2.10E+01	2.10E+01	2.10E+01	2.10E+01
$f8$	Std.	5.81E-02	7.00E-02	5.95E-02	4.33E-02	7.25E-02	5.55E-02
	Rank	5.00E+00	**1.00E+00**	2.00E+00	6.00E+00	3.00E+00	4.00E+00
	Mean	4.89E+01	3.69E+01	**3.28E+1**	4.46E+02	7.52E+01	7.12E+01
$f9$	Std.	1.16E+01	1.22E+01	6.10E+00	6.54E+01	5.14E+00	4.34E+00
	Rank	3.00E+00	2.00E+00	**1.00E+00**	6.00E+00	5.00E+00	4.00E+00
	Mean	1.27E+02	**9.55E+1**	1.24E+02	5.81E+02	2.54E+02	2.42E+02
$f10$	Std.	3.67E+01	3.81E+01	3.81E+01	1.27E+02	1.61E+01	1.55E+01
	Rank	3.00E+00	**1.00E+00**	2.00E+00	6.00E+00	5.00E+00	4.00E+00
	Mean	2.56E+01	**2.26E+1**	2.28E+01	3.89E+01	3.38E+01	3.20E+01
$f11$	Std.	3.52E+00	4.08E+00	3.56E+00	3.81E+00	1.58E+00	1.33E+00
	Rank	3.00E+00	**1.00E+00**	2.00E+00	6.00E+00	5.00E+00	4.00E+00
	Mean	**2.78E+4**	3.12E+04	2.88E+04	1.15E+06	1.85E+05	1.42E+05
$f12$	Std.	1.78E+04	2.39E+04	2.28E+04	4.80E+05	2.16E+04	1.80E+04
	Rank	**1.00E+00**	3.00E+00	2.00E+00	6.00E+00	5.00E+00	4.00E+00
	Mean	4.50E+00	**3.21E+0**	4.55E+00	4.76E+02	1.32E+01	1.16E+01
$f13$	Std.	1.05E+00	8.28E-01	1.26E+00	3.82E+02	1.24E+00	1.06E+00
	Rank	2.00E+00	**1.00E+00**	3.00E+00	6.00E+00	5.00E+00	4.00E+00
	Mean	1.29E+01	**1.27E+1**	1.28E+01	1.35E+01	1.34E+01	1.33E+01
$f14$	Std.	2.71E-01	3.79E-01	2.95E-01	2.85E-01	1.41E-01	1.73E-01
	Rank	3.00E+00	**1.00E+00**	2.00E+00	6.00E+00	5.00E+00	4.00E+00

Table 4.18: Synthesis of the optimization results for functions 15 to 25 of the thirty-dimensional CEC2005 benchmark. The optimum result is highlighted in bold.

		NS	PSO	M-PSO	CAPSO	LSHADE	jSO
	Mean	4.29E+02	3.98E+02	4.72E+02	9.78E+02	4.03E+02	**3.56E+2**
$f15$	Std.	6.36E+01	1.47E+02	1.89E+02	1.66E+02	4.22E+01	4.29E+01
	Rank	4.00E+00	2.00E+00	5.00E+00	6.00E+00	3.00E+00	**1.00E+00**
	Mean	**2.73E+2**	3.79E+02	3.12E+02	7.94E+02	2.91E+02	2.82E+02
$f16$	Std.	1.48E+02	1.83E+02	1.48E+02	1.77E+02	1.72E+01	1.26E+01
	Rank	**1.00E+00**	5.00E+00	4.00E+00	6.00E+00	3.00E+00	2.00E+00
	Mean	4.12E+02	**3.39E+2**	4.28E+02	8.69E+02	5.18E+02	4.58E+02
$f17$	Std.	1.13E+02	1.33E+02	1.92E+02	1.87E+02	3.33E+01	3.30E+01
	Rank	2.00E+00	**1.00E+00**	3.00E+00	6.00E+00	5.00E+00	4.00E+00
	Mean	**9.12E+2**	9.32E+02	9.12E+02	1.10E+03	9.27E+02	9.17E+02
$f18$	Std.	2.31E+00	1.90E+01	3.40E+00	1.06E+02	1.86E+00	1.06E+00
	Rank	**1.00E+00**	5.00E+00	2.00E+00	6.00E+00	4.00E+00	3.00E+00
	Mean	**9.13E+2**	9.44E+02	9.16E+02	1.11E+03	9.27E+02	9.17E+02
$f19$	Std.	4.48E+00	3.52E+01	1.93E+01	1.09E+02	2.24E+00	1.16E+00
	Rank	**1.00E+00**	5.00E+00	2.00E+00	6.00E+00	4.00E+00	3.00E+00
	Mean	**9.11E+2**	9.32E+02	9.12E+02	1.08E+03	9.27E+02	9.17E+02
$f20$	Std.	1.61E+00	2.74E+01	2.02E+00	7.72E+01	2.19E+00	1.22E+00
	Rank	**1.00E+00**	5.00E+00	2.00E+00	6.00E+00	4.00E+00	3.00E+00
	Mean	**7.18E+2**	8.15E+02	7.25E+02	1.28E+03	8.55E+02	7.62E+02
$f21$	Std.	2.48E+02	1.91E+02	2.79E+02	1.29E+02	3.59E+01	2.83E+01
	Rank	**1.00E+00**	4.00E+00	2.00E+00	6.00E+00	5.00E+00	3.00E+00
	Mean	**9.24E+2**	9.40E+02	9.40E+02	1.31E+03	1.05E+03	1.02E+03
$f22$	Std.	3.83E+01	4.82E+01	4.07E+01	2.13E+02	1.63E+01	1.44E+01
	Rank	**1.00E+00**	3.00E+00	2.00E+00	6.00E+00	5.00E+00	4.00E+00
	Mean	**6.26E+2**	9.20E+02	7.13E+02	1.24E+03	8.58E+02	7.80E+02
$f23$	Std.	1.71E+02	2.15E+02	2.56E+02	1.06E+02	4.26E+01	2.87E+01
	Rank	**1.00E+00**	5.00E+00	2.00E+00	6.00E+00	4.00E+00	3.00E+00
	Mean	8.91E+02	9.67E+02	9.30E+02	1.30E+03	8.27E+02	**7.79E+2**
$f24$	Std.	2.48E+02	7.41E+01	2.22E+02	2.25E+02	4.20E+01	4.87E+01
	Rank	3.00E+00	5.00E+00	4.00E+00	6.00E+00	2.00E+00	**1.00E+00**
	Mean	9.11E+02	1.08E+03	8.80E+02	1.24E+03	9.00E+02	**8.63E+2**
$f25$	Std.	2.37E+02	9.82E+01	2.39E+02	1.54E+02	5.35E+01	5.31E+01
	Rank	4.00E+00	5.00E+00	2.00E+00	6.00E+00	3.00E+00	**1.00E+00**

References

[1] Payri, F., Molina, S., Martín, J., and Armas, O. "Influence of measurement errors and estimated parameters on combustion diagnosis". In: *Applied Thermal Engineering* 26.2-3 (2006), pp. 226–236. DOI: 10.1016/j.applthermaleng.2005.05.006.

[2] Benajes, J., Olmeda, P., Martín, J., and Carreño, R. "A new methodology for uncertainties characterization in combustion diagnosis and thermodynamic modelling". In: *Applied Thermal Engineering* 71 (2014), pp. 389–399. DOI: 10.1016/j.applthermaleng.2014.07.010.

[3] *OpenFOAM website, https://openfoam.org/.*

[4] Montenegro, G., Onorati, A., Piscaglia, F., and D'Errico, G. "Integrated 1D-MultiD fluid dynamic models for the simulation of I.C.E. Intake and exhaust systems". In: *SAE Technical Papers* 2007.724 (2007), pp. 776–790. DOI: 10.4271/2007-01-0495.

[5] Lucchini, Tommaso et al. "A comprehensive model to predict the initial stage of combustion in SI engines". In: *SAE Technical Papers* 2 (2013). DOI: 10.4271/2013-01-1087.

[6] Lucchini, Tommaso et al. "Automatic Mesh Generation for CFD Simulations of Direct-Injection Engines". In: *SAE Technical Papers* 2015-April.April (2015). DOI: 10.4271/2015-01-0376.

[7] Lucchini, Tommaso, Pontoni, Daniel, D'Errico, Gianluca, and Somers, Bart. "Modeling diesel combustion with tabulated kinetics and different flame structure assumptions based on flamelet approach". In: *International Journal of Engine Research* 21.1 (2020), pp. 89–100. DOI: 10.1177/1468087419862945.

[8] Zhou, Qiyan, Lucchini, Tommaso, D'Errico, Gianluca, Hardy, Gilles, and Lu, Xingcai. "Modeling heavy-duty diesel engines using tabulated kinetics in a wide range of operating conditions". In: *International Journal of Engine Research* 22.4 (2021), pp. 1116–1132. DOI: 10.1177/1468087419896165.

[9] Ismail, H.M., Ng, H.K., Gan, S., and Lucchini, T. "Approach for the Modeling of Reacting Biodiesel Fuel Spray using OpenFOAM". In: *SAE Technical Paper Series* 1 (2014), pp. 1–9. DOI: 10.4271/2014-01-2565.

[10] D'Errico, G., Lucchini, T., Hardy, G., Tap, F., and Ramaekers, G. "Combustion Modeling in Heavy Duty Diesel Engines Using Detailed Chemistry and Turbulence-Chemistry Interaction". In: *SAE Technical Paper Series* 1 (2015), pp. 1–14. DOI: 10.4271/2015-01-0375.

[11] Dukowicz, John K. "A particle-fluid numerical model for liquid sprays". In: *Journal of Computational Physics* 35.2 (1980), pp. 229–253. DOI: 10.1016/0021-9991(80)90087-X.

[12] Yakhot, Victor and Orszag, Steven A. "Renormalization-Group Analysis of Turbulence". In: 57.14 (1986), pp. 1722–1724.

[13] Ra, Youngchul and Reitz, Rolf D. "A reduced chemical kinetic model for IC engine combustion simulations with primary reference fuels". In: *Combustion and Flame* 155.4 (2008), pp. 713–738. DOI: 10.1016/j.combustflame.2008.05.002.

[14] Zhu, Yongfei et al. "Development of diesel surrogates for reproducing the effect of fuel properties on engine combustion and emissions using an optimized decoupling physical–chemical surrogate (DPCS) model". In: *Fuel* 310.PB (2022), p. 122424. DOI: 10.1016/j.fuel.2021.122424.

[15] Peters, N. "Laminar flamelet concepts in turbulent combustion". In: *Symposium (International) on Combustion* 21.1 (1988). Twenty-First Symposuim (International on Combustion), pp. 1231–1250. DOI: https://doi.org/10.1016/S0082-0784(88)80355-2.

[16] Barths, H, Hasse, C, and Peters, N. "Computational fluid dynamics modelling of non-premixed combustion in direct injection diesel engines". In: *International Journal of Engine Research* 1.3 (2000), pp. 249–267. DOI: 10.1243/1468087001545164.

[17] Peters, N. "Laminar diffusion flamelet models in non-premixed turbulent combustion". In: *Progress in Energy and Combustion Science* 10.3 (1984), pp. 319–339. DOI: 10.1016/0360-1285(84)90114-X.

[18] D'Errico, G., Lucchini, T., Contino, F., Jangi, M., and Bai, X. S. "Comparison of well-mixed and multiple representative interactive flamelet approaches for diesel spray combustion modelling". In: *Combustion Theory and Modelling* 18.1 (2014), pp. 65–88. DOI: 10.1080/13647830.2013.860238.

[19] D'Errico, Gianluca et al. "Reduced kinetic mechanisms for diesel spray combustion simulations". In: *SAE Technical Papers* 6.Cmc (2013). DOI: 10.4271/2013-24-0014.

[20] Lucchini, T, Onorati, A, and Hardy, G. "CFD modelling of combustion in Heavy-Duty Diesel Engines". In: (2014), pp. 1–15.

[21] Zhou, Qiyan, Lucchini, Tommaso, D'Errico, Gianluca, and Hardy, Gilles. "Validation of Diesel Combustion Models with Turbulence Chemistry Interaction and Detailed Kinetics". In: *SAE Technical Papers* (2019). DOI: 10.4271/2019-24-0088.

[22] Zhou, Qiyan et al. "Computational Modeling of Diesel Spray Combustion with Multiple Injections". In: *SAE Technical Papers* 2020-April.April (2020), pp. 2839–2858. DOI: 10.4271/2020-01-1155.

[23] Heywood, John B. *Internal Combustion Engine Fundamentals. N. York: McGraw-Hill.* 1988.

[24] Leung, K. M., Lindstedt, R. P., and Jones, W. P. "A simplified reaction mechanism for soot formation in nonpremixed flames". In: *Combustion and Flame* 87.3-4 (1991), pp. 289–305. DOI: 10.1016/0010-2180(91)90114-Q.

[25] Paul, B and Ganesan, V. "Flow field development in a direct injection diesel engine with different manifolds". In: *International Journal of Engineering, Science and Technology* 2.1 (2010), pp. 80–91. DOI: 10.4314/ijest.v2i1.59089.

[26] Madras, Technology and Madras, Technology. "CFD Analysis of in-Cylinder Flow and Air-Fuel Interaction on Different Combustion Chamber Geometry in DISI Engine CFD Analysis of in-Cylinder Flow and Air-Fuel Interaction on Different Combustion Chamber Geometry in DISI Engine". In: *International Journal on Theoretical and Applied Research in Mechanical Engineering (IJTARME)* 2.3 (2013), pp. 104–108.

[27] Harshavardhan, Ballapu and Mallikarjuna, J. M. "Effect of piston shape on in-cylinder flows and air-fuel interaction in a direct injection spark ignition engine - A CFD analysis". In: *Energy* 81 (2015), pp. 361–372. DOI: 10.1016/j.energy.2014.12.049.

[28] Gugulothu, S. K. and Reddy, K. H.C. "CFD simulation of in-cylinder flow on different piston bowl geometries in a DI diesel engine". In: *Journal of Applied Fluid Mechanics* 9.3 (2016), pp. 1147–1155. DOI: 10.18869/acadpub.jafm.68.228.24397.

[29] Kaplan, Mahmut, Özbey, Mustafa, and Özcan, Hakan. "Numerical Investigation of the Effects of Intake Port Geometry on In-Cylinder Motion and Combustion in Diesel Engine". In: *Int. J. Eng. Sci.* 7 (2018), pp. 16–26. DOI: 10.9790/1813-0706021626.

[30] Baratta, Mirko, Chiriches, Silvestru, Goel, Prashant, and Misul, Daniela. "CFD modelling of natural gas combustion in IC engines under different EGR dilution and H2-doping conditions". In: *Transportation Engineering* 2.August (2020). DOI: 10.1016/j.treng.2020.100018.

[31] Silva, Mickael et al. "Computational assessment of effects of throat diameter on combustion and turbulence characteristics in a pre-chamber engine". In: *Applied Thermal Engineering* 212.April (2022), p. 118595. DOI: 10.1016/j.applthermaleng.2022.118595.

[32] Maes, Noud et al. "Heavy-Duty Diesel Engine Spray Combustion Processes: Experiments and Numerical Simulations". In: *SAE Technical Papers* 2018-September (2018), pp. 1–22. DOI: 10.4271/2018-01-1689.

[33] Borman, Gary and Nishiwaki, Kazuie. "Internal-combustion engine heat transfer". In: *Progress in Energy and Combustion Science* 13.1 (1987), pp. 1–46. DOI: 10.1016/0360-1285(87)90005-0.

[34] Dec, John E. "Advanced compression-ignition engines - Understanding the in-cylinder processes". In: *Proceedings of the Combustion Institute* 32 II.2 (2009), pp. 2727–2742. DOI: 10.1016/j.proci.2008.08.008.

[35] Komninos, N. P. and Kosmadakis, G. M. "Heat transfer in HCCI multizone modeling: Validation of a new wall heat flux correlation under motoring conditions". In: *Applied Energy* 88.5 (2011), pp. 1635–1648. DOI: 10.1016/j.apenergy.2010.11.039.

[36] Komninos, N. P. and Rakopoulos, C. D. "Heat transfer in hcci phenomenological simulation models: A review". In: *Applied Energy* 181 (2016), pp. 179–209. DOI: 10.1016/j.apenergy.2016.08.061.

[37] Decan, Gilles et al. "Evaluation of wall heat flux calculation methods for CFD simulations of an internal combustion engine under both motored and HCCI operation". In: *Applied Energy* 232 (2018), pp. 451–461. DOI: 10.1016/J.APENERGY.2018.09.214.

[38] Angelberger, C., Poinsot, T., and Delhay, B. "Improving near-wall combustion and wall heat transfer modeling in SI engine computations". In: *SAE Technical Papers* (1997). DOI: 10.4271/972881.

[39] Zhiyu Han, Rolf D. Reitz. "A temperature wall function formulation for variable-density turbulent flows with application to engine convective heat transfer modeling". In: *Int. J. Mass Transfer* 40.3 (1997), pp. 613–625. DOI: 10.1016/0017-9310(96)00117-2.

[40] Huh, Kang Y., Chang, I. Ping, and Martin, Jay K. "A comparison of boundary layer treatments for heat transfer in IC engines". In: *SAE Technical Papers* (1990). DOI: 10.4271/900252.

[41] Rakopoulos, C. D., Kosmadakis, G. M., and Pariotis, E. G. "Critical evaluation of current heat tranfsfer models used in CFD in-cylinder engine simulations and establishment of a comprehensive wall-function formulation". In: *Applied Energy* 87.5 (2010), pp. 1612–1630. DOI: 10.1016/j.apenergy.2009.09.029.

[42] Benajes, Jesus et al. "Optimization of the combustion system of a medium duty direct injection diesel engine by combining CFD modeling with experimental validation". In: *Energy Conversion and Management* 110 (2016), pp. 212–229. DOI: 10.1016/j.enconman.2015.12.010.

[43] Broatch, Alberto, Novella, Ricardo, Gomez-Soriano, Josep, Pal, Pinaki, and Som, Sibendu. "Numerical Methodology for Optimization of Compression-Ignited Engines Considering Combustion Noise Control". In: *SAE International Journal of Engines* 11.6 (2018), pp. 625–642. DOI: 10.4271/2018-01-0193.

[44] Decan, Gilles et al. "Evaluation of Wall Heat Flux Models for Full Cycle CFD Simulation of Internal Combustion Engines under Motoring Operation". In: *SAE Technical Papers* 2017-September (2017). DOI: 10.4271/2017-24-0032.

[45] Martínez Rodríguez, D. "Optimization Algorithm Based on Novelty Search Applied to the Treatment of Uncertainty in Models." PhD thesis. Universitat Politècnica de València, 2021. DOI: 10.4995/Thesis/10251/178994.

[46] Kennedy, J. and Eberhart, R. "Particle swarm optimization". In: *Proceedings of ICNN 95 - International Conference on Neural Networks*. IEEE, 1995. DOI: 10.1109/icnn.1995.488968.

[47] Lehman, Joel and Stanley, Kenneth O. "Exploiting open-endedness to solve problems through the search for novelty". In: *Artificial Life - ALIFE* (2008).

[48] Marini, Federico and Walczak, Beata. "Particle swarm optimization (PSO). A tutorial". In: *Chemometrics and Intelligent Laboratory Systems* 149 (2015), pp. 153–165. DOI: 10.1016/j.chemolab.2015.08.020.

[49] Chen, Junfeng, Ren, Ziwu, and Fan, Xinnan. "Particle Swarm Optimization with Adaptive Mutation and Its Application Research in Tuning of PID Parameters". In: *2006 1st International Symposium on Systems and Control in Aerospace and Astronautics*. IEEE, 2006. DOI: 10.1109/isscaa.2006.1627490.

[50] Beheshti, Zahra and Shamsuddin, Siti Mariyam Hj. "CAPSO: centripetal accelerated particle swarm optimization". In: *Information Sciences* 258 (2014), pp. 54–79.

[51] Piotrowski, Adam P. "L-SHADE optimization algorithms with population-wide inertia". In: *Information Sciences* 468 (2018), pp. 117–141. DOI: 10.1016/j.ins.2018.08.030.

[52] Brest, Janez, Maucec, Mirjam Sepesy, and Boskovic, Borko. "Single objective real-parameter optimization: Algorithm jSO". In: *2017 IEEE Congress on Evolutionary Computation (CEC)*. IEEE, 2017. DOI: 10.1109/cec.2017.7969456.

[53] Suganthan, P. N. et al. "Problem Definitions and Evaluation Criteria". In: *CEC 2005 Special Session on Real Parameter Optimization*. 2005.

[54] *Python programming language - https://www.python.org*. [Online; accessed 31 January 2020].

[55] *Package for scientific computing with Python - https://numpy.org*. [Online; accessed 31 January 2020].

[56] Derrac, Joaquín, García, Salvador, Molina, Daniel, and Herrera, Francisco. "A practical tutorial on the use of nonparametric statistical tests as a methodology for comparing evolutionary and swarm intelligence algorithms". In: *Swarm and Evolutionary Computation* 1.1 (2011), pp. 3–18. DOI: https://doi.org/10.1016/j.swevo.2011.02.002.

[57] Payri, Raul, Gimeno, Jaime, Novella, Ricardo, and Bracho, Gabriela. "On the rate of injection modeling applied to direct injection compression ignition engines". In: *International Journal of Engine Research* 17.10 (2016), pp. 1015–1030. DOI: 10.1177/1468087416636281.

[58] Payri, R., Salvador, F. J., Gimeno, J., and Bracho, G. "A new methodology for correcting the signal cumulative phenomenon on injection rate measurements". In: *Experimental Techniques* 32.1 (2008), pp. 46–49. DOI: 10.1111/j.1747-1567.2007.00188.x.

[59] Benajes, Jesús, Novella, Ricardo, Pastor, Jose Manuel, Hernández-López, Alberto, and Kokjohn, Sage L. "Computational optimization of the combustion system of a heavy duty direct injection diesel engine operating with dimethyl-ether". In: *Fuel* 218 (2018), pp. 127–139. DOI: 10.1016/j.fuel.2018.01.020.

[60] Benajes, Jesus et al. "Analysis of the combustion process, pollutant emissions and efficiency of an innovative 2-stroke HSDI engine designed for automotive applications". In: *Applied Thermal Engineering* 58.1-2 (2013), pp. 181–193. DOI: 10.1016/j.applthermaleng.2013.03.050.

[61] Hernández López, Alberto. "Optimization and analysis by CFD of mixing-controlled combustion concepts in compression ignition engines [Tesis doctoral no publicada]". PhD thesis. 2018. DOI: https://doi.org/10.4995/Thesis/10251/103826.

Chapter 5

Optimization of the combustion system of CI engines using conventional diesel

5.1 Introduction

From the previous literature review and methodology, it could be inferred that the CI engines running on conventional fuel still have room for improvement to fulfill the pollutant emissions standards. In this framework, this chapter focuses on the optimization of the combustion system of a 4-cylinder, 4-stroke MD engine through the combination of a numerical model with an optimization algorithm. In the first place, the objective of this process is to improve the ISFC while maintaining NO_x and soot emissions below the reference engine values. Therefore, this research focuses on understanding the requirements of the combustion system to optimize fuel consumption, respecting the emissions constraints.

Previously, the engine model was validated in Section 4.4 through the comparison of the simulation results against the experimental data of the real engine operating at the point of maximum power. This point was selected to be the bases of this study, considering it is one of the most demanded points during the operation of the engine.

A very large number of parameters to define the combustion chamber, the injection, and the air-management system can be inspected in order to lead to the optimum combustion system. The most important is to understand how each parameter can affect the combustion and how they interact with each other to match the optimum configuration. Among all these large numbers of variables that can be used, Section 5.2 presents a resume of all the chosen parameters and why each one was selected for this study.

Furthermore, this first optimization will allow the evaluation of the methodology developed in this thesis. In addition, it will provide an understanding of how explorers and conquerors particles evolve, the convergence capability of the NS algorithm, and especially that it can be capable of improving a preexisting combustion system. Furthermore, the algorithm behavior is evaluated when applied to a complex multi-variable problem. An extra challenge for this optimization is that the reference engine has been extensively developed by the manufacturer and is very efficient, increasing the difficulty of achieving a more efficient combustion system while maintaining the same emission levels.

The main barrier to the optimization process described before is its computational cost. In order to evaluate a single engine configuration (a candidate solution of the algorithm), 4 computational cores are needed, and the time to complete 1 engine simulation is nearly 20 hours. A wide range of the search space must be explored, and at the same time that a better optimum than the current engine configuration must be found. Also, the topology of the search space is not known, but several local optima may exist.

This chapter begins with the optimization parameters and objective function definition. Afterward, the results of the optimization process are presented. The evaluation of the objective function, after this, the progress of the input parameters are shown. Furthermore, the constraints and the objective parameter are analyzed for all cases simulated during the process. Subsequently, the optimized case is evaluated and compared with the reference case. Following, a parametric dependence evolution is presented in order to show what each parameter implies in the combustion system. The subsequent part is a heat transfer analysis comparing the optimized case with the reference one. The chapter ends with a summary of the chapter and the main conclusions of the results.

5.2 Optimization parameters and objective function

Among the various parameters that make up the combustion system, nine different variables were selected as inputs to the optimization process. These elements were selected according to their impact on the combustion process and subsequently implemented within the algorithm. Following all the parameters are presented:

- Geometrical parameters: These parameters are specially important once they are responsible for the geometry, the piston shape that implies directly on the CR, and for the consequence on the combustion process. The geometry strongly affects the fuel distribution inside the combustion chamber and the air-fuel mixing rate, thus also affecting pollutant emissions. The importance of the shape design in the combustion system development was already reported in [1–3].

- Number of holes: This variable directly impacts the amount of fuel injected into the combustion chamber. As the total area of the injector is maintained constant, it is necessary to adjust the hole diameter for each number of holes tested. The number of holes enhances the air-fuel mixing in the same way that the combustion chamber and the spatial distribution of the spray inside the chamber to avoid spray overlap. Increasing the diameter of the holes, or decreasing the number of holes, reduces the nozzle exit velocity, which helps to decrease the NO_x emissions while increasing the fuel consumption. Moreover, smaller orifices reduce CO, HC, and soot emissions [2, 4, 5].

- Injection pressure: Like the same way the last parameter, the injection pressure composes the injection system. Also, it is responsible for the injection of the fuel, changing the velocity of the liquid fuel, which influences the atomization of the fuel. Low values of injection pressure enlarge fuel particles and the ID time. This situation leads to an increment of NO_x, CO. On the other hand, a higher injection pressure value leads to a shorter ID and an increment in soot emissions [6–8].

- Swirl number: This parameter characterizes the swirl motion of the fluxes inside the combustion chamber. The swirl ratio improves the internal flow and atomization. Moreover, it influences the temperature and flame spread. Some studies show that increasing the swirl number reduces exhaust emissions due to the increment of in-cylinder mixing

while decreasing the power due to the higher pumping losses and wall heat loss [9–11].

- EGR: The gas recirculation has influenced the composition of the gas during the intake. The EGR is a widely known and used technique to control NO_x emissions. This parameter affects diesel engines by providing an increase in the thermal capacity of the air entering the combustion chamber as some of the inlet O_2 is replaced by CO_2 evaporating H_2O. This change in initial concentrations reduces the gas temperature inside the cylinder during the combustion process, thus generating lower emissions of NO_x. However, this reduction in O_2 concentration reduces soot oxidation during combustion, leading to higher soot emission levels from the engine [12, 13].

All the parameters used in the optimization process and their ranges are shown in Table 5.1. The limits of each parameter range were established considering technological limitations and the safe operating condition defined by the manufacturer.

Table 5.1: Range of the input parameters considered in the optimization.

Parameter	Range
Geometrical parameter 1 [-]	[-0.5, 1.0]
Geometrical parameter 2 [-]	[-1.0, 1.25]
Geometrical parameter 3 [-]	[-1.0, 1.0]
Geometrical parameter 4 [-]	[0.0, 1.0]
Geometrical parameter 5 [-]	[-1.4, 0.1]
Number of injector nozzles [-]	[4, 12]
Swirl number at IVC [-]	[1.0, 3.0]
Injection pressure [bar]	[1500, 2000]
EGR [%]	[0, 30]

Figure 5.1 shows the position of each geometrical parameter used to define the piston bowl shape. Moreover, the direction in which each point can move is presented in the figure. The bowl center position, piston radius, and crevice region are constant for all possible geometries however, in order to generate different geometries and maintain the same CR (16), the squish height is adjusted. The ability to move geometric parameters of this methodology provides a certain degree of freedom, making it possible to generate several different geometries.

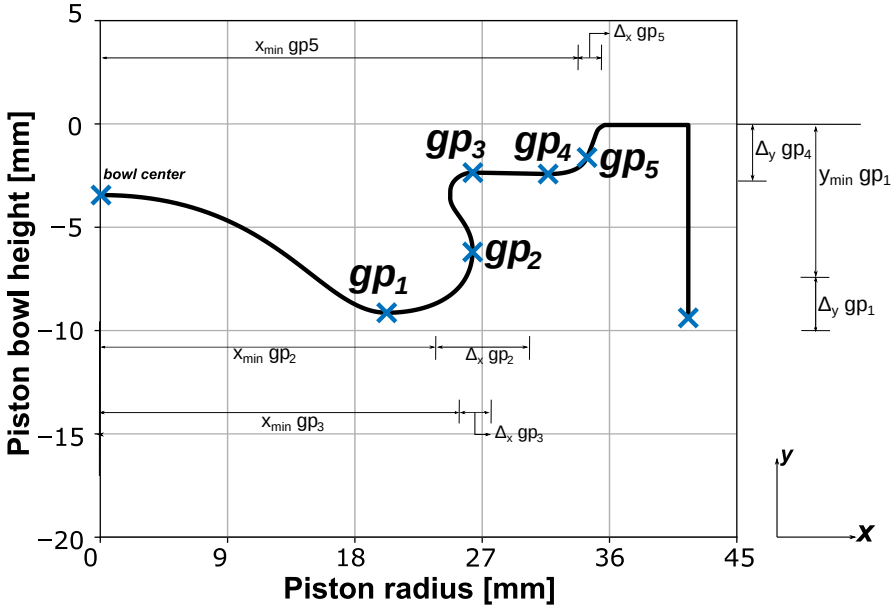

Figure 5.1: Geometrical parameters position and its respective movement.

As mentioned, this optimization aims to reduce the specific fuel consumption (ISFC) and the exhaust emissions of NO_x and soot. Additionally, the emission values were restricted to a certain level; configurations that exceed the emission constraints are penalized accordingly. The operating point used for the CFD model validation was selected as the baseline for the constraint values. This way, the objective function was formulated to consider the relative importance of ISFC, soot, and NO_x against the baseline values. These considerations were expressed in the objective function as follows:

$$OF = f_1(NO_x) \cdot coef_{NO_x} + f_2(soot) \cdot coef_{soot} + f_3(ISFC) \cdot coef_{ISFC} \quad (5.1)$$

where $f_1(NO_x)$, $f_2(soot)$, and $f_3(ISFC)$ are calculated as defined:

where f_1, f_2, and f_3 are, respectively, the functions for NO_x, soot, and ISFC. f_{CFD} is the value obtained in the CFD simulation for each variable, whereas $NO_{x,lim}$, $soot_{lim}$ and $ISFC_{lim}$ refers to the emission levels achieved in the baseline configuration. Finally, $coef_{NO_x}$, $coef_{soot}$, and $coef_{ISFC}$ are coefficients used to balance the equation according to the order of magnitude of each term. The value of the objective function is the one that feeds back the NS algorithm for the following iteration.

Table 5.2: Component functions of the parameters to optimize and the constraints.

Condition	$f_1(\mathrm{NO}_x)$ . . . . . Eq. (5.2)
if $f_{CFD} < f_{lim}$	$\frac{f_{CFD}}{f_{lim}}$
if $f_{CFD} \geq f_{lim}$	$\frac{f_{CFD}}{f_{lim}} + 100 \cdot (f_{CFD} - f_{lim})^2$
Condition	$f_2(\mathrm{soot})$ . . . . . Eq. (5.3)
if $f_{CFD} < f_{lim}$	$\frac{-log(f_{CFD})}{log(f_{lim})}$
if $f_{CFD} \geq f_{lim}$	$\frac{-log(f_{CFD})}{log(f_{lim})} + 10^6 \cdot (log(f_{CFD}) - log(f_{lim}))^2$
Condition	$f_3(\mathrm{ISFC})$ . . . . . Eq. (5.4)
if $f_{CFD} < f_{lim}$	$\frac{f_{CFD}}{f_{lim}}$
if $f_{CFD} \geq f_{lim}$	$\frac{f_{CFD}}{f_{lim}} + 100 \cdot (f_{CFD} - f_{lim})^2$

As the main objective is to increase the efficiency of the engine at the same time as it reduces its NO_x and soot emissions, the values of the coefficients used are: $coef_{ISFC} = 50$, $coef_{NO_x} = 5$ and $coef_{soot} = 5 \cdot 10^{-4}$.

5.3 Optimization results

The first step was to analyze the convergence of the objective function during the optimization process. The convergence of the NS algorithm is accomplished by the mathematical solution of the objective function value, calculated using the Equations 5.1, 4.2, 4.3, and 4.4 based on the simulation results. Figure 5.2 shows the convergence of the objective function for all the simulated cases during the optimization process. It is shown that the objective function values decrease as more cases are simulated, converging toward the minimum value. Furthermore, it can be seen that most of the particles that present small objective function values are conqueror particles. As proposed by Novelty Search, the explored particles are always looking for new positions throughout the search space, so a large part of the obtained results generates high OF values, and therefore few points are seen in the graph. Then, the conqueror particles must refine the search in positions close to the minimum

obtained by the explorers. The best particle in this optimization process was obtained around the simulated case number 780.

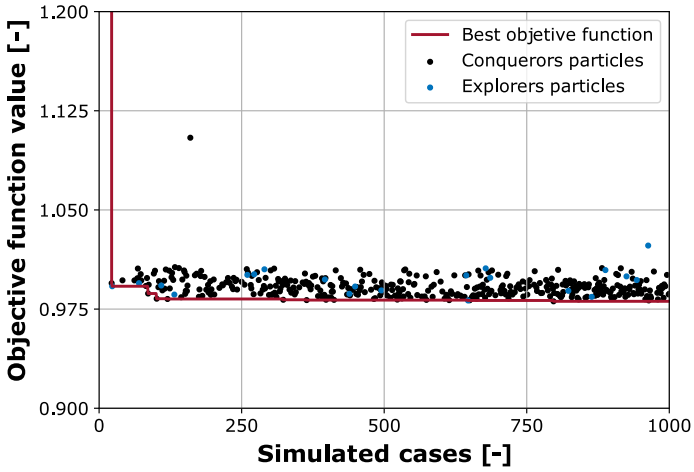

Figure 5.2: Objective function convergence.

The distribution of the inputs during all the optimization processes is shown in Figure 5.3. It is possible to see that the explorer particles (blue dots) are distributed over the domain for all particles. In contrast, the conquerors particles (black dots) are concentrated in specific areas for each input, maintaining the search for the best result in this close region of the local optimum. The distribution of the geometric parameters is throughout the domain since it is necessary to combine all five parameters to obtain the bowl geometry so that each parameter alone does not have the same effect as the injection or air-management system parameters. The injection pressure converges to higher values of pressure since the simulated case number 250. This behavior is due to the impact of this parameter in emissions once higher injection pressure values lead to lower NO_x emissions at the cost of an increment of soot. However, this reduction in NO_x has more impact on the optimization process. The swirl number shows changes during the process. Start with lower values until around case 300, after this grows and at the last 250 simulations, it goes down again. This is because the swirl number needs to be tied to the number of injector nozzles since both parameters impact the spray distribution inside the combustion chamber. The best example of particle movement is the EGR rate distribution. As the EGR rate is a widely used parameter for NO_x emission control, it can be seen that during the first simulations, until

the simulated case number 100, the EGR rate moved throughout the domain. According to the response of this parameter, the algorithm kept it in this zone (around 15% EGR) for the conquering particles once this value presented a good result, while the exploring particles were evaluated throughout the search space until the end of the algorithm execution.

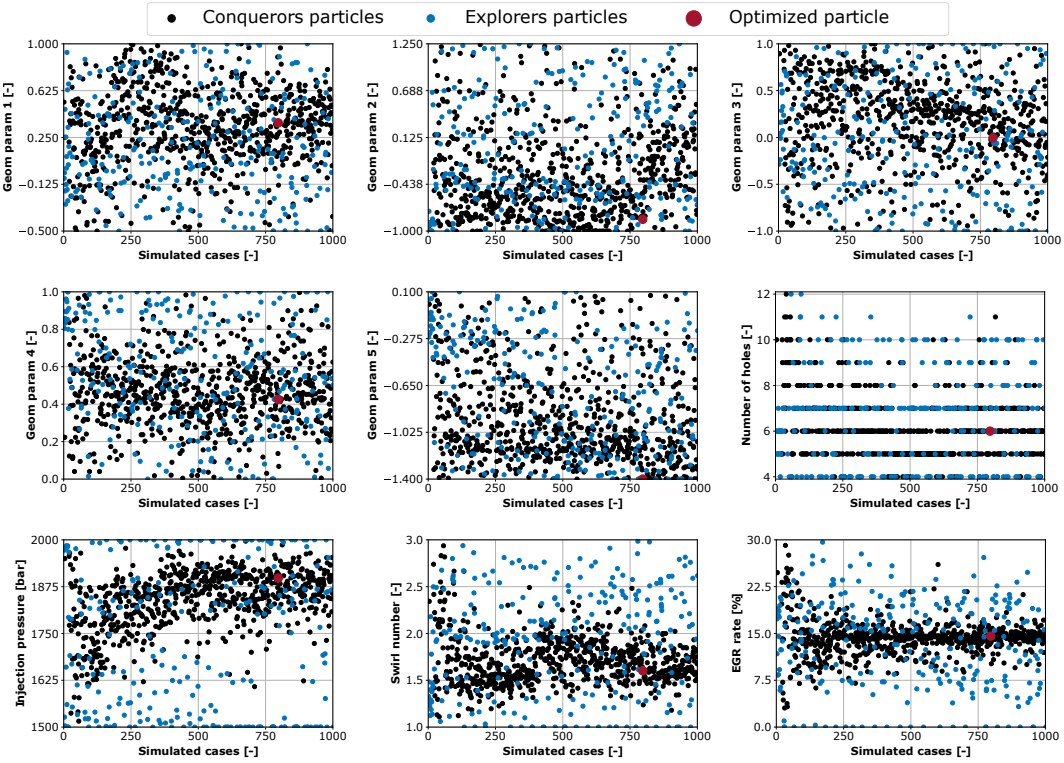

Figure 5.3: Inputs distribution during the optimization process.

Figure 5.4 shows the evolution of the swirl number during the optimization process in order to exemplify how the NS algorithm changes during its execution. It can be seen how the explorers particles move through the search space until the end of the process. Moreover, it is possible to see how the conquerors particles move to meet the optimal value at a certain iteration. Until case 250, the points are widely distributed between the values; however, the swirl number decreases to 1.5 according to the swirl value of the local optimized point. After case 300, the swirl number starts to grow, and the particles are grouped around the swirl number equal to 2, the swirl value of the optimized local

value between case 300 and 700. For the final part of the optimization, the swirl number decreases again until the optimized particle is reached. After this point, the conquerors particles are concentrated on exploring the region close to the optimized value.

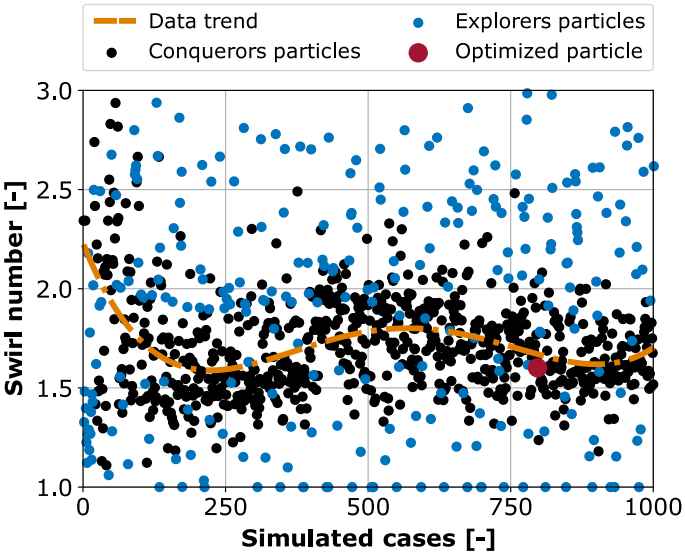

Figure 5.4: Swirl number convergence and trends of the NS algorithm to this specific parameter.

The results of the optimization in terms of the input variables against outputs are shown in Figure 5.5 and Figure 5.6. It demonstrates a thorough exploration of the design space and convergence on a solution. It is possible to see how each parameter evolves during the optimization process and how each affects the emission outputs and the objective function. From Figure 5.1, it is possible to see that the geometric parameter 1 controls the depth position of the piston and presents good results for emissions and ISFC were found for the whole range of values of this parameter, and the highest amount of particles can be found at intermediate values. The re-entrant part position is controlled by geometry parameter 2. This parameter moves the horizontal position where the re-entrant part is located. Moreover, as the value of the parameter decreases, the step part of the piston is longer and moves the lower part of the bowl closer to the bowl center. Thus promoting a better relationship between spray angle and geometry since the angle value is fixed during the optimization process.

The geometrical parameter 3 controls how re-entrant the geometry will be. From the results, it can be seen that this parameter has converged to the lowest possible values, making the bowl not re-entrant. The geometric parameter 4 is also related to the step by increasing and decreasing the height of this part. For both geometrical parameters 3 and 4, good results can be found throughout the data range, and the optimum point is near the intermediate value of both parameters. In addition, geometric parameter 5 is responsible for positioning the ramp at the end of the step. The smaller the parameter, the shorter the step length because the ramp moves towards the center of the geometry, and on the other hand, the larger the parameter, the longer the step because the ramp moves closer to the crevice.

The number of holes was reduced from 10 to 6, which led to better efficiencies (reducing the ISFC and soot) because it promotes a higher rate of heat release during the mixing phase of the combustion, in agreement with the results obtained in [14]. Therefore, the NO_x emissions are increased, thus leading the algorithm to choose the best trade-off between the constraint and objective parameter. The injection pressure was moved to a range near the maximum value to improve the atomization and evaporation of the fuel. Using this high injection pressure, the fuel particles are smaller, reducing the ID time due to the improved atomization and enhanced evaporation. Moreover, the soot emissions are reduced due to better combustion efficiency once the fuel conversion is improved. The fuel-rich region decreases with higher injection pressures due to the better mixing process, reducing soot emissions.

Furthermore, decreasing the swirl number leads to an increase in ISFC by improving air filling and aerodynamic motion consequences because the RoHR is controlled during the diffusive combustion phase [14]. Finally, the best trade-off was found for the EGR rate with intermediate values. Increasing the EGR rate is an alternative to controlling NO_x emissions. Still, as the amount of EGR increases, soot emissions and fuel consumption also increase, which affects the trade-off between NO_x, soot, and ISFC emissions. High concentrations of EGR result in a lower concentration of O_2, which deteriorates the combustion and increases soot, HC, and CO emissions simultaneously, reducing NO_x emissions. Thus, it is necessary to find the proper EGR level that can achieve the low NO_x -soot emissions trade-off being around 15 % in this thesis.

To investigate the impact and evolution of the constraints (NO_x and soot emissions) and the optimization parameter (ISFC) during the optimization process, Figure 5.7 shows the evolution of these parameters during the process. The points are separated into conquerors and explorers particles in black and

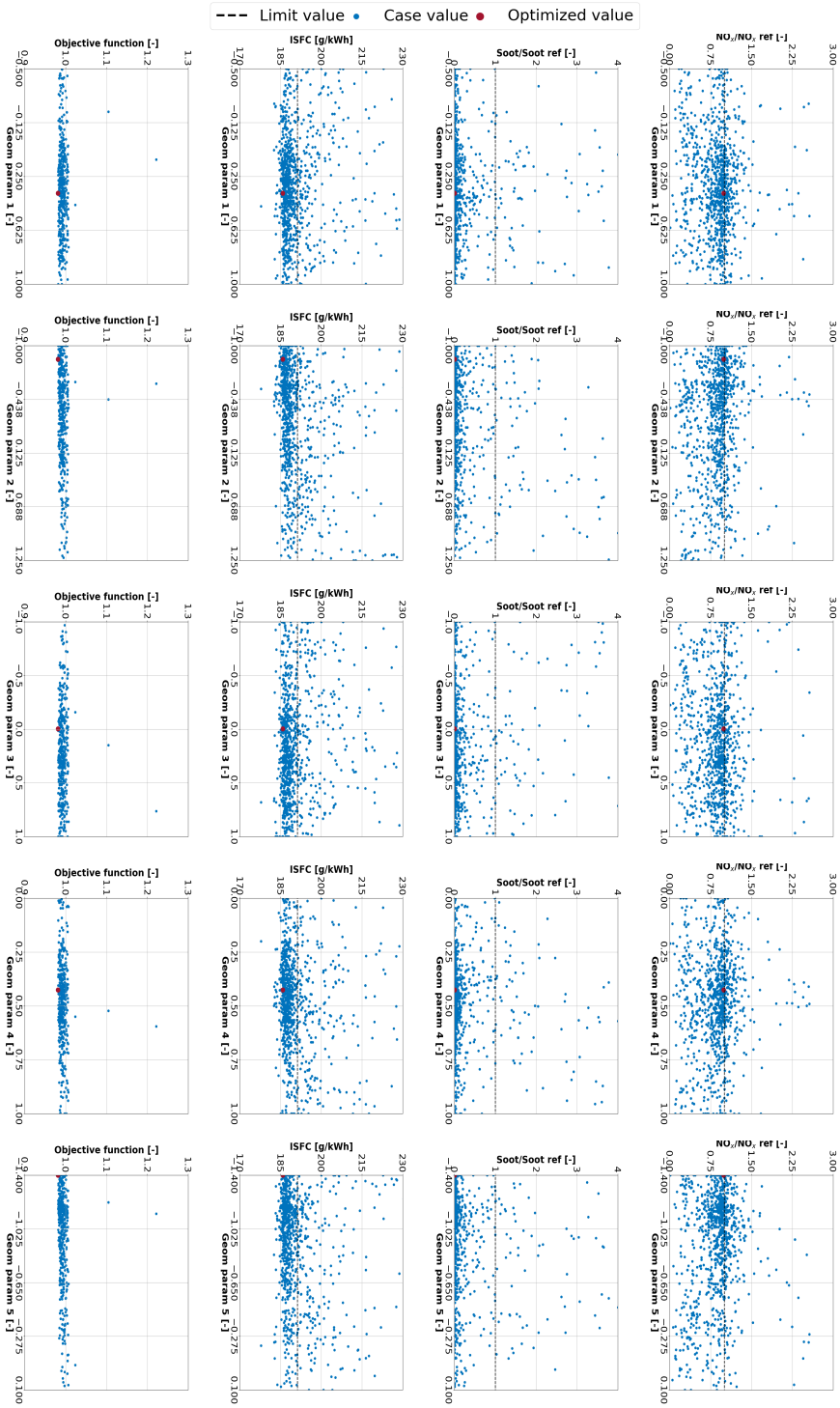

Figure 5.5: Effect of the geometrical parameters on the emissions, fuel consumption, and objective function.

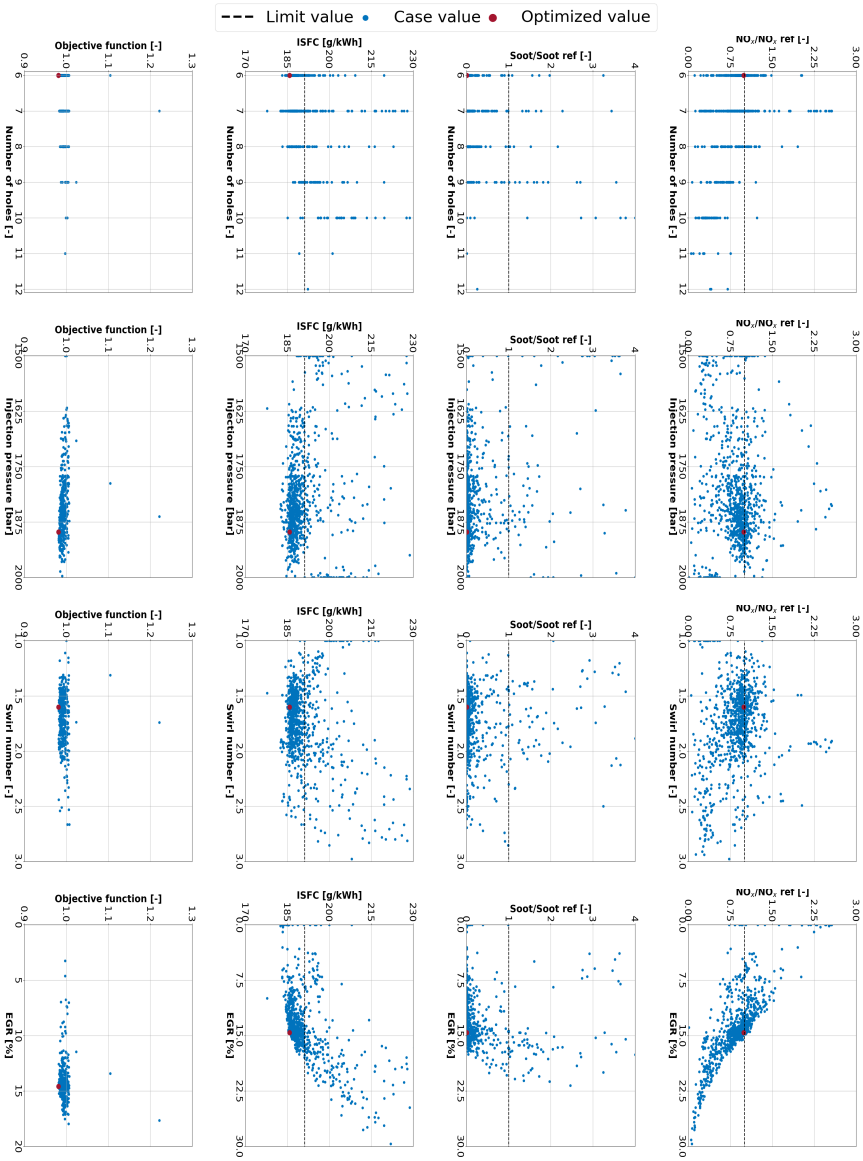

Figure 5.6: Effect of the number of holes, injection pressure, swirl number, and EGR rate on the emissions, fuel consumption, and objective function.

blue dots, respectively. The optimized particle is represented by a red dot, and the limit of each constraint and the initial value of the target output are represented by the orange dashed line. Those configurations are able to accomplish the restrictions established in Table 4.7 and have a low enough value of the objective function. This is the reason why, even if the NO_x and the soot values are below the imposed limit, if they have an ISFC value greater than the reference baseline configuration, the overall objective value is higher rather than the one from other configurations with individual worse NO_x and soot values.

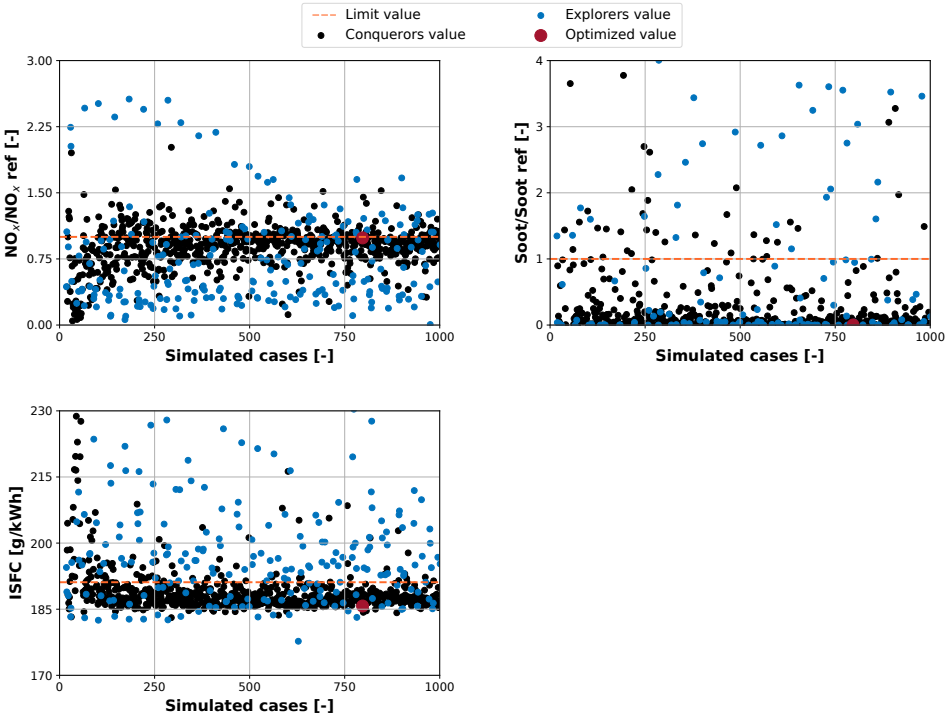

Figure 5.7: Constraints and objective parameter evolution for all the optimization process.

Figure 5.8 presents the effect of each constraint and the objective parameter on the objective function value and shows that the best case is the better trade-off between all the NO_x, soot, and ISFC results. The optimized case is not the case with the lowest ISFC value. However, when searching for the NO_x value for this particle, it can be seen that the value is higher than the NO_x

value found for the optimized case. Then the higher value of NO_x penalizes the OF calculation, underestimating the lowest ISFC case as the best.

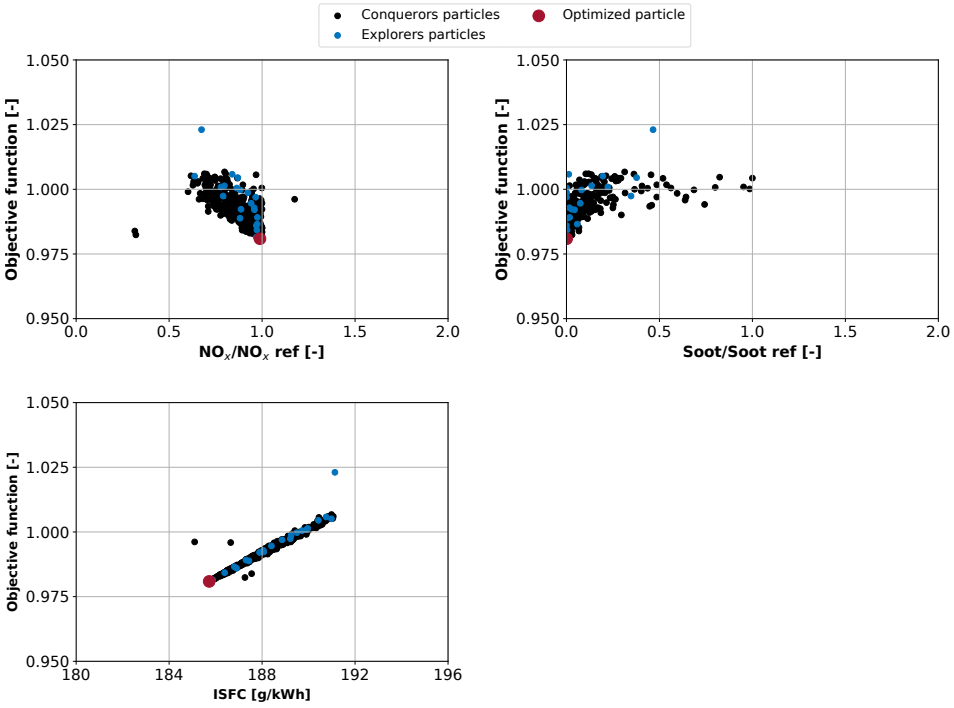

Figure 5.8: Effect of the NO_x, soot, and ISFC on the objective function.

Through the analysis of Figure 5.8, it can be seen that there are cases that present lower values for both NO_x emissions and fuel consumption but are not the optimized, which is the one with the lowest objective function. Thus, Figure 5.9 compares the piston shapes for each of these two cases in addition to the baseline case. The point with a lower ISFC value also is the case with a lower soot emissions level. The simulation with lower NO_x, minimum NO_x case, is similar to the baseline. It also has a re-entrant geometry however presents some differences in the downhill, maximum deep, and step part of the piston. When it comes to the minimum ISFC point, the re-entrant part was modified for a flat wall. Moreover, the downhill and the step of this geometry are similar to the one that presents lower NO_x emissions.

Furthermore, the set of inputs to configure the injection and air-management system of each simulation is presented in Table 5.3. In both

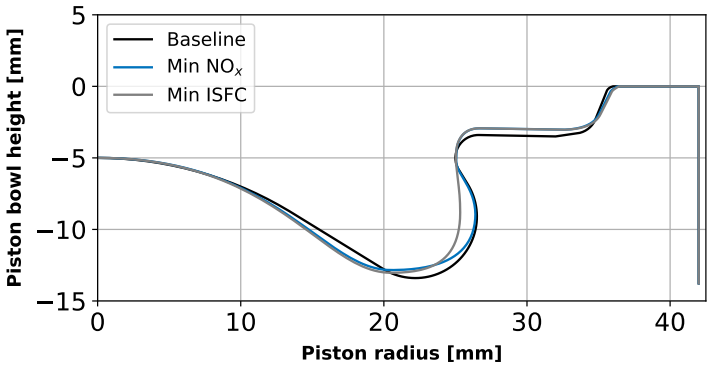

Figure 5.9: Difference between geometries of baseline and cases that present lower NO_x and ISFC values.

cases, minimum NO_x and minimum ISFC present similar configurations. The main differences are in the EGR rate and injection pressure, being that the EGR rate is the main change. These two cases present a fewer number of holes, lower swirl number, higher injection pressure, and EGR rate than the baseline configuration.

Table 5.3: Inputs comparison between baseline and cases that present lower NO_x and ISFC values.

	Baseline	Min NO_x	Min ISFC
Number of holes [-]	10	6	6
Swirl number [-]	2	1.6	1.6
Injection pressure [bar]	1800	1888	1861
EGR [%]	0	14.53	12.01

Figure 5.10 compares the in-cylinder pressure, temperature, RoHR, and normalized HR of the baseline, minimum NO_x, and ISFC cases. The results obtained for in-cylinder pressure are very similar, well adjusted during the compression phase, reaching the same maximum pressure values. For the rate of heat release (top right figure), it is possible to see that the peak of the premixed phase is higher for the baseline case, which means that the ID is also

higher for this case, most likely because of the lower injection pressure. For the diffusive combustion phase, it is possible to see that in both simulations, minimum NO_x and ISFC, there is higher energy release. Thus, the burning rate is improved for these engine configurations. In contrast to the pressure curve, the in-cylinder temperature presents differences that can start to explain the reason for these cases not being the optimized one. The minimum ISFC case presents a higher maximum temperature, which indicates that this case presents more NO_x emissions than the other cases. The temperature for the min NO_x is almost at the same level as the previously cited case however, the EGR rate for this case is higher, which helps to reduce the emissions. The normalized HR shows that the combustion efficiency of all cases is around 97-98% since the minimum ISFC case shows a little higher value. This means that almost all the injected fuel in the cycle was burned. This result was expected once the fuel consumption depended on the combustion efficiency.

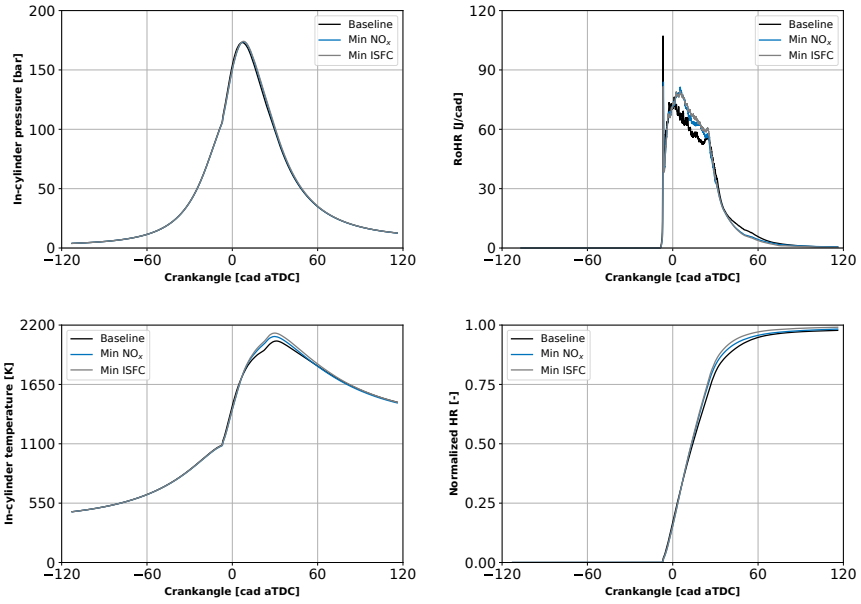

Figure 5.10: Comparison between baseline, minimum NO_x, and minimum ISFC results. Left side: In-cylinder pressure and temperature evolution. Right side: RoHR and normalized HR evolution.

Table 5.4 resumes the emissions and fuel consumption for the baseline, minimum NO_x, and ISFC values. Once the emissions of NO_x have an opposite behavior than the ISFC, the case with lower emissions of NO_x presents a higher

fuel consumption value which ends up harming the trade-off between results. Even so, the case with lower NO_x emissions shows excellent results, but since the optimization process was focused on reducing fuel consumption and the emission parameters were the constraints, this case ended up not being the optimized one. On the other hand, the case with the best ISFC value has a high level of NO_x emissions, thus not complying with the previously imposed constraint.

Table 5.4: Constraints and optimized parameter comparison between baseline and cases with lower NO_x and ISFC values.

	Baseline	Min NO_x	Min ISFC
Objective function [-]	1	0.98	0.99
NO_x [ppm]	1460	460	1715
Soot [ppm Mass]	2.1E-06	1.4E-07	3.1E-11
ISFC [g/kWh]	191	188	185

In order to locate the particle that provides the best solution within the explored range, NO_x, soot, and ISFC were compared in Figure 5.11. In both figures, the characteristic Pareto front of CI engines shows the trade-off between ISFC and NO_x, and ISFC and soot. In those plots, several solutions satisfy the restrictions imposed, improving the optimizing parameters. However, even if there are particles that present better results of NO_x, soot, or ISFC separately, the solution of the objective function could be high since it depends on all parameters together. For example, if one simulation provides a low value of ISFC, probably the result of NO_x is higher because these parameters have antagonistic behavior in engines, and the objective function presents a higher value because the NO_x value penalizes the solution. For this reason, the optimum solution is focused on optimizing the ISFC and soot while maintaining the NO_x within limits.

Based on the best solution of the objective function and the verification of the reference limits from Pareto's front, the optimized configuration was compared with the baseline configuration. In Figure 5.12, the differences between the geometries are shown. It is possible to see how the piston bowl shape changes. The greatest change in the bowl shape is in the re-entrant geometry that was actualized for a flat wall before the step. Moreover, the region that starts in the bowl center and goes until the maximum bowl depth is moved in order to a better match with the spray angle, which was maintained constant in this process. The step part is now larger and has a little less

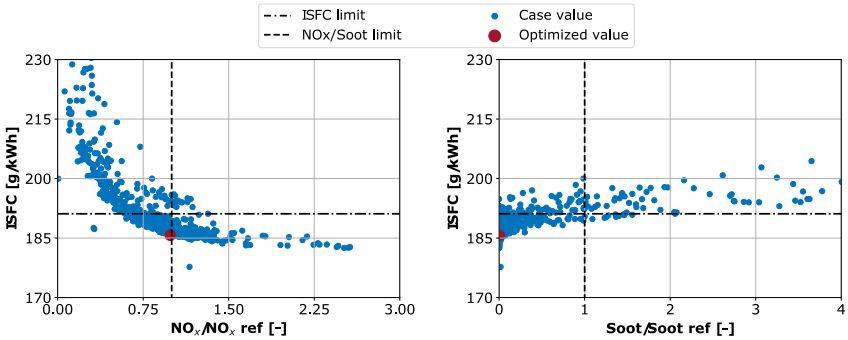

Figure 5.11: Pareto front comparison between the parameter to be optimized and the constraints: : ISFC against NO_x emissions (left) and ISFC against soot emissions (right)

height, which means that this component was moved to a closer cylinder head region. This new step position helps to direct the flame to the cylinder head.

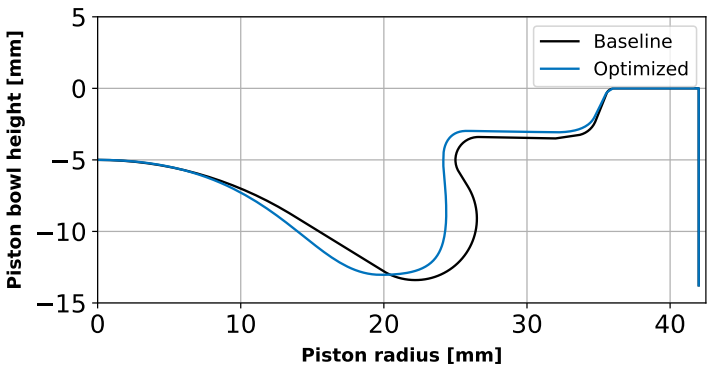

Figure 5.12: Difference between baseline and optimized geometry.

Table 5.5 shows the values of the inputs for the optimized case compared to the baseline. The new configuration counts with a lower number of holes which helps to avoid the interactions between the sprays. Moreover, the swirl level is lower, which also acts on the movement of the spray inside the combustion

chamber. With higher injection pressure, the NS algorithm searches to reduce the soot emissions and improve the ISFC of the optimized case. In the end, to control the NO_x emissions, the EGR rate is adjusted until the point that offers the best trade-off for fuel consumption emissions.

Table 5.5: Inputs comparison between baseline and optimized case.

	Baseline	Optimized
Number of holes [-]	10	6
Swirl number [-]	2	1.6
Injection pressure [bar]	1800	1898
EGR [%]	0	14.57

5.4 Engine results

5.4.1 Engine Optimization Results

This section presents the results related to the engine parameters and analysis of the optimized combustion system in comparison with the baseline one. In Figure 5.13, a comparison of in-cylinder pressure, temperature, rate of heat release, and normalized HR traces between the baseline and optimized design is presented. It can be seen that the in-cylinder pressure is similar to the baseline case, reaching the same levels of maximum pressure. However, differences in the HRR are more evident. While the premixed peak is reduced (helping to reduce combustion noise), the burning rate is increased during the diffusive combustion phase. This could promote a higher temperature of the flame which is shown in the graph on the left of the bottom line but within the limit of not generating more NO_x and provide some thermodynamic advantages. Regarding the cumulative HR, it is possible to see how the increment in the RoHR during the diffusive phase of the combustion leads to an improvement in the combustion process of the optimized case achieving better efficiency of this process.

Table 5.6 shows the values of the results for the optimized case in comparison with the baseline case, where a reduction in pollutant emissions and consumption is obtained. From Table 5.5, it can be seen that the number of holes decreases, therefore there is more space between sprays, promoting the air entrainment and avoiding the jet-to-jet interaction that enhances the combustion performance. At the same time, the injection pressure increases slightly, which is related to a higher spray momentum and better atomization

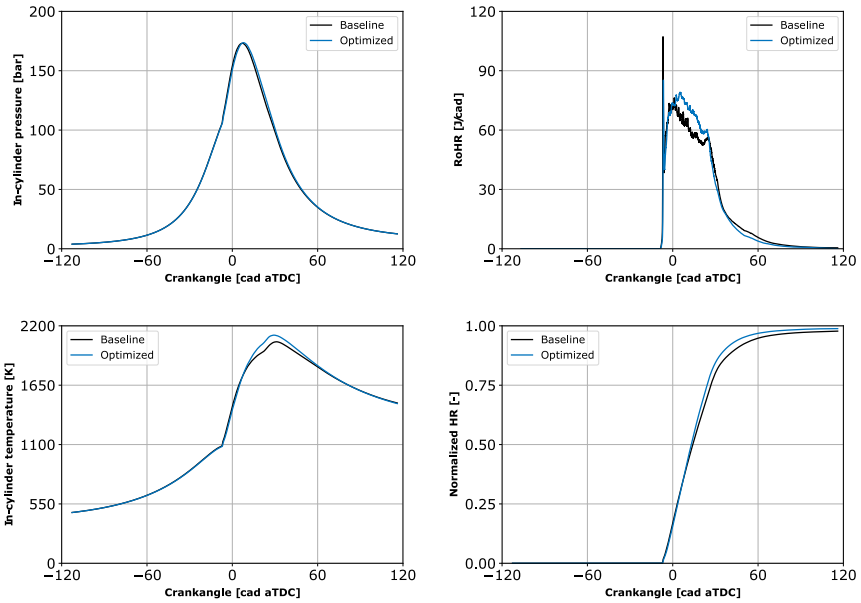

Figure 5.13: Results comparison between baseline and optimized case. Left side: In-cylinder pressure (top) and temperature (bottom) evolution. Right side: estimated rate of heat release (top) and normalized HR (bottom)

and evaporation. Moreover, the optimized case uses an EGR ratio of 14.57%, which is a well-known and effective practice for reducing NO_x emissions. All these trends corroborate that the methodology is providing reasonable results, delivering a solution that is in agreement with the performance of combustion systems reported in the literature with the added value of finding the solution in less time than other methods [15].

Table 5.6: Output comparison between baseline and optimized case.

	Baseline	Optimized
NO_x [ppm]	1460	1443
Soot [ppm Mass]	2.1e-06	1.9e-09
ISFC [g/kWh]	191	186

To better understand these trends, Figure 5.14 shows the temporal evolution of the cylinder mass over three relevant equivalence ratios for the baseline and the optimum case. Specifically, the equivalence ratio is into three different

bands bounded by 0.55, 1.05, and 1.75. It can be seen that the optimized case configuration increases the mixing rate during the non-premixed combustion, subsequently raising the burning velocity (note that near stoichiometric mixtures completely disappear after 80 CAD aTDC). In contrast, the baseline case is not able to burn all the fuel during the combustion process, keeping some stoichiometric mixture in the cylinder at the exhaust valve opening. This mixing improvement leads to enhanced combustion, which reduces soot and noise emissions while keeping the NO_x emission under control. The improved mixing conditions guaranteed by the optimized bowl correlate well with the shorter combustion duration and the improved performance, as shown previously.

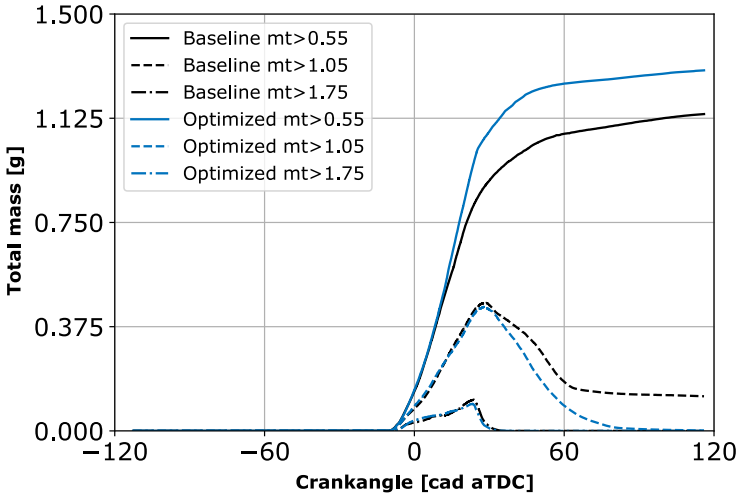

Figure 5.14: Mass with equivalence ratio evolution over three different bands: 0.55, 1.05, and 1.75 (lean mixture, near to stoichiometric, and rich mixture).

Figure 5.15 shows the temperature contours of both cases, and the white line represents the stoichiometric mixture fraction of each case. TDC snapshots show that in the optimized case, the jet penetrates faster since the injection pressure is slightly higher and also because it has a bigger nozzle hole diameter. That promotes an improved jet-wall interaction with the piston surface distributing the flame in the combustion chamber. Moreover, the optimized case presents a more homogeneous temperature distribution, thereby lowering the NO_x production.

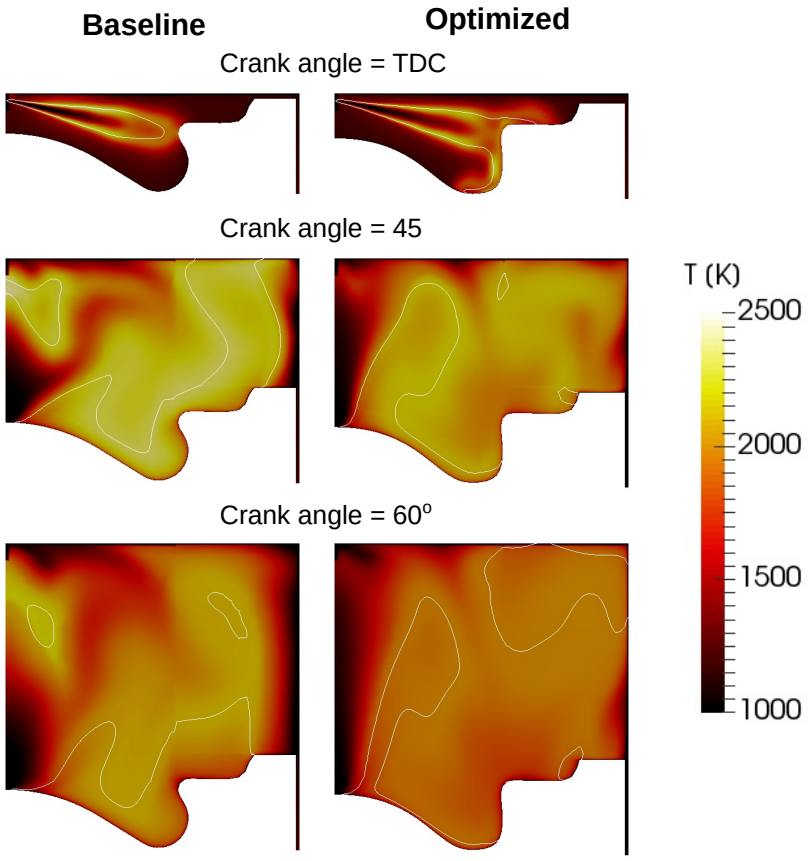

Figure 5.15: Comparison of the temperature distribution inside the combustion chamber between the baseline and optimum cases for three different crank angles instants (TDC, 45 and 60).

The mixture fraction distribution is represented in Figure 5.16. These instants of time were selected due to the great interaction of the spray with the piston when it is close to the TDC. The white line corresponds to the stoichiometric mixture fraction value during the fuel injection. Due to the higher injection pressure value, the fuel particles are smaller and penetrate with more velocity inside the combustion chamber. This is demonstrated in the crank angle -5 and TDC once there is a bigger cloud of fuel near the step region of the piston. While the baseline geometry leads the fuel to the re-entrant part and later to the bowl center direction, as can be seen after the crank angle 10, the optimized geometry leads to the step part and then

to the cylinder head direction. With this distribution of mixture fraction is understood the higher temperatures close to the cylinder head and liner in the optimized case once in the stoichiometric condition, the temperatures are higher. In general, it can be assumed by this analysis that the new geometry distributes the fuel better inside the combustion chamber.

Through the previous analysis, it is possible to see considerable differences in heat transfer losses between the baseline and optimized cases. Figure 5.17 shows the heat transfer rate evolution for each boundary of the domain. The results show that the baseline case has less heat transfer through the liner since it directs the flame to the re-entrant part of the bowl and also to the cylinder head. The optimized case, on the other hand, for having a higher injection pressure, causes the flame to penetrate faster, thus being directed to the upper part of the bowl towards the liner and the cylinder head, thus presenting a higher heat transfer through the liner. This can be seen in Figure 5.15, for the optimized case, it can be seen at the moment of TDC, the flame has already found the piston wall, and part of it was reflected the step region, while for the baseline case, the flame has not yet found the piston wall. Also, at the other time instants, it can be seen that the baseline case always maintains a smaller temperature in the liner region. As already presented in Figure 5.13, the in-cylinder mean temperature is higher than the optimized case, which in addition to the fact that the flame is conducted to the cylinder head direction from earlier, the HT of the cylinder head is higher and can be seen in the top-right figure of Figure 5.15. By contrast, the piston HT is almost the same for both cases once they have similar areas. The total heat transfer corroborates the presented by Figure 5.18, showing the higher HT for the optimized case mainly from the results of liner and cylinder head HT.

5.4.2 Parameter evolution

In this study, it is also possible to analyze the effect of each of the parameters used at a time isolated. This study was performed by changing one parameter in each simulation and comparing the energy balance. First, the geometry of the baseline case was changed to the optimized geometry while keeping all other parameters the same as the original engine parameters. In the next step, the number of holes, then the swirl number, the injection pressure, and finally the EGR rate, thus reconfiguring the optimized combustion system obtained by the NS algorithm. Figure 5.18 shows the energy balance comparison for all the simulations. First, the optimum piston bowl geometry was run, keeping all the baseline settings. This resulted in an improvement of the cycle work with a reduction of the unburned fuel, and it can be seen that the work obtained

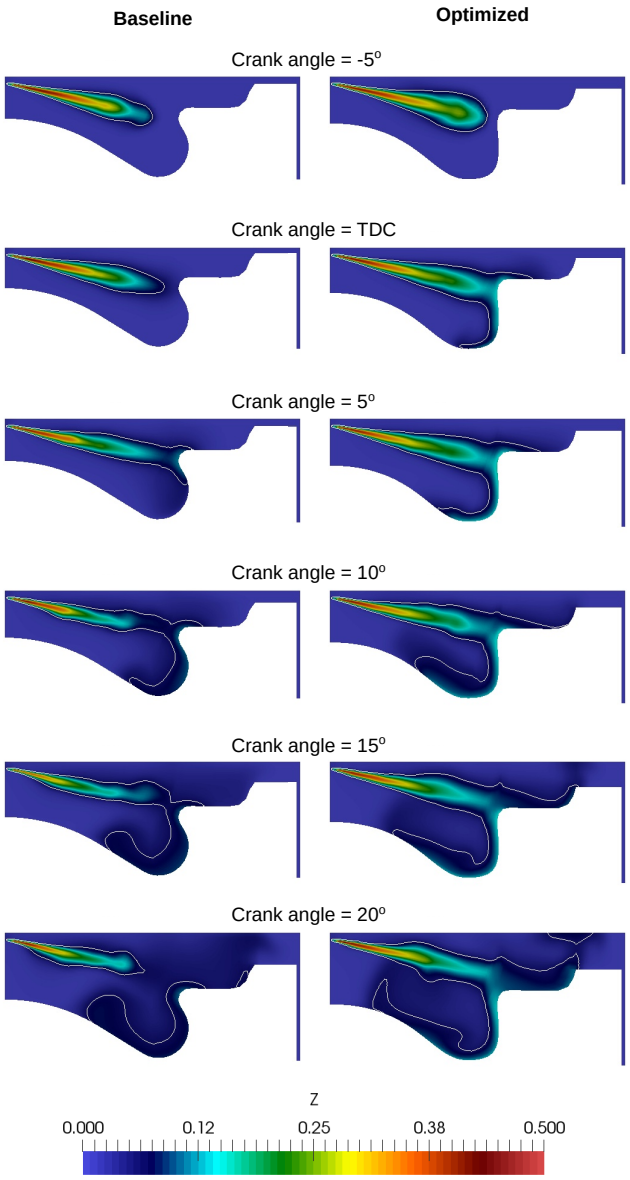

Figure 5.16: Comparison of the mixture fraction distribution inside the combustion chamber between the baseline and optimum cases for three different crank angles instants (TDC, 45 and 60).

is higher for all cases of the new combustion system when compared to the baseline case. The optimized geometry was able to improve the mixing and

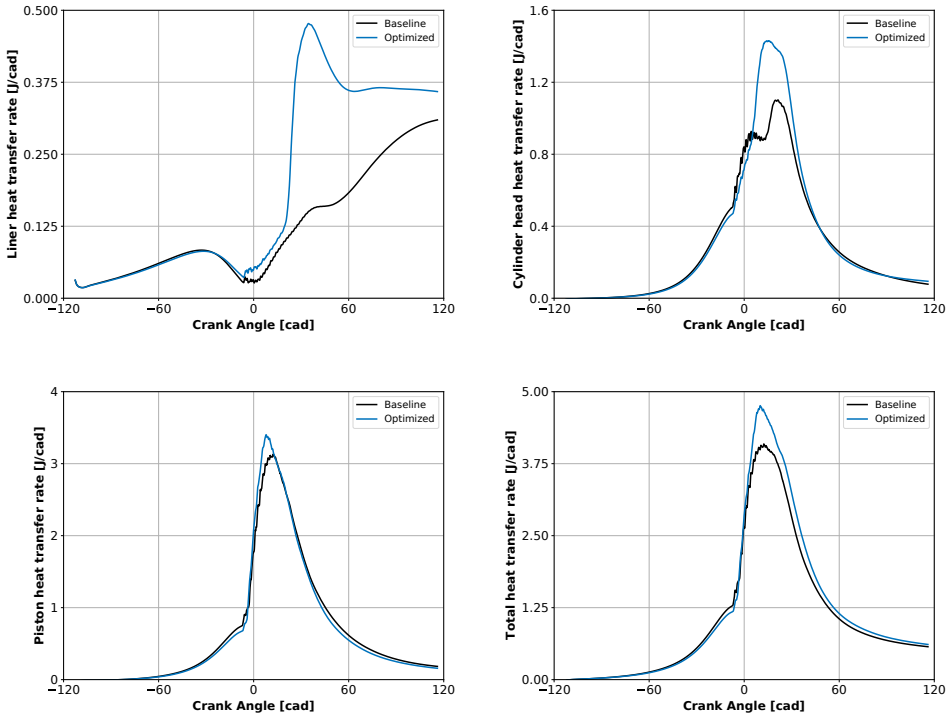

Figure 5.17: Heat transfer results comparison: baseline vs. optimum case.

efficiency and at the same time, maintain almost constant HT and exhaust losses. Following, the number of injector holes were adjusted, which results in a way better work of the cycle, reducing, even more, the exhaust losses and unburned fuel. On the other hand, the HT losses increased too. Next, the case was repeated with the optimum swirl. The results show a slight improvement in the work, but with incomplete combustion, once the unburned losses are higher than in the last case (with an adjusted number of holes). With the injection pressure adjustment, the use of a higher IP helps to improve the atomization and evaporation of the fuel resulting in mixing and combustion efficiency reducing the exhaust losses. In this particular case, the higher IP combined with a lower number of injector holes and lower swirl number helps to avoid jet-to-jet interactions. Up to this point, all the cases showed better work in comparison with the baseline case. However, none met the NO_x emissions constraint. So, the EGR rate was adjusted to a higher value (from

0 to 14.57%), penalizing the work, exhaust losses, and unburned fuel in order to meet the constraint. Higher EGR reduces the fresh air availability inside the combustion chamber, thus worsening the mixing rate and combustion efficiency of the engine.

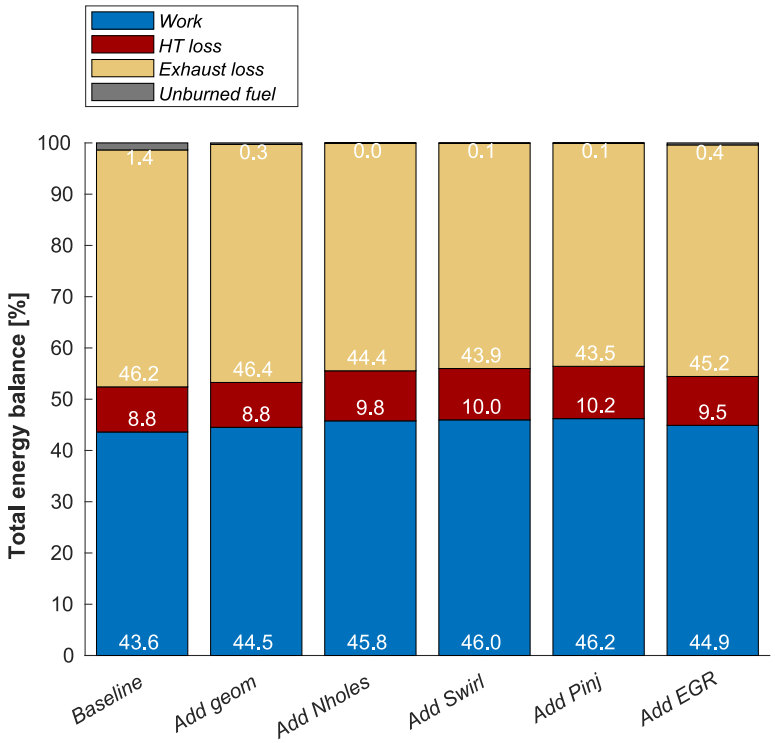

Figure 5.18: Energy balance evolution comparison.

Finally, further studies are required to investigate the implementation of other operating conditions as maximum torque or partial loads in order to analyze if this optimized bowl profile would provide good results in terms of emissions and fuel consumption for those operating conditions. Also, subsequent optimization work is necessary to understand the influence of other input parameters such as spray, including angle, nozzle tip protrusion, and the start of injection, among others.

5.5 Summary and conclusions

The current chapter had the objective of evaluating the proposed optimization methodology based on a combination of CFD modeling with a mathematical

optimization algorithm. The methodology was applied to an MD 4-cylinder 4-stroke CI engine in order to reduce ISFC while keeping NO_x and soot emissions under a defined value based on a real engine. In addition to the optimal configuration, with the use of this methodology, it is possible to obtain a cause-and-effect relationship between the control parameters and the defined objective. Thus, improving the understanding of the combustion system of CI engines and how it can be improved.

After the end of the optimization process, it was obtained a new combustion system that combines a new geometry with an adjusted injection and air-management system. This new combustion system improves the ISFC by around 3% while reducing the soot emissions and maintaining the NO_x constant. The study also indicated that the injection pressure and EGR level are the most critical parameters to obtain this improvement in engine operation. Moreover, it also is necessary to adjust the number of holes and swirl level according to the bowl shape of the combustion chamber.

Additionally, the cases that presented interesting results were analyzed in order to understand the reason the algorithm moved in different directions during the optimization process. Furthermore, a strong trade-off between ISFC and NO_x was found, proving a very limited potential for improving the CI engines.

It is clear from the study conducted in this chapter that an optimization approach is a design tool with a lot of promise since it produces precise results in a fair amount of time. The maximum number of parameters allowed for optimization was 9, which had a restriction on the potential of the optimums. Moreover, the new limits of NO_x standards can penalize the ISFC in the future to achieve the required values. At the same time, this suggests that the CI engines are already optimized, and it is difficult to improve efficiency, being necessary to move to other optimization strategies such as after-treatment or alternative fuels.

References

[1] Wickman, D. D., Senecal, P. K., and Reitz, R. D. “Diesel engine combustion chamber geometry optimization using genetic algorithms and multi-dimensional spray and combustion modeling”. In: *SAE Technical Papers* 110 (2001), pp. 487–507. DOI: 10.4271/2001-01-0547.

[2] Choi, Seungmok, Shin, Seung Hyup, Lee, Jeongwoo, Min, Kyoungdoug, and Choi, Hoimyung. "The effects of the combustion chamber geometry and a double-row nozzle on the diesel engine emissions". In: *Proceedings of the Institution of Mechanical Engineers, Part D: Journal of Automobile Engineering* 229.5 (2015), pp. 590–598. DOI: 10.1177/0954407014547748.

[3] Lee, Seokhwon, Jeon, Joonho, and Park, Sungwook. "Optimization of combustion chamber geometry and operating conditions for compression ignition engine fueled with pre-blended gasoline-diesel fuel". In: *Energy Conversion and Management* 126 (2016), pp. 638–648. DOI: 10.1016/j.enconman.2016.08.046.

[4] Kim, Byong Seok, Yoon, Wook Hyeon, Ryu, Sung Hyup, and Ha, Ji Soo. "Effect of the injector nozzle hole diameter and number on the spray characteristics and the combustion performance in medium-speed diesel marine engines". In: *SAE Technical Papers* 724 (2005). DOI: 10.4271/2005-01-3853.

[5] Vijay Kumar, M., Veeresh babu, A., Ravi Kumar, P., and Manoj Kumar Dundi, T. "Influence of different nozzle hole orifice diameter on performance, combustion and emissions in a diesel engine". In: *Australian Journal of Mechanical Engineering* 18.2 (2020), pp. 179–184. DOI: 10.1080/14484846.2018.1453975.

[6] Çelikten, Ismet. "An experimental investigation of the effect of the injection pressure on engine performance and exhaust emission in indirect injection diesel engines". In: *Applied Thermal Engineering* 23.16 (2003), pp. 2051–2060. DOI: 10.1016/S1359-4311(03)00171-6.

[7] Han, Sangwook and Bae, Choongsik. "The influence of fuel injection pressure and intake pressure on conventional and low temperature diesel combustion". In: *SAE Technical Papers* (2012). DOI: 10.4271/2012-01-1721.

[8] Kattimani, Sunilkumar S., Topannavar, S. N., Shivashimpi, M. M., and Dodamani, B. M. "Experimental investigation to optimize fuel injection strategies and compression ratio on single cylinder DI diesel engine operated with FOME biodiesel". In: *Energy* 200 (2020), p. 117336. DOI: 10.1016/j.energy.2020.117336.

[9] Jafarmadar, S., Taghavifar, Hadi, Taghavifar, Hamid, and Navid, A. "Numerical assessment of flow dynamics for various di diesel engine designs considering swirl number and uniformity index". In: *Energy Conversion and Management* 110 (2016), pp. 347–355. DOI: 10.1016/j.enconman.2015.12.035.

[10] Broatch, Alberto, Olmeda, Pablo, García, Antonio, Salvador-Iborra, Josep, and Warey, Alok. "Impact of swirl on in-cylinder heat transfer in a light-duty diesel engine". In: *Energy* 119 (2017), pp. 1010–1023. DOI: 10.1016/j.energy.2016.11.040.

[11] Yoon, Sungjun, Lee, Seungpil, Kwon, Hyuckmo, Lee, Joonkyu, and Park, Sungwook. "Effects of the swirl ratio and injector hole number on the combustion and emission characteristics of a light duty diesel engine". In: *Applied Thermal Engineering* 142.March (2018), pp. 68–78. DOI: 10.1016/j.applthermaleng.2018.06.076.

[12] Zhang, Wei et al. "Influence of EGR and oxygen-enriched air on diesel engine NO-Smoke emission and combustion characteristic". In: *Applied Energy* 107 (2013), pp. 304–314. DOI: 10.1016/j.apenergy.2013.02.024.

[13] Mobasheri, Raouf and Khabbaz, Seyed Alireza. "Modeling the effects of high EGR rates in conjunction with optimum multiple injection techniques in a heavy duty di diesel engine". In: *SAE Technical Papers* 1 (2014). DOI: 10.4271/2014-01-1124.

[14] Cursente, V., Pacaud, P., and Gatellier, B. "Reduction of the compression ratio on a hsdi diesel engine: Combustion design evolution for compliance the future emission standards". In: *SAE International Journal of Fuels and Lubricants* 1.1 (2009), pp. 420–439. DOI: 10.4271/2008-01-0839.

[15] Broatch, Alberto, Novella, Ricardo, Gomez-Soriano, Josep, Pal, Pinaki, and Som, Sibendu. "Numerical Methodology for Optimization of Compression-Ignited Engines Considering Combustion Noise Control". In: *SAE International Journal of Engines* 11.6 (2018), pp. 625–642. DOI: 10.4271/2018-01-0193.

Chapter 6

Optimization of the combustion system of CI engines fueled with OME

6.1 Introduction

This chapter of the thesis describes the results obtained from the optimization of a combustion system performed for an engine to be able to use e-fuel. As already known, CI engines fueled with conventional fuel are one of the most efficient thermal engines. However, they produce higher quantities of pollutant gas emissions, especially soot and NO_x. According to the previous chapter, optimizing the actual combustion system is possible. However, it is expected that the new emission standards will have even lower limits and thus raise the cost of after-treatment systems for conventional CI engines. For this reason, this chapter is focused on the obtention of a combustion system that is able to run efficiently using alternative synthetic fuel. The potential of this new fuel is that it can be obtained from renewable sources and is designed to produce lower soot emissions.

Synthetic fuels from renewable sources are good alternatives for reducing GHG emissions. Between these fuels, the Oxymethylene Ethers (OMEs) have gained attention since they are able to reduce and even eliminate soot emissions and CO levels as reported in some studies [1–6]. OME synthesis begins with methanol, which is created through the reaction of H_2 and CO_2 [7, 8].

An essential point to the use of OMEs fuels and their blends in substitution of diesel is the possibility of maintaining the same engine architecture that exists on the market, only making minor modifications. Some of OME advantages are the high oxygen content in its composition, the lack of a C-C bond in the molecule structure, which avoids the processes of alkene synthesis, avoiding soot production during the combustion process [4, 9]. Due to this property, it is possible to operate the engine with a high EGR level to control NO_x pollutant emissions [10]. However, the injection system must be adapted to deliver better performance once the physical properties of the OME are different from the conventional diesel fuel. Most of the studies in this area concentrated on using OME and its blends in pre-existing engines in order to evaluate the combustion system efficiency and pollutant emissions. Based on previous studies, the performance of the CI engines fueled with OME can be improved using a combustion system developed to attend to the specific requirements of this fuel. Gaukel et al. in [11] tested different piston bowls geometries being possible to obtain a specific configuration that reduced the NO_x emissions at the same time, maintaining the efficiency at the same level as the original engine. Based on the results, it was concluded that the piston shape strongly influences the combustion process. It is necessary to study the combined effect of geometry, injection, and EGR strategy.

The aim of this chapter is to provide the best combustion system design for an OME fuel-dedicated CI engine using the optimization methodology previously presented. The baseline diesel model presented in the last chapter was used as a reference in this optimization process. The following step is the change of the fuel to OME and calibrating the model to maintain the same amount of energy in the cycle. With the first OME engine model, the NS algorithm was used to optimize the engine. To perform the process, 12 parameters were used simultaneously as the inputs of the algorithm. These 12 parameters are divided into 6 parameters to define the piston bowl shape, the number of injector nozzles, spray angle, injection pressure, swirl number, EGR rate, and IVC pressure to adapt the characteristics of the combustion chamber to the requirements of this renewable fuel. The target of the optimization process is to maximize engine efficiency while reducing NO_x emissions.

This chapter is structured as follows. First, the fuel characteristics are presented. The second part presents the optimization parameters used in the NS algorithm and the objective functions used to evaluate each simulation. The third part is composed of optimization and engine analysis. The next topic of the chapter presents a parametric study performed with a neural network methodology to evaluate the optimized case. At the end of the chapter, the main conclusions are summarized.

6.2 Investigated fuel characteristics

The alternative synthetic fuel used in this part of the study is Oxymethylene Ether 1 (OME_1) with the constitutional formula CH_3-O-$(CH_2$-O$)_1$-CH_3 was used due to its fuel characteristics. One of the main characteristics of this fuel is that it generates negligible soot amount due to the high quantity of oxygen and no C-C bonds in the molecule. Although it produces low levels of soot emissions, it tends to increase the NO_x amount compared to conventional diesel fuel being necessary to use a high EGR rate to control this pollutant emission. Moreover, OME_1 seems convenient in engine applications since its general physicochemical properties are relatively similar to conventional diesel, not requiring significant modifications in the engine. However, as well as other oxygenated compounds, OME_1 has different properties compared to traditional diesel (viscosity, density, lower heating value).

To summarize the main characteristics of this fuel, the main properties for OME_1 used in this study are listed in Table 6.1. Moreover, the effect each property will have on a CI engine working with the new fuel is presented in Table 6.1. With OME_1 already established as the fuel in this part of the thesis, it will be referred to as OME.

Table 6.1: Physical and chemical properties of the fuel.

Fuel	Diesel	OME	Effect in CI engine
Density (15^oC [kg/m^3])	839.91	865.80	It is necessary to adapt the injector diameter
Viscosity (15^o C [Pa · s])	0.0016	0.00032	Due to the lower viscosity it is necessary an additional lubrication
Cetane number [-]	54.18	29	OME fuel ignites with higher temperatures
Lower heating value [MJ/kg]	44.6	22.4	More fuel is necessary to maintain the same energy level in the cycle
Initial Boiling point [^{o}C]	155.1	37.4	Fast evaporation
Final Boiling point [^{o}C]	363.1	38	Fast evaporation
Oxygen content [wt%]	≈ 0	42.1 [1]	Possibility of working with lean combustion
Air fuel relation	15.09	9.02	Possibility of working with lean combustion

Considering the differences between the characteristics of the fuel, especially the lower heating value (LHV) of OME needs to be compensated to obtain the same amount of released energy during the combustion compared to the one obtained with diesel fuel. Different strategies can be employed for compensating this decrease in LHV. One of them is to extend the injection duration to deliver more fuel mass into the combustion chamber, which reduces the combustion efficiency because part of the combustion occurs late. A second possibility could be increasing the rail pressure to deliver a higher mass flow rate, keeping the injection duration short. However, this strategy might affect the spray structure and the wall impingement and the limitation on the maximum pressure that the pump system can supply. The third option is to increase the total area of the nozzle, either by increasing the hole number, or scaling the hole diameter, or both simultaneously. The maximum hole number for this option is limited due to manufacturing and enough space in the nozzle tip to arrange many holes. For this investigation, a combination of the total area scaling is considered. The scaling factor for the same energy flow rate of OME and Diesel is determined by Equations 6.1 and 6.2 based on the energy available in the fuel and Bernoulli's principle for incompressible flows (assuming that the velocity of the flow would be similar when the pressure difference is the same).

$$\dot{m}_{ome1} \cdot LHV_{ome1} = \dot{m}_d \cdot LHV_d \tag{6.1}$$

$$A_{ome1} \cdot \rho_{ome1} \cdot u \cdot LHV_{ome1} = A_d \cdot \rho_d \cdot u \cdot LHV_d, \tag{6.2}$$

where A is the total area in the nozzle, LHV is the lower heating value, ρ is the density of the fuel, and u is the flow velocity in the nozzle exit. The subscripts *ome* and d denote OME and diesel fuel, respectively. The total area is defined as Equation 6.3, being n the number of holes and d_o the exit hole diameter.

$$A = \frac{n \cdot \pi \cdot d_o^2}{4} \tag{6.3}$$

The first step is to perform an OME-fueled engine simulation to verify that the model can qualitatively capture the changes in combustion characteristics expected when diesel fuel is replaced. The engine configuration in terms of boundary conditions and geometry was maintained equal to the diesel case described in Table 4.2 and Figure 4.14 using the coarse mesh. Though, all physical and chemical properties related to the fuel are updated accordingly, as well as the amount of fuel. As commented, the quantity of OME injected in

the combustion chamber is adjusted to reach an equivalent amount of energy since OME has a lower LHV than conventional diesel. Thus, from Equation 6.2, it can be seen that the area must be adjusted to compensate for the differences in density and LHV between the fuels. Since in this simulation, the engine conditions are considered to be the same, the number of holes is also equal to 10, so it is necessary to adjust the exit hole diameter. Considering that the fuel is injected at 60^oC, the density of diesel is higher than that of OME. This leads to an increase in the area and, consequently, the diameter of the hole (from 112 μm to 168 μm) for the case using OME as fuel.

Figure 6.1 shows the results obtained from the case running with OME against the diesel model previously calibrated. Analyzing the heat release rate traces confirmed that the mass fuel adjusted provides a similar quantity of energy released. The pressure trace when OME fuel is injected is slightly higher but still below the limit of 180 bar recommended by the manufacturer to preserve the cylinder's structural integrity. However, using more fuel, there is a higher maximum pressure. As the LHV of the OME is lower than the diesel, it is necessary to use a higher amount of fuel to maintain the same energy in the cycle. The bottom part of Figure 6.1 shows these differences in mass. Moreover, it is possible to note that the ID for OME is lower than the diesel since comparing the start of fuel injection with the rise in the heat release curve happens earlier for OME. The heat release rate traces are comparable in terms of ignition delay; however, in the combustion diffusion phase, OME presents faster combustion and shows a short burn-out phase related to the higher volume of injected fuel. The same behavior can be observed in the work of García et al. [12].

Regarding the pollutant emissions, Table 6.2 shows the predicted results of PMI, soot, and NO_x. As expected, the PMI of the case using OME as fuel is higher, like the differences in the in-cylinder pressure traces. The soot emissions almost disappear when the engine is fueled with OME, although the NO_x levels are more than double that of the diesel reference case. From this initial analysis, it can be seen that the combustion with OME has an acceptable performance when used in traditional architecture for conventional fuel in terms of soot, although the NO_x emissions are unacceptable. Nevertheless, it seems that there is room for improvement if the combustion system is adapted to the OME fuel requirements by means of the optimization procedure.

Figure 6.2 shows a comparison of the mixture fraction and NO concentration between diesel and OME cases with the same configuration. In all figures, the white line is the stoichiometric mixture fraction value in the slice of the simulated case. In the first two columns, it is possible to see the mixture frac-

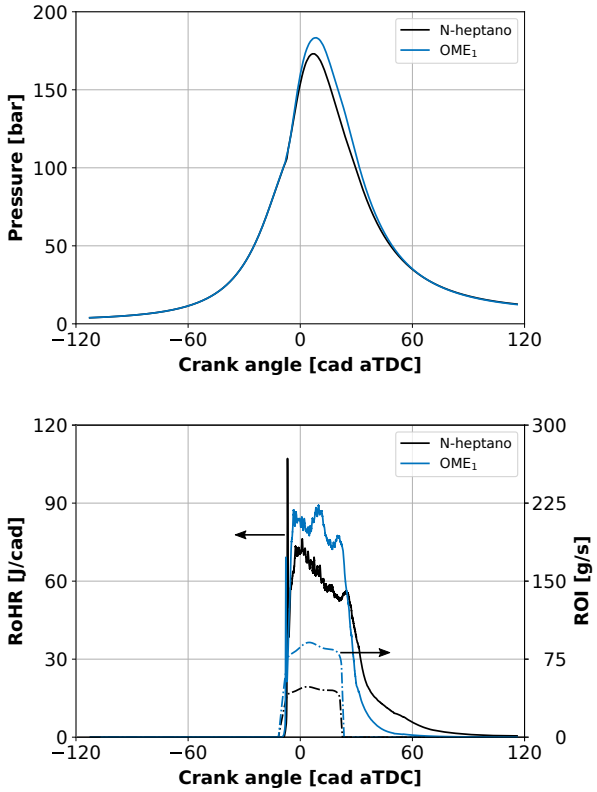

Figure 6.1: Comparison between conventional diesel and OME fuel. Top part: Evolution of the in-cylinder pressure. Bottom part: Estimated Rate of Heat Release and Rate of Injection.

Table 6.2: Pollutant emissions results - Baseline Diesel and OME fuel.

Fuel	PMI [bar]	NO_x [mg/s]	Soot [mg/s]
Diesel	22.50	230.9	0.354
OME1	24.08	773.6	1e-14

tion comparison. In this evolution, it is possible to see how the difference in the amount of fuel interacts with the piston bowl shape. More fuel interacts with the walls, conducted to the re-entrant part and the step region. Furthermore, this higher quantity of fuel inside the combustion chamber will increase the temperature during the combustion process, which leads to a higher wall

temperature. The critical parameters for NO_x formation are high temperature, oxygen enrichment, and high temperature duration. Combining the in-cylinder combustion temperature and NO_x distribution, it can be seen that the formation zone is concentrated near to re-entrant part, and in the first step of the geometry is the result of spray motion after interacting with the walls. Moreover, this rise in temperature will increase the NO_x emissions, and this behavior can be observed in the third and fourth columns of the figure. In general, the relation between the ignition delay and NO_x generation is that decreasing the ignition delay can reduce the reaction time of free nitrogen and oxygen, hence inhibiting the synthesis of NO_x. As combustion proceeds, it can be seen that the NO concentration is higher in the case of using OME as fuel. Unacceptable levels of NO emissions were reached using the same combustion system for both cases. However, considering the soot emissions were practically eliminated, we see potential in using this fuel with a combustion system specifically designed for it. By combining a new geometry with specific injection and air-management systems, it would be possible to obtain a better functioning engine, competitive against a conventional CI engine.

Thus, it is possible to see that many parameters interfere with the engine analysis, many with overlapping characteristics, interacting with each other and being highly non-linear. Therefore, the alternative to obtain a specific combustion system for an engine operating with OME is to use the optimization methodology coupling the NS algorithm with CFD simulations developed and validated in Chapter 5 of this thesis.

6.3 Optimization parameters and objective function

Aiming to optimize the combustion system for the use of OME as fuel, twelve relevant parameters were chosen where:

- Six of them are related to the geometry definition of the bowl.
- Three parameters define the injection system: number of injection nozzle holes, spray angle, and injection pressure.
- The last three parameters, the swirl number at IVC, EGR rate, and IVC pressure, were used to configure the air-management system to define the in-cylinder gas conditions.

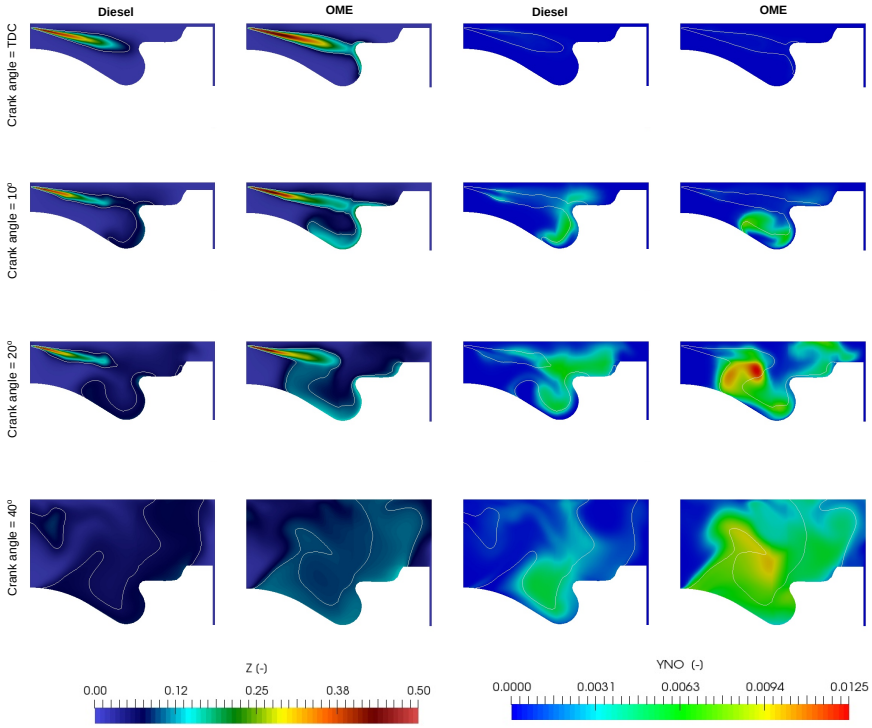

Figure 6.2: Comparison between conventional diesel and OME fuel. Mixture fraction and concentration of NO_x emissions for the reference case adapted to work with OME.

The ranges of those input variables are shown in Table 6.3. When comparing the new inputs against those used in the optimization of the conventional CI engine, the extra geometrical parameter is used to obtain more flexibility for the piston shape generation. The six geometrical points used to generate the bowl profile are presented in Figure 6.3. The blue line represents the profile using the minimum value, while the red line represents the profile obtained using the maximum value possible of the range of each parameter. The black line refers to a geometry using the average values. The gp_1, gp_2, gp_3, and gp_6 are represented by the points, while the gp_4 and gp_5 are the green squares. The gp_1 input will determine the horizontal position of the point and, at the same time, the bottom part of the piston. Moreover, the gp_2 and gp_3 have horizontal positioning and determine the position of the bowl wall and the start of the squish region, respectively. In contrast to the optimization performed in the previous chapter, the gp_4 and gp_5 control the corresponding

curvature between gp_3-gp_2 and gp_2-gp_1. Additionally, the gp_5 impacts the gp_1 vertical movement to better adjust the curvature of the piston shape. The gp_6 controls the bowl center position and can be moved in the vertical direction. The position of the start and end of the crevice region is represented by the x, and its position is the same for all geometries. The spray angle was implemented in this process since there is more variation in bowl geometry, and a better match between these factors is needed. Figure 6.3 shows the angle range of change. The maximum and minimum values of the spray angle (SA_{max} = 170 deg and SA_{min} = 155 deg) are possible for the algorithm to select values between this range.

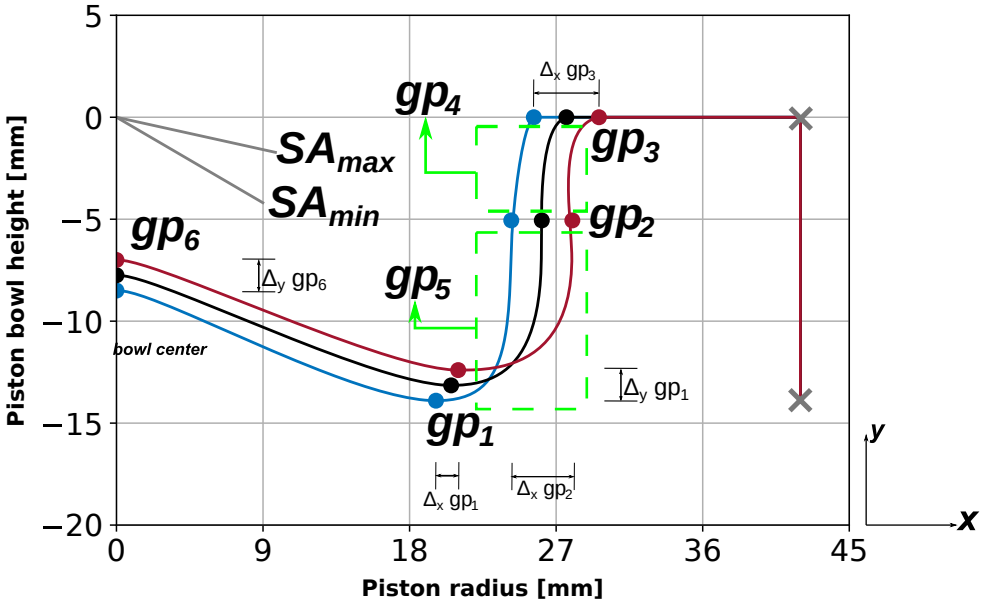

Figure 6.3: Geometrical parameters position and its respective movement and maximum y minimum spray angles used in the optimization process.

The injection pressure range was increased due to the differences in the liquid properties between the fuels and the amount of fuel needed each cycle. Figure 6.4 shows a comparison between several tested cases. The left graph shows a comparison between the ROI for all the injectors for diesel and OME fuels. In order to sustain the same level of energy throughout the cycle, a greater quantity of fuel is injected. With this difference in the amount of

Table 6.3: Parameters and ranges considered in the optimization process.

Parameter	Range
Geometrical parameter 1 [-]	[-0.5, 1.0]
Geometrical parameter 2 [-]	[-1.0, 1.25]
Geometrical parameter 3 [-]	[-1.0, 2.0]
Geometrical parameter 4 [-]	[0.0, 1.0]
Geometrical parameter 5 [-]	[-1.4, 0.1]
Geometrical parameter 6 [-]	[-0.5, 1.0]
Number of injector nozzles [-]	[7, 12]
Spray angle [°]	[155, 170]
Swirl number at IVC [-]	[1.0, 3.0]
Injection pressure [bar]	[1600, 2400]
EGR rate [%]	[0, 25]
IVC pressure [bar]	[3.4, 4.4]

fuel, it is necessary to adjust the diameter of each orifice to maintain the injector permeability once the injection pressure and the number of holes are the same for both cases. In the medium graph, it is possible to see the effect of the injection pressure on the ROI. All the curves were generated using OME fuel, an injector with 10 holes, and as a consequence, the same diameter and the same amount of fuel. As higher injection pressures are used, the total fuel injection duration is shorter due to the higher speed. The right graph of the figure is shown a comparison of the ROI for different numbers of holes and diameters, maintaining the same injection pressure and amount of fuel. Moreover, this graph shows the injection for each injector nozzle in order to show the differences once the total ROI (for the injector) is the same. With fewer holes, the diameter is bigger to maintain the same characteristics. IVC pressure was implemented as an input once the air/fuel ratio between diesel and OME was not negligible. Higher air intake pressure means more pumping work; hence, the increase in reported efficiency must compensate for the increase in pumping effort, which is highly dependent on the efficiency of the turbo system and its operating conditions.

To evaluate the simulation results, the global objective function was defined in order to reduce emissions and improve engine efficiency an is present as follows in Equation 6.4:

$$OF = f_1(NO_x) \cdot coef_{NO_x} + f_2(soot) \cdot coef_{soot} + f_3(eff) \cdot coef_{eff} \qquad (6.4)$$

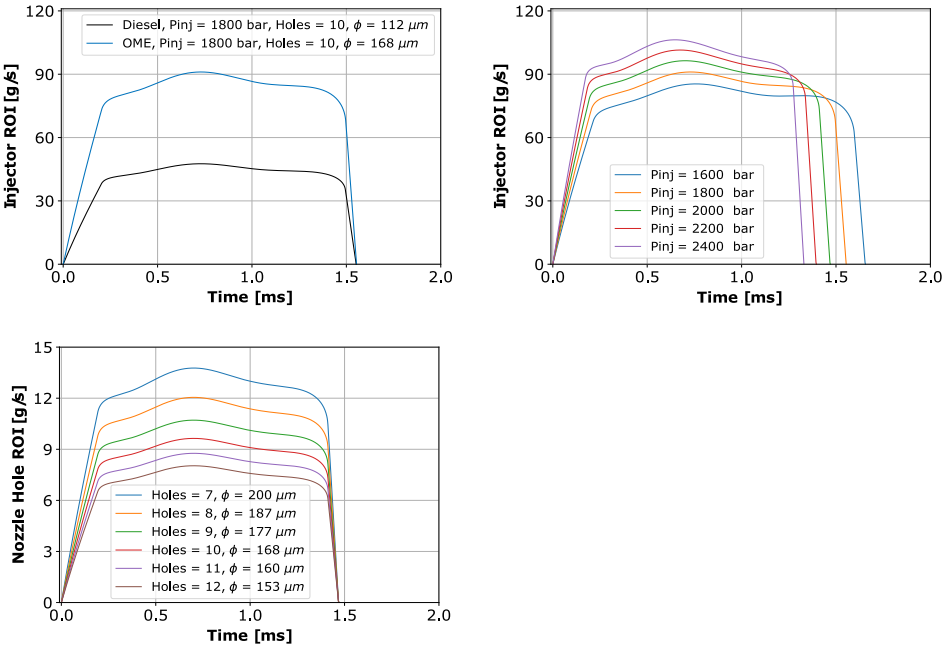

Figure 6.4: Rate of injection for different cases. A comparison between fuels, injection pressure values, and several numbers of injector nozzles.

where $f_1(NO_x)$, $f_2(soot)$ and $f_3(eff)$ are the sub-objectives functions and its values are obtained from the Equations 6.5, 6.6, 6.7 presented in Table 6.4. The, $coef_{NO_x}$, $coef_{soot}$, and $coef_{eff}$ are coefficients used to adjust the equation according to the order of importance of the parameters in the optimization. As the main objective is to increase the efficiency of the engine at the same time as it reduces NO_x and soot emissions, the values of the coefficients used are: $coef_{NO_x} = 0.05$, $coef_{soot} = 0.001$ and $coef_{eff} = 1$. In Equations 6.5 - 6.7 the f_{lim} refers to the respective value of the reference engine and the f_{CFD} is the value obtained from the CFD simulation of each case.

6.4 Optimization results

Optimization evolution analysis

The initial step of the results analysis was the algorithm convergence verification through the mathematical analysis of the objective function value for all

Table 6.4: Sub-objective functions used to perform the optimization with OME fuel.

Condition	$f_1(\mathrm{NO}_x)$ . . . . . Eq. (6.5)
if $f_{CFD} < f_{lim}$	$\frac{f_{CFD}}{f_{lim}}$
if $f_{CFD} \geq f_{lim}$	$\frac{f_{CFD}}{f_{lim}} + 100 \cdot (f_{CFD} - f_{lim})^2$
Condition	$f_2(\mathrm{soot})$ . . . . . Eq. (6.6)
if $f_{CFD} < f_{lim}$	$\frac{-log(f_{CFD})}{log(f_{lim})}$
if $f_{CFD} \geq f_{lim}$	$\frac{-log(f_{CFD})}{log(f_{lim})} + 10^6 \cdot (log(f_{CFD}) - log(f_{lim}))^2$
Condition	$f_3(\mathrm{eff})$ . . . . . Eq. (6.7)
if $f_{CFD} > f_{lim}$	$\frac{-log(f_{CFD})}{-log(f_{lim})}$
if $f_{CFD} \leq f_{lim}$	$\frac{-log(f_{CFD})}{-log(f_{lim})} + 100 \cdot (log(f_{CFD}) - log(f_{lim}))^2$

particles calculated from the CFD data simulation. Figure 6.5 shows how the NS algorithm consistently decreases the objective function value, converging towards a minimum value. The best particle would be the one with the minimum value of the objective function until that iteration. At the beginning of the procedure, it is observed how the objective function suddenly decreases due to the NS rapid convergence capacity, until case number 780, where it reaches the minimum value of the objective function.

To obtain the location of the particle that provides the best solution in the explored range, the efficiency and NO_x were compared in a Pareto front that is presented in the upper plot of Figure 6.6. In this graph all the simulated particles were used to show the trade-off between both parameters, the NO_x constraint and the efficiency that is the objective of the optimization. The optimum value is shown on the figure as a red dot. Moreover, from Figure 6.6 it is possible to find particles that provide better results than the optimized particle for each separate output. Sacrificing part of the efficiency it is possible to obtain better NO_x emissions and the opposite is also possible, sacrificing fractions of NO_x it is possible to obtain better efficiencies. The bottom part of the Figure 6.6 present the trade-off of the soot against the efficiency. It

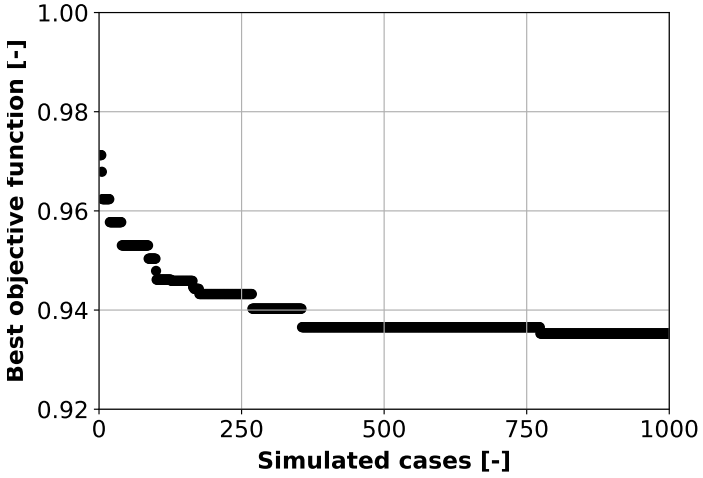

Figure 6.5: Objective function convergence.

is possible to see that almost all particles show very small values for these emissions, and can be considered as 0 emissions, due to the fuel composition.

Based on the results of the objective function, the optimized configuration was compared with the reference diesel case that was used to reproduce the experimental conditions. In Figure 6.7, the differences between bowl geometry and spray angle can be observed. Regarding the optimized geometry, a re-entrant bowl shape is used instead of a step-bowl profile. One of the purposes of the step-bowl geometry is to deflect the spray towards the cylinder head to prevent an excess of spray-wall impingement on the liner, avoiding soot-in-oil generation. Since OME is a low sooting fuel, this deflection is not required because there is negligible risk for generating soot particles near the liner region. This new geometry may also decrease the heat transfer through the cylinder head, preserving the mechanical integrity of this component and contributing to a better efficiency. Furthermore, the spray angle is adjusted with the bowl piston shape.

Additionally, Table 6.5 lists the complete set of parameters of the combustion system for both cases. The number of injector nozzle holes is decreased to 9 which leads to larger orifice diameters in order to maintain the same nozzle area. The spray angle is 10 degrees greater which enables the spray to match the geometry of the bowl. The injection pressure is higher than the reference value, enhancing the mixing rate due to a higher spray momentum, improved

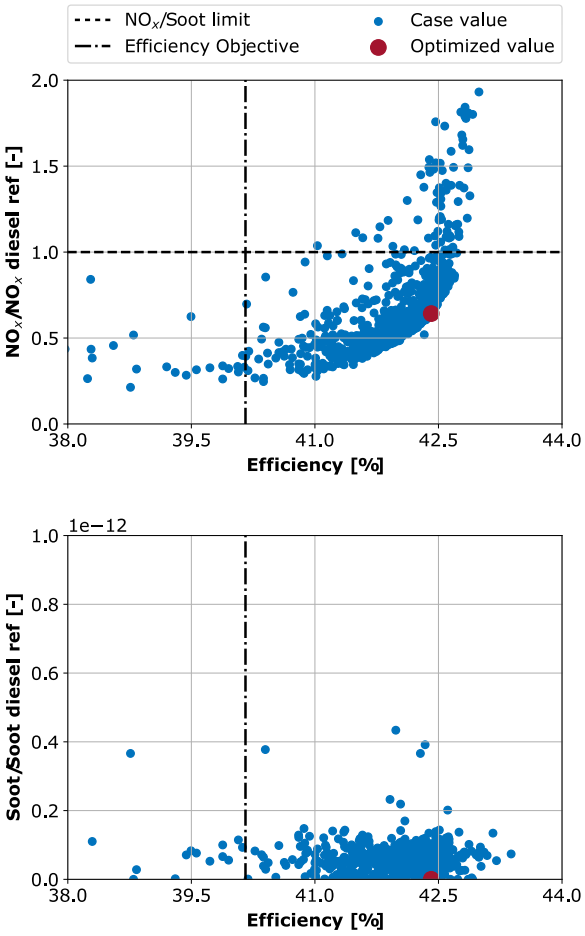

Figure 6.6: Pareto front of NO_x emissions vs. efficiency (top) and soot emissions vs. efficiency (bottom) of the engine. The blue dots are the results of all cases simulated in the optimization process and the red dot is the optimized case.

atomization, and faster evaporation. Apart from that, the optimized case has an EGR rate of 17.3% and an IVC pressure slightly higher than the initial baseline configuration.

Combustion system comparison

In Figure 6.8, the in-cylinder pressure, rate of heat release and normalized HR comparison between the reference diesel case, baseline OME case and

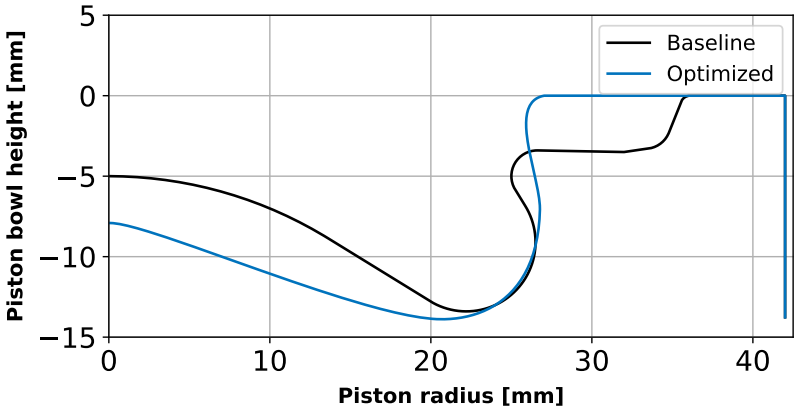

Figure 6.7: Bowl profile comparison between reference diesel case and optimized OME case.

Table 6.5: Inputs comparison between baseline OME and optimized OME cases.

Parameter	OME Baseline case	Optimized case
Number of holes [-]	10	9
Spray angle [deg]	154	164
Swirl number [-]	2.00	2.83
Injection pressure [bar]	1800	2216
EGR rate [%]	0	17.3
IVC pressure [bar]	3.89	4.04

the optimized OME case are shown. The baseline OME case has the same configuration of the diesel reference case while using OME as the fuel. The optimized OME case obtained from the NS using OME as fuel is presented in this figure as well. By examining the pressure trace, it is possible to note the differences between all cases. The differences related to the maximum peak of pressure obtained for the cases using OME can be a result of the greater amount of fuel needed to compensate the lower LHV of the OME. A

combination of the higher injection pressure together with the larger nozzle holes leads to a faster energy delivery causing a higher cylinder pressure level.

The heat release rate of the optimized case with OME presents a higher burn rate compared with the reference diesel case, showing a higher peak of the premixed phase, and for the rest of the combustion duration. Furthermore, the heat release rate is slightly shortened since the injection pressure is higher, decreasing the duration of the injection event to ensure that the same amount of energy is injected for all cases. The high levels of heat release combined with a shorter duration improves the combustion performance, and leads to thermodynamic advantages, such as improved combustion efficiency and a thermodynamic cycle closer to the ideal one. The enhanced combustion process is related to a better distribution of the mixture within the system as is discussed later on. The normalized HR was normalized with respect to the maximum of the total theoretical energy available in the cycle, which is calculated as the product of the total injected mass and the low heating value of the fuel injected $HR_{max} = \dot{m}_{diesel} \cdot LHV_{diesel}$ or $HR_{max} = \dot{m}_{OME} \cdot LHV_{OME}$ This curve shows that both OME cases arrives to the same combustion efficiency and which are slightly higher than the values of the reference diesel case. However, all cases show a good combustion efficiency, consuming almost all the injected fuel, reaching to heat releases levels close to the theorical one.

The results obtained from the optimized case are shown in Table 6.6 where they are compared against the reference diesel case and the OME baseline case. Comparing the reference diesel against the optimized case, a combustion system was obtained that produces 35.7% less NO_x, 2.2% higher efficiency, and a great reduction of soot due to the non-sooting characteristics of OME. Even though the baseline OME case has a higher efficiency than the other two cases, the NO_x value is unacceptable, therefore it is necessary to slightly sacrifice part of the efficiency in order to reduce the NO_x level.

In general, the combination of a higher injection pressure with higher swirl ratio contributes to have better atomization and evaporation and shortens combustion duration. With the new configuration there is more space between the sprays avoiding spray interaction resulting in NO_x reduction with better efficiency. The great NO_x reduction can be explained principally by the EGR rate of the optimized case. The EGR reduces the local temperature near the flame regions leading to a lower NO_x concentration.

The temporal evolution of the NO_x emission as the combustion progresses is shown in bottom graph of Figure 6.9. Compared to the reference diesel case, the NO_x formation in the baseline OME case has the highest values, and correlates well with the maximum mean temperature in the cylinder be-

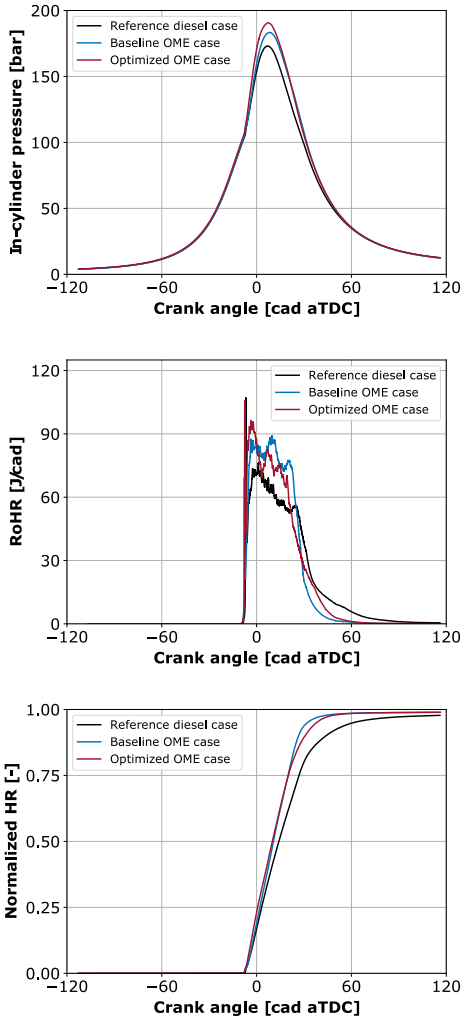

Figure 6.8: Comparison of in-cylinder pressure and rate of heat release between reference diesel case, baseline OME case, and optimized OME case.

tween 12 and 40 CAD, as can be seen on the bottom part of the same figure. This increment can be attributed to an excess of local temperature above 1800K promoting an exponential NO_x formation as previously demonstrated by Turns in [13] and Drake in [14]. Regarding the optimized case, the mean temperature overlaps with that of the OME baseline during the premixed phase of the combustion. However, during the later stages, the temperature of the optimized case is lower due to the EGR rate used that provides an

Table 6.6: NO_x, soot and efficiency comparison between reference, baseline and optimized cases.

Case	NO_x [mg/s]	Soot [mg/s]	Efficiency [%]
Reference case	230.95	0.355	40.2
Baseline OME case	773.60	< 0.0001	43.0
Optimized OME case	148.32	< 0.0001	42.4

increase in the heat capacity of the mixture acting as NO_x controller. The vertical dashed lines in Figure 6.9 represent five crankangles (0, 12, 27, 40, and 60) selected for comparing the temperature distribution in the combustion chamber for the analyzed cases.

Figure 6.10 shows the temperature contours for the diesel reference case, the baseline OME case (with the same geometry of the initial diesel engine) using OME as fuel and the best case obtained from the optimization. Mainly, the changes in the bowl profile increases the distance between the nozzle hole outlet and the walls of the piston bowl, which is in agreement with previous studies [11, 15], that presented larger combustion chambers when oxygenated fuels are used due to the longer mixing lengths for those fuel sprays. In addition, the optimized case exhibits a faster jet penetration, which occurs due to bigger orifice diameters and higher injection pressure. The included spray angle that matches the bowl profile is wider than the reference case, directing the spray towards the inferior side of the re-entrant edge of the profile when the piston is at top dead center, as can be seen from the first image at the bottom left side. The onset of combustion appears to consume the air present in the piston bowl mainly. As the piston moves towards the bottom dead center, the spray impacts the edge of the bowl, splits, and then finds the air available in the outer regions of the bowl, increasing the mixing rate and improving the distribution of the flame inside the combustion chamber. Moreover, the optimized case has a higher swirl number that could produce an overlap of the plumes promoting unfavorable combustion conditions, however, this inconvenience is surpassed by using a nozzle with one less hole compared to the initial configuration. The use of the 9 hole configuration restricts the plume-to-plume interaction and avoids the formation of fuel-rich zones. Therefore, in the last stage of the combustion, a more homogeneous temperature distribution is found, leading to a better performance of the system, corroborating the behavior previously shown in Figure 6.9.

Figure 6.11 shows the mixture fraction contours of several crank angles. As already mentioned, the mixture fraction in the reference diesel case is well

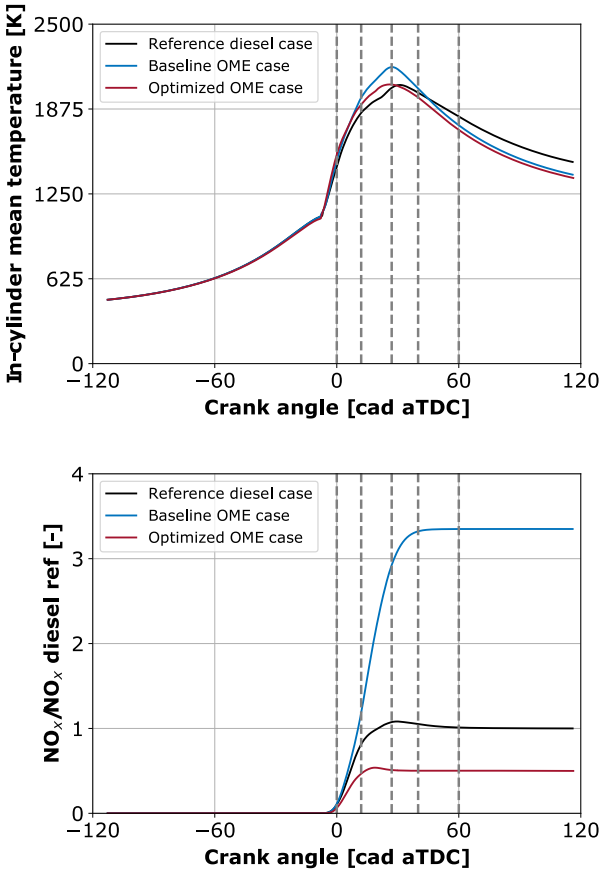

Figure 6.9: In-cylinder mean temperature and NO_x emissions, a comparison between the reference diesel case, baseline OME case, and the optimized OME case. The gray dashed lines represent the five crank angles selected to compare the temperature distribution.

distributed, with a little interaction with the bowl wall and results to be adequately consumed at the end of the combustion process. On the other hand, the baseline OME case just adapt the diesel configuration with a new fuel. In order to maintain the same amount of energy in the cycle the mass fuel injected was corrected. With this fuel correction, more fuel is injected and consequently more fuel collides with the wall, characterizing high impingement, and promoting a poor combustion phasing. This way, a considerable part of the fuel remains on the combustion chamber until the end of the cycle, which affect the emissions and can be seen in the Figure 6.11 on the brightest

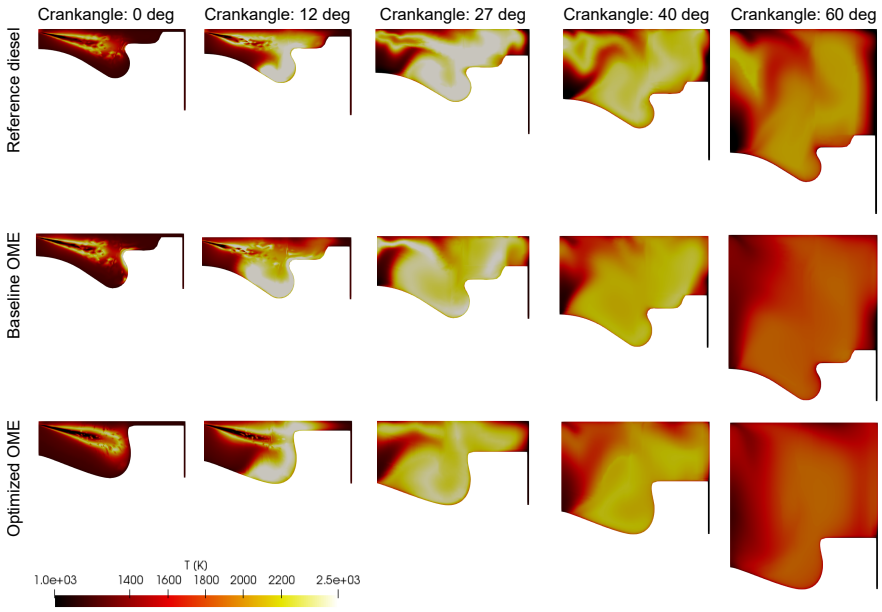

Figure 6.10: In-cylinder temperature contours comparison between the reference diesel case, baseline OME case, and the optimized OME case.

blue colors. Now, it is possible to recover the combustion process for the optimized case, the new geometry with its parameters of the air-management and injection systems. With the new number of holes, the diameter of each injector hole is bigger, which makes the injected fuel droplets larger. In general, this modification harms the fuel atomization and penetration. However with the higher injection pressure, swirl number and IVC pressure it is possible to revert and further improve atomization, evaporation, and consequently the mixing rate. Furthermore, with the new piston geometry there is a better fuel distribution inside the combustion chamber, with less fuel impact on the walls. Comparing the optimized case against the baseline OME at the crank angle 60^o.

The NO is the main component of NO_x emissions. Therefore, Figure 6.12 shows the temporal evolution of NO concentration inside the combustion chamber. In the reference diesel case it is observed a progressive generation of NO but after this, some part of the NO was oxidized. However, with the engine configuration using 0% of EGR a lot of NO is formed. When this case is reproduced with OME, and more fuel mass is injected to maintain the energy, it is possibly to see that the NO emissions were increased to a unacceptable level. Due to the amount of fuel, characteristics, there is more

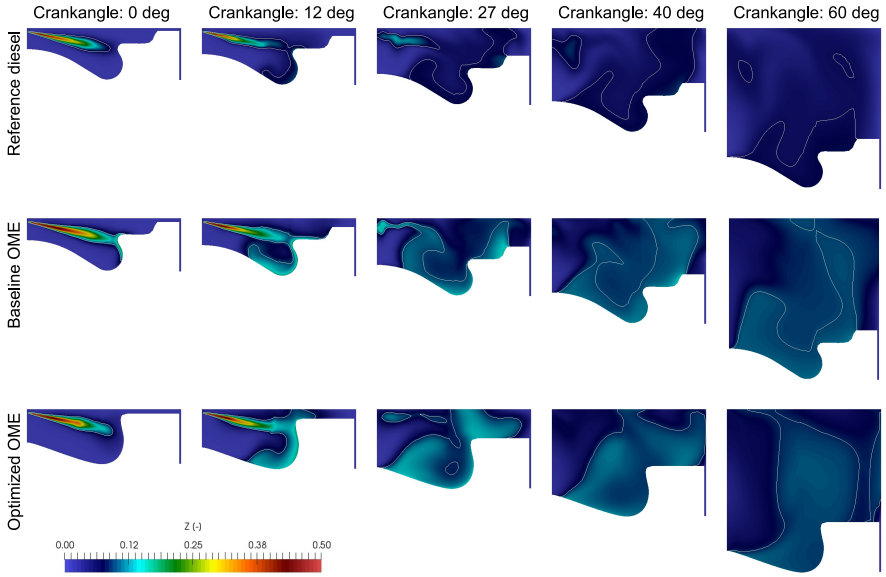

Figure 6.11: Mixture fraction contours comparison between the reference diesel case, baseline OME case, and the optimized OME case.

spray velocity, which promotes a rise in pressure and temperature resulting in more NO production and poor combustion. For the optimized case it is possible to see that the new combustion system was able to reduce the NO emissions. The better atomization and mixing rate contributes to a quickly temperature reduction leading to a higher oxidation of the NO formed during the combustion process. However, the main reason of this reduction is the EGR rate (17.3%) used to the optimized case. Being that, in the end of the cycle the optimized case was capable to reduce the NO emissions in almost 6 times when compared with the baseline OME case and 1.5 times when compared against the diesel reference case. Moreover, the OME combustion is faster than the diesel due to its physical properties.

Parameter evolution

As the NS algorithm changes all parameters at the same time during the optimization process, a parameter evolution study of the optimized case was performed to analyze the energy balance of each combustion system modification. The first step was to convert the engine to work with OME, adapting the physical characteristics of the injection system, such as the hole exit diameter, in order to maintain the same amount of energy in the simulated cycle.

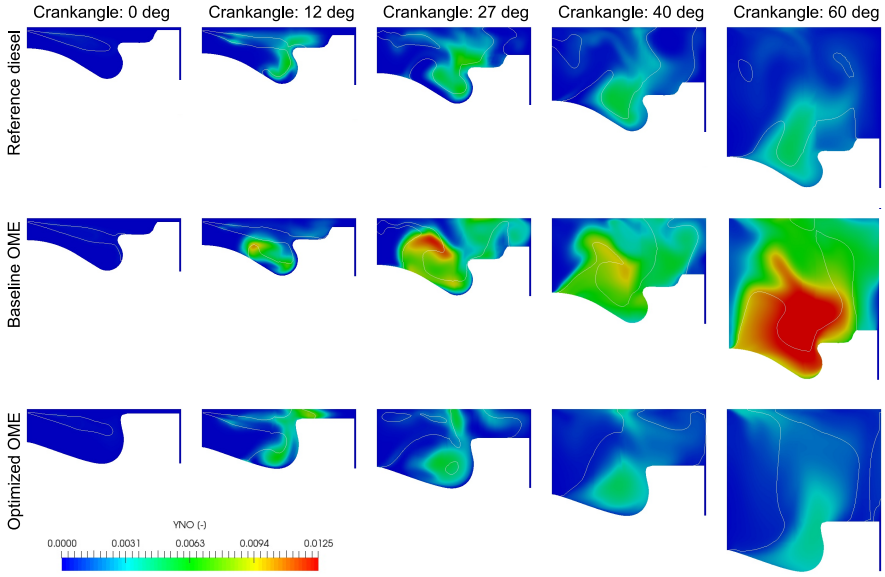

Figure 6.12: NO concentration contours comparison between the reference diesel case, baseline OME case, and the optimized OME case.

This configuration presents better work than the diesel reference, with fewer losses in the exhaust, and in unburned fuel meantime, the heat transfer losses and the NO_x emissions are increased. The HT losses are 2.4% higher due to the difference in the amount of the fuel that results in more fuel reaching the piston surface, thereby causing piston wetting, engine impingement, and the NO_x emissions increases more than 3 times.

The next step is the change of the reference geometry by the optimized one. Changing the geometry, the energy balance of the baseline case is maintained, there is just a little reduction in the work and exhaust losses but with an increment on the unburned fuel. Adding the new number of holes, obtaining a slight reduction of the NO_x emissions is possible while maintaining the same energy distribution. These better emissions results came from the fact that with this new number of holes exists more space inside the combustion chamber, avoiding jet-to-jet interactions.

The next step consists in adapting the new spray angle. The new angle is better adjusted with the geometry preventing spray from being directed onto the piston surface, which helps to reduce the NO_x emissions. After this, the swirl number was adjusted, reducing the emissions but still being above the

value of the constraint. The swirl value increment helps increase the mixing rate, which helps a better combustion process.

Next, the case was updated, configuring the optimum injection pressure. This higher injection pressure helps to improve mixing and combustion efficiency reducing the exhaust losses and increasing the thermal efficiency from 44.8% to 45.4%. Additionally, the HT losses and NO_x emissions are increased once the higher injection pressure leads to higher in-cylinder pressure and temperature. The next simulation was made using the optimized pressure in the IVC instant resulting in the best cycle work of these simulations but with 3 times more NO_x than the constraint value.

Finally, in the last simulation, the EGR rate was adjusted in order to control the emissions. The EGR rate changes from 0% to 17.3%, which reduces the fresh air available inside the combustion chamber, worsening the mixing rate, and combustion efficiency resulting in lower work, but at the same time, the HT losses and unburned fuel were reduced in comparison to the last case. This new EGR configuration has proven to be able to greatly reduce NO_x emissions, staying below the value set for the constraint but sacrificing some of the engine's efficiency. However, the optimized combustion system could improve the work efficiency, exhaust losses, and unburned fuel quantities compared to the reference diesel case fulfilling the optimization objective.

To better understand the difference in HT, Fig 6.14 shows the HT rate of each boundary and the HT total for the diesel reference case, baseline OME and optimized OME. For all boundaries, the HT is higher for the optimum case maintaining the same total HT as the baseline case. Since the new geometry does not have the step, more temperature is concentrated in the zones close to the liner, and the HT distribution can be observed in the top-left part of Figure 6.14. Due to the higher amount of fuel, combined with the new injection pressure and the position of the spray, the HT in the cylinder head is higher for the optimized case, and it is presented in the top-right part of Figure 6.14. The higher piston HT can be related to the higher in-cylinder temperatures due to the new injection pressure; once a great part of the flame is concentrated in the reentrant part of the bowl, raising the temperature at that point promotes a higher HT for the piston.

6.5 Parametric study for sensitivity analysis

This section presents the results obtained from a parametric study realized using machine learning methods. The NS methodology presented in Section 6.3 enabled an optimum design in a reasonable number of simulations. Also, it

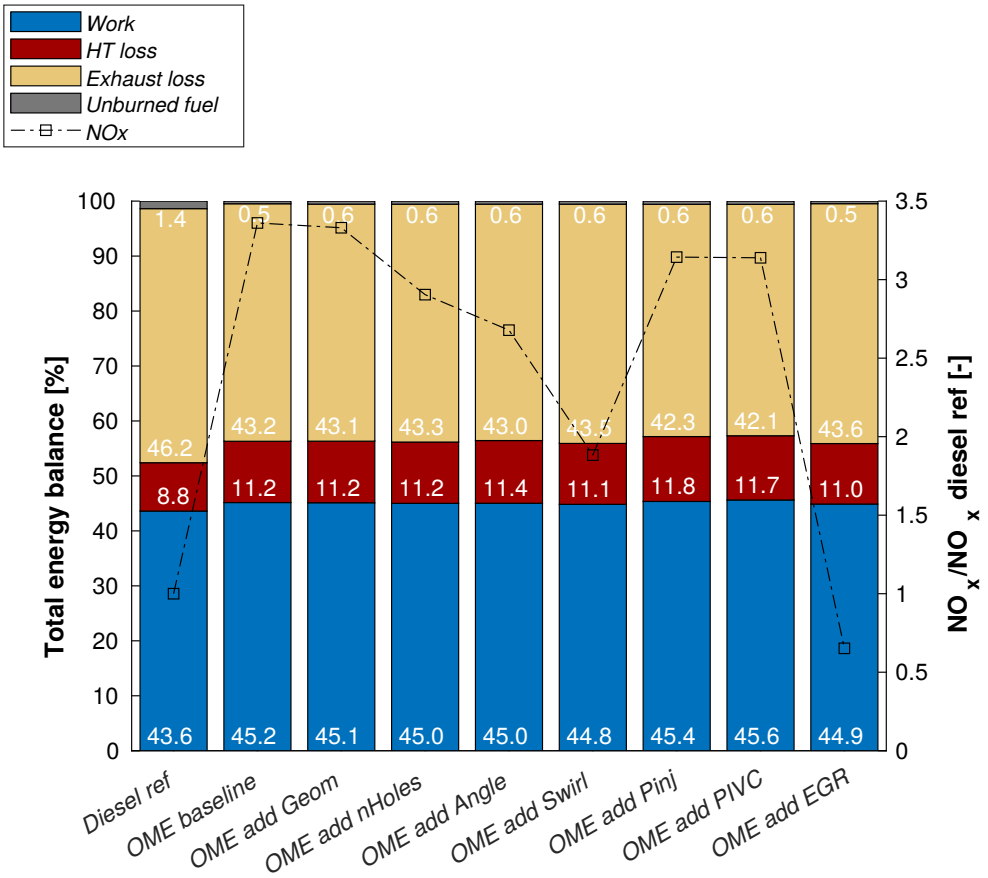

Figure 6.13: Energy balance comparison.

generated an extensive data set with helpful information about the combustion system. In order to use the information and explore the optimized combustion system obtained from the previous steps, a neural network model was trained from the available data with the target of performing a sensitivity analysis. A model is a mathematical approach that acts as a surrogate model for CFD simulations. Two different NN were trained from the data generated during the optimization process where the first predicts the engine efficiency behavior, and the second reproduces the NO_x emissions behavior. A NN model for soot emissions was neglected since the values obtained during the optimization process were imperceptible (as expected due to the low-sooting capability of this fuel).

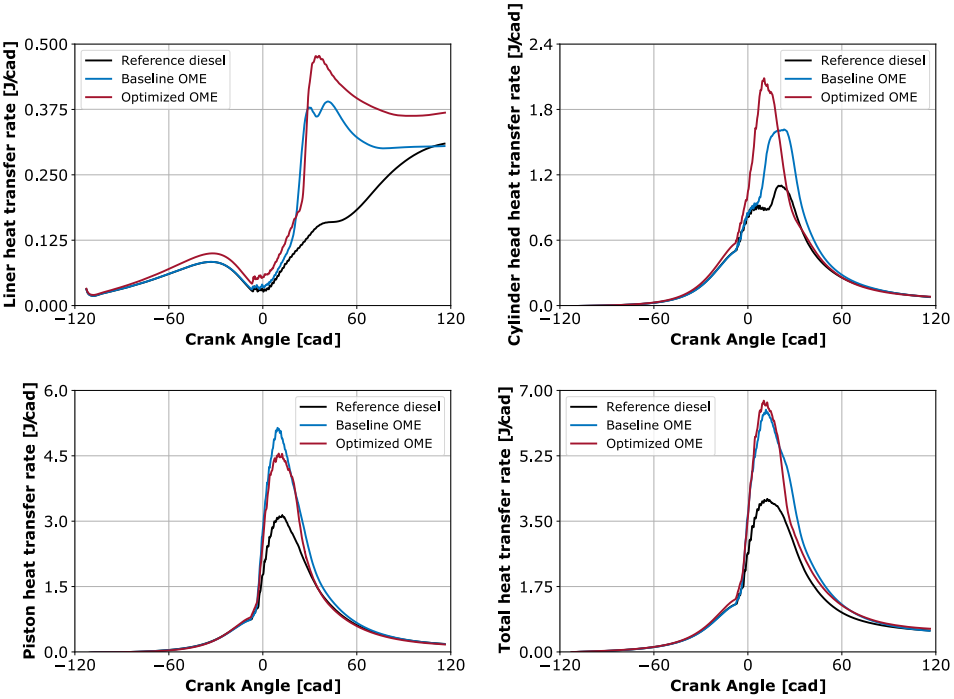

Figure 6.14: Heat transfer analysis.

The NN used in this work was developed in Python [16] using packages as Numpy together with the open-source libraries Keras [17]. A kernel L2 regularization was used for all hidden layers to improve the accuracy of the prediction during the training phase [18]. Adam optimization algorithm [19] was used with the training algorithm for updating the NN weights. The maximum number of iterations of the algorithm was set to 500. In order to choose the best set of parameters for the NN, a KerasRegressor has been implemented. Also, a k-fold cross validation was used, which consists of an iterative division of the data used in the training process and other data for the testing. The NN was trained with 67% of the total data (that is two thirds of the 950 simulated cases) and tested with 33% of the remaining data, selected randomly.

In order to evaluate the quality of the prediction, both NNs were tested using the optimum case configuration, predicting the outputs of this case and comparing them against the results obtained from the CFD simulation. The predictions of efficiency and NO_x emissions resulted in 42.4% (42.415)

and 155.67 mg/s respectively for the NN, compared to the efficiency and NO_x emissions from the CFD case of 42.4% (42.412) and 148.32 mg/s, which means a difference of 0.008% for the efficiency and 4.96% for NO_x emissions. Moreover, Figure 6.15 shows the predicted values obtained from the NN regression vs the CFD results for efficiency (top plot) and for the NO_x values (bottom plot).

In general, the prediction of the NOx concentration is more precise than the prediction of the efficiency. This behavior was observed by other authors before. For instance, Owoyele et al. [20] also found that the NN predictions are more accurate for the NOx results than for other variables such as ISFC or soot emissions. Overall, the NN reproduces the efficiency and NO_x emissions trend quite well with a reasonable accuracy level.

A sensitivity analysis was performed based on the trained NN to aim at a better understanding of the combustion system. For this part of the study, the piston bowl design was kept the same while other parameters were varied, such as the number of holes of the injector, the spray angle, the injection pressure, the EGR rate, and the IVC pressure. The goal was to evaluate the behavior of the efficiency and NO_x emissions of the optimum geometry with different parameters focusing on the engine settings and operation. The proposed parameters with their respective range for this sensitivity analysis are presented in Table 6.7.

Table 6.7: Parameters used to study the optimum combustion chamber behavior.

Parameter	Range
Number of holes [-]	[8, 10]
Spray angle [def]	[161, 165]
Injection pressure [bar]	[2000, 2400]
EGR rate [%]	[14, 20]
IVC pressure [bar]	[3.9, 4.1]

To isolate the effect of each parameter, a matrix of cases was created, varying just one parameter each time, it means the cases used to the study influence of the number of holes in the combustion chamber have the same configuration as the optimized, except to the number of holes. The same procedure was applied to the others parameters that were tested in this analysis.

Figure 6.16 shows all the results obtained from this parametric study for efficiency and NO_x emissions. From a general perspective, the parameters

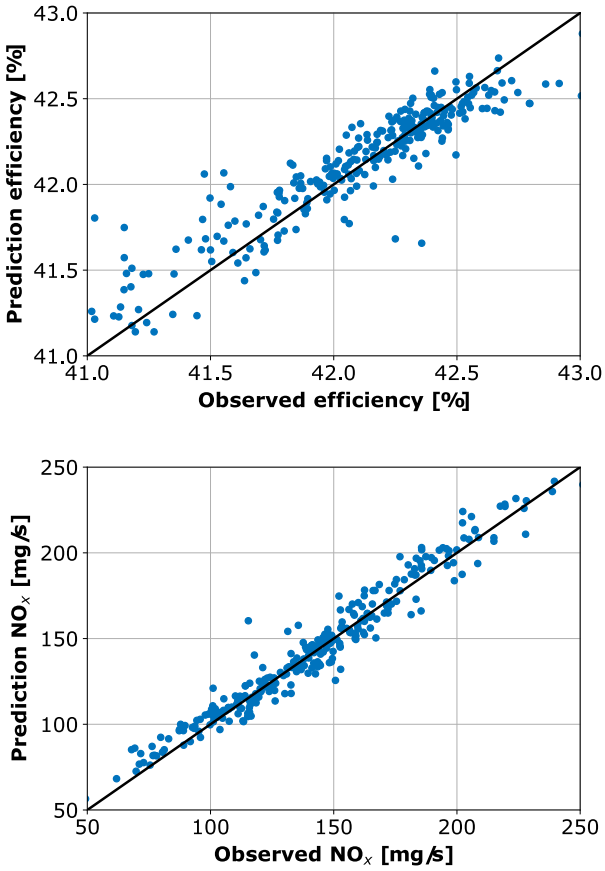

Figure 6.15: NN-based predicted vs CFD observed. The top figure plot: efficiency regression. The bottom figure plot: NO_x prediction

that have a considerable influence are the injection pressure and the EGR rate on NO_x emissions and efficiency. Meanwhile, the nozzle configuration and the IVC pressure have a lower effect. The effect of nozzle hole number on NO_x and efficiency is shown in Figure 6.16, and it is possible to note that a maximum value was obtained for the efficiency when the injector has 9 holes. Hence, a compromise should be taken since reducing the number of holes would lead to bigger droplets being injected due to the larger hole diameters. This, in turn, worsens the atomization and mixing process between the fuel and air. On the contrary, increasing the number of holes would cause a significant plume-to-plume interaction, negatively impacting the combustion process. This could

also lead to a higher number of rich zones and a reduced efficiency having a similar behavior to that presented by Mohiuddin in [21]. Regarding the NO_x emissions trend, increasing the number of holes while maintaining the same operating conditions results in a smaller droplet size of fuel, which means a better-atomized spray enhances the mixture and reduces emissions.

Concerning the included spray angle, it must be noted that when the bowl design is decided, the injector configuration is usually kept constant. Nevertheless, small variations of the spray angle have very little consequence on the efficiency and NO_x emissions. In addition, the impact of the IVC pressure on both efficiency and NO_x emissions is negligible, as can be seen in the figures where the plot is constant. Regarding the EGR rate and injection pressure, it is possible to observe that these parameters greatly influence efficiency and NO_x emissions in the range evaluated. When the EGR rate is increased, the burning rate of the non-premixed combustion phase increases, leading to a reduction in efficiency and NO_x emissions. This effect was also observed in literature in some works presented by Shi and Reitz in [22], Benajes in [23] and Mohiuddin [21]. The last parameter evaluated was the injection pressure that substantially influences the efficiency and NO_x emissions. The injection pressure increases the liquid phase momentum and the evaporation. When the injection pressure is increased, better mixing is expected, which promotes improved combustion and leads to a higher temperature inside the combustion chamber. On the one hand, the higher temperature improves the efficiency, and on the other hand, it promotes the formation of NO_x. Based on this study, it is possible to predict the behavior of the engine and to evaluate further settings and configurations that can be used on an engine test bench.

Finally, a variability study is shown in Table 6.8 where the variations for each parameter are calculated aiming to obtain an analytical representation of the results showed in Figure 6.16. From Table 6.8, it is possible to observe that the appropriate set of parameters could improve efficiency up to 1.2%. For what concerns the NO_x emissions, the correct set of the injection pressure and EGR can reduce the emissions in the engine by 60%. The interesting point is that these two parameters, injection pressure and EGR rate, can be changed directly during engine operation, allowing a quick adjustment in the set of parameters to obtain better NO_x emissions. The information this part of the study offers is valid in the case the system is manufactured, facilitates a better understanding of its sensitivity to the parameters, and could be useful even for guiding engine calibration strategies.

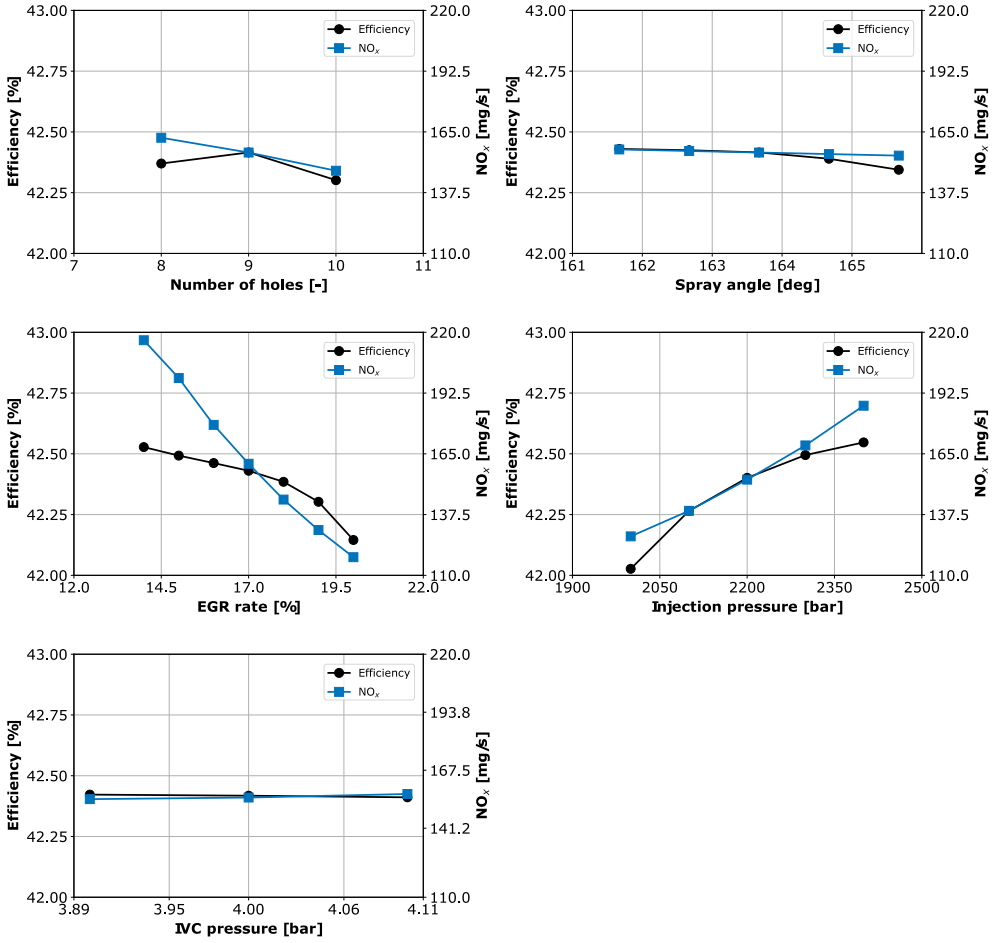

Figure 6.16: Efficiency and NO_x results from the parametric study using machine learning tools.

6.6 Summary and conclusions

This chapter had the objective of evaluating the NS algorithm optimization methodology and proposing a new combustion system explicitly developed for a CI engines fueled with OME. The results provided an optimum configuration of the combustion system through engine optimization with the NS algorithm. Moreover, a database with valuable information was generated, providing a cause-and-effect database. The methodology validated in a CI engine fueled

Table 6.8: Variability of each parameter based on the optimum value.

	Efficiency variation [%]	NO_x variation [%]
Number of holes [-]	0.27	9.59
Spray angle [def]	0.20	1.79
Injection pressure [bar]	1.23	37.99
EGR rate [%]	0.90	63.08
IVC pressure [bar]	0.03	1.49

with conventional fuel was applied to a MD 4-cylinder 4-stroke CI engine in order to improve the efficiency while keeping NO_x emissions under the established limit.

The optimization process considered 12 parameters, where 6 were responsible for the geometry, 3 for the injection system, and 3 for the air management system. After the end of the optimization process, it was obtained a new combustion system designed for this specific fuel that improves the engine efficiency by 2.2% with a significant reduction of the NO_x, from 230.95 mg/s to 148.32 mg/s, totaling a reduction of almost 36% and soot elimination, from 0.355 mg/s to a virtual 0, when compared against the reference diesel engine. Moreover, using OME as fuel, it is possible to use a higher EGR rate to reduce NO_x emissions due to the higher oxygen content in the fuel molecule and its characteristics. The injection system, especially the injection pressure and diameter of the holes, must be adjusted considering the physical properties of the fuel. Furthermore, a NN methodology was used to explore even more the characteristics of the new combustion system.

This chapter demonstrates that OME is a potential fuel for next-generation CI engines and gives suggestions for designing OME-fueled CI engines. The non-sooting nature of OME, along with the optimization algorithm capacity to regulate NO_x emissions, enables the new combustion system to manage NO_x and soot emissions while retaining diesel-like efficiency totally.

References

[1] Lautenschütz, Ludger et al. “Physico-chemical properties and fuel characteristics of oxymethylene dialkyl ethers”. In: *Fuel* 173 (2016), pp. 129–137. DOI: 10.1016/j.fuel.2016.01.060.

[2] Iannuzzi, Stefano Emanuele, Barro, Christophe, Boulouchos, Konstantinos, and Burger, Jakob. "Combustion behavior and soot formation/oxidation of oxygenated fuels in a cylindrical constant volume chamber". In: *Fuel* 167 (2016), pp. 49–59. DOI: 10.1016/j.fuel.2015.11.060.

[3] Liu, Haoye, Wang, Zhi, Zhang, Jun, Wang, Jianxin, and Shuai, Shijin. "Study on combustion and emission characteristics of Polyoxymethylene Dimethyl Ethers/diesel blends in light-duty and heavy-duty diesel engines". In: *Applied Energy* 185 (2017), pp. 1393–1402. DOI: 10.1016/j.apenergy.2015.10.183.

[4] Omari, Ahmad, Heuser, Benedikt, and Pischinger, Stefan. "Potential of oxymethylenether-diesel blends for ultra-low emission engines". In: *Fuel* 209.May (2017), pp. 232–237. DOI: 10.1016/j.fuel.2017.07.107.

[5] Tan, Yong Ren et al. "Sooting characteristics of polyoxymethylene dimethyl ether blends with diesel in a diffusion flame". In: *Fuel* 224.November 2017 (2018), pp. 499–506. DOI: 10.1016/j.fuel.2018.03.051.

[6] Ferraro, Federica, Russo, Carmela, Schmitz, Robert, Hasse, Christian, and Sirignano, Mariano. "Experimental and numerical study on the effect of oxymethylene ether-3 (OME3) on soot particle formation". In: *Fuel* 286.P1 (2021), p. 119353. DOI: 10.1016/j.fuel.2020.119353.

[7] Burger, Jakob, Siegert, Markus, Ströfer, Eckhard, and Hasse, Hans. "Poly(oxymethylene) dimethyl ethers as components of tailored diesel fuel: Properties, synthesis and purification concepts". In: *Fuel* 89.11 (2010), pp. 3315–3319. DOI: 10.1016/j.fuel.2010.05.014.

[8] Burger, Jakob, Ströfer, Eckhard, and Hasse, Hans. "Production process for diesel fuel components poly(oxymethylene) dimethyl ethers from methane-based products by hierarchical optimization with varying model depth". In: *Chemical Engineering Research and Design* 91.12 (2013), pp. 2648–2662. DOI: 10.1016/j.cherd.2013.05.023.

[9] Härtl, Martin, Seidenspinner, Philipp, Jacob, Eberhard, and Wachtmeister, Georg. "Oxygenate screening on a heavy-duty diesel engine and emission characteristics of highly oxygenated oxymethylene ether fuel OME1". In: *Fuel* 153 (2015), pp. 328–335. DOI: 10.1016/j.fuel.2015.03.012.

[10] Deutz, Sarah et al. “Cleaner production of cleaner fuels: Wind-to-wheel-environmental assessment of CO2-based oxymethylene ether as a drop-in fuel”. In: *Energy and Environmental Science* 11.2 (2018), pp. 331–343. DOI: 10.1039/c7ee01657c.

[11] Gaukel, Kai, Dworschak, Patrick, Pélerin, Dominik, Härtl, Martin, and Wachtmeister, Georg. “Combustion process optimization for oxymethylene ether fuels in a heavy-duty application”. In: (2019), pp. 351–367. DOI: 10.1007/978-3-658-26528-1_21.

[12] García, Antonio, Gil, Antonio, Monsalve-Serrano, Javier, and Lago Sari, Rafael. “OMEx-diesel blends as high reactivity fuel for ultra-low NOx and soot emissions in the dual-mode dual-fuel combustion strategy”. In: *Fuel* 275.April (2020), p. 117898. DOI: 10.1016/j.fuel.2020.117898.

[13] Turns, Stephen R. *An introduction to combustion : concepts and applications*. 3rd ed.. New York: New York : McGraw-Hill, 2012., 2012.

[14] Drake, Michael C and Blint, Richard J. “Calculations of NOx Formation Pathways in Propagating Laminar, High Pressure Premixed CH4/Air Flames”. In: *Combustion Science and Technology* 75.4-6 (1991), pp. 261–285. DOI: 10.1080/00102209108924092.

[15] Zubel, Marius, Ottenwälder, Tamara, Heuser, Benedikt, and Pischinger, Stefan. “Combustion system optimization for dimethyl ether using a genetic algorithm”. In: *International Journal of Engine Research* 22.1 (2021), pp. 22–38. DOI: 10.1177/1468087419851577.

[16] *Python programming language - https://www.python.org*. [Online; accessed 31 January 2020].

[17] Chollet, François et al. *Keras*. https://keras.io. 2015.

[18] Kukačka, Jan, Golkov, Vladimir, and Cremers, Daniel. “Regularization for Deep Learning: A Taxonomy”. In: (2017), pp. 1–23.

[19] Kingma, Diederik P. and Ba, Jimmy Lei. “Adam: A method for stochastic optimization”. In: *3rd International Conference on Learning Representations, ICLR 2015 - Conference Track Proceedings* (2015), pp. 1–15.

[20] Owoyele, Opeoluwa, Pal, Pinaki, and Torreira, Alvaro Vidal. “An automated machine learning-genetic algorithm (AutoML-GA) framework with active learning for design optimization”. In: *ASME 2020 Internal Combustion Engine Division Fall Technical Conference, ICEF 2020* November (2021). DOI: 10.1115/ICEF2020-3000.

[21] Mohiuddin, Khawar, Kwon, Heesun, Choi, Minhoo, and Park, Sungwook. "Experimental investigation on the effect of injector hole number on engine performance and particle number emissions in a light-duty diesel engine". In: *International Journal of Engine Research* (2020). DOI: 10.1177/1468087420934605.

[22] Shi, Y. and Reitz, R. D. "Optimization study of the effects of bowl geometry, spray targeting, and swirl ratio for a heavy-duty diesel engine operated at low and high load". In: *International Journal of Engine Research* 9.4 (2008), pp. 325–346. DOI: 10.1243/14680874JER00808.

[23] Benajes, Jesus et al. "Optimization of the combustion system of a medium duty direct injection diesel engine by combining CFD modeling with experimental validation". In: *Energy Conversion and Management* 110 (2016), pp. 212–229. DOI: 10.1016/j.enconman.2015.12.010.

Chapter 7

Optimization of the combustion system of oxy-fuel combustion engines

7.1 Introduction

This chapter of the thesis is focused on describing the results obtained from the combustion system optimization of a compression-ignited engine applied to operate in oxy-fuel combustion mode. In this concept, the air injected is replaced by oxygen, removing the nitrogen of the oxidant. This process results in high temperatures, thus being necessary to dilute the mixture with a high EGR rate to control the temperature. This system demonstrates an advantage in terms of emissions once removing the nitrogen of the intake air mixture implies no NO_x emissions. Furthermore, this combustion can be coupled with CO_2 capture technologies. More benefits, restrictions, and descriptions of the oxy-fuel combustion concept can be found in Section 2.5.

To apply this concept in vehicles, some points can affect the performance of the system. First is the high cost of obtaining oxygen with the necessary purity. Second, when thinking in the CO_2 capture, the necessity of a new deposit increases the weight of the vehicle and, consequently, the fuel consumption. To solve the oxygen supply issue, mixed ionic-electronic conducting membranes (MIEC) can be applied. The researches of Bauman et al. and Catalán-Martinez et al. [1, 2] studied both the experimental and nu-

merical performance of the membrane to transport oxygen. Thus, the results showed that the MIEC operating conditions are met, allowing to obtain the necessary quantity of oxygen for an engine operation.

In order to couple the oxy-fuel combustion concept with CI engine, the operating condition must attend MIEC requirements. The exhaust gases of the engine must be within a specific temperature range to heat up the membrane for the correct operation. Serrano et al. [3] have already studied this approach to eliminate soot, CO, NO_x, and HC engine emissions through a 1D ICE model. The results show a similar brake power and indicated efficiency compared to conventional engines running at high speeds.

Considering the trade-off between the advantages and drawbacks, the oxy-fuel combustion concept shows the potential to reduce the gas emissions of a CI engine. This way, this chapter is structured as follows in order to explore this new concept. First, the oxy-fuel combustion model is described. The engine configuration and operating conditions are presented. Moreover, the validation of the concept in CFD is discussed. In the second part, the optimization parameters and the objective function used to evaluate each simulation are presented. The third part is composed of the optimization and engine results. The next part of the chapter is an analysis of an extended operating range of the optimized combustion system. To finish the chapter, the main conclusions are summarized.

7.2 Oxy-fuel combustion model

The feasibility of the oxy-fuel combustion concept was analyzed in a preliminary work performed by Serrano et al. [4]. As previously commented, they implemented a numerical methodology to assess oxy-fuel combustion features and the potential of this concept in optimal conditions. They simulated a conventional CI engine with a 0D-1D in-house simulation software named Virtual Engine Model (VEMOD) [5], where they also integrated the oxygen membrane (MIEC) model technology.

In that preliminary study, [3], the gas composition that entered the cylinder was formed by O_2, CO_2, and H_2O, avoiding the presence of N_2. The concentration of each specie depends on the operating condition and the EGR rate. It was observed that the optimal operative conditions and the original volumetric compression ratio of the engine (with a CR of 16) operating in oxy-combustion mode, with an EGR rate of 70% and without N_2, had a lower trapped mass than conventional air combustion, which means lower in-cylinder pressure if the temperature of the charge is maintained. For this reason, they

performed a sensitivity study, increasing the CR value in order to maximize the engine torque and effective efficiency, varying different parameters in the engine, like intake pressure and temperature, among others (to fulfill the restriction of the exhaust temperature at 1000ºC and to respect the in-cylinder pressure limit). The outcome was that the CR was changed from 16 to 28, and indirectly the conditions at the IVC changed slightly from the initial case, improving the trapped mass.

Moreover, the minimum area of the MIEC required for supplying an appropriate amount of oxygen was calculated, obtaining a value of 10 m^2 for delivering the necessary O_2 amount for the engine. As a consequence, the value of the oxygen-fuel ratio (λ), based on the mass ratio, was maintained constant and with a relatively low value of 1.1 (compared to traditional CI values). The reason for this low value is that the oxygen separation onboard is costly due to the high surface and thermal requirements of the MIEC to operate correctly.

The information obtained from this 0D-1D evaluation, in terms of optimum compression ratio, EGR rate, and gas composition, is used for defining the boundary conditions for the CFD calculations performed in the current work. Specifically, the calibrated case presented in Section 4.4.5 was updated considering the oxy-fuel operation characteristics and parameters from the 0D-1D simulations. The boundary conditions for the 3D model (so-called "Baseline oxy-combustion") are presented in Table 7.1.

Table 7.1: Oxy-fuel combustion model boundary conditions.

Compression Ratio [-]	28:1
Engine speed [rpm]	3500
IMEP [bar]	20.25
Fuel mass [mg/cc]	62
Fuel LHV [MJ/kg]	44.6
SOI [deg]	-11.5
Temperature at IVC [K]	387
Pressure at IVC [bar]	1.83
O_2 [-]	0.364
H_2O [-]	0.203
CO_2 [-]	0.433
EGR [%]	70

A comparison of the in-cylinder pressure, RoHR, and the HR between the reference Diesel case and the baseline oxy-combustion case is presented in Fig-

ure 7.1. The in-cylinder thermodynamic conditions are different in both cases due to differences in the gas composition, promoting a higher delay in the start of combustion in the oxy-fuel concept. In terms of in-cylinder pressure (top graph in Figure 7.1), the reduction in the pressure values when the oxy-fuel combustion concept is used can be explained by the differences between CO_2 and N_2 properties, the different trapped masses and the different volumetric compression ratio. Despite the higher CR, the oxy-fuel combustion case shows lower peak pressure values in both compression and combustion phases. The carbon dioxide molecule has a lower specific heat capacity than oxygen and nitrogen (the dominant parts of the air). So, the increment of CO_2 in the combustion chamber, maintaining the same intake temperature and pressure, will vary the specific heat capacity of the mixture, causing a lower temperature rise and a more considerable ignition delay period [6, 7]. Regarding the RoHR (the graph in the middle), the ignition delay is higher for the oxy-fuel combustion configuration. Thus the combustion happens practically in the premixed combustion phase. Also, the combustion slows down at around 20 cad aTDC because jet-wall interaction might interfere with the flame sustainability since the higher CR requires a smaller combustion chamber volume.

All these differences impact the total energy losses, which can be seen in the normalized cumulative HR plot. The results from the simulations were normalized concerning the maximum of the theorical total energy available in each cycle, which is calculated by the amount of fuel injected in a cycle multiplied by the low heating value of the fuel. The engine working in the oxy-fuel combustion concept is not able to keep the combustion efficiency at acceptable values, compromising the engine efficiency.

Based on this initial analysis, it can be seen that the new oxy-fuel combustion concept has an unsatisfactory efficiency when used in an existing CI Diesel combustion chamber designed for conventional air combustion. As stated in the objectives, this work intends to find a new combustion system adapted to this particular combustion concept requirements.

The number of variables that define the combustion system is typically high, which all contribute to the combustion performance, which has cross-interaction between them and non-linear trends. Finding the right combination of all the factors that provide an optimal engine design is still a challenge nowadays.

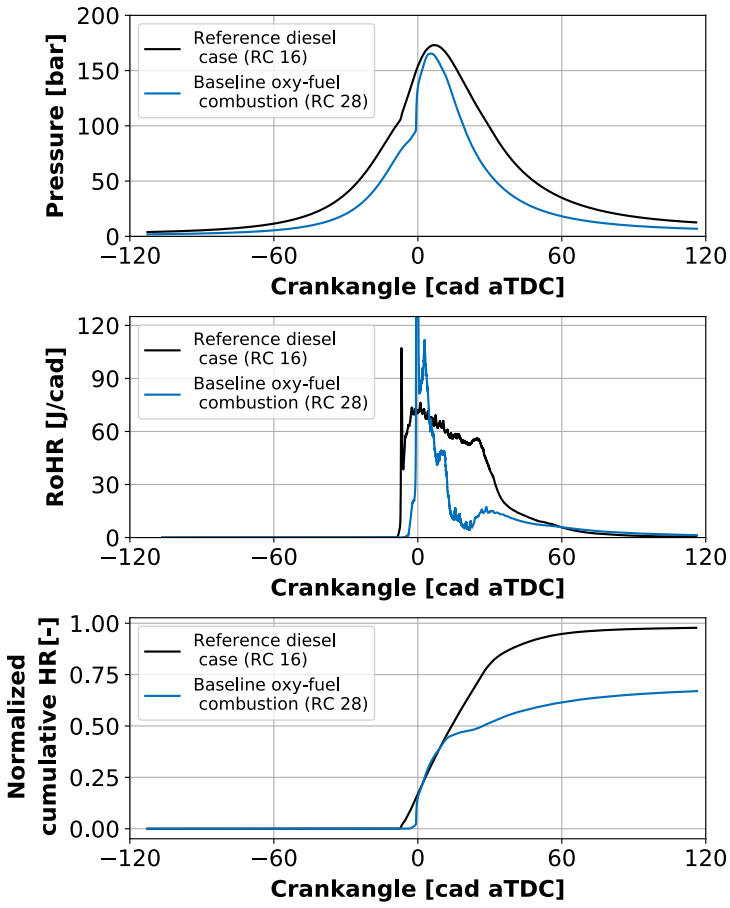

Figure 7.1: Comparison between the simulations of the reference Diesel case against the baseline oxy-fuel combustion case, results of in-cylinder pressure (top), RoHR (middle), and normalized cumulative HR (bottom).

7.3 Optimization definition

7.3.1 Optimization parameters and objective function

As mentioned in previous sections, this chapter aims to find a suitable combustion system configuration that improves the performance of the oxy-fuel concept. Therefore, eleven parameters associated with the combustion system were selected as variables:

- Six factors are geometrical parameters related to the piston bowl defi-

nition and are shown in Figure 7.2. As can be seen in the figure, the $GP1$ and $GP6$ can move in the vertical direction. The points, $GP2$ and $GP3$ are able to move in the horizontal direction. At the same time, the $GP4$ and $GP5$ are defined to control the curvature of the line, to better adjust the shape of these parts. The $p5$ and $p6$ have a fixed position for all the cases, maintaining the same crevice.

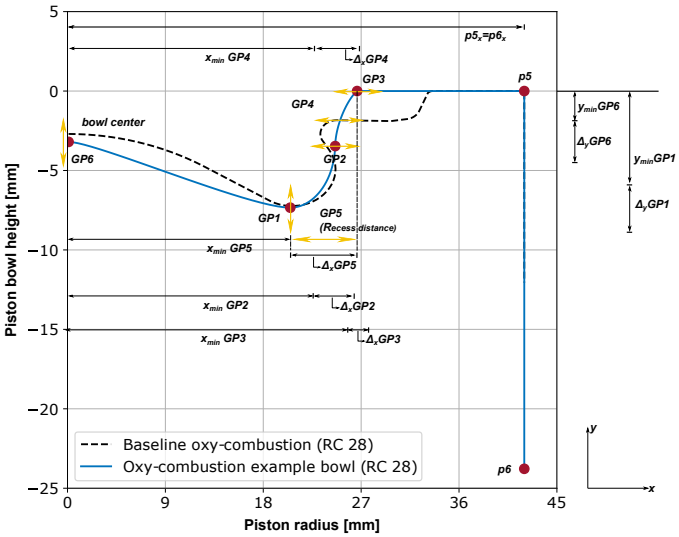

Figure 7.2: Geometrical points for piston bowl definition.

- Four parameters are used to characterize the injection system (nozzle hole number, spray angle, injection pressure, and start of injection). The left graph of Figure 7.3 shows the variation of the ROI for the injector when the injection pressure is changed using the same number of holes and injected mass. The right graph exemplifies the ROI for each nozzle injector hole when this parameter change at constant injection pressure and amount of fuel.
- The final one is the swirl number to describe the in-cylinder gas motion. The range of all parameters used as inputs for the optimization process is presented in Table 7.2.

To define the first particles, the Latin Hypercube methodology was used to create 100 distinct particles equally distributed in each input's range. Later,

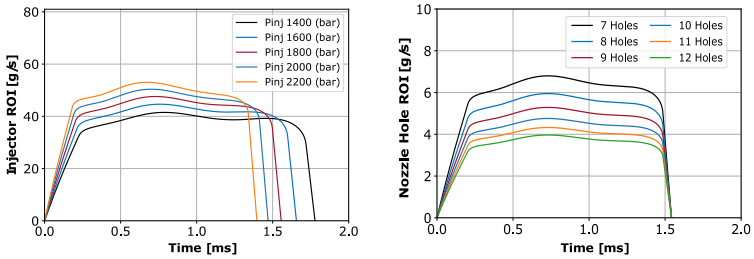

Figure 7.3: ROI examples for different parameters: left - injection pressure, right - number of injector holes.

Table 7.2: Inputs parameters and their ranges considered in the optimization process.

Parameter	Range
Geometrical parameter 1 [-]	[-0.5, 1.0]
Geometrical parameter 2 [-]	[-1.0, 1.25]
Geometrical parameter 3 [-]	[-1.0, 2.0]
Geometrical parameter 4 [-]	[0.0, 1.0]
Geometrical parameter 5 [-]	[-1.4, 0.1]
Geometrical parameter 6 [-]	[-0.5, 1.0]
Number of injector holes [-]	[7, 12]
Spray angle [°]	[155, 175]
Swirl number at IVC [-]	[1.0, 3.0]
Injection pressure [bar]	[1000, 2200]
SOI [cad aTDC]	[-25, 0]

the results of these parameters were used as a database for the initialization of the optimization algorithm. In the next step, NS starts the optimization process by generating the 30 standard particles and 10 particles that explore the search space.

The optimization algorithm will combine all the input variables in order to maximize the engine efficiency and, at the same time, minimize the soot emissions. Additionally, the algorithm should consider two constraints: the maximum in-cylinder pressure (to ensure the mechanical integrity of the cylinder, established by the manufacturer) and the CO emissions, which should be lower than the value of the baseline case. To meet these requirements, the objective function (OF) is defined based on the relative importance of soot,

efficiency, the maximum pressure (p_{max}), and CO emissions against the baseline values. The mathematical definition of the OF is presented in Equation 7.1,

$$\begin{aligned} OF = f_1(soot) \cdot coef_{\text{soot}} + f_2(\text{eff}) \cdot coef_{\text{eff}} \\ + f_3(p_{max}) \cdot coef_{p_{max}} + f_4(\text{CO}) \cdot coef_{\text{CO}} \end{aligned} \tag{7.1}$$

where the *coef* indexes are coefficients used to adjust the equation in order of importance of each term. In this work, the main objective of the optimization process is to obtain a combustion system that minimizes soot emissions. The second objective is to obtain the best efficiency value possible. For these reasons, the coefficients used for these values are higher and play a major role in the objective function. The choice of lower values for the CO and maximum pressure coefficients is because these parameters are constraints of the optimization and should have a minor influence on the objective function. In addition, the objective of soot oxidation is aligned with the objective of *CO* and C_xH_y oxidation. The absence of N_2 fully breaks the trade-off between oxidation and reduction reactions to eliminate pollutants within the combustion chamber. Despite C_xH_y is not within the optimization function, it will be checked that it is not needed since the *CO* optimization will also cause a C_xH_y oxidation below the standard air combustion levels. The values of those coefficients were $coef_{\text{soot}} = 1$, $coef_{\text{eff}} = 0.75$, $coef_{Pmax} = 0.1$ and $coef_{\text{CO}} = 0.1$. Moreover, the total objective function is composed of four sub-functions that are defined for each output. Those functions are detailed in Equations (7.2, 7.3, 7.4, 7.5), where the *CFD* index represents the value obtained from the CFD simulation, and the *lim* index represents the baseline level of each component. The objective function is essential in the optimization process because it is the one that feeds the NS algorithm with the evaluation of the inputs and their effect on the efficiency and emission reduction, leading to the convergence of the solution.

7.4 Results and discussion

This section summarizes the results obtained from the optimization process. First, the convergence of the optimization algorithm is presented, and the evolution of the output parameters is analyzed. Then, the optimized combustion system results are compared against the reference case to understand better this new system that should maximize the benefits of the oxy-fuel combustion concept.

Table 7.3: Component functions of the parameters to optimize and the constraints.

Condition	f_1(soot) . . . . . Eq. (7.2)
if $f_{CFD} < f_{lim}$	$\frac{f_{CFD}}{f_{lim}}$
if $f_{CFD} \geq f_{lim}$	$\frac{f_{CFD}}{f_{lim}} + 1000 \cdot (log(f_{CFD}) - log(f_{lim}))^2$
Condition	f_2(eff) . . . . . Eq. (7.3)
if $f_{CFD} > f_{lim}$	$\frac{f_{lim}}{f_{CFD}}$
if $f_{CFD} \leq f_{lim}$	$\frac{f_{lim}}{f_{CFD}} + 100 \cdot (log(f_{CFD}) - log(f_{lim}))^2$
Condition	$f_3(p_{max})$ . . . . . Eq. (7.4)
if $f_{CFD} < f_{lim}$	$\frac{f_{CFD}}{f_{lim}}$
if $f_{CFD} \geq f_{lim}$	$\frac{f_{CFD}}{f_{lim}} + 50 \cdot (f_{CFD} - f_{lim})^2$
Condition	f_4(CO) . . . . . Eq. (7.5)
if $f_{CFD} < f_{lim}$	$\frac{f_{CFD}}{f_{lim}}$
if $f_{CFD} \geq f_{lim}$	$\frac{f_{CFD}}{f_{lim}} + 100 \cdot (f_{CFD} - f_{lim})^2$

7.4.1 Optimization process results

The initial step of the analysis of the results was the verification of the algorithm convergence. Figure 7.4 presents the evolution of the global objective function for all the cases simulated with CFD. It can be seen how the NS algorithm decreases the value of the objective function as it progresses, converging toward a minimum value. The definition of the best particle refers to the one with the minimum value of the objective function until that current iteration. The capability of the NS for rapid convergence is observed since the objective function decreases quickly from the beginning of the procedure. In this figure, the black line represents the path of the minimum objective function value during the optimization process. Meanwhile, the blue represents the conquerors or standard particles, while the red dots denote the explorers particles. The best particle with the lowest objective function was obtained around the simulated case 720.

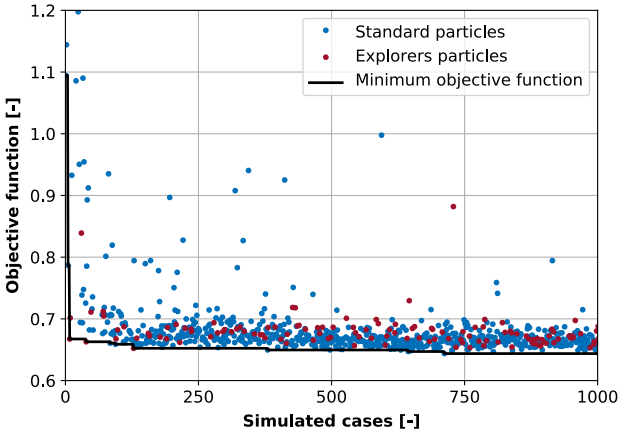

Figure 7.4: Objective function convergence evolution.

Subsequently, the optimization targets and constraints were analyzed to verify these parameters evolution during the optimization process. Figure 7.5 shows the progression of these parameters for each simulated case. The results obtained for soot and efficiency are shown in the bottom graphs and show a significant improvement in both variables. While the optimization process could reduce the soot emissions close to a virtual zero, the efficiency exhibits an improvement of 8.8% concerning the baseline oxy-fuel combustion case (marked with the horizontal dashed line). Likewise, all the graphs evidence common information, the high variability of the outputs at the beginning of the optimization process with results that do not meet the values of the constraints. As the simulations evolve, the majority of the points try to reach the optimized region. However, some points seem to be scattered with relatively bad results in terms of soot or efficiency. These dispersed points are explorer particles that seek new positions throughout the search space, away from the optimal region.

Moreover, the top graphs represent the evolution of the constraints of the objective function: CO and maximum pressure, respectively. In this figure, the blue dots represent each simulated case, and the black dashed line is the constraint obtained from the baseline engine configuration operating under oxy-fuel conditions. Along the progress of the optimization, the blue dots tend to move far from their respective constraint value, especially on the reduction of the CO values, due to the high correlation between the reduction

of CO emissions and the increase in efficiency, also reported by Zubel et al. [8]. Finally, the optimized case is represented by the red dot in the four plots.

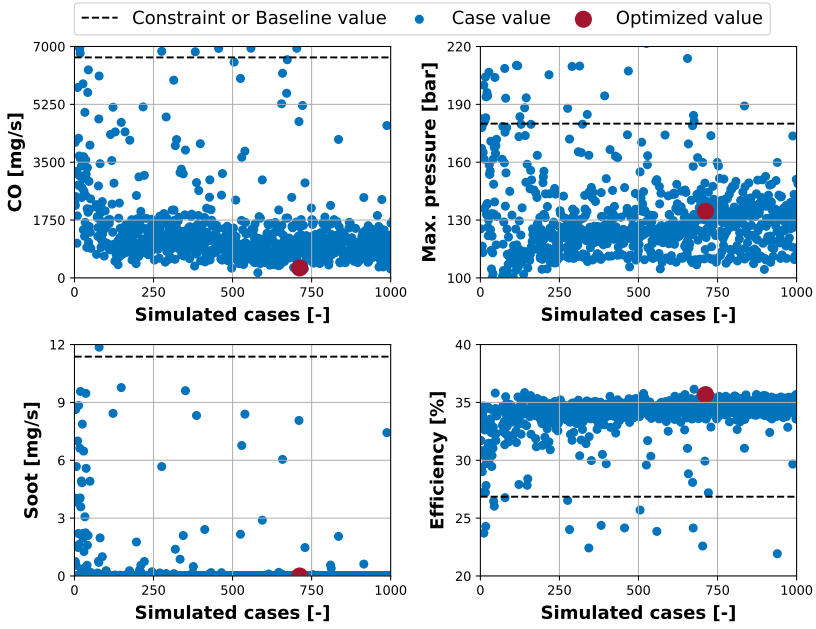

Figure 7.5: Evolution of constraints and objectives outputs towards the optimized value.

The dependency of the objective function value on the geometrical parameters is shown in Figure 7.6 where again, the red dot represents the optimized case, whereas the blue dot is the value of each parameter for each case. The geometrical parameter 1 (GP1) adjusts the depth of the piston and is presented in the left-top graph. The optimization process tends to move the value of GP1 towards regions near this parameter's maximum limit, decreasing the piston bowl height. For the geometrical parameter 2, most points are concentrated near the maximum limit of this parameter, suggesting that the bowl diameter increment would enhance the performance of the oxy-fuel combustion concept. The evolution of the geometrical parameter 3 during the optimization process starts with some cases in the minimum limit moving to an intermediate region of the entire range but nearer to the maximum limit. This evolution modifies the point GP3 in Figure 4.20, changing the initial geometry of the deep re-entrant piston towards an almost no re-entrant geometry. The geometrical parameters 4 and 5 are responsible for adjusting the curvature between the

GP2 and GP3 (shown in Figure 4.20) and the alignment between GP1 and GP2, respectively. The GP4 has values in the middle of the parameter range in order to obtain a smoother bowl shape with a lower objective function. Then, the GP5 was conducted to the maximum range value, again avoiding the re-entrant condition. The last parameter, the GP6, can update the bowl center depth. The results for this parameter converge close to the maximum value possible.

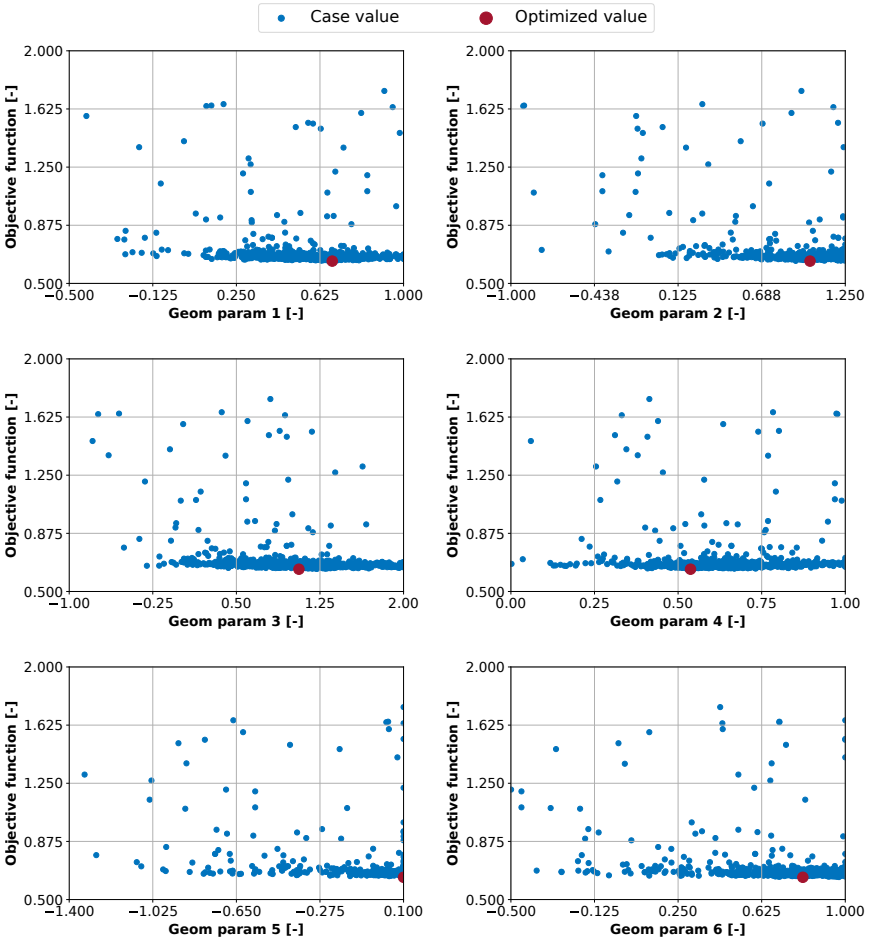

Figure 7.6: Objective function value for the geometrical parameters.

Figure 7.7 summarizes the distribution of the objective function in the domain of each parameter related to the injection system and the swirl number. Analogous to previous figures, the blue dots represent each simulated case,

and the red dot is the best configuration found for the oxy-fuel concept. The top-left graph shows that the most suitable number of orifices is the minimum in the studied range, leading to a big orifice diameter. This preference for fewer orifices is related to the reduction of CO emissions, in agreement with the results of Yoon et al. in [9]. Furthermore, the NS algorithm explores all the possible ranges for the spray angle value. The best case is located in the spray angle value that matches with the piston geometry [10]. Regarding the injection settings, the best case moves to the maximum level in the explored range, which is related to the fact that higher injection pressure improves the atomization and evaporation of the fuel, enhancing the mixture and the ability to react with the oxygen present in the combustion chamber [11].

Moreover, the SOI distribution during the optimization evidence that when the injection is advanced, the combustion performance deteriorates since it promotes a longer ignition delay with a higher gap between fuel injection and the start of combustion. Thus, the heat release rate had a significant peak in the premixed combustion phase, and a maximum in-cylinder pressure value beyond the constraint of the optimization process [12]. On the other hand, when the SOI moves towards the top dead center, the ignition delay is reduced, with a smoother start of combustion.

Lastly, the reduction of the swirl number is related to the increment of the bowl diameter that will reduce the gas velocity in the bowl and, at the same time, could reduce heat transfer and other energy losses [13].

The plots in Figure 7.8 corroborate that the best case (the red dot with the minimum objective function) is obtained for the lowest soot level and the maximum efficiency, which were the objectives of the optimization process. Also, the constraints are respected, with a high CO emissions reduction associated with the maximum efficiency trend.

The Pareto fronts can be seen in the left side of Figure 7.9 where the initial Diesel reference case is the black dot, and the optimum case is represented with the red dot. In both plots, the vertical dashed line represents the efficiency of the baseline case, and the horizontal dashed lines indicate the respective levels for the constraints. In both graphs, several cases meet the restrictions (are below the horizontal dashed lines) and provide better efficiency than the oxy-fuel baseline case. Since the objective function is composed of four parameters with different coefficients that define the optimization priorities, combining the constraints and objectives with the best trade-off between all these outputs simultaneously is the best solution. The plots on the right side of Figure 7.9 illustrate how the optimum case tries to reach the lowest HC level maximizing the efficiency. The most promising result can be seen in

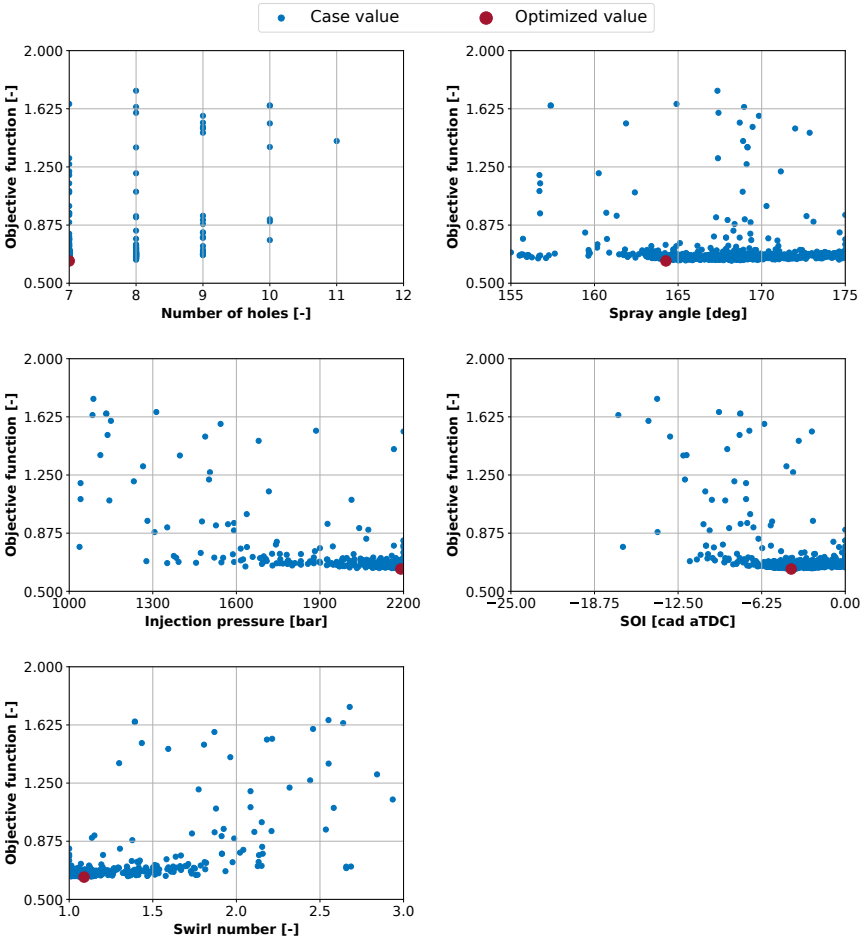

Figure 7.7: Objective function value for inputs of the injection system and swirl number.

the soot vs. HC comparison (bottom-right plot in Figure 7.9), where both pollutant emissions were drastically reduced from the oxy-fuel baseline case, even reaching values much lower than the initial Diesel-reference case, with plenty of solutions still under the constraints.

Based on the results, the optimized geometry profile was compared against the baseline geometry, which is the same as the original Diesel engine but adapted to the CR 28. The comparison of both geometries is shown in Figure 7.10. The baseline step-bowl profile changed to a new geometry without the step, where the re-entrant configuration has also disappeared. Initially, one objective of the step-bowl was to split the fuel spray into two parts, one

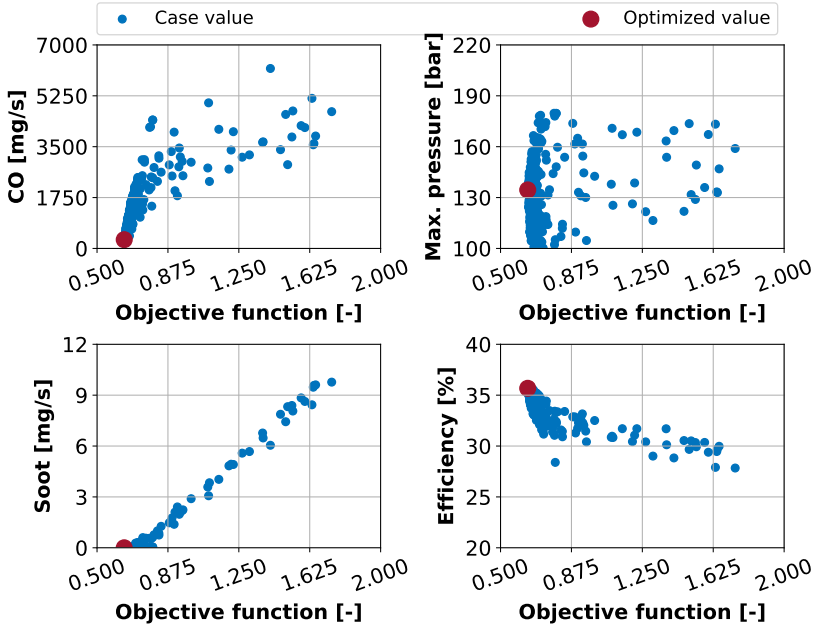

Figure 7.8: Objective function value evolution for the constraints and objective parameters.

direction towards the cylinder head and the other part into the bowl. This avoided the spray reaching the squish zone, resulting in less soot generated close to the cylinder walls, decreasing the soot-in-oil production in the engine [14, 15]. The new bath-tube geometry is a result of the optimization process that reduces the soot emissions and, at the same time, improves the efficiency since this new geometry is focused on area reduction, which reduces the heat transfer losses and improves the engine efficiency [16]. Additionally, the spray angle changes in order to match the new geometry. The spray angle in the baseline case conduces the injected fuel within the piston bowl, promoting spray-wall impingement. Meanwhile, in the new configuration, the angle is wider. Therefore, the distribution of the spray in the chamber volume is more uniform, increasing the interaction between the injected fuel with the gas mixture available inside the chamber.

Finally, Table 7.4 summarizes the parameters that describe the combustion system for the baseline and the optimized cases. The oxy-fuel combustion concept requires an injector with a lower orifice number (a higher diameter to keep the same nozzle area). A wider spray angle matches the new piston bowl

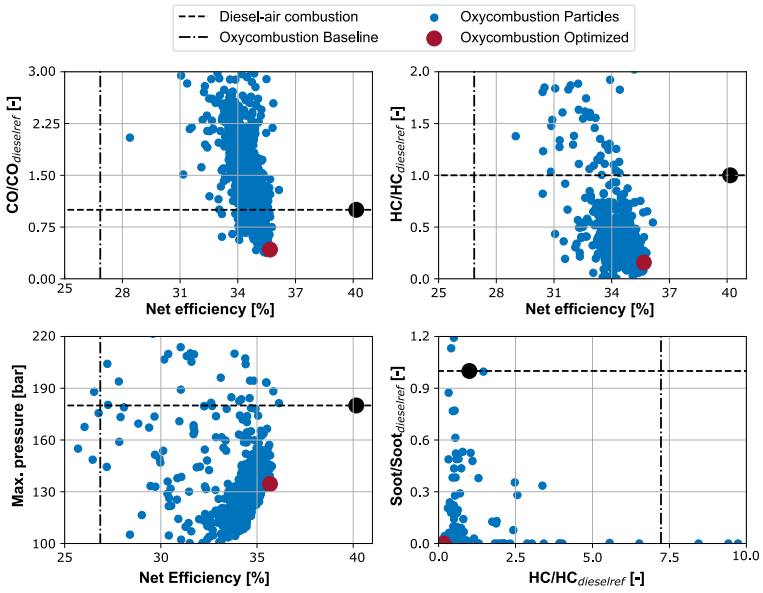

Figure 7.9: Pareto front of maximum pressure of the engine vs. efficiency, CO emissions, HC and soot evolution vs. efficiency. The reference Diesel case value normalizes the pollutant emissions.

geometry and avoids excessive fuel impingement with the walls. Moreover, the optimal number of holes depends on the engine operating condition and compression ratio. Still, in general, a low number of holes conducts to good efficiencies because it promotes the highest rate of heat release during the mixing combustion phase [15, 17]. Swirl number was reduced following the number of injector nozzles behavior. The injection pressure increases, improving the spray momentum, atomization, and mixing rate. The last parameter is the SOI. It was delayed until an instant when it is possible to control the peak of in-cylinder pressure within the limit of the engine operation.

7.4.2 Engine results

In Figure 7.11 the comparison between the in-cylinder pressure, temperature, rate of heat release, and the cumulative heat release are presented. The lower in-cylinder pressure trace in the oxy-fuel cases comes from the differences in the gas properties due to the absence of nitrogen, as already mentioned in Section 7.2. Both oxy-fuel combustion cases, baseline, and optimized cases have the same CR, and the differences in the peak of pressure are due to the

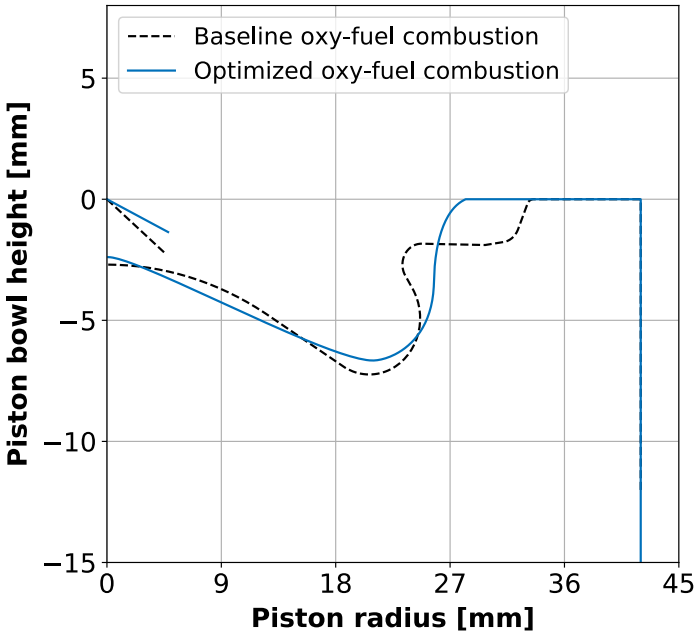

Figure 7.10: Comparison between the baseline and the optimized geometry.

Table 7.4: Inputs comparison between the baseline and optimized oxy-fuel combustion cases configuration.

	Baseline case	Oxy-fuel combust. best case
Number of injector holes [-]	10	7
Spray angle [deg]	154	164
Swirl number [-]	2.00	1.08
Injection pressure [bar]	1800	2190
SOI [cad aTDC]	-11.5	-4.04

differences in the engine settings. For instance, the optimization procedure indicates that for a proper operation in oxy-fuel mode, the start of injection should be delayed, near the top dead center, with higher injection pressure. The benefit of this strategy is evidenced in the heat release rate curves, where the start of combustion occurs sooner since the ignition delay is shorter because the injection occurs when the gas in the chamber is at a higher temperature and pressure. The wider bowl shape without the re-entrant edge minimizes the wall impingement and avoids the slowdown of the combustion observed in

the blue curve around 15 cad. Another factor responsible for this improvement is the higher injection pressure that atomizes the fuel better and helps find the oxygen available in the chamber, enhancing the mixture distribution. The cumulative rate of heat release curves corroborates this behavior (bottom-right graph in Figure 7.11). The modifications in the combustion system allow to burn the fuel supplied in the engine more efficiently, with a combustion efficiency more similar to those of conventional air-Diesel engines.

Moreover, the evolution of the mean temperature along the cycle is analyzed since it is an important parameter for the correct operation of the MIEC. The bottom-left graph in Figure 7.11 shows that the temperature level in oxy-fuel cases is lower from the IVC and during the compression stroke. However, as soon as the combustion starts, the temperature trace in the optimized configuration increases and reaches levels similar to the conventional Diesel operation mode, delivering an exhaust gas with temperatures higher than 1500K. Then this energy can be used for the O_2 separation in the MIEC membrane. This result is consistent with the RoHR curves (see upper-right plot in Figure 7.11). This result represents the EGR level settled in the boundary conditions for the current study. However, this might vary for different EGR rates, as was determined by Serrano et al. in [18].

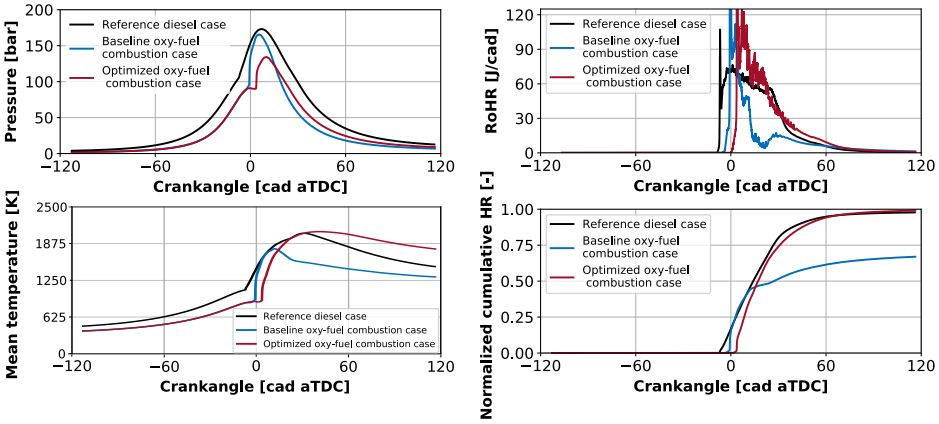

Figure 7.11: Comparison between in-cylinder pressure, RoHR, and normalized cumulative HR for the reference Diesel case, baseline, and optimized oxy-fuel combustion case.

The improvement in terms of emissions per cylinder is listed in Table 7.5. Comparing the combustion system of the optimized oxy-fuel combustion case against the reference Diesel case, it is possible to see that the soot emissions

are widely reduced, obtaining values near a virtual zero. Regarding the CO emissions, the initial baseline engine operating with the oxy-fuel combustion concept produced an unacceptable level of this pollutant specie, 10 times higher than the standard reference Diesel. The new chamber hardware, combined with adequate engine settings, allowed to decrease the CO emissions to a level than the reference Diesel. This result is obtained even with the restricted oxygen quantity in the system (lambda is 1.1 since its production in the membrane is costly). The unburned hydrocarbon emissions showed a similar trend, where it can be noticed that the new combustion configuration produces lower HC (in mg/s per cylinder) than the initial Diesel reference case, which is in agreement with the combustion efficiency observed in the cumulative HR curves presented in Figure 7.11. In the preliminary stage, the baseline oxy-fuel case generated extremely high levels of unburned hydrocarbons due to strong jet-wall interaction that slowed down the combustion combined with the formation of very rich zones near the squish, with little O_2 availability, that stopped the combustion process. However, the configuration found by the optimization procedure was able to promote the mixture formation and the O_2 consumption, as corroborated in the last part of this section.

Additionally, the net indicated efficiency was also evaluated. It is net indicated efficiency since, for this analysis, only the high pressure indicated work is taken into account because the study is focused on the closed cycle and the combustion process. It can be seen that the changes in the system produced an increase in the net indicated efficiency of the engine compared to the baseline oxy-fuel combustion (from 26.6% to 35.7%). However, this value is still far from the initial value of the conventional Diesel case (40.1%). Since the carbon dioxide molecule has a lower specific heat capacity compared with oxygen and nitrogen, the increment of CO_2 in the combustion chamber due to the higher EGR rate used in the oxy-fuel combustion concept will vary the specific heat capacity of the mixture. Therefore, the adiabatic expansion coefficient (γ) when operating with EGR + O_2 is lower than considering pure N_2, then the efficiency in the oxy-fuel case is lower compared to the reference one, although they have similar cumulative HR. Although all the efforts made during the study, this is one weakness of the concept that remains. On the other side, it must be highlighted that this is compensated by the absence of NO_x emissions in the exhaust gases. Also, since there is no N_2, the CO_2 can be easily separated from the water vapor (by water condensation) and compressed until supercritical conditions. It means capturing it as a dense supercritical liquid of high purity (more than 95%). Therefore, the increment in BSFC does not mean an increment in CO_2 emissions.

Table 7.5: Comparison between the efficiency, soot, and CO between the reference Diesel case, baseline, and optimized oxy-fuel combustion cases.

	Reference Diesel	Baseline oxy-fuel C.	Optimized oxy-fuel C.
Efficiency [%]	40.1	26.6	35.7
Soot [mg/s]	0.35	11.4	< 0.0001
CO [mg/s]	177	1929	81
HC [mg/s]	28	206	4.5

Figure 7.12 shows the energy balance for each of the three cases presented in Table 7.5. For the Baseline oxy-fuel combustion case, it can be seen that some part of the energy is lost due to the unburned fuel since it cannot find the oxygen available in the chamber. On the other hand, the Optimized oxy-fuel combustion case can burn most of the fuel, recovering part of the energy wasted in the Baseline oxy-fuel combustion case (comparable to that of the reference diesel-air case). However, higher losses were found through the walls, where the most significant difference is in the liner region due to the difference in compression ratio and bowl shape. Also, an important part of the energy is lost in the exhaust gases as a consequence of the lower adiabatic expansion coefficient of the gas.

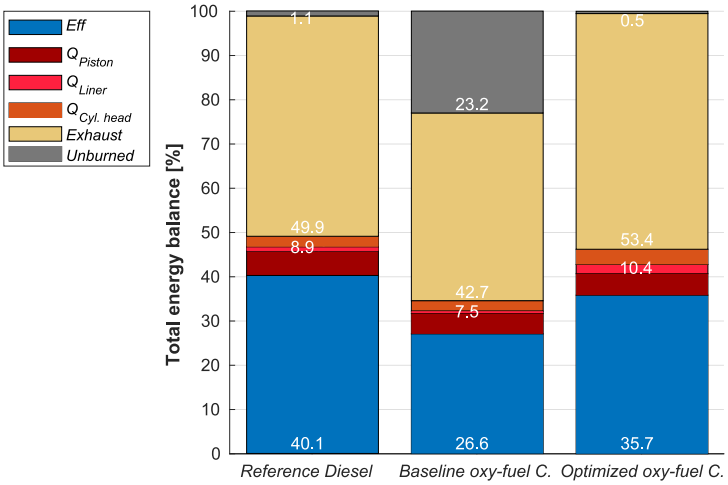

Figure 7.12: Energy balance for the three simulated cases.

Lastly, to understand the mixture's distribution in the system, Figure 7.13 shows the contours of the oxygen concentration inside the combustion chamber during the combustion process. The columns of the figure correspond to the instants of 10% (CA10), 25% (CA25), 50% (CA50), 75% (CA75), and 90% (CA90) of burned mass, and the rows represent each one of the three simulated cases. For the reference Diesel case, the oxygen concentration available at IVC is lower than in the other cases due to the air composition (oxygen and nitrogen). In this case, the fuel jets can easily find oxygen inside the chamber, with a small amount of oxygen remaining in the crevice region and near the injector at the end of combustion (CA90). The CA10, CA25, and CA50 phases occur almost at the same crank angle during the premixed combustion phase for the baseline oxy-fuel combustion case. Higher quantities of oxygen remained in the squish region that did not reach the fuel, evidencing rich zones and incomplete combustion, which are responsible for the soot formation. On the contrary, the optimized oxy-fuel combustion case shows a better oxygen consumption at the end of combustion (from CA50 to CA90) compared to the baseline configuration, with a similar distribution compared to the reference air-Diesel engine evincing the advantages of the optimization procedure.

Figure 7.14 illustrates the temperature contour inside the combustion chamber for the Diesel reference and the optimized configuration. Although the new combustion chamber has a smaller volume, the jet is able to distribute and progress within the domain until it reaches the bowl wall. The matching between the jet and the bowl corner can be seen, re-distributing the spray inside the bowl and some other parts towards the squish, where fresh oxygen is available (in agreement with Figure 7.13). After CA50 phases, the temperature contours show higher values for the optimized case than the Diesel one, which is also evenly distributed. This is also consistent with the temperature traces in Figure 7.11. In this combustion concept, the high-temperature levels can be afforded since there is no N_2 in the trapped gas in the cylinder, then there is no NO_x production. Also, relatively high-temperature levels are desired in order to provide sufficient energy to the MIEC, as mentioned before.

7.5 Analysis of an extended operating range

During the optimization process, the combustion system was strongly analyzed in terms of the best SOI value against maximum pressure, soot, CO, HC emissions, efficiency, and objective function. Figure 7.15 summarizes how the SOI affects each parameter. In a general way, moving the SOI to a region with a good value of efficiency produces a reduction in CO, soot, and HC emissions.

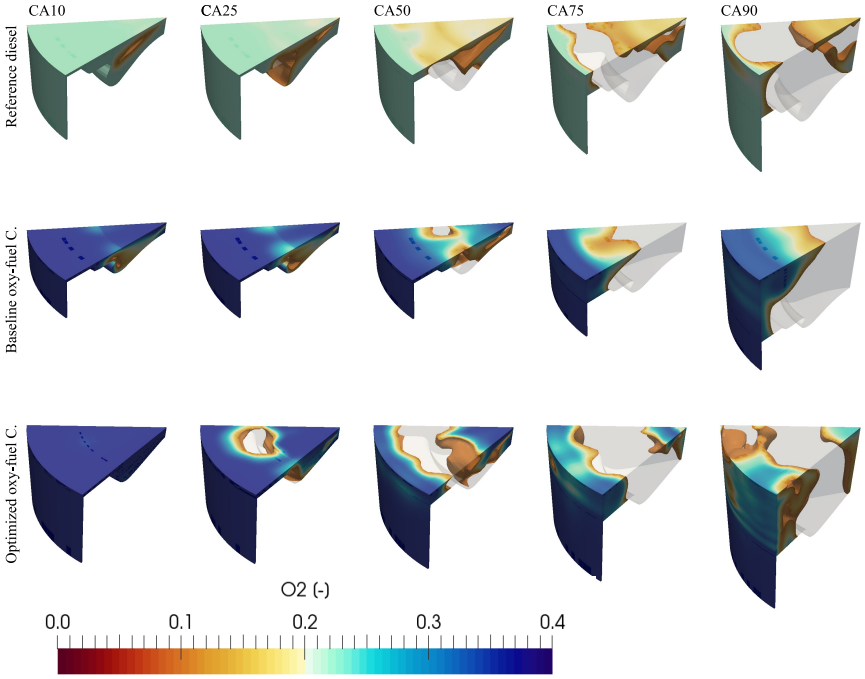

Figure 7.13: O_2 distribution inside the combustion chamber for several combustion periods (CA) comparison between the reference Diesel, baseline, and optimized oxy-fuel combustion case.

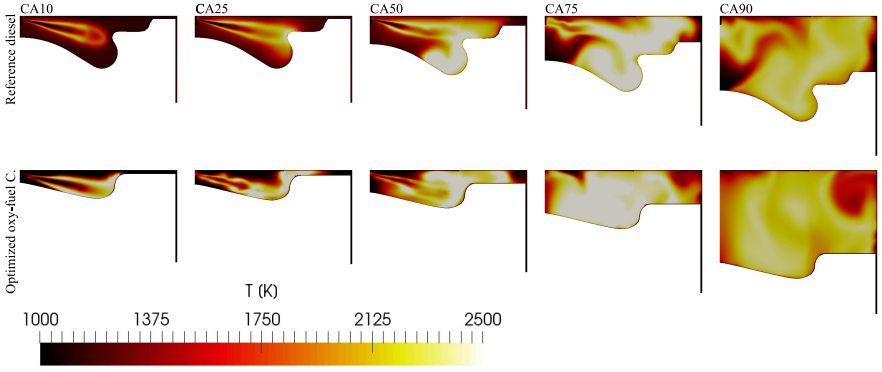

Figure 7.14: Temperature distribution inside the combustion chamber for several combustion periods (CA) comparison between the reference Diesel and optimized oxy-fuel combustion case.

Moreover, when the SOI is advanced, the combustion performance is affected, resulting in higher peaks in the RoHR and in-cylinder pressure inside the combustion chamber, which leads to worse values of objective function once the maximum pressure is an essential constraint of the system.

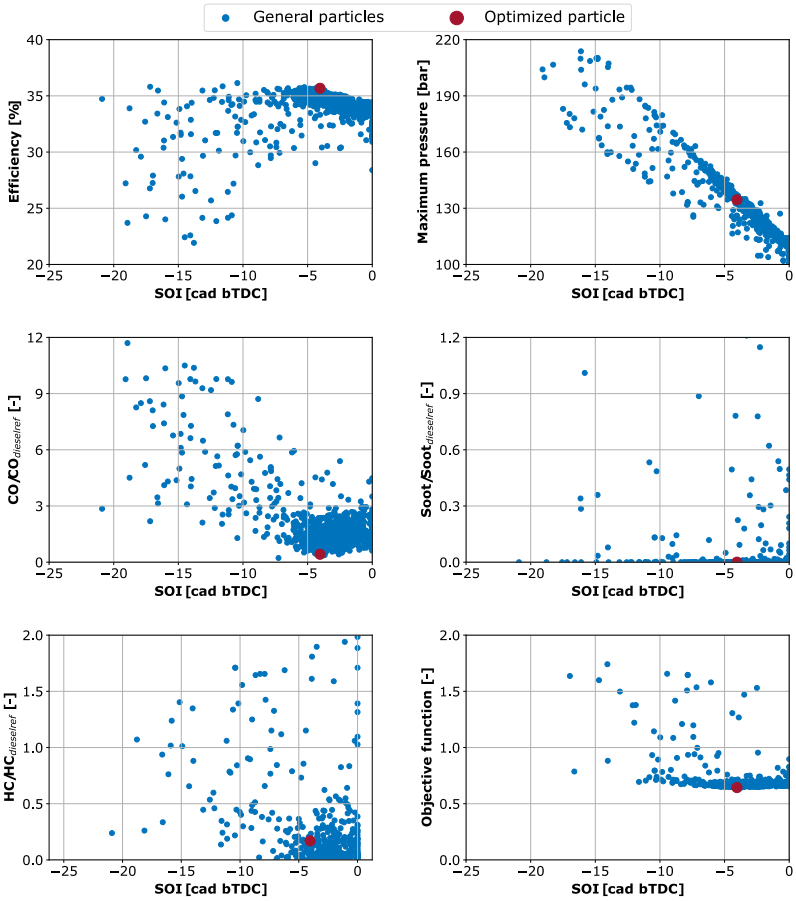

Figure 7.15: Effect of the SOI in the outputs of the engine.

This review of the effect of the SOI in the system is important to clarify the results that will be presented in the following sections related to the simulations performed to extend the information for new operating conditions of the engine.

The left part of Figure 7.16 shows all the cases simulated during the optimization process. From these cases, three of them were selected based on their configuration. They present a high-efficiency value, similar geometry,

and parameters, being that the most significant difference is the SOI moment. The cases are named in the graph as *Opt*, *C*15, and *C*22, meaning optimized, Conquerors 15 and Conquerors 22, respectively. On the right graph of Figure 7.16 the piston bowl geometry and the spray angle of the cases are presented.. Moreover, all the parameters obtained from the optimization process are described in Table 7.6.

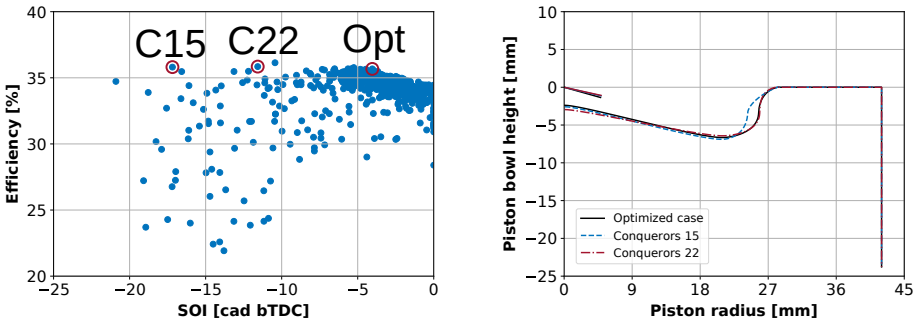

Figure 7.16: Selected cases to the SOI analysis. Left graph: Efficiency distribution in relation to the SOI position. Right: Piston bowl geometry of the selected cases.

Table 7.6: Comparison between combustion system configuration.

	Optimized case	Conquerors 15	Conquerors 22
Number of Holes [-]	7	7	7
Spray angle [deg]	164	167	168
Injection pressure [bar]	2190	2190	2200
Swirl number [-]	1.1	1.6	1.0
SOI [deg]	-4.04	-17.18	-11.58

Furthermore, Figure 7.17 presents the case results of in-cylinder pressure, RoHR, and normalized cumulative HR. The in-cylinder pressure trace shows how advancing the start of injection increases the pressure drastically, values higher than those of safe engine operation for both cases (Conquerors 22 and Conquerors 15). This higher pressure is reflected on the RoHR , since at the fuel injection instant the in-cylinder gas is at low temperature and pressure conditions, increasing the ignitions delay, leading to the increment of the ignition delay. So, when the mixture reaches a favorable condition for ignite, there

is already too much fuel in the combustion chamber, which causes a peak in the RoHR, resulting in all combustion taking place in the pre-mixed phase. This behavior is reproduced on the normalized HR, showing a reduction in combustion efficiency due to the very advanced SOI.

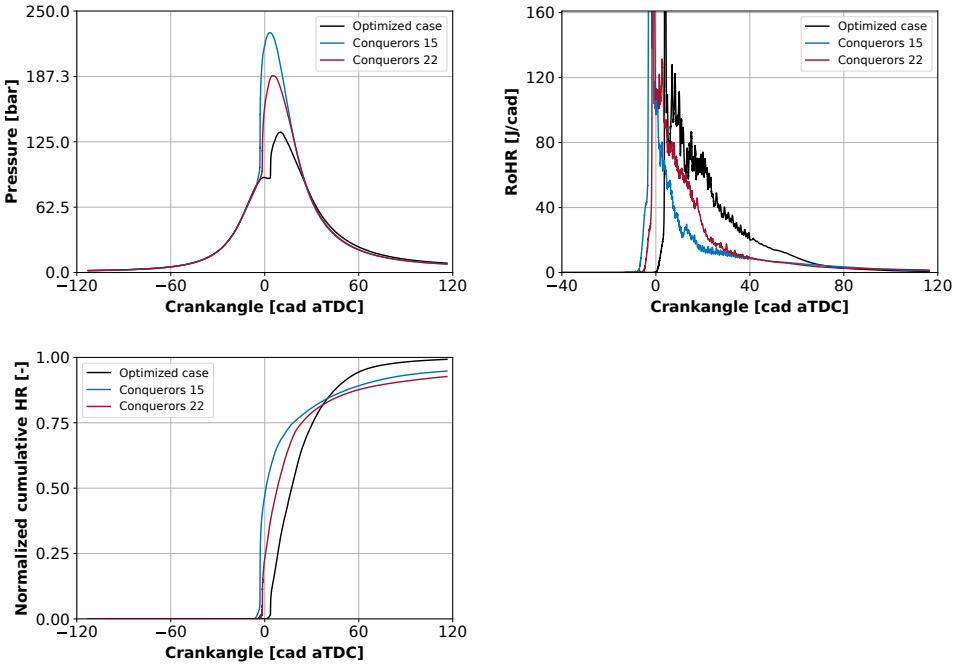

Figure 7.17: In-cylinder pressure, RoHR, and normalized cumulative HR for the selected cases of the SOI study.

Figure 7.18 shows the contour of the temperature of the reference diesel, optimized, Conquerors 15 and Conquerors 22 cases. As the SOI of the cases is different, the comparison was made using representative instant of combustion points (CA10, CA25, CA50, CA75, and CA90). It is possible to see that the combustion occurs mainly until CA50 with a higher temperature value. Furthermore, when combustion takes place predominantly in the premixed phase, the temperature fields are concentrated in the center of the combustion chamber and do not interact much with the liner region in comparison to the other cases.

Some combustion results were compared in Table 7.7. The SOC considered in this study was 0.5% of burned mass. Advancing the SOI, more time is

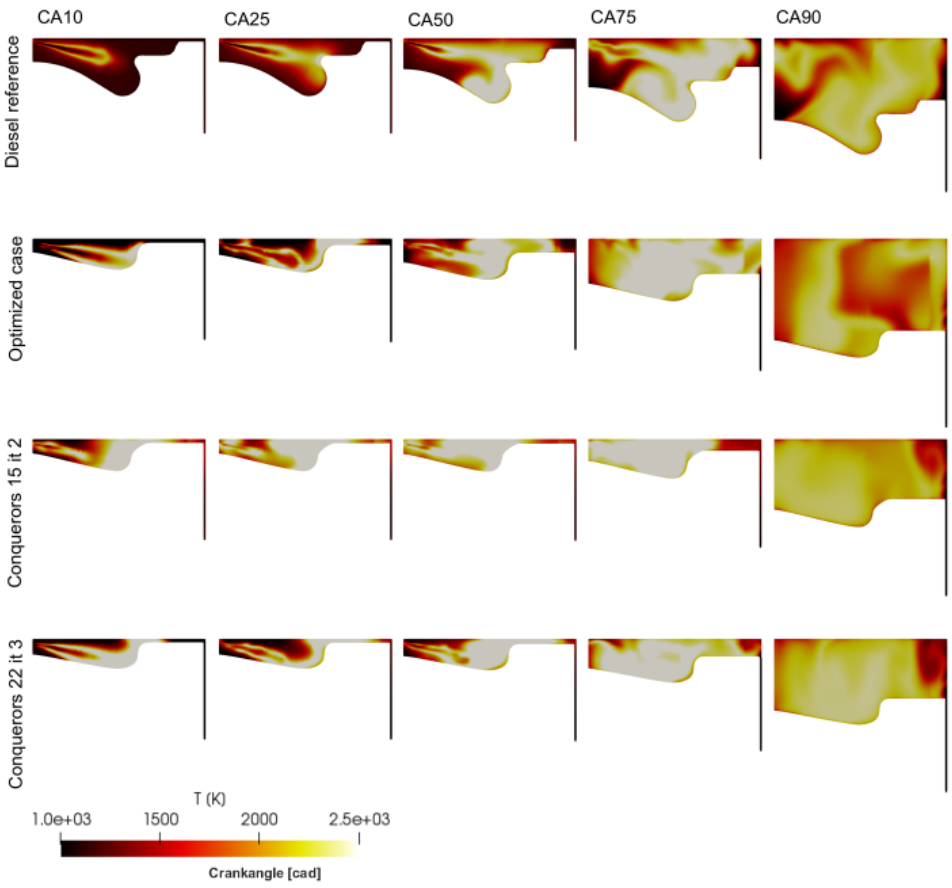

Figure 7.18: Analysis of temperature contours comparing different combustion events.

needed to start the combustion in the simulations due to the combustion chamber mixture conditions.

Figure 7.19 shows the mixture fraction distribution for all the cases. While the diesel reference and the optimized cases have almost no mixture fractions after CA90, the Conquerors cases 15 and 22 have a higher amount of mixture fraction inside the combustion chamber due to the lower combustion efficiency. This behavior is the result of the lower combustion efficiency once 5 to 7% of the fuel is not burned, thus remaining inside the combustion chamber.

Figure 7.20 presents the temporal evolution of the cylinder mass over different equivalent ratios, confirming the information shown in the mixture frac-

Table 7.7: Comparison between combustion results.

Case	SOI [deg]	SOC [deg]	Combustion efficiency [%]
Reference diesel case	-11.65	-7.87	98.53
Optimized case	-4.04	0.91	99.12
Conquerors 15	-17.18	-7.03	94.63
Conquerors 22	-11.57	-4.77	92.88

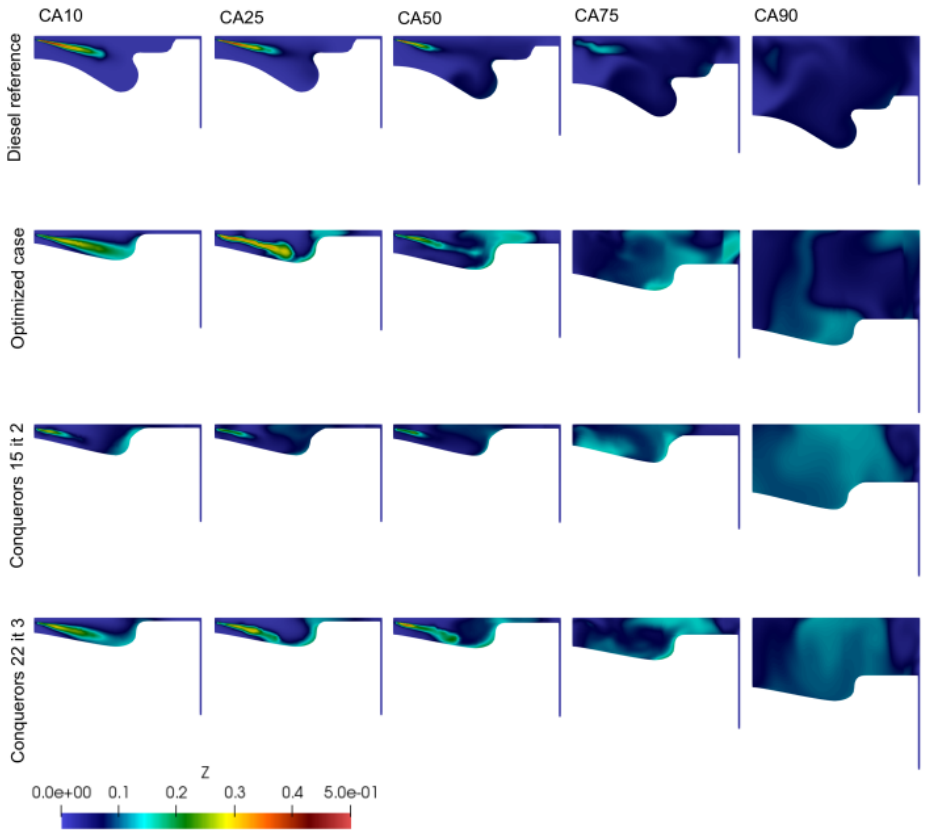

Figure 7.19: Analysis of mixture fraction contours comparing different combustion events.

tion contour. This equivalence ratio evolution represents the bounds of 0.55, 1.05, and 1.75. It can be seen that all the cases are capable of burning rich

mixtures. However, when it comes to the stoichiometric mixture, just the optimized case is able to burn all the fuel in this condition due to the better mixing, especially during the diffusive combustion phase raising the burning velocity. In contrast, the other cases are not able to burn all the fuel during the combustion process, keeping stoichiometric mixtures in the cylinder at the EVO. This better combustion process is assured by the new combustion system implemented, which provides a better match between the bowl geometry, injection, and air-management systems.

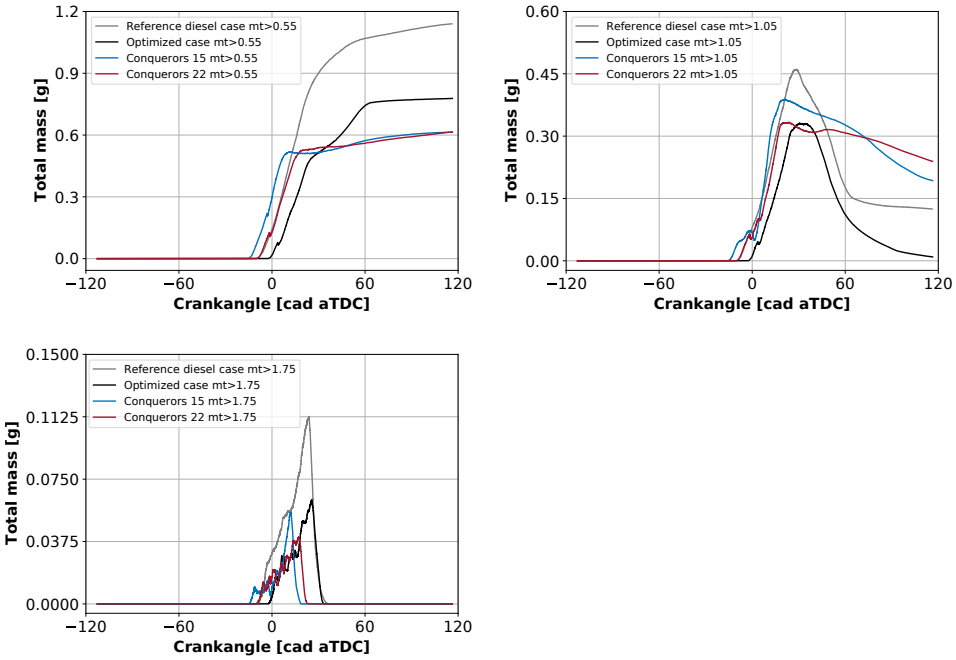

Figure 7.20: Cylinder mass over several equivalent ratios.

With the optimization results, it was noticed that there is a possibility to improve even more the system. This fact is based on the in-cylinder pressure trace of the optimized case, which is below the limit one (180 bar). To evaluate the possibilities, the 1D model used to provide the boundary conditions for the oxy-fuel combustion study was updated with the optimized combustion system. A new 1D study was performed considering the new information available in order to confirm and extend the knowledge obtained from the optimization process. In this new study, the objective was to obtain the

maximum power operating point to maximize the engine's power and efficiency with the new combustion system configuration through 1D optimization. At the end of the iteration process, new boundary conditions were obtained. This new optimum configuration is presented and compared against those one used in the CFD optimization process in Table 7.8.

Table 7.8: New boundary conditions.

Parameter	BC optimized case	BC new case
SOI [deg]	-4.04	-10.64
T_{IVC} [K]	387	430
P_{IVC} [bar]	1.83	2.30
T_{liner} [K]	430	381
$T_{cyl.head}$ [K]	508	502
T_{piston} [K]	543	488
O_2 [-]	0.3641	0.3366
CO_2 [-]	0.4332	0.4520
H_2O [-]	0.2027	0.2113
Fuel [mg/cc]	62	63.71

Figure 7.21 shows the results of the simulations using the new boundary conditions for the max power point. It can be seen that the in-cylinder pressure was recovered, even going a bit over the limit of engine operation when compared with the optimized case. The RoHR shows the same behavior as expected, and there is a reduction in the maximum in-cylinder mean temperature obtained for the new case. Moreover, the normalized HR of the optimized case and the new one are at the same level, showing that the combustion efficiency is similar for both cases.

After obtaining the new boundary conditions for the maximum power point, several operation points of the engine were explored. During this step, it was observed that the pressure inside the cylinder already exceeded the operating limit of 180 bar already in the engine compression phase, thus making it unfeasible to operate the engine at these points using the previously predetermined CR 28. As a result, a new study was needed to obtain the best CR for this engine with the new combustion system. Thus, an exploring process based on 1D simulations was launched using the VEMOD software to obtain a new engine compression ratio value. At the end of this new study, a compression ratio equal to 20 was obtained as the best engine option. These new boundary conditions obtained for RC20 are shown in Table 7.9 and compared against the BC used in the CFD combustion system optimization study.

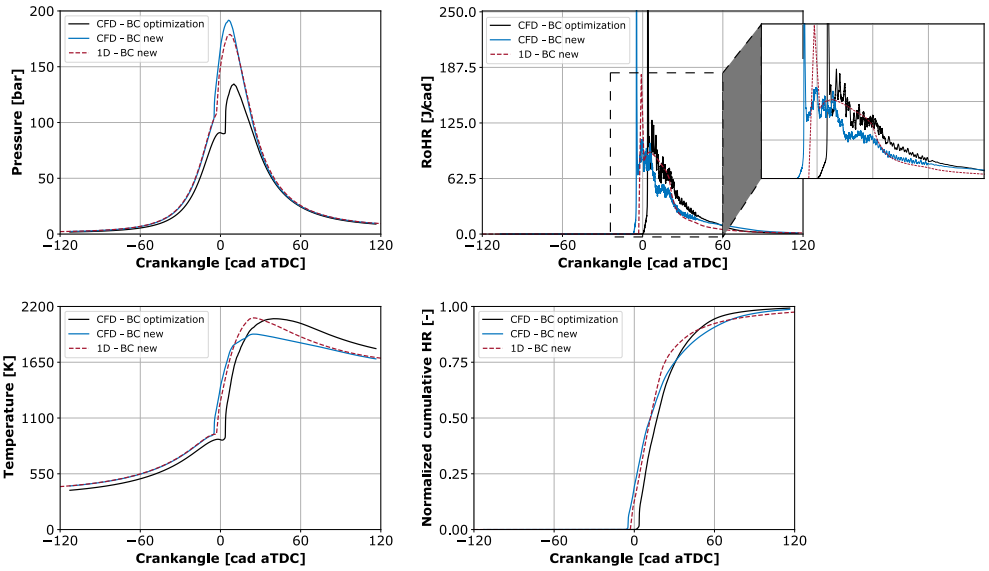

Figure 7.21: Comparison between the new and old boundary conditions results for in-cylinder pressure, RoHR, in-cylinder mean temperature, and normalized cumulative HR.

With lower CR, the IVC conditions need to be adjusted with higher values of pressure and temperature. The EGR rate was increased by almost 4%, this implies different composition of the mixture in the IVC instant to maintain the same air-fuel ratio λ. Moreover, it was necessary to adjust the amount of fuel injected in each cycle.

The first simulation was performed directly using the BC obtained from the 1D calculation. However, as already observed in the analyses of how SOI affects combustion, it happens abruptly in the premixed phase leading to big gradients of the thermodynamic variables (p and T), indicating abnormal combustion. So, considering this fact, other SOI values were tested. Figure 7.22 shows the results obtained for all SOI tested. In all simulations, the same BC was maintained; just the SOI was actualized. Using the SOI of -18 cad bTDC the simulation predicts huge gradients of p and T, then it was discarded. On the other hand, using SOI of -15 deg or more advanced, the combustion evolves normally. As the start of injection value is advanced, the maximum pressure and temperature inside the combustion chamber are lower. For RoHR, the lower the peak in the premixed phase, the longer the diffusive

Table 7.9: New boundary conditions for CR 20 engine configuration.

Parameter	BC CR 28	BC CR 20
SOI [deg]	-4.04	-20.3
T_{IVC} [K]	387	432
P_{IVC} [bar]	1.83	2.29
T_{liner} [K]	430	382
$T_{cyl.head}$ [K]	508	512
T_{piston} [K]	543	497
O_2 [-]	0.3641	0.3356
CO_2 [-]	0.4332	0.4527
H_2O [-]	0.2027	0.2116
Fuel [mg/cc]	62	63.69
EGR [%]	68	71.4

phase of combustion. On the other hand, the reduction of the pressure and temperature values in the chamber causes a decrease in the normalized RoHR, i.e. the combustion efficiency.

To better understand the minimum necessary conditions in the SOI instant, Figure 7.23 shows the ignition delay time as a function of the SOI temperature and pressure for all the tested cases. The points inside the red circles are the ones that the simulation predicts abnormal combustion behavior. It is possible to see that the cases with a higher ID show at the same time a combination of lower in-cylinder temperature and pressure, which means that there is a lot of fuel inside the combustion chamber, leading to a great fuel impingement, causing abrupt combustion when the combustion chamber reaches the conditions to ignite the air-fuel mixture that results in a peak of the RoHR. Based on this information, it has been stipulated that the maximum SOI value that can be used in 1D calculations is equal to -15 deg.

An extended investigation was performed in a different operation point condition. A partial load point at 2500 rpm was tested in CFD and compared to the 1D results in order to analyze the engine behavior in a different condition. The boundary conditions of this point were obtained from the 1D study and are listed in Table 7.10 using the CR of 20.

Figure 7.24 shows the comparison between 1D and CFD results to the tested point. The CFD simulation correctly reproduces the in-cylinder pressure trace obtained numerically, being slightly higher for the maximum value found, which is normal when considering that the CFD calculation solves and

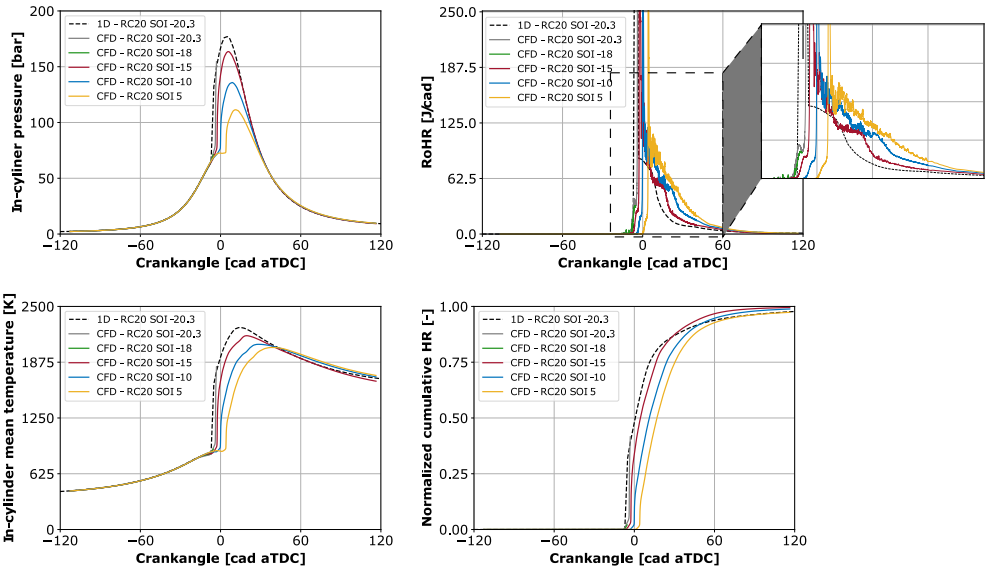

Figure 7.22: Validation of the new BC for CR20. In-cylinder pressure, RoHR, in-cylinder temperature, and normalized HR traces.

Table 7.10: New boundary conditions for CR 20 engine configuration at partial load.

Parameter	BC full load	BC partial load
SOI [deg]	-20.27 (-5)	-5.05
T_{IVC} [K]	432	415
P_{IVC} [bar]	2.29	2.16
T_{liner} [K]	382	376
$T_{cyl.head}$ [K]	512	451
T_{piston} [K]	497	453
O_2 [-]	0.3356	0.3136
CO_2 [-]	0.4527	0.4677
H_2O [-]	0.2116	0.2186
Fuel [mg/cc]	63.69	51
EGR [%]	71.4	65.11

models a more significant number of equations than the 1D calculation. For the in-cylinder temperature, the two curves are also in agreement, and the

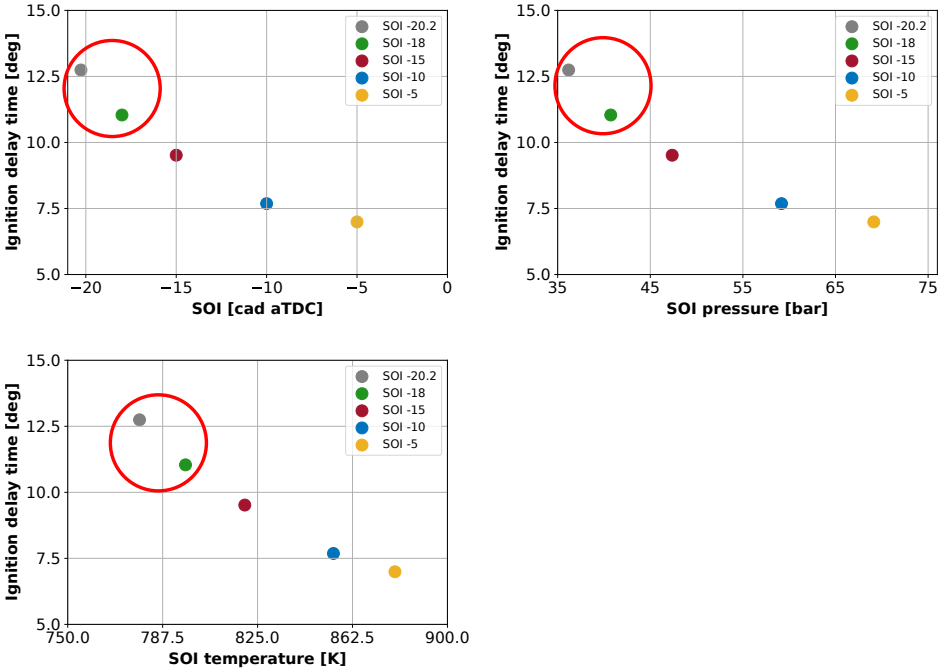

Figure 7.23: Analysis of the in-cylinder pressure and temperature conditions at SOI instant. The red circles show the location of the points where the simulations predicted abnormal combustion behavior.

temperature at the end of the cycle is slightly lower when simulated computationally. When it comes to RoHR, it is possible to observe that the peak obtained in the CFD simulation is higher than that reported by the 1D mathematical model, but they are centered when compared to each other. Another difference is that the non-premixed phase of combustion is more prolonged for the CFD simulation. These differences in heat release rates occur because the CFD model solves several equations and considers a larger amount of phenomenological effects happening inside the combustion chamber. In contrast, the 1D model can be explained as a mathematical model calibrated with previous results in order to describe the combustion phenomena for an engine operating in oxy-fuel combustion mode. Both models achieve a good normalized HR, which means that almost all fuel was burned during the combustion inside the chamber.

After the partial load point analysis, it was observed that the 1D and

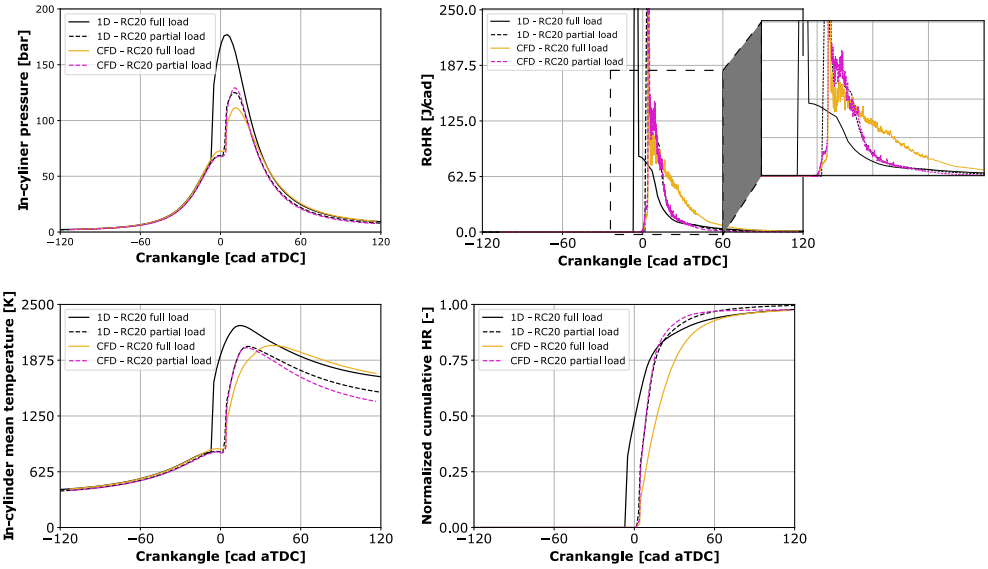

Figure 7.24: Partial load case evaluation. Left column: In-cylinder pressure and mean temperature. Right column: Rate of heat release and normalized cumulative heat release analysis.

CFD models could predict well the engine behavior. However, analyzing the engine emissions, it was seen that there was a large amount of CO_2 in addition to a large amount of O_2 available that was being eliminated by the exhaust gases, which could be reused in combustion, increasing the mechanical energy of the engine to move the volumetric compressors. So a 1D study of different recirculating O_2 + CO_2 + H_2O compositions was planned to the maximum power point where the gains can be higher. A new 1D optimization process to maximize the brake power and efficiency was performed using VEMOD. At the end of the procedure, new boundary conditions that improve the engine efficiency were found and are presented in Table 7.12.

With the new boundary conditions, a CFD simulation was performed to analyze the agreement between the models and evaluate the emissions. To perform the CFD simulations of the case with CR 20 and without gas recirculation, it was used the SOI value of -15^o once the simulation with the original one diverged. Moreover, this value is closer to the SOI value of the case with gas recirculation. Furthermore, the colors on the graph were maintained the

Table 7.11: New boundary conditions for CR 20 engine configuration with gas recirculation.

Parameter	CR 20 without gas recirculation	CR 20 with gas recirculation
SOI [deg]	-15 (-20.27)	-12.8
T_{IVC} [K]	432	400
P_{IVC} [bar]	2.29	2.24
T_{liner} [K]	382	392
$T_{cyl.head}$ [K]	512	504
T_{piston} [K]	497	474
O_2 [-]	0.3356	0.3256
CO_2 [-]	0.4527	0.4669
H_2O [-]	0.2116	0.2073
Fuel [mg/cc]	63.69	67.1

same as the Figure 7.22 to facilitate the visualization and association of the results since it is the same case.

Figure 7.25 compares the 1D VEMOD values case against the CFD results for in-cylinder pressure and mean temperature, RoHR, and normalized cumulative HR of the recirculating gas cases. With the new BC, the in-cylinder pressure and mean temperature in IVC changed to smaller values than the original. Therefore, it was necessary to increase these two values a little to keep the same conditions in the combustion chamber in order to be able to simulate the case. Even with these changes, the simulation reproduces the behavior found in the 1D calculation well. The case with gas recirculation was compared with the one without gas recirculation, thus making it possible to compare the gas's influence on the results. With more CO_2 inside the combustion chamber, the in-cylinder pressure and temperature are slightly low, which can lead to a reduction of the combustion efficiency and, consequently, higher emissions. In terms of RoHR, the peak of both cases is in the same order of magnitude but much higher than the one calculated by VEMOD, showing that combustion happens mainly during the premixed phase and abruptly by the mixing conditions inside the combustion chamber. These differences in pressure, temperature, and RoHR are reflected in the normalized HR, which shows the combustion efficiency is slower than the case without this gas recirculation.

Figure 7.26 compares the emissions of soot, CO, HC, and combustion efficiency of both cases. It is possible to see that the increment of the CO_2

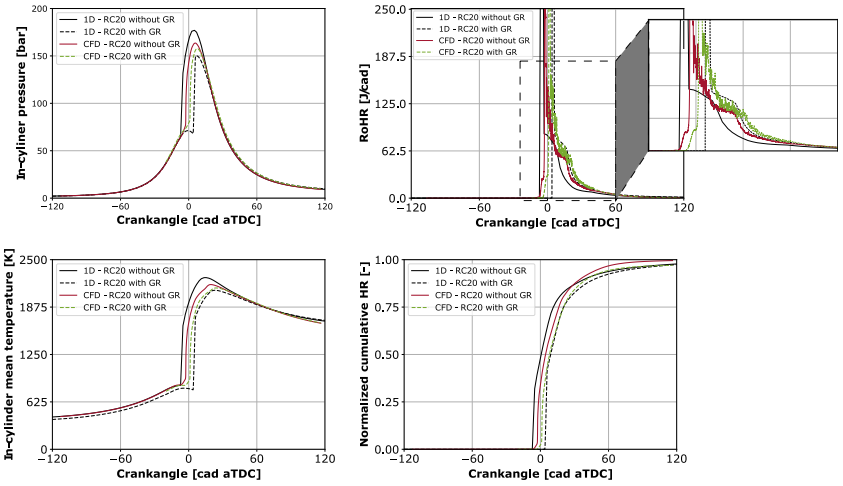

Figure 7.25: Gas recirculation boundary conditions validation.

inside the combustion chamber at IVC generates more soot, CO, and HC emissions due to the worst combustion process that is not able to oxidize the molecules due to lower temperatures in the combustion chamber. Moreover, the combustion efficiency is reduced by almost 2.5 %.

Another test performed to improve the performance of the engine operating in oxy-fuel combustion was the recirculation of H_2O, searching to increase the γ of the mixture, thus increasing engine performance and improving the efficiency. CO_2 has higher specific heat than H2O as high temperatures, however, the H2O molecule has higher thermal-diffusivity. The wet EGR is able to produce superior performance in relation to dry EGR, with higher fuel-conversion efficiency.Adding water to the combustion chamber reduces the temperatures, increasing the ignition delay and thus allowing more time to premix the air-fuel mixture. Moreover, the water injection can considerably reduce the wall heat transfer leading to a reduction in brake efficiency. On the other hand, H_2O recirculation also promotes better exhaust gas temperature control, which is a fundamental condition for the proper functioning of the membrane.

Figure 7.27 shows the comparison of in-cylinder pressure, mean temperature, RoHR, and normalized cumulative HR between the case without and with H_2O recirculation. It is possible to see that the increment of H_2O helps to reduce the maximum in-cylinder pressure and temperature inside the combustion chamber. When it comes to ignition delay, it is not possible to pinpoint

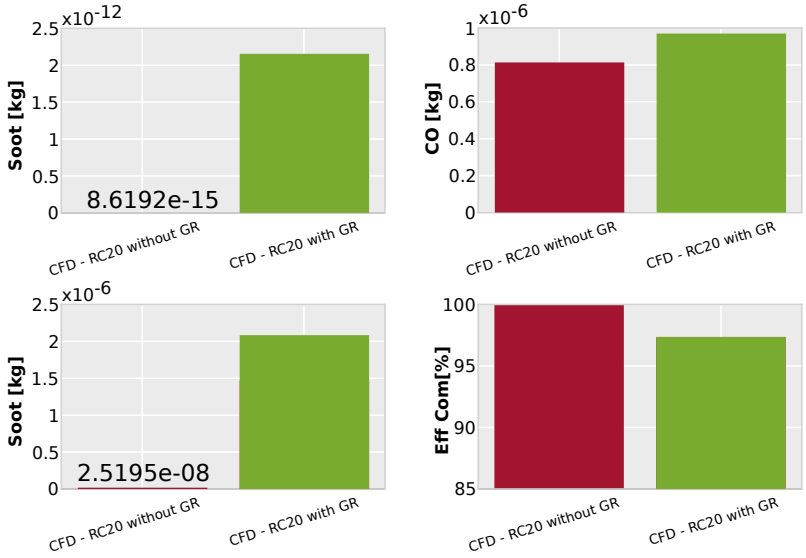

Figure 7.26: Analysis of the emissions with gas recirculation boundary conditions.

Table 7.12: New boundary conditions for CR 20 engine configuration with H_2O recirculation.

Parameter	CR 20 without H_2O recirculation	CR 20 with H_2O recirculation
SOI [deg]	-15 (20.27)	-12.4
T_{IVC} [K]	432	475
P_{IVC} [bar]	2.29	2.58
T_{liner} [K]	382	382
$T_{cyl.head}$ [K]	512	500
T_{piston} [K]	497	483
O_2 [-]	0.3356	0.3103
CO_2 [-]	0.4527	0.4294
H_2O [-]	0.2116	0.2602
Fuel [mg/cc]	63.69	62.3
EGR [%]	71.4	67

precisely how the water affects the system once there are differences in the IVC conditions and the start of injection of the fuel. The case without water recirculation has lower pressure and temperature in IVC with a more advanced

SOI than the case with water recirculation. These differences in IVC lead to a peak of heat release in the premixed phase once more fuel was injected until the start of the combustion. Since more fuel was consumed in the premixed phase, the diffusive combustion phase happens faster than the case without recirculation. Moreover, this higher H_2O content allied with the new BC conditions helps to reduce the peak during the premixed combustion phase due to the lower mixture reactivity inside the combustion chamber. From the normalized cumulative HR, it is possible to observe that the case with the higher water percentage has a little less combustion efficiency, being a consequence of the lower combustion temperatures and ignition delay but remains in the same order of magnitude compared to the original one.

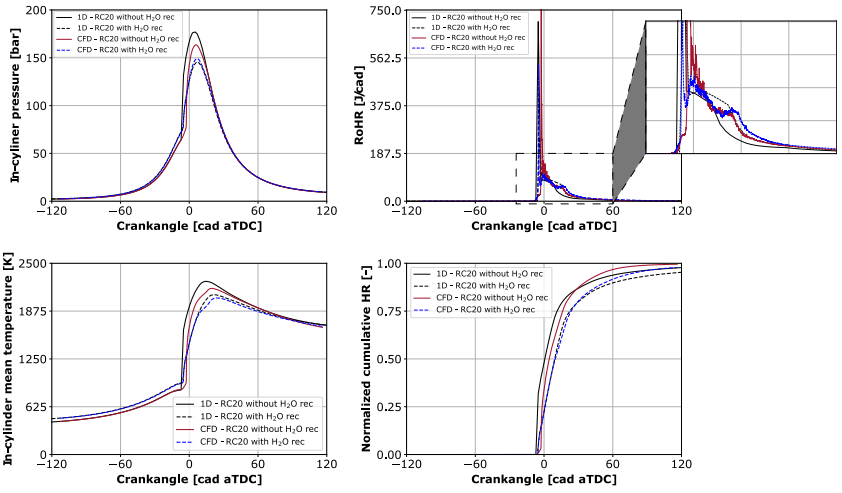

Figure 7.27: H_2O recirculation boundary conditions validation.

On the other hand, Figure 7.28 shows that the CO and HC emissions are higher than the case with H_2O once the combustion is less efficient and not consuming the same amount of gases when compared to the case without the addition of water. Once there are more products not consumed by the combustion process, the emissions grow up.

7.6 Summary and conclusions

This chapter applies the previously established optimization methodology for the optimization and analysis of a CI engine operating in oxy-fuel mode. Furthermore, with the final result of the optimization, a study extrapolating the

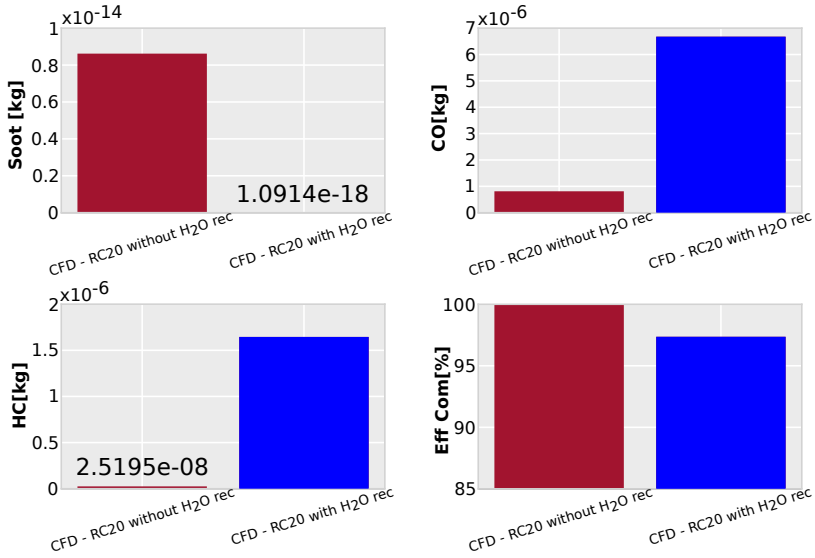

Figure 7.28: Analysis of the emissions with H_2O recirculation boundary conditions.

operating range of the engine was performed. Since this is a new engine architecture, a proprietary combustion system is required, designed specifically to obtain the maximum possible efficiency and the lowest possible levels of soot emissions.

The NS algorithm was used for the optimization process taking into account 11 parameters. Of these, 6 are responsible for defining the bowl profile and the combustion chamber geometry. 4 different parameters characterize the injection system, and finally, the last parameter is responsible for defining the air management system. With the coupling of the CFD algorithm and computational code, the optimization process was carried out through computer simulations. In total, 1100 simulations were performed, with each simulation concerning each of the combustion systems generated by the algorithm. Among these 1100 simulations, it is essential to note that the first 100 simulations were based on the Latin hypercube system to obtain the parameters and a first database. After the end of these simulations, the optimization process was started with the NS algorithm.

The new combustion system changed the piston geometry significantly, and the baseline geometry gave way to a bathtub geometry, thus increasing the efficiency of the engine and reducing heat transfer losses. In addition, the number of injector nozzles has been changed from 10 to 7 to improve air-fuel

mixing inside the combustion chamber. The injection pressure was increased significantly, improving fuel atomization and evaporation. Additionally, the spray angle was adjusted to better adapt to the new geometry. With the new injection system, it was possible to prevent the sprays collision. Finally, the SOI was adjusted in order to control the maximum in-cylinder pressure.

Overall, the optimized combustion system for the oxy-fuel combustion case improved the efficiency levels of the engine compared to the base configuration, increasing the efficiency value from 26.6 % to 35.7 %. At the same time, soot emissions were reduced from 11.37 mg/s to practically zero. In this context, reducing soot emissions is especially important in this engine concept because the energy in the exhaust gases needs to be recovered to increase the temperature so that the MIEC membrane can separate the oxygen from the nitrogen.

In addition, this new combustion system was able to reduce CO emissions to a level similar to a conventional diesel engine. The C_xH_y emissions remained below the reference values of a conventional diesel engine as there is no oxidation of hydrocarbons and no reduction of NO_x. This advantage results from the removal of nitrogen already in the air-fuel mixture, thus avoiding the formation of pollutants. Furthermore, from the emission levels obtained, it would be easy to design an after-treatment system. One point that could be pointed out as a deficiency of the concept is the lower efficiency, but there is the possibility of capturing CO2 that can compensate for this loss.

From this, oxy-fuel combustion in a CI engine could be an interesting solution to the emission problem. This concept eliminates the NO_x emissions, and it is possible to drastically reduce the soot emissions.

References

[1] Baumann, S. et al. “Ultrahigh oxygen permeation flux through supported Ba0.5Sr0.5Co0.8Fe0.2O3-δ membranes”. In: *Journal of Membrane Science* 377.1-2 (2011), pp. 198–205. DOI: 10.1016/j.memsci.2011.04.050.

[2] Catalán-Martínez, D., Santafé-Moros, A., Gozálvez-Zafrilla, J. M., García-Fayos, J., and Serra, J. M. “Characterization of oxygen transport phenomena on BSCF membranes assisted by fluid dynamic simulations including surface exchange”. In: *Chemical Engineering Journal* 387.October 2019 (2020), p. 124069. DOI: 10.1016/j.cej.2020.124069.

[3] Serrano, J.R., Arnau, F.J., García-Cuevas, L.M., and Farias, V.H. "Oxy-fuel combustion feasibility of compression ignition engines using oxygen separation membranes for enabling carbon dioxide capture". In: *Energy Conversion and Management* 247 (2021), p. 114732. DOI: 10.1016/j.enconman.2021.114732.

[4] Serrano, J.R. et al. "Oxy-fuel combustion engine for highly efficient onboard CO2 capture. Another step forward in the path to a CO2 circular economy". In: Sustainable Internal Combustion Engine Virtual 'Live' (Stuttgart, Germany, Feb. 3–4, 2021). 2021.

[5] Martin, Jaime, Arnau, Francisco, Piqueras, Pedro, and Auñon, Angel. "Development of an Integrated Virtual Engine Model to Simulate New Standard Testing Cycles". In: *SAE Technical Papers* 2018-April (2018), pp. 1–17. DOI: 10.4271/2018-01-1413.

[6] Tan, Qinming and Hu, Yihuai. "A study on the combustion and emission performance of diesel engines under different proportions of O2 & N2 & CO2". In: *Applied Thermal Engineering* 108 (2016), pp. 508–515. DOI: 10.1016/j.applthermaleng.2016.07.151.

[7] Kang, Zhe et al. "Study of the Combustion Characteristics of a HCCI Engine Coupled with Oxy-Fuel Combustion Mode". In: *SAE International Journal of Engines* 10.3 (2017). DOI: 10.4271/2017-01-0649.

[8] Zubel, Marius, Ottenwälder, Tamara, Heuser, Benedikt, and Pischinger, Stefan. "Combustion system optimization for dimethyl ether using a genetic algorithm". In: *International Journal of Engine Research* 22.1 (2021), pp. 22–38. DOI: 10.1177/1468087419851577.

[9] Yoon, Sungjun, Lee, Seungpil, Kwon, Hyuckmo, Lee, Joonkyu, and Park, Sungwook. "Effects of the swirl ratio and injector hole number on the combustion and emission characteristics of a light duty diesel engine". In: *Applied Thermal Engineering* 142.March (2018), pp. 68–78. DOI: 10.1016/j.applthermaleng.2018.06.076.

[10] Shi, Yu and Reitz, Rolf D. "Assessment of optimization methodologies to study the effects of bowl geometry, spray targeting and swirl ratio for a heavy-duty diesel engine operated at High-Load". In: *SAE International Journal of Engines* 1.1 (2009), pp. 537–557. DOI: 10.4271/2008-01-0949.

[11] Han, Sangwook and Bae, Choongsik. "The influence of fuel injection pressure and intake pressure on conventional and low temperature diesel combustion". In: *SAE Technical Papers* (2012). DOI: 10.4271/2012-01-1721.

[12] Agarwal, Avinash Kumar et al. "Effect of fuel injection timing and pressure on combustion, emissions and performance characteristics of a single cylinder diesel engine". In: *Fuel* 111 (2013), pp. 374–383. DOI: 10.1016/j.fuel.2013.03.016.

[13] Yaliwal, V. S. et al. "Effect of nozzle and combustion chamber geometry on the performance of a diesel engine operated on dual fuel mode using renewable fuels". In: *Renewable Energy* 93 (2016), pp. 483–501. DOI: 10.1016/j.renene.2016.03.020.

[14] Dreisbach, Rolf, Graf, Gernot, Kreuzig, Gerhard, Theissl, Helmut, and Pfahl, Ulrich. "HD base engine development to meet future emission and power density challenges of a DDI™ engine". In: *SAE Technical Papers* 724 (2007). DOI: 10.4271/2007-01-4225.

[15] Miles, Paul C. and Andersson, Öivind. "A review of design considerations for light-duty diesel combustion systems". In: *International Journal of Engine Research* 17.1 (2016), pp. 6–15. DOI: 10.1177/1468087415604754.

[16] Benajes, Jesús, Pastor, José V., García, Antonio, and Monsalve-Serrano, Javier. "An experimental investigation on the influence of piston bowl geometry on RCCI performance and emissions in a heavy-duty engine". In: *Energy Conversion and Management* 103 (2015), pp. 1019–1030. DOI: 10.1016/j.enconman.2015.07.047.

[17] Cursente, V., Pacaud, P., and Gatellier, B. "Reduction of the compression ratio on a hsdi diesel engine: Combustion design evolution for compliance the future emission standards". In: *SAE International Journal of Fuels and Lubricants* 1.1 (2009), pp. 420–439. DOI: 10.4271/2008-01-0839.

[18] Serrano, J.R., Martin, J., Gomez-Soriano, J., and Raggi, R. "Theoretical and experimental evaluation of the spark-ignition premixed oxy-fuel combustion concept for future CO 2 captive powerplants". In: *Energy Conversion and Management* 244 (2021), p. 114498. DOI: 10.1016/j.enconman.2021.114498.

Chapter 8

Conclusions and future works

8.1 Introduction

This last chapter of the doctoral thesis aims to present the main conclusions obtained during the investigation. The conclusions obtained for each of the different activities developed are included here. From the conclusions, it is also possible to verify whether the proposed objectives were fulfilled or not. In addition, in the end, some topics of interest are presented as possible future work in order to use and further develop the knowledge obtained during the development of this research.

8.2 Conclusions

Before presenting the most significant conclusions of this work, it is important to remember the objectives of this thesis. In chapter 1, it was presented that the fundamental objective of this thesis is to develop and apply an optimization methodology for the combustion system of CI engines coupling computational simulation with an optimization algorithm to improve efficiency and reduce contaminant emissions. In addition, the introduction describes the motivation behind this study and the steps taken in order to achieve the final objective.

In chapters 2 and 3, the review of the specific literature about engines and the combustion process demonstrated the need for new strategies to reduce contaminant emissions in compression ignition engines. Different alternatives can be taken in order to achieve this target. However, some strategies are

preferred over others. Some of the classical strategies are modification of the combustion systems characteristics, such as altering the piston geometry, changing the injection, and air management system components and configurations. Nevertheless, as the decades go by, the emission laws become more and more restrictive, limiting these traditional methodologies once they are already close to their robustness limits. For this reason, other alternatives are needed to meet these more restrictive limits. Among the new alternatives is the design of specific combustion systems using mathematical algorithms in order to, from an already known configuration, estimate contaminating gas emissions and fuel consumption and, iteratively, reach a completely new design that fulfills the imposed requirements. Other possibilities are the use of alternative fuels such as OME and also the use of different engine architectures or alternative combustion modes.

Chapter 4 presents in detail the methodology developed. One of the objectives of the thesis is to develop a new methodology for CI engine optimization by coupling CFD calculation with the NS algorithm. The steps followed to be possible obtain this new method are shown in this chapter. The characterization and validation of an engine operating point were performed computationally. Essential information was presented, starting with the mesh discretization and going through all the models used in the calculations. Besides the validation of the mathematical models and the operating point, the benchmark results obtained for the NS algorithm in comparison against possible competitors are shown. Numerical tools, such as the fuel injection rate generator, were also presented.

Therefore, the results of this thesis have been divided into three main parts. The first concerns the validation of the methodology through the optimization of a CI engine operating with conventional fuel. The second contemplates the results of the optimization of the CI engine for the use of alternative fuel. The last part discusses a new engine architecture and a new combustion model for CI engines. In all blocks, the goal was to improve engine performance, increase efficiency and decrease fuel consumption, and reduce the levels of contaminant emissions, mainly NO_x and soot.

8.3 Conventional diesel CI engines combustion system optimization

Chapter 5 shows the results obtained for the optimization process of a CI engine operating on conventional fuel demonstrate that the methodology meets

the requirements established at the beginning of the work. By applying computational algorithms with CFD modeling on a MD 4-cylinder 4-stroke CI engine, it was possible to obtain an improvement in fuel consumption at the same time, NO_x, and soot emissions remained below values based on real engines. Furthermore, the methodology makes it possible to generate an extensive database for cause and effect analysis of each of the parameters used, thus improving the understanding of the combustion process.

The new combustion system obtained combines a new geometry with a specific injection and air management system, improving the combination between them. Thus, it was possible to achieve a reduction of around 3 % for ISFC while keeping the emission levels constant. This new system indicates that the injection pressure and EGR rate should be increased and are the main parameters used in this particular optimization. Other parameters, such as the number of injector nozzles and the number of swirl, should be adjusted according to each system.

In general, it has been shown that the optimization methodology generates good results within a reasonable amount of time. Still, it is dependent on the number of parameters that are used during the process. It is clear here that as emission laws have become more restrictive, it is challenging to improve CI engines using conventional fuel without after-treatment strategies or alternative fuels once these engines have been optimized.

8.4 CI engine fueled with OME combustion system optimization

The chapter 6 report the results of the second optimization that is focused on using the developed optimization methodology on CI engines operating with alternative fuel, in this case, the OME. Initially, the process started from a CI engine operating with conventional fuel that was converted to run with OME since the fuel characteristics of the new fuel allow its use without significant physical changes in the engine.

Based on the simulations of the baseline case, it was observed that it is necessary to develop a combustion system specific for an engine that uses OME fuel. From this point on, the optimization methodology coupling the NS algorithm and CFD calculations was used to generate a new combustion system dedicated to OME. To optimize the engine 12 parameters were selected to define the geometry, injection, and air management systems. During the optimization process, over 1100 simulations were performed, of which 100 were

initially generated by the Latin hypercube methodology. The information generated by these 100 simulations provided a database for later initializing the NS algorithm. The remaining 1000 simulations were performed during the execution of the NS algorithm.

At the end of the optimization process, a combustion system dedicated to a CI engine operating with OME was obtained. This new system presented an efficiency 2.2% higher than the real diesel engine used as a reference. Moreover, there was a drastic reduction in NO_x emissions, around 36%, and it was possible to eliminate soot emissions. The NO_x decrease is due to the possibility of using high EGR rates, and the elimination of soot comes from the characteristics of OME. The injection system was specially adjusted because the physical characteristics of OME are different from diesel.

Furthermore, using the data generated by the optimization process and neural networks, it was possible to further extend the study about the characteristics of this new combustion system.

8.5 Oxy-combustion engine combustion system optimization

In the last chapter of the results, chapter 7, the NS-CFD methodology was applied in order to obtain a new combustion system for a CI engine running with an oxy-fuel combustion mode. In this case, the NS algorithm considered 11 different parameters, with 6 responsible for the geometry, 4 for the injection system, and the last parameter responsible for defining the air management system. Again, 1100 simulations were performed. Of this total, 100 were generated through the Latin hypercube methodology and served as the initial database, and the remaining 1000 were used to run the NS algorithm.

The new combustion system significantly changed the geometry compared to the baseline geometry. The injection system was also changed, the injection pressure was increased, and the number of injector holes was reduced from 10 to 7. These new parameters are necessary to improve the atomization, evaporation, and mixing rate of the fuel with the air. The spray angle was also adjusted to have a better match with the geometry. Finally, the SOI was changed, seeking to control the maximum pressure value inside the cylinder.

Overall, the new combustion system increased the efficiency from 26.6% to 35.7%. At the same time, soot emissions were reduced to practically zero. This reduction in soot emissions is essential because the exhaust gases are

reused by the MIEC to separate the oxygen used by the engine. The CO and HC emissions found remained close to those in conventional diesel engines.

Moreover, the optimized combustion system was used to explore other areas of the engine map. With the data obtained from the optimization, the 1D study of the poly-cylinder engine was fed back in order to obtain an operation map of the new engine. Initially, it was verified if the previously defined boundary conditions still provided the best operating conditions for this new system. Thus, it was observed that some changes could be made to obtain the best engine operation. Subsequently, it was obtained that reducing the compression ratio would eventually provide a better engine operating regime. With this new compression ratio, partial load points were explored, and the effects of gas and water recirculation on this oxy-fuel combustion model were also studied.

8.6 Future works

In the course of this work, some questions that could not be answered at the moment appeared. To answer these questions, some recommendations for future work were formulated.

- As during the development of this thesis, the study was focused on computational simulation, it is necessary to validate the results experimentally since the computational results are promising. The combustion systems, both for conventional CI engines and engines using OME and oxy-fuel combustion, should be manufactured and experimentally tested in order to prove the results obtained.

- Explore other operation points from the new combustion system obtained for the engine fueled with OME. That is, to expand the study to the entire engine map in order to understand how this combustion system behaves in different operating situations.

- Currently, it was only possible to work with 1 single fuel in each optimization. Thus, an important task would be to adapt the codes used to explore using fuel mixtures or two different fuels in the same cycle as an optimization parameter. This could be applied to engines with different combustion modes, such as RCCI.

- A possible next step would be to couple the knowledge about using OME with the concept of oxy-fuel combustion. Ideally, this new concept could

remove both NO_x and soot emissions due to the characteristics of OME and the absence of nitrogen in the oxy-fuel model. However, it is a critical study and verifies the engine behavior and the efficiencies that can be obtained from this new power plant architecture.

- Explore the possibility of hybridizing the NS algorithm with some other algorithm to improve the robustness of the algorithm and the time needed for the optimization process. Today there is a variety of neural networks for different applications so that neural networks could be implemented in the NS algorithm. As the optimization process evolves, the neural network is fed with additional information to increase the convergence speed of the algorithm.

- Given that the combustion model was adopted due to its characteristic of requiring less time for numerical calculation, an alternative future work is to use another combustion model. With this new model, the baseline and optimized cases can be reproduced, aiming to improve the results already obtained.

Global Bibliography

Abraham, B M, Asbury, J G, Lynch, E P, and Teotia, A P.S. "Coal-oxygen process provides CO/sub 2/ for enhanced recovery". In: *Oil Gas J.; (United States)* (1982) (cited on page 28).

Agarwal, Avinash Kumar et al. "Effect of fuel injection timing and pressure on combustion, emissions and performance characteristics of a single cylinder diesel engine". In: *Fuel* 111 (2013), pp. 374–383. DOI: 10.1016/j.fuel.2013.03.016 (cited on pages 23, 191).

Angelberger, C., Poinsot, T., and Delhay, B. "Improving near-wall combustion and wall heat transfer modeling in SI engine computations". In: *SAE Technical Papers* (1997). DOI: 10.4271/972881 (cited on page 81).

Aradi, Allen, Higgins, Brian, and Siebers, Dennis L. "Diesel-Spray Ignition and Premixed-Burn Behavior". In: (2000). DOI: https://doi.org/10.4271/2000-01-0940 (cited on page 14).

Arnau, F.J., García-Cuevas, L.M., Novella, R., and Gutiérrez, F. "Adapting an internal combustion engine to oxy-fuel combustion with in-situ oxygen production". In: *ASME - ICEF. The Internal Combustion Engine Fall Conference. Virtual Conference, Online:* (October 13-15, 2021) (cited on page 30).

Bae, Choongsik and Kim, Jaeheun. "Alternative fuels for internal combustion engines". In: *Proceedings of the Combustion Institute* 36.3 (2017), pp. 3389–3413. DOI: 10.1016/j.proci.2016.09.009 (cited on pages 24, 25).

Baratta, Mirko, Chiriches, Silvestru, Goel, Prashant, and Misul, Daniela. "CFD modelling of natural gas combustion in IC engines under different EGR dilution and H2-doping conditions". In: *Transportation Engineering* 2.August (2020). DOI: 10.1016/j.treng.2020.100018 (cited on page 75).

Barths, H, Hasse, C, and Peters, N. "Computational fluid dynamics modelling of non-premixed combustion in direct injection diesel engines". In: *International Journal of Engine Research* 1.3 (2000), pp. 249–267. DOI: 10.1243/1468087001545164 (cited on pages 66, 67).

Bartok, W. and Sarofim, A.F. *Fossil Fuel Combustion: A Source Book*. Wiley, 1991 (cited on page 18).

Baumann, S. et al. "Ultrahigh oxygen permeation flux through supported Ba0.5Sr0.5Co0.8Fe0.2O3-δ membranes". In: *Journal of Membrane Science* 377.1-2 (2011), pp. 198–205. DOI: 10.1016/j.memsci.2011.04.050 (cited on pages 29, 179).

Beheshti, Zahra and Shamsuddin, Siti Mariyam Hj. "CAPSO: centripetal accelerated particle swarm optimization". In: *Information Sciences* 258 (2014), pp. 54–79 (cited on pages 88, 90).

Beheshti, Zahra and Siti, Siti Mariyam. "CAPSO: Centripetal accelerated particle swarm optimization". In: *Information Sciences* 258 (2014), pp. 54–79. DOI: 10.1016/j.ins.2013.08.015 (cited on page 51).

Benajes, J., Olmeda, P., Martín, J., and Carreño, R. "A new methodology for uncertainties characterization in combustion diagnosis and thermodynamic modelling". In: *Applied Thermal Engineering* 71 (2014), pp. 389–399. DOI: 10.1016/j.applthermaleng.2014.07.010 (cited on page 64).

Benajes, Jesus et al. "Analysis of the combustion process, pollutant emissions and efficiency of an innovative 2-stroke HSDI engine designed for automotive applications". In: *Applied Thermal Engineering* 58.1-2 (2013), pp. 181–193. DOI: 10.1016/j.applthermaleng.2013.03.050 (cited on page 98).

Benajes, Jesus et al. "Optimization of the combustion system of a medium duty direct injection diesel engine by combining CFD modeling with experimental validation". In: *Energy Conversion and Management* 110 (2016), pp. 212–229. DOI: 10.1016/j.enconman.2015.12.010 (cited on pages 19, 81, 97, 172).

Benajes, Jesús, García, Antonio, Pastor, José Manuel, and Monsalve-Serrano, Javier. "Effects of piston bowl geometry on reactivity controlled compression ignition heat transfer and combustion losses at different engine loads". In: *Energy* 98 (2016), pp. 64–77. DOI: 10.1016/j.energy.2016.01.014 (cited on page 19).

Benajes, Jesús, Novella, Ricardo, Pastor, Jose Manuel, Hernández-López, Alberto, and Kokjohn, Sage L. "Computational optimization of the combustion system of a heavy duty direct injection diesel engine operating with dimethyl-ether". In: *Fuel* 218 (2018), pp. 127–139. DOI: 10.1016/j.fuel.2018.01.020 (cited on page 97).

Benajes, Jesús, Pastor, José V., García, Antonio, and Monsalve-Serrano, Javier. "An experimental investigation on the influence of piston bowl geometry on RCCI performance and emissions in a heavy-duty engine". In: *Energy Conversion and Management* 103 (2015), pp. 1019–1030. DOI: 10.1016/j.enconman.2015.07.047 (cited on pages 19, 21).

Benajes, Jesús, Pastor, José V., García, Antonio, and Monsalve-Serrano, Javier. "An experimental investigation on the influence of piston bowl geometry on RCCI performance and emissions in a heavy-duty engine". In: *Energy Conversion and Management* 103 (2015), pp. 1019–1030. DOI: 10.1016/j.enconman.2015.07.047 (cited on page 193).

Bengio, Yoshua. "Practical Recommendations for Gradient-Based Training of Deep Architectures". In: *Neural Networks: Tricks of the Trade: Second Edition*. Ed. by Grégoire Montavon, Geneviève B. Orr, and Klaus-Robert Müller. Berlin, Heidelberg: Springer Berlin Heidelberg, 2012, pp. 437–478. DOI: 10.1007/978-3-642-35289-8_26 (cited on page 55).

Bergh, FVD. "An analysis of particle swarm optimizers. PhD Thesis". In: *University of Pretoria, South Africa* (2001). DOI: http://repository.up.ac.za/bitstream/handle/2263/24297/00thesis.pdf (cited on page 49).

Biyiklioğlu, Onur and Tat, Mustafa Ertunc. "Tribological assessment of NiCr, Al2O3/TiO2, and Cr3C2/NiCr coatings applied on a cylinder liner of a heavy-duty diesel engine". In: *International Journal of Engine Research* 22.7 (2021), pp. 2267–2280. DOI: 10.1177/1468087420930164 (cited on page 29).

Borman, Gary and Nishiwaki, Kazuie. "Internal-combustion engine heat transfer". In: *Progress in Energy and Combustion Science* 13.1 (1987), pp. 1–46. DOI: 10.1016/0360-1285(87)90005-0 (cited on page 79).

Brest, Janez, Maucec, Mirjam Sepesy, and Boskovic, Borko. “Single objective real-parameter optimization: Algorithm jSO”. In: *2017 IEEE Congress on Evolutionary Computation (CEC)*. IEEE, 2017. DOI: 10.1109/cec.2017.7969456 (cited on pages 88, 90).

Brest, Janez, Maučec, Mirjam Sepesy, and Bošković, Borko. “Single objective real-parameter optimization: Algorithm jSO”. In: *2017 IEEE Congress on Evolutionary Computation, CEC 2017 - Proceedings* (2017), pp. 1311–1318. DOI: 10.1109/CEC.2017.7969456 (cited on page 51).

Broatch, Alberto, Novella, Ricardo, Gomez-Soriano, Josep, Pal, Pinaki, and Som, Sibendu. “Numerical Methodology for Optimization of Compression-Ignited Engines Considering Combustion Noise Control”. In: *SAE International Journal of Engines* 11.6 (2018), pp. 625–642. DOI: 10.4271/2018-01-0193 (cited on page 81).

Broatch, Alberto, Novella, Ricardo, Gomez-Soriano, Josep, Pal, Pinaki, and Som, Sibendu. “Numerical Methodology for Optimization of Compression-Ignited Engines Considering Combustion Noise Control”. In: *SAE International Journal of Engines* 11.6 (2018), pp. 625–642. DOI: 10.4271/2018-01-0193 (cited on page 134).

Broatch, Alberto, Olmeda, Pablo, García, Antonio, Salvador-Iborra, Josep, and Warey, Alok. “Impact of swirl on in-cylinder heat transfer in a light-duty diesel engine”. In: *Energy* 119 (2017), pp. 1010–1023. DOI: 10.1016/j.energy.2016.11.040 (cited on pages 24, 118).

Burger, Jakob, Siegert, Markus, Ströfer, Eckhard, and Hasse, Hans. “Poly(oxymethylene) dimethyl ethers as components of tailored diesel fuel: Properties, synthesis and purification concepts”. In: *Fuel* 89.11 (2010), pp. 3315–3319. DOI: 10.1016/j.fuel.2010.05.014 (cited on page 25).

Burger, Jakob, Siegert, Markus, Ströfer, Eckhard, and Hasse, Hans. “Poly(oxymethylene) dimethyl ethers as components of tailored diesel fuel: Properties, synthesis and purification concepts”. In: *Fuel* 89.11 (2010), pp. 3315–3319. DOI: 10.1016/j.fuel.2010.05.014 (cited on page 145).

Burger, Jakob, Ströfer, Eckhard, and Hasse, Hans. “Production process for diesel fuel components poly(oxymethylene) dimethyl ethers from methane-based products by hierarchical optimization with varying model depth”. In: *Chemical Engineering Research and Design* 91.12 (2013), pp. 2648–2662. DOI: 10.1016/j.cherd.2013.05.023 (cited on page 25).

Burger, Jakob, Ströfer, Eckhard, and Hasse, Hans. "Production process for diesel fuel components poly(oxymethylene) dimethyl ethers from methane-based products by hierarchical optimization with varying model depth". In: *Chemical Engineering Research and Design* 91.12 (2013), pp. 2648–2662. DOI: 10.1016/j.cherd.2013.05.023 (cited on page 145).

Busch, Stephen, Zha, Kan, Perini, Federico, and Reitz, Rolf D. "Piston Bowl Geometry Impacts on Late-Cycle Flow and Mixing in a Small-Bore Diesel Engine." In: (2017) (cited on page 21).

Catalán-Martínez, D., Santafé-Moros, A., Gozálvez-Zafrilla, J. M., García-Fayos, J., and Serra, J. M. "Characterization of oxygen transport phenomena on BSCF membranes assisted by fluid dynamic simulations including surface exchange". In: *Chemical Engineering Journal* 387.October 2019 (2020), p. 124069. DOI: 10.1016/j.cej.2020.124069 (cited on pages 29, 30, 179).

Çelikten, Ismet. "An experimental investigation of the effect of the injection pressure on engine performance and exhaust emission in indirect injection diesel engines". In: *Applied Thermal Engineering* 23.16 (2003), pp. 2051–2060. DOI: 10.1016/S1359-4311(03)00171-6 (cited on pages 22, 117).

Chaichan, Miqdam T. "Combustion and emission characteristics of E85 and diesel blend in conventional diesel engine operating in PPCI mode". In: *Thermal Science and Engineering Progress* 7.April (2018), pp. 45–53. DOI: 10.1016/j.tsep.2018.04.013 (cited on page 27).

Chen, Junfeng, Ren, Ziwu, and Fan, Xinnan. "Particle Swarm Optimization with Adaptive Mutation and Its Application Research in Tuning of PID Parameters". In: *2006 1st International Symposium on Systems and Control in Aerospace and Astronautics*. IEEE, 2006. DOI: 10.1109/isscaa.2006.1627490 (cited on pages 88, 90).

Chen, Junfeng, Ren, Ziwu, and Fan, Xinnan. "Particle swarm optimization with adaptive mutation and its application research in tuning of PID parameters". In: *2006 1st International Symposium on Systems and Control in Aerospace and Astronautics*. 2006, 5 pp.–994. DOI: 10.1109/ISSCAA.2006.1627490 (cited on page 49).

Choi, Seungmok, Shin, Seung Hyup, Lee, Jeongwoo, Min, Kyoungdoug, and Choi, Hoimyung. "The effects of the combustion chamber geometry and a double-row nozzle on the diesel engine emissions". In: *Proceedings of the Institution of Mechanical Engineers, Part D: Journal of Automobile Engineering* 229.5 (2015), pp. 590–598. DOI: 10.1177/0954407014547748 (cited on page 117).

Chollet, François et al. *Keras*. https://keras.io. 2015 (cited on page 169).

Christensen, Magnus, Hultqvist, Anders, and Johansson, Bengt. "Demonstrating the multi fuel capability of a homogeneous charge compression ignition engine with variable compression ratio". In: *SAE Technical Papers* 724 (1999). DOI: 10.4271/1999-01-3679 (cited on page 27).

Clow, Brian and White, Tony. "An evolutionary race: A comparison of genetic algorithms and particle swarm optimization used for training neural networks". In: *Proceedings of the International Conference on Artificial Intelligence, IC-AI'04* 2 (2004), pp. 582–588 (cited on page 54).

Cursente, V., Pacaud, P., and Gatellier, B. "Reduction of the compression ratio on a hsdi diesel engine: Combustion design evolution for compliance the future emission standards". In: *SAE International Journal of Fuels and Lubricants* 1.1 (2009), pp. 420–439. DOI: 10.4271/2008-01-0839 (cited on pages 124, 194).

D'Errico, G., Lucchini, T., Contino, F., Jangi, M., and Bai, X. S. "Comparison of well-mixed and multiple representative interactive flamelet approaches for diesel spray combustion modelling". In: *Combustion Theory and Modelling* 18.1 (2014), pp. 65–88. DOI: 10.1080/13647830.2013.860238 (cited on page 68).

D'Errico, Gianluca et al. "Reduced kinetic mechanisms for diesel spray combustion simulations". In: *SAE Technical Papers* 6.Cmc (2013). DOI: 10.4271/2013-24-0014 (cited on page 68).

D'Errico, G., Lucchini, T., Hardy, G., Tap, F., and Ramaekers, G. "Combustion Modeling in Heavy Duty Diesel Engines Using Detailed Chemistry and Turbulence-Chemistry Interaction". In: *SAE Technical Paper Series* 1 (2015), pp. 1–14. DOI: 10.4271/2015-01-0375 (cited on page 65).

Dahlstrom, Jessica, Andersson, Oivind, Tuner, Martin, and Persson, Håkan. "Experimental Comparison of Heat Losses in Stepped-Bowl and Re-Entrant Combustion Chambers in a Light Duty Diesel Engine". In: *SAE Technical Papers* (2016). DOI: 10.4271/2016-01-0732 (cited on page 21).

Das, Swagatam, Mullick, Sankha Subhra, and Suganthan, P. N. "Recent advances in differential evolution-An updated survey". In: *Swarm and Evolutionary Computation* 27 (2016), pp. 1–30. DOI: 10.1016/j.swevo.2016.01.004 (cited on page 51).

De Lima Moradell, DA. "Analysis of combustion concepts in a poppet valve two-stroke downsized compression ignition engine designed for passenger car applications [Tesis doctoral no publicada]". In: *Universitat Politècnica de València* (2016). DOI: https://doi.org/10.4995/Thesis/10251/68502 (cited on page 5).

Dec, John E. "A Conceptual Model of DI Diesel Combustion Based on Laser-Sheet Imaging*". In: *International Congress & Exposition*. SAE International, 1997. DOI: https://doi.org/10.4271/970873 (cited on pages 15–17).

Dec, John E. "Advanced compression-ignition engines - Understanding the in-cylinder processes". In: *Proceedings of the Combustion Institute* 32 II.2 (2009), pp. 2727–2742. DOI: 10.1016/j.proci.2008.08.008 (cited on page 79).

Dec, John E. and Canaan, Robert E. "PLIF Imaging of NO Formation in a DI Diesel Engine". In: *International Congress & Exposition*. SAE International, 1998. DOI: https://doi.org/10.4271/980147 (cited on page 17).

Dec, John E. and Espey, Christoph. "Ignition and Early Soot Formation in a DI Diesel Engine Using Multiple 2-D Imaging Diagnostics". In: *International Congress & Exposition*. SAE International, 1995. DOI: https://doi.org/10.4271/950456 (cited on page 15).

Decan, Gilles et al. "Evaluation of Wall Heat Flux Models for Full Cycle CFD Simulation of Internal Combustion Engines under Motoring Operation". In: *SAE Technical Papers* 2017-September (2017). DOI: 10.4271/2017-24-0032 (cited on page 82).

Decan, Gilles et al. "Evaluation of wall heat flux calculation methods for CFD simulations of an internal combustion engine under both motored and HCCI operation". In: *Applied Energy* 232 (2018), pp. 451–461. DOI: 10.1016/J.APENERGY.2018.09.214 (cited on pages 79, 82).

Dempsey, Adam B., Walker, N. Ryan, and Reitz, Rolf D. "Effect of Piston Bowl Geometry on Dual Fuel Reactivity Controlled Compression Ignition (RCCI) in a Light-Duty Engine Operated with Gasoline/Diesel and Methanol/Diesel". In: *SAE International Journal of Engines* 6.1 (2013), pp. 78–100. DOI: https://doi.org/10.4271/2013-01-0264 (cited on page 21).

Derrac, Joaquín, García, Salvador, Molina, Daniel, and Herrera, Francisco. "A practical tutorial on the use of nonparametric statistical tests as a methodology for comparing evolutionary and swarm intelligence algorithms". In: *Swarm and Evolutionary Computation* 1.1 (2011), pp. 3–18. DOI: https://doi.org/10.1016/j.swevo.2011.02.002 (cited on page 90).

Desantes, J. et al. "Motor de combustion interna de hidrocarburos auto transportable que no emite gases nocivos ni CO2; secuestra CO2 atmosférico y fabrica CO2 líquido subcrítico". In: (Patent WO 2020/193833 A1) (cited on pages 29, 31).

Deutz, Sarah et al. "Cleaner production of cleaner fuels: Wind-to-wheel-environmental assessment of CO2-based oxymethylene ether as a drop-in fuel". In: *Energy and Environmental Science* 11.2 (2018), pp. 331–343. DOI: 10.1039/c7ee01657c (cited on pages 24, 26, 146).

Divekar, Prasad S., Chen, Xiang, Tjong, Jimi, and Zheng, Ming. "Energy efficiency impact of EGR on organizing clean combustion in diesel engines". In: *Energy Conversion and Management* 112 (2016), pp. 369–381. DOI: 10.1016/j.enconman.2016.01.042 (cited on page 22).

Dolak, Jonathan George, Shi, Yu, and Reitz, Rolf. "A computational investigation of stepped-bowl piston geometry for a light duty engine operating at low load". In: *SAE Technical Papers* (2010). DOI: 10.4271/2010-01-1263 (cited on page 21).

Drake, Michael C and Blint, Richard J. "Calculations of NOx Formation Pathways in Propagating Laminar, High Pressure Premixed CH4/Air Flames". In: *Combustion Science and Technology* 75.4-6 (1991), pp. 261–285. DOI: 10.1080/00102209108924092 (cited on page 161).

Dreisbach, Rolf, Graf, Gernot, Kreuzig, Gerhard, Theissl, Helmut, and Pfahl, Ulrich. "HD base engine development to meet future emission and power density challenges of a DDI™ engine". In: *SAE Technical Papers* 724 (2007). DOI: 10.4271/2007-01-4225 (cited on page 193).

Dukowicz, John K. "A particle-fluid numerical model for liquid sprays". In: *Journal of Computational Physics* 35.2 (1980), pp. 229–253. DOI: 10.1016/0021-9991(80)90087-X (cited on page 65).

Dumouchel, Christophe. "On the experimental investigation on primary atomization of liquid streams". In: *Experiments in Fluids* 45.3 (2008), pp. 371–422. DOI: 10.1007/s00348-008-0526-0 (cited on page 14).

Espey, Christoph and Dec, John E. "Chemiluminescence Imaging of Autoignition in a DI Diesel Engine". In: *International Fall Fuels and Lubricants Meeting and Exposition*. SAE International, 1998. DOI: https://doi.org/10.4271/982685 (cited on page 15).

Ferraro, Federica, Russo, Carmela, Schmitz, Robert, Hasse, Christian, and Sirignano, Mariano. "Experimental and numerical study on the effect of oxymethylene ether-3 (OME3) on soot particle formation". In: *Fuel* 286.P1 (2021), p. 119353. DOI: 10.1016/j.fuel.2020.119353 (cited on page 24).

Ferraro, Federica, Russo, Carmela, Schmitz, Robert, Hasse, Christian, and Sirignano, Mariano. "Experimental and numerical study on the effect of oxymethylene ether-3 (OME3) on soot particle formation". In: *Fuel* 286.P1 (2021), p. 119353. DOI: 10.1016/j.fuel.2020.119353 (cited on page 145).

Funayama, Yoshihiro, Nakajima, Hiroshi, and Shimokawa, Kiyohiro. "A Study on the Effects of a Higher Compression Ratio in the Combustion Chamber on Diesel Engine Performance". In: *SAE 2016 World Congress and Exhibition*. SAE International, 2016. DOI: https://doi.org/10.4271/2016-01-0722 (cited on page 20).

Gandomi, Amir Hossein, Yun, Gun Jin, Yang, Xin She, and Talatahari, Siamak. "Chaos-enhanced accelerated particle swarm optimization". In: *Communications in Nonlinear Science and Numerical Simulation* 18.2 (2013), pp. 327–340. DOI: 10.1016/j.cnsns.2012.07.017 (cited on page 51).

García, Antonio, Gil, Antonio, Monsalve-Serrano, Javier, and Lago Sari, Rafael. "OMEx-diesel blends as high reactivity fuel for ultra-low NOx and soot emissions in the dual-mode dual-fuel combustion strategy". In: *Fuel* 275.April (2020), p. 117898. DOI: 10.1016/j.fuel.2020.117898 (cited on page 149).

García, Antonio, Monsalve-Serrano, Javier, Lago Sari, Rafael, and Martinez-Boggio, Santiago. "Energy sustainability in the transport sector using synthetic fuels in series hybrid trucks with RCCI dual-fuel engine". In: *Fuel* 308.August 2021 (2022), p. 122024. DOI: 10.1016/j.fuel.2021.122024 (cited on page 3).

García, Antonio, Monsalve-Serrano, Javier, Martinez-Boggio, Santiago, and Gaillard, Patrick. "Impact of the hybrid electric architecture on the performance and emissions of a delivery truck with a dual-fuel RCCI engine". In: *Applied Energy* 301.February (2021), p. 117494. DOI: 10.1016/j.apenergy.2021.117494 (cited on page 3).

García, Antonio et al. “Potential of e-Fischer Tropsch diesel and oxymethyl-ether (OMEx) as fuels for the dual-mode dual-fuel concept”. In: *Applied Energy* 253.July (2019), p. 113622. DOI: 10.1016/j.apenergy.2019.113622 (cited on page 26).

García Carrero, AA. “Experimental Study of the Fuel Effect on Diffusion Combustion and Soot Formation under Diesel Engine-Like Conditions [Tesis doctoral]”. In: *Universitat Politècnica de València* (2021). DOI: https://doi.org/10.4995/Thesis/10251/179997 (cited on page 6).

Gaukel, Kai, Dworschak, Patrick, Pélerin, Dominik, Härtl, Martin, and Wachtmeister, Georg. “Combustion process optimization for oxymethylene ether fuels in a heavy-duty application”. In: (2019), pp. 351–367. DOI: 10.1007/978-3-658-26528-1_21 (cited on pages 146, 162).

Ge, Mengpin and Friedrich, Johannes. *4 Charts Explain Greenhouse Gas Emissions by Countries and Sectors*. 2020 (cited on page 2).

Genzale, Caroline L., Reitz, Rolf D., and Wickman, David D. “A computational investigation into the effects of spray targeting, bowl geometry and swirl ratio for low-temperature combustion in a heavy-duty diesel engine”. In: *SAE Technical Papers* 2007.724 (2007), pp. 776–790. DOI: 10.4271/2007-01-0119 (cited on pages 22, 24).

Glassman, Irvin and Yetter, Richard A. “Chapter 9 - Combustion of Non-volatile Fuels”. In: *Combustion (Fourth Edition)*. Ed. by Irvin Glassman and Richard A. Yetter. Fourth Edition. Burlington: Academic Press, 2008, pp. 495–550. DOI: https://doi.org/10.1016/B978-0-12-088573-2.00009-9 (cited on page 16).

Gómez Soriano, J. “Computational assessment of combustion noise of automotive compression-ignited engines [Tesis doctoral]”. In: *Universitat Politècnica de València* (2018). DOI: https://doi.org/10.4995/Thesis/10251/112726 (cited on page 5).

Gray, Allen W. and Ryan, Thomas W. “Homogeneous charge compression ignition (HCCI) of diesel fuel”. In: *SAE Technical Papers* 412 (1997). DOI: 10.4271/971676 (cited on page 27).

Gugulothu, S. K. and Reddy, K. H.C. “CFD simulation of in-cylinder flow on different piston bowl geometries in a DI diesel engine”. In: *Journal of Applied Fluid Mechanics* 9.3 (2016), pp. 1147–1155. DOI: 10.18869/acadpub.jafm.68.228.24397 (cited on page 75).

Han, Sangwook and Bae, Choongsik. "The influence of fuel injection pressure and intake pressure on conventional and low temperature diesel combustion". In: *SAE Technical Papers* (2012). DOI: 10.4271/2012-01-1721 (cited on page 24).

Han, Sangwook and Bae, Choongsik. "The influence of fuel injection pressure and intake pressure on conventional and low temperature diesel combustion". In: *SAE Technical Papers* (2012). DOI: 10.4271/2012-01-1721 (cited on pages 117, 191).

Hanak, Dawid P., Powell, Dante, and Manovic, Vasilije. "Techno-economic analysis of oxy-combustion coal-fired power plant with cryogenic oxygen storage". In: *Applied Energy* 191 (2017), pp. 193–203. DOI: 10.1016/j.apenergy.2017.01.049 (cited on page 29).

Harshavardhan, Ballapu and Mallikarjuna, J. M. "Effect of piston shape on in-cylinder flows and air-fuel interaction in a direct injection spark ignition engine - A CFD analysis". In: *Energy* 81 (2015), pp. 361–372. DOI: 10.1016/j.energy.2014.12.049 (cited on page 75).

Härtl, Martin, Seidenspinner, Philipp, Jacob, Eberhard, and Wachtmeister, Georg. "Oxygenate screening on a heavy-duty diesel engine and emission characteristics of highly oxygenated oxymethylene ether fuel OME1". In: *Fuel* 153 (2015), pp. 328–335. DOI: 10.1016/j.fuel.2015.03.012 (cited on pages 26, 146).

Hassan, Rania, Cohanim, Babak, De Weck, Olivier, and Venter, Gerhaid. "A comparison of particle swarm optimization and the genetic algorithm". In: *Collection of Technical Papers - AIAA/ASME/ASCE/AHS/ASC Structures, Structural Dynamics and Materials Conference* 2.April (2005), pp. 1138–1150. DOI: 10.2514/6.2005-1897 (cited on page 54).

Hernández López, Alberto. "Optimization and analysis by CFD of mixing-controlled combustion concepts in compression ignition engines [Tesis doctoral no publicada]". PhD thesis. 2018. DOI: https://doi.org/10.4995/Thesis/10251/103826 (cited on pages 5, 98).

Heywood, John B. *Internal Combustion Engine Fundamentals. N. York: McGraw-Hill.* 1988 (cited on pages 1, 12–16, 68).

Hsu, Bertrand D. *Diesel-Engine Combustion Analysis Practical Combustion Analysis.* 2022 (cited on page 16).

Hu, Jiancun, Chen, Ziqiang, Yao, Ye, Shi, Lei, and Deng, Kangyao. "Study on control-oriented emission predictions of PPCI diesel engine with two-stage fuel injection". In: *Fuel* 320.January (2022), p. 123984. DOI: 10.1016/j.fuel.2022.123984 (cited on page 27).

Huh, Kang Y., Chang, I. Ping, and Martin, Jay K. "A comparison of boundary layer treatments for heat transfer in IC engines". In: *SAE Technical Papers* (1990). DOI: 10.4271/900252 (cited on page 81).

Hyvönen, Jari, Haraldsson, Göran, and Johansson, Bengt. "Supercharging HCCI to extend the operating range in a multi-cylinder VCR-HCCI engine". In: *SAE Technical Papers* 2003.724 (2003). DOI: 10.4271/2003-01-3214 (cited on page 27).

Iannuzzi, Stefano Emanuele, Barro, Christophe, Boulouchos, Konstantinos, and Burger, Jakob. "Combustion behavior and soot formation/oxidation of oxygenated fuels in a cylindrical constant volume chamber". In: *Fuel* 167 (2016), pp. 49–59. DOI: 10.1016/j.fuel.2015.11.060 (cited on page 4).

Iannuzzi, Stefano Emanuele, Barro, Christophe, Boulouchos, Konstantinos, and Burger, Jakob. "Combustion behavior and soot formation/oxidation of oxygenated fuels in a cylindrical constant volume chamber". In: *Fuel* 167 (2016), pp. 49–59. DOI: 10.1016/j.fuel.2015.11.060 (cited on pages 24, 26).

Iannuzzi, Stefano Emanuele, Barro, Christophe, Boulouchos, Konstantinos, and Burger, Jakob. "Combustion behavior and soot formation/oxidation of oxygenated fuels in a cylindrical constant volume chamber". In: *Fuel* 167 (2016), pp. 49–59. DOI: 10.1016/j.fuel.2015.11.060 (cited on page 145).

Intergovernmental Panel on Climate Change. *Climate Change 2014 Mitigation of Climate Change*. 2014. DOI: 10.1017/cbo9781107415416 (cited on page 2).

Ismail, H.M., Ng, H.K., Gan, S., and Lucchini, T. "Approach for the Modeling of Reacting Biodiesel Fuel Spray using OpenFOAM". In: *SAE Technical Paper Series* 1 (2014), pp. 1–9. DOI: 10.4271/2014-01-2565 (cited on page 65).

Jafarmadar, S., Taghavifar, Hadi, Taghavifar, Hamid, and Navid, A. "Numerical assessment of flow dynamics for various di diesel engine designs considering swirl number and uniformity index". In: *Energy Conversion and Management* 110 (2016), pp. 347–355. DOI: 10.1016/j.enconman.2015.12.035 (cited on page 118).

Jain, Ayush, Singh, Akhilendra Pratap, and Agarwal, Avinash Kumar. "Effect of fuel injection parameters on combustion stability and emissions of a mineral diesel fueled partially premixed charge compression ignition (PCCI) engine". In: *Applied Energy* 190 (2017), pp. 658–669. DOI: 10.1016/j.apenergy.2016.12.164 (cited on page 27).

Jin, Chao and Zheng, Zunqing. "A review on homogeneous charge compression ignition and low temperature combustion by optical diagnostics". In: *Journal of Chemistry* 2015 (2015). DOI: 10.1155/2015/910348 (cited on page 27).

Kakaee, Amir Hasan, Nasiri-Toosi, Ali, Partovi, Babak, and Paykani, Amin. "Effects of piston bowl geometry on combustion and emissions characteristics of a natural gas/diesel RCCI engine". In: *Applied Thermal Engineering* 102 (2016), pp. 1462–1472. DOI: 10.1016/j.applthermaleng.2016.03.162 (cited on pages 19, 21).

Kang, Zhe et al. "Study of the Combustion Characteristics of a HCCI Engine Coupled with Oxy-Fuel Combustion Mode". In: *SAE International Journal of Engines* 10.3 (2017), pp. 908–916. DOI: 10.4271/2017-01-0649 (cited on page 30).

Kang, Zhe et al. "Study of the Combustion Characteristics of a HCCI Engine Coupled with Oxy-Fuel Combustion Mode". In: *SAE International Journal of Engines* 10.3 (2017). DOI: 10.4271/2017-01-0649 (cited on page 182).

Kaplan, Mahmut, Özbey, Mustafa, and Özcan, Hakan. "Numerical Investigation of the Effects of Intake Port Geometry on In-Cylinder Motion and Combustion in Diesel Engine". In: *Int. J. Eng. Sci.* 7 (2018), pp. 16–26. DOI: 10.9790/1813-0706021626 (cited on page 75).

Karra, Prashanth and Kong, Song Charng. "Application of particle swarm optimization for diesel engine performance optimization". In: *SAE Technical Papers* (2010). DOI: 10.4271/2010-01-1258 (cited on page 49).

Kattimani, Sunilkumar S., Topannavar, S. N., Shivashimpi, M. M., and Dodamani, B. M. "Experimental investigation to optimize fuel injection strategies and compression ratio on single cylinder DI diesel engine operated with FOME biodiesel". In: *Energy* 200 (2020), p. 117336. DOI: 10.1016/j.energy.2020.117336 (cited on page 117).

Kennedy, J. and Eberhart, R. "Particle swarm optimization". In: *Proceedings of ICNN 95 - International Conference on Neural Networks*. IEEE, 1995. DOI: 10.1109/icnn.1995.488968 (cited on pages 49, 86).

Kidoguchi, Yoshiyuki, Yang, Changlin, and Miwa, Kei. "Effect of high squish combustion chamber on simultaneous reduction of NOx and particulate from a direct-injection diesel engine". In: *SAE Technical Papers* 724 (1999). DOI: 10.4271/1999-01-1502 (cited on page 21).

Kim, Byong Seok, Yoon, Wook Hyeon, Ryu, Sung Hyup, and Ha, Ji Soo. "Effect of the injector nozzle hole diameter and number on the spray characteristics and the combustion performance in medium-speed diesel marine engines". In: *SAE Technical Papers* 724 (2005). DOI: 10.4271/2005-01-3853 (cited on pages 22, 117).

Kimura, N., Omata, K., Kiga, T., Takano, S., and Shikisima, S. "The characteristics of pulverized coal combustion in O2/CO2 mixtures for CO2 recovery". In: *Energy Conversion and Management* 36.6-9 (1995), pp. 805–808. DOI: 10.1016/0196-8904(95)00126-X (cited on page 29).

Kingma, Diederik P. and Ba, Jimmy Lei. "Adam: A method for stochastic optimization". In: *3rd International Conference on Learning Representations, ICLR 2015 - Conference Track Proceedings* (2015), pp. 1–15 (cited on page 169).

Klaus Mollenhauer, Helmut Tschöke. *Handbook of Diesel Engines*. Springer Berlin, Heidelberg, 2010. DOI: https://doi.org/10.1007/978-3-540-89083-6 (cited on pages 14, 17).

Kokjohn, S. L., Hanson, R. M., Splitter, D. A., and Reitz, R. D. "Fuel reactivity controlled compression ignition (RCCI): A pathway to controlled high-efficiency clean combustion". In: *International Journal of Engine Research* 12.3 (2011), pp. 209–226. DOI: 10.1177/1468087411401548 (cited on page 28).

Komninos, N. P. and Kosmadakis, G. M. "Heat transfer in HCCI multi-zone modeling: Validation of a new wall heat flux correlation under motoring conditions". In: *Applied Energy* 88.5 (2011), pp. 1635–1648. DOI: 10.1016/j.apenergy.2010.11.039 (cited on page 79).

Komninos, N. P. and Rakopoulos, C. D. "Heat transfer in hcci phenomenological simulation models: A review". In: *Applied Energy* 181 (2016), pp. 179–209. DOI: 10.1016/j.apenergy.2016.08.061 (cited on page 79).

König, Andrea, Marquardt, Wolfgang, Mitsos, Alexander, Viell, Jörn, and Dahmen, Manuel. "Integrated design of renewable fuels and their production processes: recent advances and challenges". In: *Current Opinion in Chemical Engineering* 27 (2020), pp. 45–50. DOI: 10.1016/j.coche.2019.11.001 (cited on page 24).

Kukačka, Jan, Golkov, Vladimir, and Cremers, Daniel. "Regularization for Deep Learning: A Taxonomy". In: (2017), pp. 1–23 (cited on page 169).

Kweon, Chol Bum et al. "Effect of injection timing on detailed chemical composition and particulate size distributions of diesel exhaust". In: *SAE Technical Papers* (2003). DOI: 10.4271/2003-01-1794 (cited on page 23).

Ladommatos, N., Abdelhalim, S., and Zhao, H. "The effects of exhaust gas recirculation on diesel combustion and emissions". In: *International Journal of Engine Research* 1.1 (2000), pp. 107–126. DOI: 10.1243/1468087001545290 (cited on page 23).

Lago Sari, R. "Dual Mode Dual Fuel Combustion: Implementation on a Real Medium Duty Engine Platform [Tesis doctoral]". In: *Universitat Politècnica de València* (2021). DOI: https://doi.org/10.4995/Thesis/10251/165366 (cited on page 5).

Lautenschütz, Ludger et al. "Physico-chemical properties and fuel characteristics of oxymethylene dialkyl ethers". In: *Fuel* 173 (2016), pp. 129–137. DOI: 10.1016/j.fuel.2016.01.060 (cited on page 4).

Lautenschütz, Ludger et al. "Physico-chemical properties and fuel characteristics of oxymethylene dialkyl ethers". In: *Fuel* 173 (2016), pp. 129–137. DOI: 10.1016/j.fuel.2016.01.060 (cited on page 24).

Lautenschütz, Ludger et al. "Physico-chemical properties and fuel characteristics of oxymethylene dialkyl ethers". In: *Fuel* 173 (2016), pp. 129–137. DOI: 10.1016/j.fuel.2016.01.060 (cited on pages 145, 147).

Leach, Felix, Ismail, Riyaz, Davy, Martin, Weall, Adam, and Cooper, Brian. "The effect of a stepped lip piston design on performance and emissions from a high-speed diesel engine". In: *Applied Energy* 215.November 2017 (2018), pp. 679–689. DOI: 10.1016/j.apenergy.2018.02.076 (cited on page 21).

Lee, Seokhwon, Jeon, Joonho, and Park, Sungwook. "Optimization of combustion chamber geometry and operating conditions for compression ignition engine fueled with pre-blended gasoline-diesel fuel". In: *Energy Conversion and Management* 126 (2016), pp. 638–648. DOI: 10.1016/j.enconman.2016.08.046 (cited on page 117).

Lehman, Joel and Stanley, Kenneth O. "Exploiting open-endedness to solve problems through the search for novelty". In: *Artificial Life - ALIFE* (2008) (cited on pages 52, 87).

Lehman, Joel and Stanley, Kenneth O. "Efficiently evolving programs through the search for novelty". In: *Proceedings of the 12th Annual Genetic and Evolutionary Computation Conference, GECCO '10* (2010), pp. 837–844. DOI: 10.1145/1830483.1830638 (cited on page 52).

Lehman, Joel and Stanley, Kenneth O. "Novelty Search and the Problem with Objectives". In: *Genetic Programming Theory and Practice IX*. Ed. by Rick Riolo, Ekaterina Vladislavleva, and Jason H. Moore. New York, NY: Springer New York, 2011, pp. 37–56. DOI: 10.1007/978-1-4614-1770-5_3 (cited on page 52).

Leung, K. M., Lindstedt, R. P., and Jones, W. P. "A simplified reaction mechanism for soot formation in nonpremixed flames". In: *Combustion and Flame* 87.3-4 (1991), pp. 289–305. DOI: 10.1016/0010-2180(91)90114-Q (cited on page 69).

Liu, Haoye, Wang, Zhi, Zhang, Jun, Wang, Jianxin, and Shuai, Shijin. "Study on combustion and emission characteristics of Polyoxymethylene Dimethyl Ethers/diesel blends in light-duty and heavy-duty diesel engines". In: *Applied Energy* 185 (2017), pp. 1393–1402. DOI: 10.1016/j.apenergy.2015.10.183 (cited on page 24).

Liu, Haoye, Wang, Zhi, Zhang, Jun, Wang, Jianxin, and Shuai, Shijin. "Study on combustion and emission characteristics of Polyoxymethylene Dimethyl Ethers/diesel blends in light-duty and heavy-duty diesel engines". In: *Applied Energy* 185 (2017), pp. 1393–1402. DOI: 10.1016/j.apenergy.2015.10.183 (cited on page 145).

Liu, Haoye et al. "Recent progress in the application in compression ignition engines and the synthesis technologies of polyoxymethylene dimethyl ethers". In: *Applied Energy* 233-234.June 2018 (2019), pp. 599–611. DOI: 10.1016/j.apenergy.2018.10.064 (cited on page 26).

Lucchini, T, Onorati, A, and Hardy, G. "CFD modelling of combustion in Heavy-Duty Diesel Engines". In: (2014), pp. 1–15 (cited on page 68).

Lucchini, Tommaso, Pontoni, Daniel, D'Errico, Gianluca, and Somers, Bart. "Modeling diesel combustion with tabulated kinetics and different flame structure assumptions based on flamelet approach". In: *International Journal of Engine Research* 21.1 (2020), pp. 89–100. DOI: 10.1177/1468087419862945 (cited on page 64).

Lucchini, Tommaso et al. "A comprehensive model to predict the initial stage of combustion in SI engines". In: *SAE Technical Papers* 2 (2013). DOI: 10.4271/2013-01-1087 (cited on page 64).

Lucchini, Tommaso et al. "Automatic Mesh Generation for CFD Simulations of Direct-Injection Engines". In: *SAE Technical Papers* 2015-April.April (2015). DOI: 10.4271/2015-01-0376 (cited on pages 64, 69).

Ma, Cheng et al. "Analysis of PPCI mode and multi-objective comprehensive optimization for a dual-fuel engine". In: *Fuel* 303.April (2021), p. 121296. DOI: 10.1016/j.fuel.2021.121296 (cited on page 27).

Ma, Cheng et al. "Multi-objective optimization of dual-fuel engine performance in PPCI mode based on preference decision". In: *Fuel* 312.October 2021 (2022), p. 122901. DOI: 10.1016/j.fuel.2021.122901 (cited on page 27).

Ma, Xiao et al. "PLII-LEM and OH∗ Chemiluminescence Study on Soot Formation in Spray Combustion of PODEn-Diesel Blend Fuels in a Constant Volume Vessel". In: *SAE Technical Papers* 2017-October (2017). DOI: 10.4271/2017-01-2329 (cited on page 26).

Madras, Technology and Madras, Technology. "CFD Analysis of in-Cylinder Flow and Air-Fuel Interaction on Different Combustion Chamber Geometry in DISI Engine CFD Analysis of in-Cylinder Flow and Air-Fuel Interaction on Different Combustion Chamber Geometry in DISI Engine". In: *International Journal on Theoretical and Applied Research in Mechanical Engineering (IJTARME)* 2.3 (2013), pp. 104–108 (cited on page 75).

Maes, Noud et al. "Heavy-Duty Diesel Engine Spray Combustion Processes: Experiments and Numerical Simulations". In: *SAE Technical Papers* 2018-September (2018), pp. 1–22. DOI: 10.4271/2018-01-1689 (cited on pages 75, 77).

Mancaruso, Ezio, Todino, Michele, and Vaglieco, Bianca Maria. "Analysis of dual fuel combustion in single cylinder research engine fueled with methane and diesel by ir diagnostics". In: *SAE Technical Papers* 2019-April.April (2019). DOI: 10.4271/2019-01-1165 (cited on page 28).

Mancaruso, Ezio and Vaglieco, Bianca Maria. "UV-Visible Spectroscopic Measurements of Dual-Fuel PCCI Engine". In: *SAE International Journal of Fuels and Lubricants* 4.2 (2011), pp. 271–281. DOI: 10.4271/2011-24-0061 (cited on page 28).

Mancaruso, Ezio and Vaglieco, Bianca Maria. "UV-visible imaging of PCCI engine running with ethanol/diesel fuel". In: *SAE Technical Papers* (2012). DOI: 10.4271/2012-01-1238 (cited on page 28).

Mancaruso, Ezio and Vaglieco, Bianca Maria. "Characterization of PCCI combustion in a single cylinder CI engine fuelled with RME and bio-ethanol". In: *SAE Technical Papers* 2 (2013). DOI: 10.4271/2013-01-1672 (cited on page 28).

Mancini, N. D. and Mitsos, A. "Conceptual design and analysis of ITM oxy-combustion power cycles". In: *Physical Chemistry Chemical Physics* 13.48 (2011), pp. 21351–21361. DOI: 10.1039/c1cp23027a (cited on page 29).

Marini, Federico and Walczak, Beata. "Particle swarm optimization (PSO). A tutorial". In: *Chemometrics and Intelligent Laboratory Systems* 149 (2015), pp. 153–165. DOI: 10.1016/j.chemolab.2015.08.020 (cited on pages 88, 90).

Martin, Jaime, Arnau, Francisco, Piqueras, Pedro, and Auñon, Angel. "Development of an Integrated Virtual Engine Model to Simulate New Standard Testing Cycles". In: *SAE Technical Papers* 2018-April (2018), pp. 1–17. DOI: 10.4271/2018-01-1413 (cited on page 180).

Martínez Rodríguez, D. "Optimization Algorithm Based on Novelty Search Applied to the Treatment of Uncertainty in Models." PhD thesis. Universitat Politècnica de València, 2021. DOI: 10.4995/Thesis/10251/178994 (cited on page 86).

Martins, Mario et al. "HCCI of wet ethanol on dedicated cylinder of a diesel engine using exhaust heat recovery". In: *SAE Technical Papers* September (2018). DOI: 10.4271/2018-36-0191 (cited on page 27).

Miles, Paul C. and Andersson, Öivind. "A review of design considerations for light-duty diesel combustion systems". In: *International Journal of Engine Research* 17.1 (2016), pp. 6–15. DOI: 10.1177/1468087415604754 (cited on pages 20–22).

Miles, Paul C. and Andersson, Öivind. "A review of design considerations for light-duty diesel combustion systems". In: *International Journal of Engine Research* 17.1 (2016), pp. 6–15. DOI: 10.1177/1468087415604754 (cited on pages 24, 193, 194).

Mito, Yuko, Tanaka, Daisuke, Lee, Seang Wock, Daisho, Yasuhiro, and Kusaka, Jin. "The effect of intake, injection parameters and fuel properties on diesel combustion and emissions". In: *SAE Technical Papers* (2003). DOI: 10.4271/2003-01-1793 (cited on page 23).

Mobasheri, Raouf, Aitouche, Abdel, Peng, Zhijun, and Li, Xiang. "A numerical study of the effects of oxy-fuel combustion under homogeneous charge compression ignition regime". In: *International Journal of Engine Research* 23.4 (2022), pp. 649–660. DOI: 10.1177/1468087421993359 (cited on page 30).

Mobasheri, Raouf, Izza, Nadia, Aitouche, Abdel, Peng, Jun, and Bakir, Boualem. "Investigation of oxyfuel combustion on engine performance and emissions in a di Diesel HCCI Engine". In: *2019 8th International Conference on Systems and Control, ICSC 2019* (2019), pp. 411–416. DOI: 10.1109/ICSC47195.2019.8950525 (cited on page 30).

Mobasheri, Raouf and Khabbaz, Seyed Alireza. "Modeling the effects of high EGR rates in conjunction with optimum multiple injection techniques in a heavy duty di diesel engine". In: *SAE Technical Papers* 1 (2014). DOI: 10.4271/2014-01-1124 (cited on pages 29, 118).

Mohammed, Abdulrahman, Masurier, Jean Baptiste, Elkhazraji, Ali, and Johansson, Bengt. "Oxy-Fuel HCCI Combustion in a CFR Engine with Carbon Dioxide as a Thermal Buffer". In: *SAE Technical Papers* 2019-September.September (2019). DOI: 10.4271/2019-24-0119 (cited on page 30).

Mohiuddin, Khawar, Kwon, Heesun, Choi, Minhoo, and Park, Sungwook. "Experimental investigation on the effect of injector hole number on engine performance and particle number emissions in a light-duty diesel engine". In: *International Journal of Engine Research* (2020). DOI: 10.1177/1468087420934605 (cited on page 172).

Moneib, Hany A., Abdelaal, Mohsen, Selim, Mohamed Y.E., and Abdallah, Osama A. "NOx emission control in SI engine by adding argon inert gas to intake mixture". In: *Energy Conversion and Management* 50.11 (2009), pp. 2699–2708. DOI: 10.1016/j.enconman.2009.05.032 (cited on page 28).

Monsalve Serrano, J. "Dual-fuel compression ignition: towards clean, highly efficient combustion [Tesis doctoral no publicada]". In: *Universitat Politècnica de València* (2016). DOI: https://doi.org/10.4995/Thesis/10251/75109 (cited on page 5).

Montenegro, G., Onorati, A., Piscaglia, F., and D'Errico, G. "Integrated 1D-MultiD fluid dynamic models for the simulation of I.C.E. Intake and exhaust systems". In: *SAE Technical Papers* 2007.724 (2007), pp. 776–790. DOI: 10.4271/2007-01-0495 (cited on page 64).

Musculus, Mark P. B. “On the Correlation between NOx Emissions and the Diesel Premixed Burn”. In: *SAE 2004 World Congress & Exhibition*. SAE International, 2004. DOI: https://doi.org/10.4271/2004-01-1401 (cited on page 16).

Neri, Ferrante and Tirronen, Ville. “Recent advances in differential evolution: A survey and experimental analysis”. In: 33.1-2 (2010), pp. 61–106. DOI: 10.1007/s10462-009-9137-2 (cited on page 51).

Omari, Ahmad, Heuser, Benedikt, and Pischinger, Stefan. “Potential of oxymethylenether-diesel blends for ultra-low emission engines”. In: *Fuel* 209.May (2017), pp. 232–237. DOI: 10.1016/j.fuel.2017.07.107 (cited on pages 24, 26).

Omari, Ahmad, Heuser, Benedikt, and Pischinger, Stefan. “Potential of oxymethylenether-diesel blends for ultra-low emission engines”. In: *Fuel* 209.May (2017), pp. 232–237. DOI: 10.1016/j.fuel.2017.07.107 (cited on pages 145, 146).

OpenFOAM website, https://openfoam.org/ (cited on page 64).

Osman, Azmi. “Feasibility study of a novel combustion cycle involving oxygen and water”. In: *SAE Technical Papers* 3 (2009). DOI: 10.4271/2009-01-2808 (cited on page 29).

Owoyele, Opeoluwa, Pal, Pinaki, and Torreira, Alvaro Vidal. “An automated machine learning-genetic algorithm (AutoML-GA) framework with active learning for design optimization”. In: *ASME 2020 Internal Combustion Engine Division Fall Technical Conference, ICEF 2020* November (2021). DOI: 10.1115/ICEF2020-3000 (cited on page 170).

Package for scientific computing with Python - https://numpy.org. [Online; accessed 31 January 2020] (cited on page 88).

Pamminger, Michael, Wang, Buyu, Hall, Carrie M., Vojtech, Ryan, and Wallner, Thomas. “The impact of water injection and exhaust gas recirculation on combustion and emissions in a heavy-duty compression ignition engine operated on diesel and gasoline”. In: *International Journal of Engine Research* 21.8 (2020), pp. 1555–1573. DOI: 10.1177/1468087418815290 (cited on page 29).

Pastor, José V. et al. “Effect of a novel piston geometry on the combustion process of a light-duty compression ignition engine: An optical analysis”. In: *Energy* 221 (2021). DOI: 10.1016/j.energy.2021.119764 (cited on pages 21, 26).

Paul, B and Ganesan, V. “Flow field development in a direct injection diesel engine with different manifolds”. In: *International Journal of Engineering, Science and Technology* 2.1 (2010), pp. 80–91. DOI: 10.4314/ijest.v2i1.59089 (cited on page 75).

Payri, F., Molina, S., Martín, J., and Armas, O. “Influence of measurement errors and estimated parameters on combustion diagnosis”. In: *Applied Thermal Engineering* 26.2-3 (2006), pp. 226–236. DOI: 10.1016/j.applthermaleng.2005.05.006 (cited on page 64).

Payri, R., Salvador, F. J., Gimeno, J., and Bracho, G. “A new methodology for correcting the signal cumulative phenomenon on injection rate measurements”. In: *Experimental Techniques* 32.1 (2008), pp. 46–49. DOI: 10.1111/j.1747-1567.2007.00188.x (cited on page 96).

Payri, Raul, Gimeno, Jaime, Novella, Ricardo, and Bracho, Gabriela. “On the rate of injection modeling applied to direct injection compression ignition engines”. In: *International Journal of Engine Research* 17.10 (2016), pp. 1015–1030. DOI: 10.1177/1468087416636281 (cited on page 96).

Pélerin, Dominik, Gaukel, Kai, Härtl, Martin, Jacob, Eberhard, and Wachtmeister, Georg. “Potentials to simplify the engine system using the alternative diesel fuels oxymethylene ether OME1 and OME3-6 on a heavy-duty engine”. In: *Fuel* 259.January 2019 (2020). DOI: 10.1016/j.fuel.2019.116231 (cited on page 26).

Pellegrini, Leonardo et al. “Combustion behaviour and emission performance of neat and blended polyoxymethylene dimethyl ethers in a light-duty diesel engine”. In: *SAE Technical Papers* (2012). DOI: 10.4271/2012-01-1053 (cited on page 26).

Peters, N. “Laminar diffusion flamelet models in non-premixed turbulent combustion”. In: *Progress in Energy and Combustion Science* 10.3 (1984), pp. 319–339. DOI: 10.1016/0360-1285(84)90114-X (cited on page 67).

Peters, N. “Laminar flamelet concepts in turbulent combustion”. In: *Symposium (International) on Combustion* 21.1 (1988). Twenty-First Symposuim (International on Combustion), pp. 1231–1250. DOI: https://doi.org/10.1016/S0082-0784(88)80355-2 (cited on page 65).

Pickett, Lyle M., Kook, Sanghoon, and Williams, Timothy C. “Visualization of Diesel Spray Penetration, Cool-Flame, Ignition, High-Temperature Combustion, and Soot Formation Using High-Speed Imaging”. In: *SAE International Journal of Engines* 2.1 (2009), pp. 439–459. DOI: https://doi.org/10.4271/2009-01-0658 (cited on page 15).

Piotrowski, Adam P. "L-SHADE optimization algorithms with population-wide inertia". In: *Information Sciences* 468 (2018), pp. 117–141. DOI: 10.1016/j.ins.2018.08.030 (cited on pages 88, 90).

Plee, Steven L. and Ahmad, Tanvir. "Relative Roles of Premixed and Diffusion Burning in Diesel Combustion". In: *1983 SAE International Fall Fuels and Lubricants Meeting and Exhibition*. SAE International, 1983. DOI: https://doi.org/10.4271/831733 (cited on page 15).

Poláková, Radka and Valenta, Daniel. "jSO and GWO Algorithms Optimize Together". In: *CEUR Workshop Proceedings* 3226 (2022), pp. 159–166 (cited on page 51).

Portillo, Esmeralda, Alonso-Fariñas, Bernabé, Vega, Fernando, Cano, Mercedes, and Navarrete, Benito. "Alternatives for oxygen-selective membrane systems and their integration into the oxy-fuel combustion process: A review". In: *Separation and Purification Technology* 229.January (2019), p. 115708. DOI: 10.1016/j.seppur.2019.115708 (cited on page 29).

Prashanth, K, Shaik, Amjad, T, Srinivasa Rao, and B, Pavan Bharadwaja. "Experimental investigation of argon gas induction on diesel engine performance and emission characteristics : A comprehensive study on de-NO x techniques". In: *Process Safety and Environmental Protection* 152 (2021), pp. 471–481. DOI: 10.1016/j.psep.2021.06.036 (cited on page 28).

Python programming language - https://www.python.org. [Online; accessed 31 January 2020] (cited on pages 88, 169).

Ra, Youngchul and Reitz, Rolf D. "A reduced chemical kinetic model for IC engine combustion simulations with primary reference fuels". In: *Combustion and Flame* 155.4 (2008), pp. 713–738. DOI: 10.1016/j.combustflame.2008.05.002 (cited on page 65).

Rakopoulos, C. D., Kosmadakis, G. M., and Pariotis, E. G. "Critical evaluation of current heat tranfsfer models used in CFD in-cylinder engine simulations and establishment of a comprehensive wall-function formulation". In: *Applied Energy* 87.5 (2010), pp. 1612–1630. DOI: 10.1016/j.apenergy.2009.09.029 (cited on pages 81, 82).

Reddy, Abhishek G, Pratap Singh, Nirmal, V Sai Krishna, Kolluri R, Priyedarshi, Anurag, and Singh, SN. "Effect Of Compression Ratio On The Performance Of Diesel Engine At Different Loads". In: *Journal of Engineering Research and Applications www.ijera.com ISSN* 5.102 (2015), pp. 2248–962262 (cited on page 20).

Reitz, Rolf D. and Duraisamy, Ganesh. "Review of high efficiency and clean reactivity controlled compression ignition (RCCI) combustion in internal combustion engines". In: *Progress in Energy and Combustion Science* 46 (2015), pp. 12–71. DOI: 10.1016/j.pecs.2014.05.003 (cited on page 28).

Sanz, Wolfgang, Jericha, Herbert, Bauer, Bernhard, and Göttlich, Emil. "Qualitative and Quantitative Comparison of Two Promising Oxy-Fuel Power Cycles for CO2 Capture". In: *Journal of Engineering for Gas Turbines and Power* 130.3 (2008). 031702. DOI: 10.1115/1.2800350 (cited on page 29).

Serrano, J.R., Arnau, F.J., García-Cuevas, L.M., and Farias, V.H. "Oxy-fuel combustion feasibility of compression ignition engines using oxygen separation membranes for enabling carbon dioxide capture". In: *Energy Conversion and Management* 247 (2021), p. 114732. DOI: 10.1016/j.enconman.2021.114732 (cited on pages 30, 31, 180).

Serrano, J.R., Martin, J., Gomez-Soriano, J., and Raggi, R. "Theoretical and experimental evaluation of the spark-ignition premixed oxy-fuel combustion concept for future CO 2 captive powerplants". In: *Energy Conversion and Management* 244 (2021), p. 114498. DOI: 10.1016/j.enconman.2021.114498 (cited on pages 31, 196).

Serrano, J.R. et al. "Oxy-fuel combustion engine for highly efficient onboard CO2 capture. Another step forward in the path to a CO2 circular economy". In: Sustainable Internal Combustion Engine Virtual 'Live' (Stuttgart, Germany, Feb. 3–4, 2021). 2021 (cited on page 180).

Shen, Yong, Liang, Ziyuan, Kang, Hongwei, Sun, Xingping, and Chen, Qingyi. "A Modified jSO Algorithm for Solving Constrained Engineering Problems". In: *Symmetry* 13.1 (2021). DOI: 10.3390/sym13010063 (cited on page 51).

Sher, Eran. "Handbook of Air Pollution From Internal Combustion Engines". In: San Diego: Academic Press, 1998, pp. 653–663. DOI: https://doi.org/10.1016/B978-012639855-7/50056-9 (cited on page 23).

Shi, Y. and Reitz, R. D. "Optimization study of the effects of bowl geometry, spray targeting, and swirl ratio for a heavy-duty diesel engine operated at low and high load". In: *International Journal of Engine Research* 9.4 (2008), pp. 325–346. DOI: 10.1243/14680874JER00808 (cited on page 172).

Shi, Yu and Reitz, Rolf D. "Assessment of optimization methodologies to study the effects of bowl geometry, spray targeting and swirl ratio for a heavy-duty diesel engine operated at High-Load". In: *SAE International Journal of Engines* 1.1 (2009), pp. 537–557. DOI: 10.4271/2008-01-0949 (cited on pages 22, 191).

Silva, Mickael et al. "Computational assessment of effects of throat diameter on combustion and turbulence characteristics in a pre-chamber engine". In: *Applied Thermal Engineering* 212.April (2022), p. 118595. DOI: 10.1016/j.applthermaleng.2022.118595 (cited on page 75).

Skeen, Scott, Manin, Julien, and Pickett, Lyle M. "Visualization of Ignition Processes in High-Pressure Sprays with Multiple Injections of n-Dodecane". In: *SAE International Journal of Engines* 8.2 (2015), pp. 696–715. DOI: https://doi.org/10.4271/2015-01-0799 (cited on page 15).

Song, H. H. and Edwards, C. F. "Understanding chemical effects in low-load-limit extension of homogeneous charge compression ignition engines via recompression reaction". In: *International Journal of Engine Research* 10.4 (2009), pp. 231–250. DOI: 10.1243/14680874JER03409 (cited on page 27).

Splitter, Derek, Hanson, Reed, Kokjohn, Sage, Wissink, Martin, and Reitz, Rolf. "Injection effects in low load RCCI dual-fuel combustion". In: *SAE Technical Papers* (2011). DOI: 10.4271/2011-24-0047 (cited on page 28).

Splitter, Derek, Wissink, Martin, Delvescovo, Dan, and Reitz, Rolf. "RCCI engine operation towards 60% thermal efficiency". In: *SAE Technical Papers* 2.X (2013). DOI: 10.4271/2013-01-0279 (cited on page 28).

Splitter, Derek A. and Reitz, Rolf D. "Fuel reactivity effects on the efficiency and operational window of dual-fuel compression ignition engines". In: *Fuel* 118 (2014), pp. 163–175. DOI: 10.1016/j.fuel.2013.10.045 (cited on page 28).

Squaiella, Lucas Lázaro Ferreira, Martins, Cristiane Aparecida, and Lacava, Pedro T. "Strategies for emission control in diesel engine to meet Euro VI". In: *Fuel* 104 (2013), pp. 183–193. DOI: 10.1016/j.fuel.2012.07.027 (cited on page 23).

Stanglmaier, Rudolf H and Roberts, Charles E. "(HCCI): Benefits , Compromises , and Future Engine Applications". In: *Engineering* 724 (2012) (cited on page 27).

Stone, R. and Ball, J.K. *Automotive Engineering Fundamentals*. Premiere Series Bks. SAE International, 2004 (cited on pages 12, 14).

Suganthan, P. N. et al. “Problem Definitions and Evaluation Criteria”. In: *CEC 2005 Special Session on Real Parameter Optimization*. 2005 (cited on pages 88, 89, 92, 94).

Tan, Qinming and Hu, Yihuai. “A study on the combustion and emission performance of diesel engines under different proportions of O2 & N2 & CO2”. In: *Applied Thermal Engineering* 108 (2016), pp. 508–515. DOI: 10.1016/j.applthermaleng.2016.07.151 (cited on page 30).

Tan, Qinming and Hu, Yihuai. “A study on the combustion and emission performance of diesel engines under different proportions of O2 & N2 & CO2”. In: *Applied Thermal Engineering* 108 (2016), pp. 508–515. DOI: 10.1016/j.applthermaleng.2016.07.151 (cited on page 182).

Tan, Yong Ren et al. “Sooting characteristics of polyoxymethylene dimethyl ether blends with diesel in a diffusion flame”. In: *Fuel* 224.November 2017 (2018), pp. 499–506. DOI: 10.1016/j.fuel.2018.03.051 (cited on page 24).

Tan, Yong Ren et al. “Sooting characteristics of polyoxymethylene dimethyl ether blends with diesel in a diffusion flame”. In: *Fuel* 224.November 2017 (2018), pp. 499–506. DOI: 10.1016/j.fuel.2018.03.051 (cited on page 145).

Tanabe, Ryoji and Fukunaga, Alex. “Evaluating the performance of SHADE on CEC 2013 benchmark problems”. In: *2013 IEEE Congress on Evolutionary Computation, CEC 2013* 1 (2013), pp. 1952–1959. DOI: 10.1109/CEC.2013.6557798 (cited on page 51).

Tanaka, Shigeyuki, Ayala, Ferran, Keck, James C., and Heywood, John B. “Two-stage ignition in HCCI combustion and HCCI control by fuels and additives”. In: *Combustion and Flame* 132.1-2 (2003), pp. 219–239. DOI: 10.1016/S0010-2180(02)00457-1 (cited on page 27).

Tree, Dale R. and Svensson, Kenth I. “Soot processes in compression ignition engines”. In: *Progress in Energy and Combustion Science* 33.3 (2007), pp. 272–309. DOI: 10.1016/j.pecs.2006.03.002 (cited on page 18).

Tufail, K. *Turbocharging and air-path management for light-duty diesel engines*. x. Woodhead Publishing Limited, 2009, pp. 175–214. DOI: 10.1533/9781845697457.1.175 (cited on page 23).

Turns, Stephen R. *An introduction to combustion : concepts and applications*. 3rd ed.. New York: New York : McGraw-Hill, 2012., 2012 (cited on page 161).

Valentino, Gerardo, Allocca, Luigi, and Marchitto, Luca. "PIV investigation of high swirl flow on spray structure and its effect on emissions in a diesel-like environment". In: *SAE 2011 World Congress and Exhibition* (2011). DOI: 10.4271/2011-01-1286 (cited on page 4).

Van Blarigan, Andrew et al. "Experimental Study of Methane Fuel Oxycombustion in a Spark-Ignited Engine". In: *Journal of Energy Resources Technology* 136.1 (2014). DOI: 10.1115/1.4024974 (cited on page 30).

Vargas Lewiski, FD. "Analysis of the combustion process and soot formation in a single cylinder optical engine fueled with e-fuels and using different piston geometries [Tesis doctoral]". In: *Universitat Politècnica de València* (2021). DOI: 10.4995/Thesis/10251/180351 (cited on pages 6, 14, 21).

Vijay Kumar, M., Veeresh babu, A., Ravi Kumar, P., and Manoj Kumar Dundi, T. "Influence of different nozzle hole orifice diameter on performance, combustion and emissions in a diesel engine". In: *Australian Journal of Mechanical Engineering* 18.2 (2020), pp. 179–184. DOI: 10.1080/14484846.2018.1453975 (cited on page 117).

Voratas Kachitvichyanukul. "Comparison of Three Evolutionary Algorithms :" in: *Industrial Engineering & Management Systems* 11.3 (2012), pp. 215–223 (cited on pages 53, 54).

Wang, Dan, Zhu, Gangli, Li, Zhen, Xue, Machen, and Xia, Chungu. "Conceptual design of production of eco-friendly polyoxymethylene dimethyl ethers catalyzed by acid functionalized ionic liquids". In: *Chemical Engineering Science* 206 (2019), pp. 10–21. DOI: 10.1016/j.ces.2019.05.017 (cited on page 25).

Wang, Sun-Chong. "Artificial Neural Network". In: *Interdisciplinary Computing in Java Programming*. Boston, MA: Springer US, 2003, pp. 81–100. DOI: 10.1007/978-1-4615-0377-4_5 (cited on page 54).

Wang, Xi, Ting, David S.K., and Henshaw, Paul. "Mutation particle swarm optimization (M-PSO) of a thermoelectric generator in a multivariable space". In: *Energy Conversion and Management* 224.June (2020), p. 113387. DOI: 10.1016/j.enconman.2020.113387 (cited on page 49).

Wei, Xiaoyu, Manovic, Vasilije, and Hanak, Dawid P. "Techno-economic assessment of coal- or biomass-fired oxy-combustion power plants with supercritical carbon dioxide cycle". In: *Energy Conversion and Management* 221.July (2020), p. 113143. DOI: 10.1016/j.enconman.2020.113143 (cited on page 29).

Westbrook, C. K. et al. "The effects of pressure, temperature, and concentration on the reactivity of alkanes: Experiments and modeling in a rapid compression machine". In: *Symposium (International) on Combustion* 27.1 (1998), pp. 371–378. DOI: 10.1016/S0082-0784(98)80425-6 (cited on page 15).

Westbrook, Charles K. et al. "Diesel Combustion: An Integrated View Combining Laser Diagnostics, Chemical Kinetics, And Empirical Validation". In: *Future Transportation Technology Conference & Exposition*. SAE International, 1999. DOI: https://doi.org/10.4271/1999-01-0509 (cited on page 16).

Wickman, D. D., Senecal, P. K., and Reitz, R. D. "Diesel engine combustion chamber geometry optimization using genetic algorithms and multidimensional spray and combustion modeling". In: *SAE Technical Papers* 110 (2001), pp. 487–507. DOI: 10.4271/2001-01-0547 (cited on pages 19, 117).

Winklinger, JF. "Implementation of a combustion model based on the flamelet concept and its application to turbulent reactive sprays [Tesis doctoral no publicada]". In: *Universitat Politècnica de València* (2014). DOI: https://doi.org/10.4995/Thesis/10251/48488 (cited on page 4).

Xuan, T. "Optical investigations on Diesel spray dynamics and in-flame soot formation [Tesis doctoral]". In: *Universitat Politècnica de València* (2017). DOI: 10.4995/Thesis/10251/94626 (cited on page 13).

Yakhot, Victor and Orszag, Steven A. "Renormalization-Group Analysis of Turbulence". In: 57.14 (1986), pp. 1722–1724 (cited on page 65).

Yaliwal, V. S. et al. "Effect of nozzle and combustion chamber geometry on the performance of a diesel engine operated on dual fuel mode using renewable fuels". In: *Renewable Energy* 93 (2016), pp. 483–501. DOI: 10.1016/j.renene.2016.03.020 (cited on page 191).

Yao, Mingfa, Zheng, Zhaolei, and Liu, Haifeng. "Progress and recent trends in homogeneous charge compression ignition (HCCI) engines". In: *Progress in Energy and Combustion Science* 35.5 (2009), pp. 398–437. DOI: 10.1016/j.pecs.2009.05.001 (cited on page 27).

Yoon, Sungjun, Lee, Seungpil, Kwon, Hyuckmo, Lee, Joonkyu, and Park, Sungwook. "Effects of the swirl ratio and injector hole number on the combustion and emission characteristics of a light duty diesel engine". In: *Applied Thermal Engineering* 142.March (2018), pp. 68–78. DOI: 10.1016/j.applthermaleng.2018.06.076 (cited on page 118).

Yoon, Sungjun, Lee, Seungpil, Kwon, Hyuckmo, Lee, Joonkyu, and Park, Sungwook. "Effects of the swirl ratio and injector hole number on the combustion and emission characteristics of a light duty diesel engine". In: *Applied Thermal Engineering* 142.March (2018), pp. 68–78. DOI: 10.1016/j.applthermaleng.2018.06.076 (cited on page 191).

Zhang, Wei et al. "Influence of EGR and oxygen-enriched air on diesel engine NO-Smoke emission and combustion characteristic". In: *Applied Energy* 107 (2013), pp. 304–314. DOI: 10.1016/j.apenergy.2013.02.024 (cited on page 118).

Zhang, Xiaolei, Kumar, Amit, Arnold, Ulrich, and Sauer, Jörg. "Biomass-derived oxymethylene ethers as diesel additives: A thermodynamic analysis". In: *Energy Procedia* 61 (2014), pp. 1921–1924. DOI: 10.1016/j.egypro.2014.12.242 (cited on page 24).

Zhang, Xiaolei et al. "An optimized process design for oxymethylene ether production from woody-biomass-derived syngas". In: *Biomass and Bioenergy* 90.x (2016), pp. 7–14. DOI: 10.1016/j.biombioe.2016.03.032 (cited on page 24).

Zhiyu Han, Rolf D. Reitz. "A temperature wall function formulation for variable-density turbulent flows with application to engine convective heat transfer modeling". In: *Int. J. Mass Transfer* 40.3 (1997), pp. 613–625. DOI: 10.1016/0017-9310(96)00117-2 (cited on page 81).

Zhou, Qiyan, Lucchini, Tommaso, D'Errico, Gianluca, and Hardy, Gilles. "Validation of Diesel Combustion Models with Turbulence Chemistry Interaction and Detailed Kinetics". In: *SAE Technical Papers* (2019). DOI: 10.4271/2019-24-0088 (cited on page 68).

Zhou, Qiyan, Lucchini, Tommaso, D'Errico, Gianluca, Hardy, Gilles, and Lu, Xingcai. "Modeling heavy-duty diesel engines using tabulated kinetics in a wide range of operating conditions". In: *International Journal of Engine Research* 22.4 (2021), pp. 1116–1132. DOI: 10.1177/1468087419896165 (cited on pages 64, 68).

Zhou, Qiyan et al. "Computational Modeling of Diesel Spray Combustion with Multiple Injections". In: *SAE Technical Papers* 2020-April.April (2020), pp. 2839–2858. DOI: 10.4271/2020-01-1155 (cited on pages 68, 75–77).

Zhu, Yongfei et al. "Development of diesel surrogates for reproducing the effect of fuel properties on engine combustion and emissions using an optimized decoupling physical–chemical surrogate (DPCS) model". In: *Fuel* 310.PB (2022), p. 122424. DOI: 10.1016/j.fuel.2021.122424 (cited on page 65).

Zubel, Marius, Ottenwälder, Tamara, Heuser, Benedikt, and Pischinger, Stefan. "Combustion system optimization for dimethyl ether using a genetic algorithm". In: *International Journal of Engine Research* 22.1 (2021), pp. 22–38. DOI: 10.1177/1468087419851577 (cited on pages 162, 189).